



UNIVERSITEIT • STELLENBOSCH • UNIVERSITY
jou kennisvennoot • your knowledge partner

Rocking shear wall foundations in regions of moderate seismicity

by

Johann Eduard van der Merwe

Thesis presented for the degree of Master of Science at the Department of Civil Engineering of the University of Stellenbosch



Supervisor

Professor J. A. Wium

Stellenbosch

November 2009



Fakulteit Ingenieurswese
Faculty of Engineering



DECLARATION

I, the undersigned, declare that the work contained in this dissertation is my own original work and has not previously been submitted at any University for a degree

Signature: _____

Date: _____

SYNOPSIS

In regions of moderate seismicity it has been shown that a suitable structural system is created when designing the shear wall with a plastic hinge zone at the lower part of the wall, with the shear walls resisting lateral loads and all other structural elements designed to resist gravity loads. A suitably stiff foundation is required for the assumption of plastic hinge zones to hold true. This foundation should have limited rotation and should remain elastic when lateral loads are applied to the structure.

Ensuring a foundation with a greater capacity than the shear wall results in excessively large shear wall foundations being required in areas of moderate seismicity for buildings with no basement level.

This study aims to investigate the feasibility of reducing the size of shear wall foundations in areas of moderate seismicity for buildings with no basement level. The investigation is aimed at allowing shear wall foundation rocking and taking into account the contribution of structural frames to the lateral stiffness of the structure. An example building was chosen to investigate this possibility.

Firstly, lateral force-displacement capacities were determined for a shear wall and an internal reinforced concrete frame of this investigated building. Nonlinear moment-rotation behaviour was determined for the wall foundation size that would traditionally be required as well as for six other smaller foundations.

The above capacity curves against lateral loads were then used to compile a simplified model of the structural systems assumed to contribute to the lateral stiffness of the building. This simplified model therefore combined the effect of the shear wall, internal frame and wall foundation.

Nonlinear time-history analyses were performed on this simplified model to investigate the dynamic response of the structure with different wall foundation sizes. By assessing response results on a global and local scale, it was observed that significantly smaller shear wall foundations are possible when allowing foundation rocking and taking into account the contribution of other structural elements to the lateral stiffness of the building.

SAMEVATTING

Daar is reeds getoon dat 'n voldoende strukturele sisteem verkry word in gebiede van gematigde seismiese risiko indien 'n skuifmuur ontwerp word met 'n plastiese skarnier sone naby die ondersteuning van die muur. Skuifmure word dan ontwerp om weerstand te bied teen laterale kragte met alle ander strukturele elemente ontwerp om gravitasie kragte te weerstaan. Vir die aanname van plastiese skarnier sones om geldig te wees word 'n fondasie met voldoende styfheid benodig. Só 'n fondasie moet beperkte rotasie toelaat en moet elasties bly wanneer laterale kragte aan die struktuur aangewend word.

'n Fondasie met 'n groter kapasiteit as dié van die skuifmuur lei daartoe dat uitermate groot fondasies benodig word in gebiede van gematigde seismiese risiko vir geboue met geen kelder vlak.

Hierdie studie is daarop gemik om die moontlikheid van kleiner skuifmuur fondasies te ondersoek vir geboue met geen kelder vlak in gebiede van gematigde seismiese risiko. Die ondersoek het ten doel om skuifmuur fondasie wieg aksie toe te laat en die bydrae van strukturele rame tot die laterale styfheid van die struktuur in ag te neem.

Eerstens is die laterale krag-verplasing kapasiteit van 'n skuifmuur en 'n interne gewapende beton raam van die gekose gebou bepaal. Nie-lineêre moment-rotasie gedrag is bepaal vir die skuifmuur fondasie grootte wat tradisioneel benodig sou word asook vir ses ander kleiner fondasie grotes.

Die bogenoemde kapasiteit kurwes is gebruik om 'n vereenvoudigde model van die strukturele sisteme wat aanvaar word om laterale styfheid tot die gebou te verleen, op te stel. Hierdie vereenvoudigde model kombineer gevolglik die effek van die skuifmuur, interne raam en skuifmuur fondasie.

Nie-lineêre tydgeskiedenis analyses is uitgevoer op die vereenvoudigde model ten einde die dinamiese reaksie van die struktuur te ondersoek vir verskillende fondasie grotes. Resultate is beoordeel op 'n globale en lokale vlak. Daar is waargeneem dat aansienlik kleiner skuifmuur fondasies moontlik is deur wieg aksie van die fondasie toe te laat en die bydrae van ander strukturele elemente tot die laterale styfheid van die gebou in ag te neem.

ACKNOWLEDGEMENTS

I would like to thank the following people for their contribution:

- My heavenly Father without Whom nothing is possible.
- Professor J.A. Wium for his excellent technical knowledge and simplistic approach to complex problems.
- Doctor K. Beyer for her assistance in solving numerical modelling issues.
- My fellow postgraduate students at the department of Structural Engineering, Esteé, Christo and Talita for their friendship, support and brainstorm sessions.
- My family for their emotional support and prayers.

TABLE OF CONTENTS

DECLARATION	i
SYNOPSIS.....	ii
SAMEVATTING	iii
ACKNOWLEDGEMENTS	iv
LIST OF FIGURES	ix
LIST OF TABLES	xii
NOTATION.....	xiv
ACRONYMS.....	xix
TERMINOLOGY	xx
1 INTRODUCTION	21
1.1 Background.....	21
1.2 Aim of the study.....	22
1.3 Methodology of study	22
1.4 Overview of the document	24
2 LITERATURE REVIEW	26
2.1 Background.....	26
2.1.1 Causes of seismic activity	27
2.1.2 Natural versus mining induced seismic activity	28
2.1.3 Structural systems	30
2.1.4 Capacity design philosophy	31
2.2 Methods of seismic analysis	32
2.2.1 Overview of seismic analysis methods	33
2.2.2 Modal response spectrum method	34
2.2.3 Nonlinear static pushover analysis.....	35
2.2.4 Nonlinear adaptive pushover analysis	38
2.2.5 Nonlinear time-history analysis	38
2.2.6 Capacity spectrum method.....	44
2.3 Bilinear approximation of a capacity curve.....	45
2.4 Effective slab width models	49
2.5 Flat slab-column connections	53
2.6 Rigid foundation rocking.....	56

2.7	Confinement of concrete	62
3	DESCRIPTION OF STRUCTURE	66
3.1	Objectives.....	66
3.2	Building design	67
3.3	Material properties	72
3.3.1	Concrete material properties.....	73
3.3.2	Reinforcement steel material properties	76
3.4	Performance criteria	77
3.4.1	Internal force performance criteria	78
3.4.2	Material performance criteria	79
3.4.3	Element rotation performance criteria	80
4	NUMERICAL MODELLING	84
4.1	Objectives.....	84
4.2	Numerical analysis software.....	85
4.2.1	Nonlinearity and modelling assumptions.....	86
4.3	Input parameters.....	88
4.3.1	Material properties.....	88
4.3.2	Sections.....	92
4.3.3	Element classes.....	94
4.4	Element meshing	98
4.4.1	Elements per member length	98
4.4.2	Fibre element mesh.....	103
4.5	Verification of software.....	108
4.5.1	Slab element internal forces.....	108
4.5.2	Bending moment failure	111
4.5.3	Roof displacement	112
4.5.4	Strain calculation	113
4.6	Capacity curves	116
4.6.1	Internal frame.....	116
4.6.2	Shear wall	120
4.6.3	Edge frame.....	122
5	FOUNDATION BEHAVIOUR.....	126
5.1	Objectives.....	126
5.2	Foundation parameters.....	127
5.3	Conditions of foundation behaviour	131
5.4	Comparison of nonlinear behaviour.....	133
5.5	Verification of procedure to analyse foundation behaviour	135
5.6	Conversion of capacity curve	137

6	TIME-HISTORY DATA	141
6.1	Objectives.....	141
6.2	Selection of real ground motion	142
6.2.1	Elastic response spectrum	144
6.2.2	Final choice of ground motion data	145
6.3	Scaling of selected ground motion	146
7	NONLINEAR MODELLING OF COMBINED MODEL	149
7.1	Objectives.....	149
7.2	Choice of structural systems.....	150
7.2.1	Stiffness contribution.....	152
7.2.2	Elastic comparison.....	152
7.3	Component geometry	155
7.3.1	Wall foundation	155
7.3.2	Shear wall	155
7.3.3	Internal frame.....	156
7.3.4	Combined model.....	158
7.4	Nonlinear material response.....	159
7.4.1	Shear wall	160
7.4.2	Internal frame.....	164
7.4.3	Hysteretic response properties	169
7.5	Damping properties.....	170
7.5.1	Theoretical response	170
7.5.2	Shear wall material damping coefficient	171
7.5.3	Internal frame material damping coefficient.....	173
8	ANALYSES, RESULTS AND ASSESSMENT	175
8.1	Objectives.....	175
8.2	Nonlinear time-history analyses.....	176
8.2.1	Determining the appropriate time-step	176
8.2.2	<i>Nonlinear Transient Dynamic</i> procedure.....	179
8.2.3	Response quantities for result assessment	180
8.3	Local assessment of results	180
8.3.1	Internal frame.....	181
8.3.2	Foundations	184
8.3.3	Shear wall	186
8.4	Global assessment of results	190
8.4.1	Vision 2000 performance levels	190
8.4.2	Global capacity curve	192
8.4.3	Global assessment.....	195
9	SUMMARY, CONCLUSIONS AND RECOMMENDATIONS	198
9.1	Summary	198

9.2	Conclusions	198
9.2.1	Global performance	199
9.2.2	Internal frame performance	199
9.2.3	Foundation performance	199
9.2.4	Shear wall performance	200
9.2.5	Overall performance	200
9.3	Recommendations	201
	REFERENCES.....	203
	APPENDICES.....	210
A	CONFINEMENT CALCULATIONS	211
A.1	Ground to second floor columns	212
A.2	Second floor to roof columns	214
A.3	Shear wall.....	216
B	GROUND MOTION.....	218
B.1	Scaled response spectra.....	219
B.2	Scaled accelerograms	223

LIST OF FIGURES

FIGURE 1-1: INVESTIGATION METHODOLOGY	23
FIGURE 2-1: TECTONIC PLATES	27
FIGURE 2-2: FAULT MECHANISMS	28
FIGURE 2-3: SEISMIC ZONES OF SOUTH AFRICA [2].....	28
FIGURE 2-4: NOMINAL PEAK GROUND ACCELERATION FOR SOUTH AFRICA [4].....	29
FIGURE 2-5: STRUCTURAL RESPONSE TO SEISMIC ACTIVITY [2]	30
FIGURE 2-6: LATERAL FORCE DISTRIBUTION PATTERNS.....	36
FIGURE 2-7: BAD COMPARISON	41
FIGURE 2-8: GOOD COMPARISON	42
FIGURE 2-9: CAPACITY SPECTRUM METHOD [18].....	44
FIGURE 2-10: FEMA 440 FORCE-DISPLACEMENT IDEALIZATION [20].....	46
FIGURE 2-11: ATC-40 FORCE-DISPLACEMENT IDEALIZATION [22]	47
FIGURE 2-12: MOMENT-CURVATURE IDEALIZATION [2].....	48
FIGURE 2-13: EFFECTIVE SLAB WIDTH MODEL PROPOSED BY LUO AND DURRANI [26] [27]	50
FIGURE 2-14: EFFECTIVE SLAB WIDTH FOR STRENGTH (A) AND STIFFNESS (B) [23].....	52
FIGURE 2-15: ADDITION OR SUBTRACTION OF UNBALANCED BENDING MOMENT	54
FIGURE 2-16: SHEAR STRESSES AT A FLAT SLAB-COLUMN CONNECTION	54
FIGURE 2-17: MOMENT-DRIFT HYSTERESIS LOOP [32]	56
FIGURE 2-18: SCHEMATIC OF MOMENT-ROTATION RESPONSE STATES [35]	58
FIGURE 2-19: SDOF OSCILLATOR (REGULAR PENDULUM) VS ROCKING BLOCK (INVERTED PENDULUM) [19].....	59
FIGURE 2-20: SCHEMATIC OF A WINKLER SOIL MODEL [35].....	61
FIGURE 2-21: TWO SPRING-DAMPER WINKLER SOIL MODEL [39].....	62
FIGURE 2-22: CONFINED AND UNCONFINED CONCRETE STRESS-STRAIN BEHAVIOUR [5]	63
FIGURE 2-23: CONFINEMENT BY TRANSVERSE AND LONGITUDINAL REINFORCEMENT [5]	64
FIGURE 2-24: DETERMINATION OF CONFINED STRENGTH RATIO [5].....	64
FIGURE 3-1: CHAPTER THREE OBJECTIVES	66
FIGURE 3-2: PLAN LAYOUT.....	68
FIGURE 3-3: COLUMN REINFORCEMENT DETAILING.....	70
FIGURE 3-4: PLASTIC DETAILING OF SHEAR WALL	70
FIGURE 3-5: ELASTIC DETAILING OF SHEAR WALL	71
FIGURE 3-6: ASSUMPTION FOR THE DETERMINATION OF FLEXURAL RESISTANCE	78
FIGURE 3-7: FEMA 273 BUILDING PERFORMANCE LEVELS [49].....	81

FIGURE 4-1: CHAPTER FOUR OBJECTIVES	85
FIGURE 4-2: LOCAL DEGREES OF FREEDOM [9].....	86
FIGURE 4-3: ELEMENT INTERNAL FORCES [9].....	86
FIGURE 4-4: SEISMOSTRUCT ELEMENT MODELLING [9].....	87
FIGURE 4-5: CONFINED CONCRETE STRESS-STRAIN RELATIONSHIP	89
FIGURE 4-6: UNCONFINED CONCRETE STRESS-STRAIN RELATIONSHIP.....	91
FIGURE 4-7: SLAB REINFORCEMENT MODELLING	93
FIGURE 4-8: UNDEFORMED EDGE FRAME.....	95
FIGURE 4-9: DEFORMED EDGE FRAME	96
FIGURE 4-10: SEISMOSTRUCT EDGE FRAME MODEL	97
FIGURE 4-11: SLAB ELEMENT SECTION.....	98
FIGURE 4-12: ELEMENT MESHING PUSHOVER CURVES	101
FIGURE 4-13: SLAB AND COLUMN ELEMENT MESH.....	102
FIGURE 4-14: SHEAR WALL ELEMENT MESH	103
FIGURE 4-15: COLUMN FIBRE ELEMENT SENSITIVITY ANALYSIS.....	104
FIGURE 4-16: SLAB FIBRE ELEMENT SENSITIVITY ANALYSIS.....	105
FIGURE 4-17: SHEAR WALL SENSITIVITY ANALYSIS MODEL	106
FIGURE 4-18: SHEAR WALL FIBRE ELEMENT SENSITIVITY ANALYSIS – PLASTIC SECTION	107
FIGURE 4-19: SHEAR WALL FIBRE ELEMENT SENSITIVITY ANALYSIS – ELASTIC SECTION	107
FIGURE 4-20: CONTINUOUS BEAM MODEL	109
FIGURE 4-21: BENDING MOMENT RESULTS.....	110
FIGURE 4-22: SHEAR FORCE RESULTS	110
FIGURE 4-23: THREE STOREY FRAME MODEL	112
FIGURE 4-24: SABS 0100-1 BENDING ASSUMPTION	115
FIGURE 4-25: INTERNAL FRAME	117
FIGURE 4-26: INTERNAL FRAME, TRIANGULAR FORCE DISTRIBUTION.....	118
FIGURE 4-27: INTERNAL FRAME, UNIFORM FORCE DISTRIBUTION	118
FIGURE 4-28: INTERNAL FRAME COMPARISON	119
FIGURE 4-29: CONTRIBUTING SLAB AREA TO SHEAR WALL	120
FIGURE 4-30: SHEAR WALL, TRIANGULAR FORCE DISTRIBUTION.....	121
FIGURE 4-31: SHEAR WALL, UNIFORM FORCE DISTRIBUTION	121
FIGURE 4-32: SHEAR WALL COMPARISON	122
FIGURE 4-33: EDGE FRAME, TRIANGULAR FORCE DISTRIBUTION.....	123
FIGURE 4-34: EDGE FRAME, UNIFORM FORCE DISTRIBUTION	124
FIGURE 4-35: EDGE FRAME COMPARISON	124
FIGURE 5-1: CHAPTER FIVE OBJECTIVES	127
FIGURE 5-2: FOUNDATION UPLIFT PRIOR TO YIELDING OF SOIL	130
FIGURE 5-3: SOIL YIELDING PRIOR TO FOUNDATION UPLIFT	130

FIGURE 5-4: RIGID FOUNDATION ROCKING RESPONSE.....	133
FIGURE 5-5: FOUNDATION CAPACITY CURVES	134
FIGURE 5-6: MOMENT-ROTATION VALIDATION CURVES	136
FIGURE 5-7: MOMENT-ROTATION AND BASE SHEAR-ROOF DISPLACEMENT RELATIONSHIP	138
FIGURE 6-1: CHAPTER SIX OBJECTIVES.....	141
FIGURE 6-2: ELASTIC RESPONSE SPECTRUM	145
FIGURE 6-3: SCALING OF GROUND MOTION DATA SET NUMBER TWO	147
FIGURE 7-1: CHAPTER SEVEN OBJECTIVES	149
FIGURE 7-2: LATERAL STIFFNESS COMBINATION OF SYSTEMS	151
FIGURE 7-3: EDGE FRAME + 100% FOOTING ELASTIC COMPARISON.....	153
FIGURE 7-4: EDGE FRAME + 40% FOOTING ELASTIC COMPARISON.....	154
FIGURE 7-5: SHEAR WALL MODEL CONCEPT (SCHEMATIC)	156
FIGURE 7-6: DISPLACED INTERNAL FRAME	157
FIGURE 7-7: INTERNAL FRAME MODEL CONCEPT (SCHEMATIC)	158
FIGURE 7-8: COMBINED MODEL CONCEPT (SCHEMATIC).....	159
FIGURE 7-9: DETERMINING ULTIMATE CURVATURE	163
FIGURE 7-10: SHEAR WALL MOMENT-CURVATURE MATERIAL RESPONSE	164
FIGURE 7-11: BENDING MOMENT DIAGRAM: INTERNAL FRAME MODEL	167
FIGURE 7-12: INTERNAL FRAME MOMENT-CURVATURE MATERIAL RESPONSE	168
FIGURE 7-13: RESPONSE OF A 5% DAMPED SYSTEM TO A SINUSOIDAL FORCE AT RESONANCE FREQUENCY	171
FIGURE 7-14: SHEAR WALL HARMONIC RESPONSE.....	173
FIGURE 7-15: INTERNAL FRAME HARMONIC RESPONSE.....	174
FIGURE 8-1: CHAPTER EIGHT OBJECTIVES	175
FIGURE 8-2: COMPARISON OF LATERAL ROOF DISPLACEMENT – ATH01	177
FIGURE 8-3: ATH04 REGION OF MAXIMUM GROUND ACCELERATION	178
FIGURE 8-4: COMPARISON OF LATERAL ROOF DISPLACEMENT – ATH04	179
FIGURE 8-5: GRAPHICAL REPRESENTATION OF MAXIMUM DISPLACEMENT RESPONSE	182
FIGURE 8-6: LATERAL DISPLACEMENT RESPONSE	183
FIGURE 8-7: FOOTING ROTATION RESPONSE.....	186
FIGURE 8-8: RELATIVE SHEAR WALL DISPLACEMENT	187
FIGURE 8-9: RELATIVE SHEAR WALL LATERAL ROOF DISPLACEMENT RESPONSE.....	189
FIGURE 8-10: SPRING ANALOGY FOR GLOBAL STIFFNESS	192
FIGURE 8-11: GLOBAL CAPACITY CURVE OF MODEL WITH FOUNDATION OF FULL OVERSTRENGTH MOMENT	194
FIGURE 8-12: COMPARISON OF BILINEAR GLOBAL CAPACITY CURVES	195
FIGURE 8-13: LATERAL ROOF DISPLACEMENT RESPONSE.....	196

LIST OF TABLES

TABLE 2-1: METHODS OF SEISMIC ANALYSIS	33
TABLE 3-1: GRID A SLAB REINFORCEMENT	69
TABLE 3-2: GRID B SLAB REINFORCEMENT	69
TABLE 3-3: WALL FOUNDATION DIMENSIONS	72
TABLE 3-4: SLAB BENDING MOMENT RESISTANCES	78
TABLE 3-5: SLAB-COLUMN PUNCHING SHEAR RESISTANCE.....	79
TABLE 3-6: FEMA 273 COLUMN PLASTIC HINGE ROTATION LIMITS [49]	82
TABLE 3-7: FEMA 273 SLAB-COLUMN PLASTIC HINGE ROTATION LIMITS [49].....	82
TABLE 3-8: FEMA 273 SHEAR WALL PLASTIC HINGE ROTATION LIMITS [49].....	83
TABLE 4-1: REINFORCEMENT STEEL MATERIAL PROPERTIES	89
TABLE 4-2: CONFINED CONCRETE MATERIAL PROPERTIES	90
TABLE 4-3: SECTION TYPES [9].....	93
TABLE 4-4: SENSITIVITY ANALYSIS MODELS	100
TABLE 4-5: CRITICAL INTERNAL FORCES – FIRST FLOOR SLAB	111
TABLE 4-6: INTERNAL FRAME STRAIN INVESTIGATION.....	116
TABLE 4-7: INTERNAL FRAME CAPACITY CURVE	119
TABLE 4-8: SHEAR WALL CAPACITY CURVE	122
TABLE 4-9: EDGE FRAME CAPACITY CURVE	125
TABLE 5-1: INVESTIGATED WALL FOUNDATION DIMENSIONS	133
TABLE 5-2: ULTIMATE MOMENT CAPACITIES	134
TABLE 5-3: FOUNDATION COMPARISON	135
TABLE 5-4: FOUNDATION PERFORMANCE POINT	136
TABLE 6-1: INITIAL SET OF 20 GROUND MOTION DATA [13].....	143
TABLE 6-2: SHEAR WALL NATURAL VIBRATION PERIODS	146
TABLE 6-3: GROUND MOTION SCALING FACTORS	148
TABLE 6-4: GROUND MOTION PGA	148
TABLE 7-1: ELASTIC STIFFNESS.....	153
TABLE 7-2: COMBINED ELASTIC STIFFNESS	154
TABLE 7-3: BILINEAR APPROXIMATION OF SHEAR WALL CAPACITY	160
TABLE 7-4: LATERAL FORCE DISTRIBUTION – SHEAR WALL.....	161
TABLE 7-5: BILINEAR APPROXIMATION OF INTERNAL FRAME CAPACITY	165
TABLE 7-6: LATERAL FORCE DISTRIBUTION – INTERNAL FRAME.....	166
TABLE 8-1: TIME-STEP INVESTIGATION RESULTS – ATH01	177
TABLE 8-2: TIME-STEP INVESTIGATION RESULTS – ATH04.....	178
TABLE 8-3: LATERAL ROOF DISPLACEMENT RESPONSE [MM].....	182
TABLE 8-4: FOOTING ROTATION ASSOCIATED WITH SOIL YIELDING	185

TABLE 8-5: FOOTING ROTATION RESPONSE [RADIANS]	185
TABLE 8-6: RELATIVE SHEAR WALL ROOF DISPLACEMENT [MM].....	188
TABLE 8-7: GLOBAL ASSESSMENT OF FOUNDATION SIZES (MAXIMUM RESPONSE).....	197

NOTATION

CAPITAL LETTERS

A	Area
A_c	Concrete area of critical perimeter and columns
A_s	Area of tensile reinforcement
A'_s	Area of compression reinforcement
B	Foundation width
D	Foundation depth
E	Modulus of elasticity
E_s	Static stress-strain modulus
E'_s	Plane strain modulus
F	Force
I	Moment of inertia
I_S	Steinbrenner influence factor
J_c	Polar moment of inertia of critical perimeter section around a column
K	Confinement ratio
K_e	Effective lateral stiffness
K_t	Torsional stiffness
L	Foundation length
M	Bending moment
M_b	Base bending moment
M_m	Maximum bending moment
M_n	Nominal yield bending moment
M_{qL}	Normalized nondimensional bending moment
M_R	Bending moment resistance
M_{Rd}^+	Overstrength bending moment
$M_{R,ultimate}$	Ultimate foundation bending moment resistance

M_u	Ultimate bending moment
M_y	Yield bending moment
M'_y	First yield bending moment
N_d	Overstrength normal force
P	Normal load
R^*	Closest Distance to Fault Rupture
S_a	Spectral acceleration
S_d	Spectral displacement
S_{pa}	Pseudo acceleration
T	Vibration period
T_n	n^{th} natural vibration period
V_b	Base shear force
V_d	Design base shear force
V_d^+	Overstrength base shear force
V_g	Shear force due to gravity loads
V_R	Shear resistance
V_y	Yield base shear

LOWER-CASE LETTERS

a_g	Peak ground acceleration
$a_{g,d}$	Design peak ground acceleration
c	Viscous damping
d	Effective depth to tensile reinforcement
$d_{r,i-j}$	Drift ratio between storeys i and j
f_1	Fundamental frequency measured in Hz
f'_c	Unconfined concrete compressive strength
f'_{cc}	Confined concrete compressive strength
$f_{c,d}$	Design concrete cube compressive strength

$f_{c,mean}$	Mean concrete cube compressive strength
$f_{c,mean,cyl}$	Mean concrete cylinder compressive strength
f_{cu}	Design concrete compressive strength
f'_ℓ	Effective confining stress of concrete
f_y	Yield strength
$f_{y,d}$	Design yield strength of steel
$f_{y,eff}$	Effective yield strength
$f_{y,h}$	Yield strength of transverse reinforcement
$f_{y,mean}$	Mean yield strength of steel
g	Gravitational acceleration
h	Height
k	Stiffness
k_s	Modulus of subgrade reaction
ℓ	Length
ℓ_w	Shear wall web length
m	Mass
q	Behaviour factor (response factor) / Soil pressure
q_u	Soil bearing capacity
t	Time
t_w	Shear wall web thickness
$u(t)$	Relative lateral displacement
$(u_{st})_0$	Maximum value of static displacement
v_c	Shear resistance of concrete
v_R	Total shear resistance
v_s	Resistance of shear reinforcement
x	Dimension parameter
z	Internal lever arm of a reinforced concrete section

GREEK CAPITAL LETTERS

Γ_n	n^{th} modal participation factor
Δ	Global (roof) displacement
Δ_d	Design roof displacement
Δ_p	Plastic displacement
Δ_{rel}	Relative roof displacement
Δ_u	Ultimate global (roof) displacement
Δ_y	Global yield (roof) displacement
X	Reduction factor for slab width

GREEK LOWER-CASE LETTERS

α_e	Exterior effective slab width factor
α_i	Interior effective slab width factor
γ	Specific weight
γ_c	Specific weight of reinforced concrete
γ_m	Partial material safety factor
γ_s	Partial material safety factor for steel / specific weight of steel
δ	Displacement
ϵ_{cc}	Concrete strain at peak stress
ϵ_{cu}	Ultimate concrete compressive strain
ϵ_s	Steel material strain
ϵ_{sm}	Steel material strain at maximum tensile stress
ϵ_{su}	Steel material fracture strain
ϵ_u	Ultimate steel material strain
ϵ_y	Yield strain
η	Correction factor
θ	Rotation
μ	Ductility / Poisson's ratio for soil / Strain hardening parameter / Mean value

μ_{Δ}	Displacement ductility
ν	Poisson's ratio
ξ	Damping ratio (percentage of critical damping)
ξ_n^*	Modal damping ratio of the n^{th} mode
ρ	Density
ρ_s	Transverse reinforcement ratio
σ	Normal stress / Standard deviation
σ_y	Yield stress
ϕ	Curvature
ϕ_i	Component of i^{th} mode shape
$\{\phi_i\}$	i^{th} mode shape
$\{\phi_n\}$	n^{th} eigenvector
ϕ_u	Ultimate curvature
ϕ_y	Yield curvature
ϕ_y'	First yield curvature
ϕ	Internal soil friction angle
ω_1	Fundamental natural circular frequency
ω_D	Damped circular natural frequency
ω_n	n^{th} natural circular frequency

ACRONYMS

ADRS	Acceleration-Displacement Response Spectra
ATH	Acceleration Time-History
CP	Collapse Prevention Performance Level
CQC	Complete Quadratic Combination Rule
DL	Permanent Loads
EL	Earthquake Loads
FEMA	Federal Emergency Management Agency
IO	Immediate Occupancy Performance Level
LC	Load Combination
LFRS	Lateral Force Resisting System
LL	Imposed Loads
LS	Life Safety Performance Level
MDOF	Multi Degrees of Freedom
NEHRP	National Earthquake Hazard Reduction Program
NLTHA	Nonlinear Time-History Analysis
PEER	Pacific Earthquake Engineering Research Centre
PGA	Peak Ground Acceleration
SDOF	Single Degree of Freedom
SLS	Serviceability Limit State
SRSS	Square Root of Sum of Squares Combination Rule
STD DEV	Standard deviation
ULS	Ultimate Limit State

TERMINOLOGY

Accelerogram	Ground acceleration recorded by strong-motion accelerographs.
Campbell's GEOCODE	Symbol to describe different soil types
Classical damping	Diagonal damping matrix resulting in uncoupled differential equations in modal coordinates.
Critical damping	The smallest damping coefficient that inhibits oscillation completely.
Ductility	The ability of structural members to deform inelastically.
Equal displacement approximation	Equal displacement of elastic and inelastic capacity curves.
Equal energy approximation	Equal area under the elastic and inelastic capacity curves resulting in the same energy of the systems.
Mode shape	The expected displacement shape of a natural mode of vibration.
Overstrength	Ratio of effective (mean) strength to the design strength of an element.
Participation factor	The contribution of a natural vibration mode to the dynamic response of a system.
Response spectrum	A plot of the maxima of the acceleration response of SDOF systems with various natural periods when subjected to an earthquake ground motion.
Soft storey	A column sway-mechanism developing in the lower storey in a building.
Winkler soil model	Foundation model when foundation flexural rigidity is taken into account modelling the foundation as a beam on an elastic foundation.
100% foundation	Foundation size required to resist the full shear wall overstrength bending moment

Chapter 1

1 INTRODUCTION

1.1 Background

Reinforced concrete structures consisting of flat slabs, columns and shear walls are common structural systems in many parts of the world. These structures are usually designed with the shear walls resisting all lateral forces which can be either wind or seismic loads. The flat slabs and columns are designed to resist only gravity loads.

In regions of moderate seismicity it has been shown that a suitable structural system is created when designing the shear wall with a plastic hinge zone at the lower part of the wall with the shear walls resisting lateral loads and all other structural elements designed to resist gravity loads. The behaviour of the columns and flat slabs then needs to be verified against lateral drift criteria and the possibility of punching shear failures in flat slabs at slab-column connections.

For the assumption of plastic hinge zones at the bottom of shear walls to hold true a suitably stiff foundation is required. This foundation should have limited rotation and should remain linear elastic when lateral loads are applied to the structure. Buildings with at least one basement level may provide such a sufficiently stiff foundation to a shear wall.

If a building has no basement level, the stiff support to the shear wall will have to be provided by the foundation. Shear walls designed to resist seismic loads lead to significantly larger foundations than with wind loading as the dominant lateral load condition depending on the height of the building and the number of shear walls in the building.

Traditionally the wall foundation is designed to have a greater capacity than the shear wall to ensure that damage does not occur in the footing where damage is difficult to assess and repair.

The result is that excessively large shear wall foundations are required even in areas of only moderate seismicity.

1.2 Aim of the study

This study aims to investigate the possibility of reducing the size of shear wall foundations in areas of moderate seismicity for buildings with no basement level. The investigation is aimed at allowing shear wall foundation rocking and taking into account the contribution of structural frames, consisting of columns and flat slab, to the lateral stiffness of the structure.

The shear wall, rocking wall foundation and the structural frame will therefore work together to resist the seismic loading on the building with the main mechanism being the rocking motion of the wall foundation. Such a reduction in shear wall foundation can potentially lead to a significant reduction in cost.

1.3 Methodology of study

The methodology of this study is set out graphically in Figure 1-1.

For the purpose of the investigation an example building was set up and was used for all comparative analyses. The example building is a flat slab structure with shear walls resisting lateral forces and no basement level. Based on a conventional design approach, all required reinforcement was calculated as well as the required size of the wall foundation.

The capacity of structural elements could be calculated taking into account the amount of reinforcement, dimensions of the elements, as well as the material properties. Failure criteria, in terms of structural capacity and material response, were defined for the numerical model.

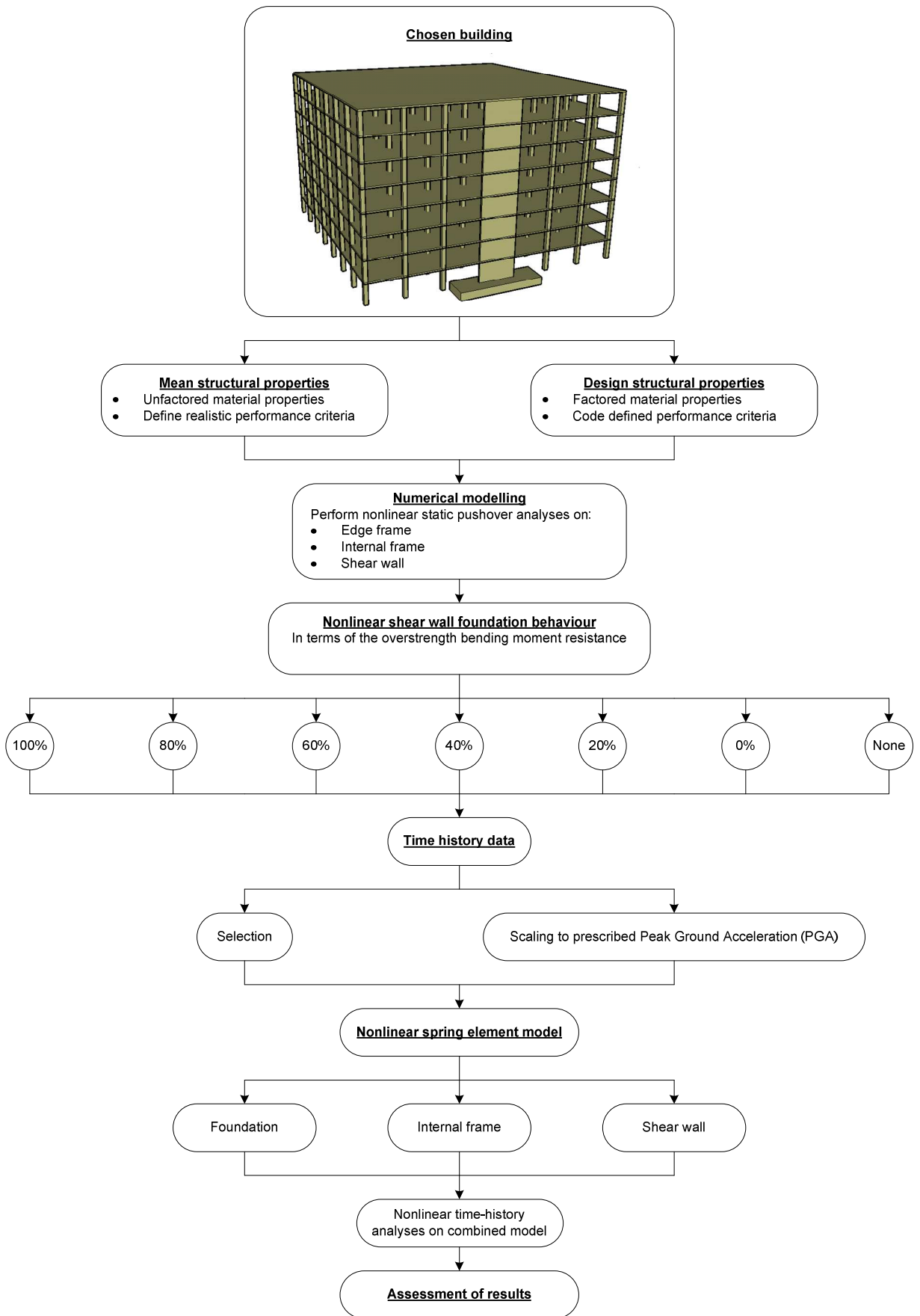


Figure 1-1: Investigation methodology

First, nonlinear static pushover analyses were performed on structural systems to determine their lateral force-displacement behaviour. These analyses were performed on structural systems assumed to contribute to the lateral stiffness of the building, being:

- A wall foundation.
- An internal frame consisting of slab and column elements.
- Either a shear wall or an edge frame consisting of a shear wall and the slab and column elements in the plane of the shear wall.

Furthermore, the nonlinear behaviour of the wall foundation was determined taking uplifting of the foundation and yielding of the underlying soil into account. For the purpose of the investigation foundation sizes were chosen, dimensioned with 0%, 20%, 40%, 60%, 80% and 100% of the shear wall overstrength bending moment applied to the foundation. Even the foundation size obtained by applying no bending moment will provide a nominal amount of bending moment resistance. It was therefore decided to investigate a seventh wall foundation support where no bending moment resistance is provided, therefore providing a pinned support to the shear wall.

Finally the three systems contributing to the structural system of the building were incorporated into a simplified finite element model. The nonlinear behaviour of the systems was modelled and several time-history analyses were performed on the system. Results from these analyses were then compared to limiting criteria.

1.4 Overview of the document

The literature review investigating previous research and publications on topics of relevance to this investigation is presented in chapter two. Important concepts that must be understood for this investigation are also presented in this chapter.

Chapter three discusses the example building that was used for all comparative analyses. This includes determining actual and design material properties as well as determining performance criteria for the various structural members.

Chapter four present the numerical modelling used to determine the nonlinear stiffness of the various superstructure systems. The software that was used to perform the nonlinear static pushover analyses is also discussed. This chapter also explains modelling assumptions that were made and shows the resulting capacity curves.

The procedure followed to determine the nonlinear response of the various foundation sizes, is set out in chapter five. Soil and foundation properties that influence the response of the foundations are also described in this chapter.

Seven ground motions were used to perform nonlinear time-history analyses. The procedure of selecting appropriate ground motions and scaling them to the relevant site and structure properties, are discussed in chapter six.

Chapter seven presents the nonlinear modelling of the combination of the various structural systems. Simplified models were used to represent these systems and the procedure followed to model the nonlinear lateral stiffness of the components is discussed.

Results from the nonlinear time-history analyses are provided in chapter eight and the assessment of the results on a local and global level are discussed.

Finally, conclusions and recommendations are made in chapter nine. This includes conclusions drawn from the assessment of the response quantities as well as recommendations for possible further research.

Chapter 2

2 LITERATURE REVIEW

This chapter presents a literature review of the following topics:

- A background into the causes of seismic activity as well as basic seismic design philosophy.
- Important concepts of seismic design.
- Methods of seismic analysis with a detailed discussion of the analysis methods used in this study.
- Different proposed methods for the bilinear approximation of capacity curves.
- The various effective slab width models proposed by different researchers.
- The effect of lateral loading on flat slab-column connections.
- Previous research regarding rigid foundation rocking.
- Material properties of confined concrete.

2.1 Background

A short discussion is provided into the causes and effects of earthquakes as general background to the philosophy of seismic engineering. An understanding of structural systems that can be used to resist the effect of earthquakes as well as the basic design philosophy are crucial in deciding on structural systems that contribute to the lateral stiffness of building structures.

2.1.1 Causes of seismic activity

Seismic activity can be divided into natural seismic activity and artificial seismic activity. Natural seismic activity can be caused by the relative movement of tectonic plates, volcanic activity and the collapse of natural underground cavities. Artificial seismic activity can be caused by blasting due to mining activity as well as nuclear blasting.

According to Tarbuck and Lutgens *an earthquake is the vibration of earth produced by the rapid release of energy* [1]. Most often natural seismic activity is caused by the relative movement between tectonic plates on the earth's crust. The earth is divided into roughly fifteen tectonic plates that can move relative to each other along what is called fault boundaries. Figure 2-1 shows these tectonic plates.

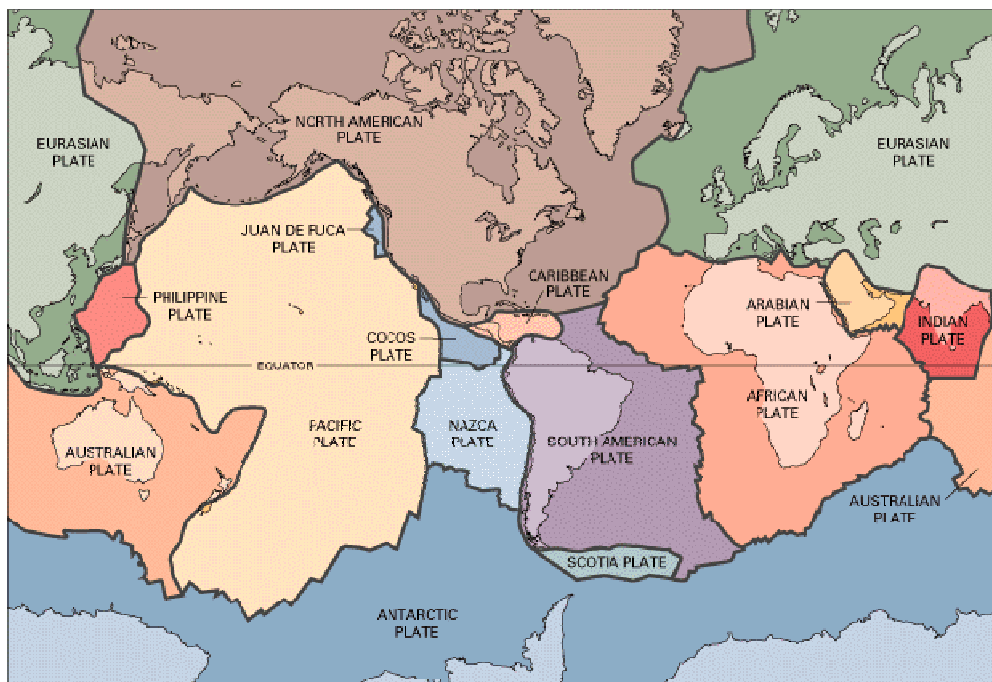


Figure 2-1: Tectonic plates

These tectonic plates move relative to each other in four ways causing shockwaves to travel through the crust of the earth. Figure 2-2 shows these four different relative movements [2].

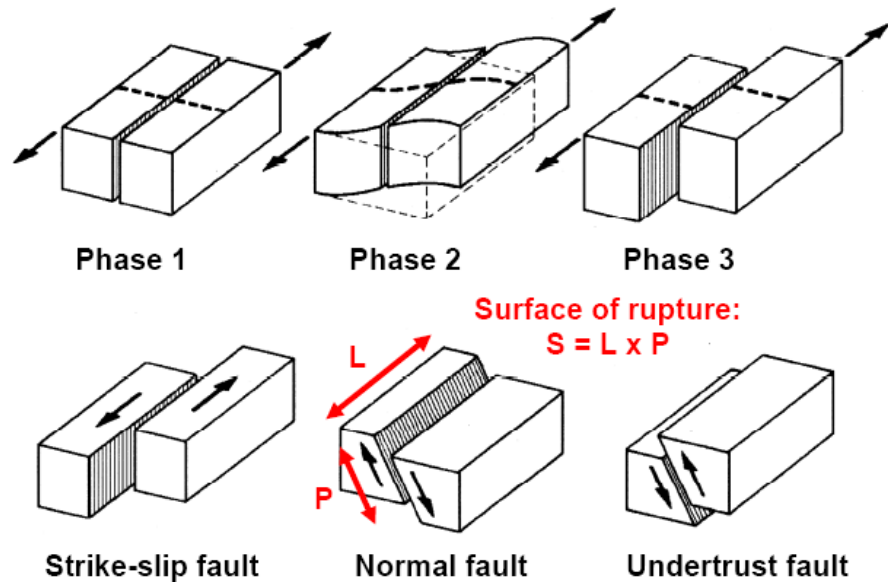


Figure 2-2: Fault mechanisms

2.1.2 Natural versus mining induced seismic activity

Regions of seismic risk in South Africa are divided into two types of zones. Zone I refers to regions of low natural seismic activity, whilst zone II refers to regions of mining-inducing seismic activity. Figure 2-3 shows these regions [3].

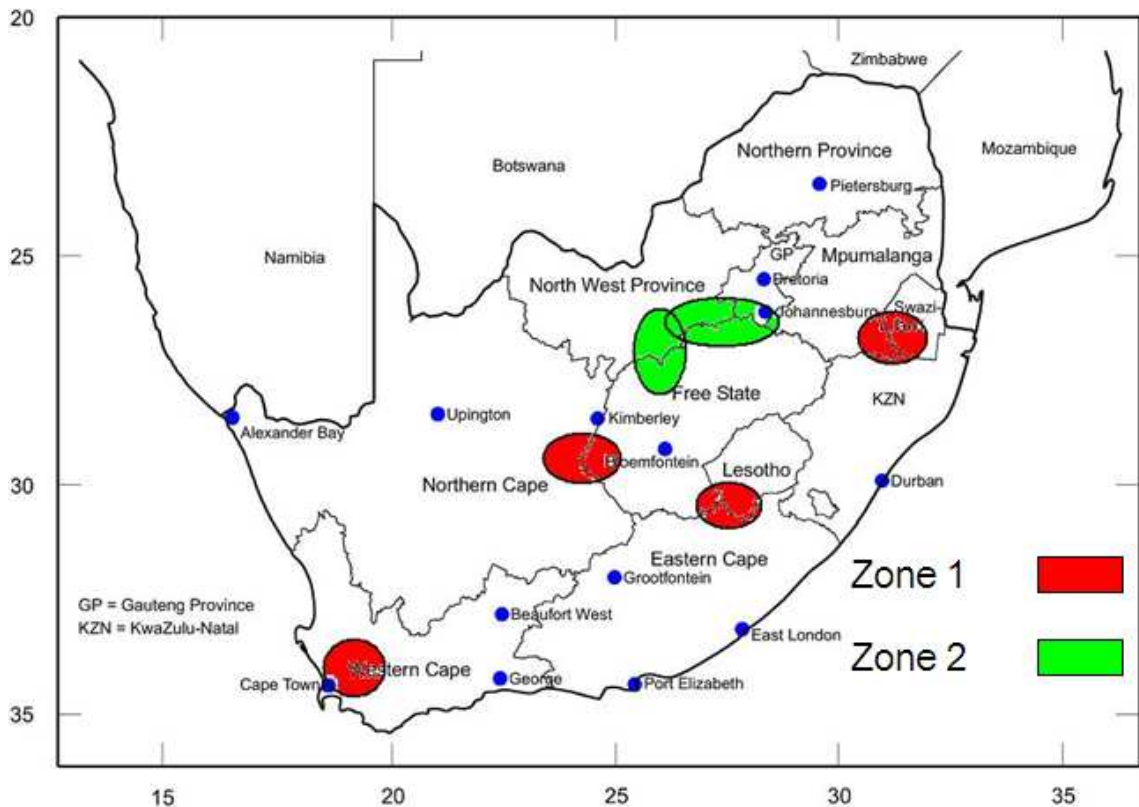


Figure 2-3: Seismic zones of South Africa [2]

In 2003 the Council for Geoscience released a contour map of nominal peak ground acceleration (PGA) for a 10% probability of occurrence in 50 years and is shown in Figure 2-4 [4].

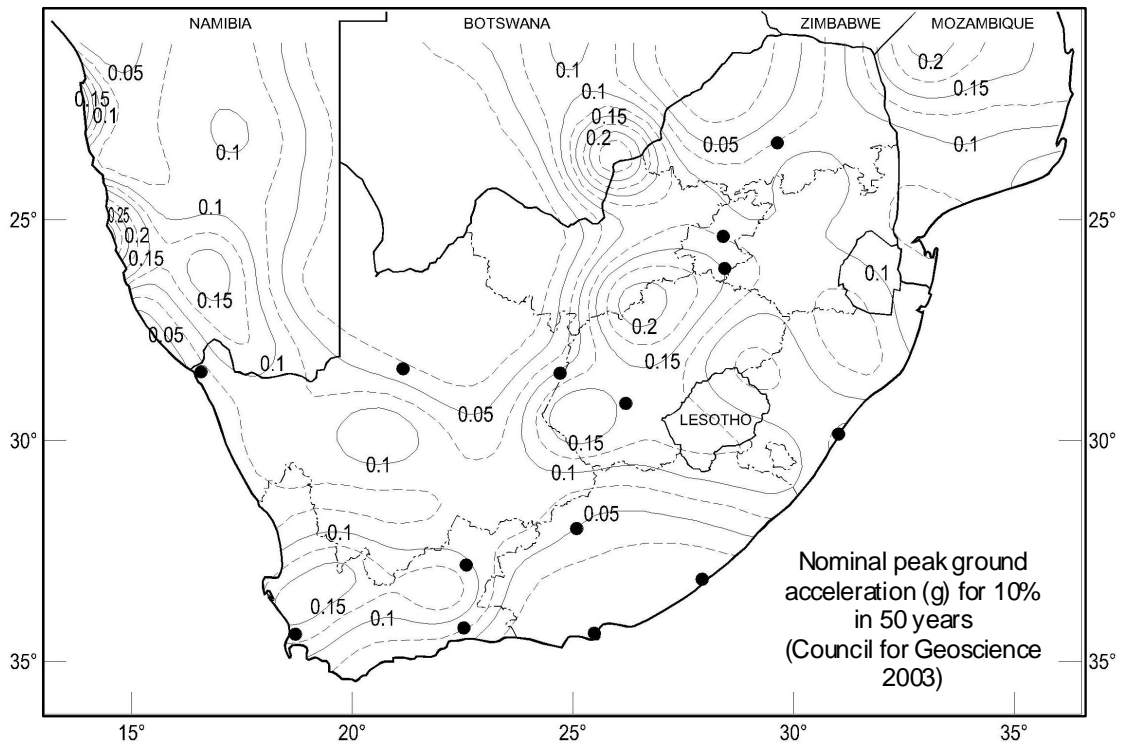


Figure 2-4: Nominal peak ground acceleration for South Africa [4]

From the above two figures it is clear that 'n larger peak ground acceleration is expected in zones of mining-inducing seismic activity than for zones of moderate natural seismic activity. The effect of natural seismic activity and mining induced seismic activity differs and as a result the structural response of buildings to the two different sources of seismic activity also differs.

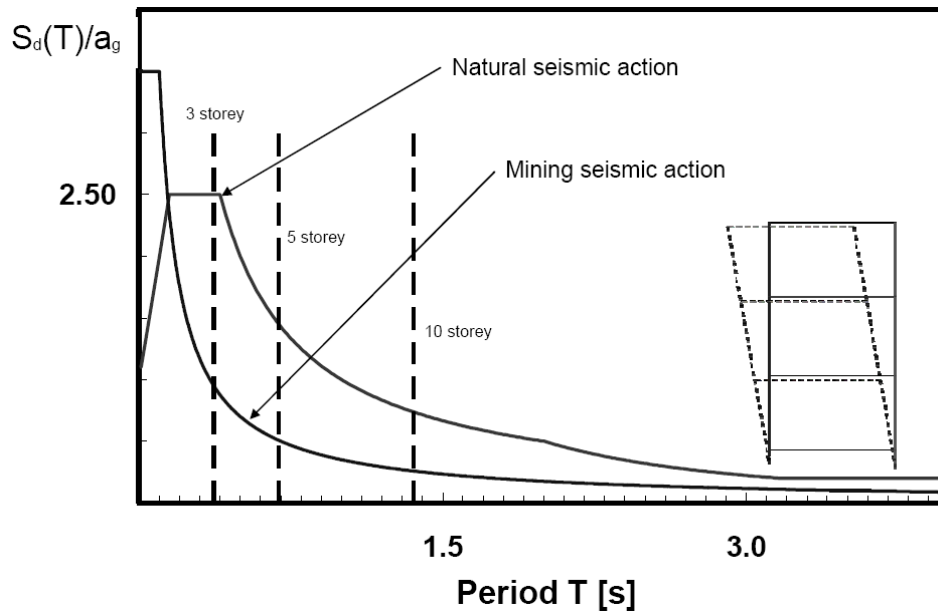


Figure 2-5: Structural response to seismic activity [2]

As can be seen from Figure 2-5 the normalized spectral displacement for mining induced seismic activity has a peak value at a low natural vibration period. The peak value of spectral displacement for natural seismic activity occurs at higher natural vibration periods. Increasing building height leads to an increasing value for the natural vibration period of a building and therefore it can be stated that mining induced seismic activity only significantly affect low rise building structures. Natural seismic activity will therefore have a more severe effect on medium to high-rise buildings [2].

2.1.3 Structural systems

All structural elements in a building are designed to support gravity loads. Buildings may however also be loaded laterally due to the effect of wind and earthquakes. The significance of the effect of these lateral forces increases with increasing building height. Lateral loading according to seismic criteria are usually more severe than the effect of wind loads for reinforced concrete buildings. For this reason it is important that structural systems be identified that will provide lateral stiffness and strength to the building structure.

Various different structural systems exist to ensure the seismic resistance of a building. These systems are discussed in the following paragraphs.

Single or coupled shear walls

These structural systems rely on reinforced concrete shear walls to provide lateral resistance to the building. Shear walls are also commonly known as structural walls, since the flexural behaviour of these walls are more important than their shear behaviour. Lateral forces usually govern the design of shear walls and therefore gravity load effects on these walls are seldom significant. Other structural elements in the building are assigned to carry gravity loads and the contribution of these elements (such as flat slabs, columns and beams) to the lateral stiffness of the building is usually neglected [5] [2].

Moment resisting frames

Multistorey reinforced concrete buildings often consist of frames with columns, floor slabs and beams. The connections between these elements are often referred to as rigid joints when designed to transfer bending moments. These frames are designed to carry gravity loads whilst also providing lateral stiffness to the building in any direction [5].

Dual systems

Dual building systems consist of reinforced shear walls and moment resisting frames that interact to provide lateral stiffness to the building as one system. Each structural element is also designed to carry its own share of gravity load. These systems are also termed hybrid or wall-frame structures [5].

These systems combine the stiffness, strength and cost effectiveness of shear walls with the large deformation capacity and ductility of moment resisting frames, which can provide lateral stiffness in case of shear wall failure. Beams, floor slabs and columns are used to carry most of the gravity load, whilst the capacity of the columns is utilized to resist the lateral forces in both horizontal directions [7].

2.1.4 Capacity design philosophy

Ensuring ductile behaviour in structures requires that yield capacity is reached first in ductile structural elements rather than in brittle ones. Capacity design ensures that brittle elements are designed to be strong enough to ensure that failure occurs in the ductile elements [6].

These failures are closely linked to energy dissipation within the structure. In the capacity design of structures, specific elements of the primary lateral force resisting system are chosen and designed and detailed for energy dissipation under severe imposed deformations. The critical regions of these elements, termed plastic hinges, are detailed to ensure inelastic flexural behaviour with sufficient resistance to avoid shear failure. All other structural elements are provided with strength greater than that corresponding to development of maximum feasible strength in the potential hinge regions to avoid failure of these elements [5].

It is therefore necessary for brittle elements to be strong enough to withstand the forces induced by yielding of the ductile members, allowing a suitable margin to give a high level of confidence that the brittle elements will not reach their failure loads. Brittle elements should therefore be stronger than the actual strength of the plastic regions. This strength almost always exceeds the minimum code requirement due to the rounding up of member dimensions or reinforcement bar diameters as well as partial safety factors for materials [6].

Refer to [5] for a description of capacity design.

2.2 Methods of seismic analysis

Various methods exist for the seismic design and analysis of buildings. These methods can be divided into force-based and displacement-based methods.

Seismic design of structures has traditionally been based on the inertia forces that are caused by earthquakes. One of the main reasons for this design choice is that other actions such as dead and live loads are considered in this manner. Structural elements are therefore safe if their capacity exceeds the applied loads.

Displacement-based seismic design of structures is not yet codified and hence, not used in this study.

2.2.1 Overview of seismic analysis methods

Table 2-1 gives a summary of the different available methods of force-based design and analysis in the order of increasing complexity [2].

Table 2-1: Methods of seismic analysis

	Equivalent lateral force method	Response spectrum method	Nonlinear static analysis	Nonlinear time-history analysis
Dynamic model	Linear SDOF system	Linear MDOF system	Nonlinear SDOF system	Nonlinear MDOF system
Geometric model	2D	2D or 3D	2D	2D or 3D
Material model	Linear	Linear	Nonlinear	Nonlinear
Damping model	Viscous	Viscous	Viscous	Viscous and hysteretic
Modes of vibration considered	Fundamental mode only	All modes	Fundamental mode only	-
Consideration of torsion	Amplification factor	Linear	Amplification factor	Nonlinear
Consideration of material nonlinearities	q-factor	q-factor	Nonlinear material model	Nonlinear material model
Seismic action	Design spectrum	Design spectrum	Design spectrum	Time-history
Output	Sectional forces and deformations	Sectional forces and deformations	Local duct. demand, sectional forces and deformation	Local duct. demand, sectional forces and deformation
Applicability	Regular buildings only	All buildings	Regular buildings only	All buildings

Typical application	Design	Design	Assessment of existing buildings	Assessment of new and existing buildings
Effort	Low	Moderate	Moderate	Large

Methods of analysis that were used in this study are discussed in detail in the following sections.

2.2.2 Modal response spectrum method

The response spectrum method can be implemented if only the maximum response of a structure to an entire time-history is of interest. According to Booth and Key [6] this method involves calculating the principal elastic modes of vibration of a structure and then calculating the maximum responses in each mode from a response spectrum.

As first step in the response spectrum method the modal quantities of the structure should be determined. Resulting from an eigenvalue analysis are the natural circular frequencies (ω_n), natural periods of vibration (T_n), the natural mode shapes ($\{\varphi_n\}$), as well as the modal participation factors (Γ_n).

In order to implement the modal response spectrum method it is required to compute the response spectrum that applies to the desired level of seismic excitation. Values for the spectral displacement and spectral acceleration that corresponds to the calculated natural frequencies can be determined using this response spectrum.

It is important to note that the maximum displacement vector for different modes does not occur at the same instant and for this reason it is impossible to calculate the maximum response exactly. A detailed discussion of methods to determine an estimate of the total maximum response from the maximum modal responses can be found in [8].

Number of modes to consider

Eurocode 8 [7] prescribes that enough modes of vibration should be taken into account that will result in a cumulative effective modal mass of 90% of the total mass of the structure in the direction of the desired response. In other words, N modes should be taken into account that will result in a cumulative modal participation factor of 0.9.

2.2.3 Nonlinear static pushover analysis

Pushover analyses are frequently utilised to estimate the horizontal capacity of structural systems. The conventional static pushover analysis is applicable in situations where the dynamic response of a structure is not significantly affected by the levels of deformation caused by the seismic action [9]. For this type of analysis the pattern of horizontal loading can be assumed to be constant. This analysis method was used to determine the lateral force-displacement behaviour of the superstructure systems that were investigated.

According to Krawinkler and Seneviratna [10] the static pushover analysis is becoming a popular tool for the evaluation of the seismic performance of both existing and new structures. They also stated that the purpose of the static pushover analysis is to evaluate the performance that can be expected from a structural system by first estimating its strength and deformation demands in design earthquakes by means of a static inelastic analysis and then comparing these demands to the capacities of the structure. This analysis can provide information on the following:

- Force demands on brittle elements in the structural system such as shear forces at beam-column connections.
- Estimation of deformation demands for elements that are required to undergo inelastic deformation in order to dissipate energy.
- Influence of strength deterioration of individual elements on the behaviour of the structural system.
- Identification of critical regions with regard to deformation demands that will have to be taken into account when detailing the structure.
- Estimation of interstorey drift.

Typically structural systems such as shear walls, moment resisting frames etc. will be required to resist a certain design base shear. In order to perform a static pushover analysis the base shear force should be distributed over the height of the lateral load resisting system. The structure is loaded with constant gravity loads and incrementally increasing lateral loads which are applied at positions of concentrated mass of the system. According to the designers' guide to EN 1998-1 and EN 1998-5 [7] these increasing lateral load simulates the inertia forces induced by a single horizontal

component of the seismic action. It is also stated in this document that this method is therefore essentially an extension of the lateral force method of linear analysis into the nonlinear regime.

No single load pattern will be able to capture the variations in the local demands in certain structural elements during a design earthquake and for this reason the Eurocode 8 prescribes that two lateral load distribution patterns must be used:

1. A uniformly distributed lateral load pattern. This corresponds to uniform unidirectional lateral acceleration at every level where the lateral forces are applied.
2. A modal pattern that depends on the type of linear analysis applicable to the structural system. In the case of structures that comply with the requirements of the lateral force analysis method, an inverted triangular unidirectional loading pattern such as the one used in the lateral force analysis method can be used.

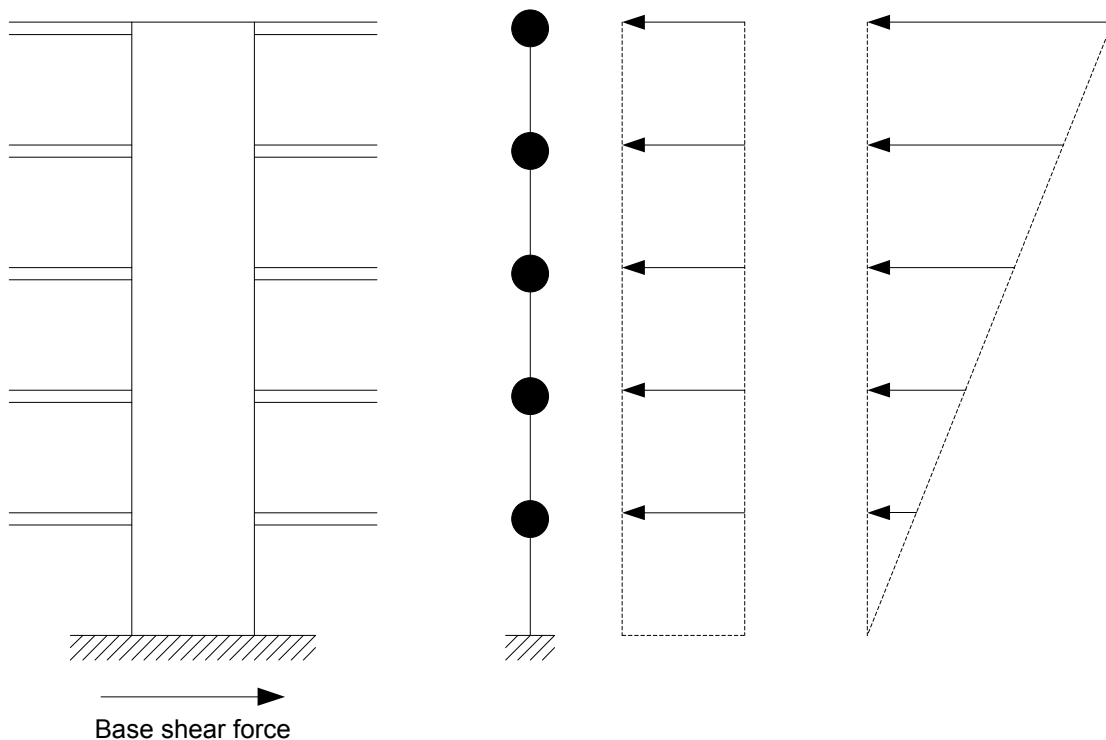


Figure 2-6: Lateral force distribution patterns

Figure 2-6 shows the position of concentrated mass of a shear wall loaded with a certain base shear and the two lateral load distribution patterns as described above. It is also stated in [7] that the most unfavourable result of the pushover analyses using the two

standard lateral load distribution patterns should be adopted. Unless perfect symmetry exists about an axis orthogonal to that of the seismic action component considered, each lateral load pattern should be applied in both directions and the most unfavourable result should be used.

Increasing lateral load will invariably lead to an increase in lateral displacement of the structure. Resulting from the static pushover analysis is a relationship of increasing base shear (and therefore an increasing lateral load at positions of mass concentration) and lateral displacement of the structure, typically measured at roof level. As this analysis is carried out into the nonlinear regime this curve is one of decreasing slope. The resulting lateral force-displacement behaviour is used in the capacity spectrum method, discussed in section 2.2.6.

Krawinkler and Seneviratna [10] identified certain aspects that are important for the static pushover analysis to be applicable. They found that most successful static pushover analyses were limited to structures with about six stories or less in which inelasticity was distributed rather uniformly over the height of the structure. Low rise structures are largely unaffected by higher mode shapes and it was found that this analysis will most likely provide a good estimation of global as well as local inelastic deformation demands for structures that vibrate primarily in the fundamental mode.

It was the above authors' opinion that the static pushover analysis can be used for all structures but should be complemented with other evaluation procedures if higher modes are expected to influence the dynamic response of the structure under seismic action. Additional analyses that can be used for this purpose are inelastic dynamic analyses with a suitable number of ground motions, and modal analyses using the unreduced design spectrum and a suitable modal contribution procedure such as SRSS and CQC.

As stated previously the capacity curve that results from the static pushover analysis is a nonlinear relationship of base shear and lateral displacement of the structure. The slope of the nonlinear graph decreases with decreasing lateral stiffness of the system as cracking of concrete, spalling of cover concrete and other inelastic deformation occur. It is convenient to approximate the capacity curve with a curve consisting of lines of

constant slope. Usually a bilinear approximation is made of the curve as will be discussed in section 2.3.

2.2.4 Nonlinear adaptive pushover analysis

Nonlinear adaptive pushover analysis is another way of determining the capacity of a structural system to lateral loading. This type of analysis is available in the seismic software package SeismoStruct [9]. According to the user manual of this program the nonlinear static pushover analysis suffers from an inability to account for the effects that the progressive degradation of stiffness has on the dynamic response characteristics of structures typically when subjected to strong earthquake motion. Nonlinear static pushover analysis assumes fixed lateral loading patterns and therefore ignores the potential redistribution of lateral loads that can occur due to the progressive degradation of stiffness. Degradation of stiffness usually leads to an elongation of the period of the structure and consequently changes the modal characteristics thereof. The resulting change in dynamic response is therefore not taken into account in the static pushover analysis.

From the above discussion it is clear that the nonlinear static pushover analysis does not yield a good estimation of the capacity of a structure when progressive stiffness degradation is expected to be prominent. Contrary to the static pushover analysis the lateral loading pattern in the adaptive pushover analysis is not kept constant but updated during every load step in the analysis according to the modal shapes and participation factors that is obtained from an eigenvalue analysis that is performed at every load step of the analysis.

This type of analysis is especially appropriate to structures where stiffness irregularities exist and where higher mode shapes can be expected to play an important role in the dynamic response of the structure. The building investigated in this study is regular in plan and elevation and therefore it was concluded that this method of analysis would not be required.

2.2.5 Nonlinear time-history analysis

As stated in Table 2-1 nonlinear time-history analysis can be used to analyse both new and existing structures. This method of analysis is however computationally expensive

but with increasing computing power and more sophisticated software this method of analysis is being used more frequently. According to [6] the use of nonlinear time-history analysis was effectively mandatory for the seismic design of tall buildings in Japan since the 1980s.

It is stated in [5] that this method is the most sophisticated level of analysis available to predict design forces and displacements due to seismic loading. This method involves a stepwise solution through time of the MDOF equations of motion that represents the response of a MDOF structure to a seismic event.

The designers' guide to EN 1998-1 and EN 1998-5 [7] states that, unlike modal response analysis, which provides only estimates of the peak response of a MDOF system, the nonlinear time-history analysis provides peak response quantities that are exact, assuming that the ground motion used is reliable and applicable to the site conditions of the investigated structure. Eurocode 8 prescribes that the analysis should be based on time-histories of ground motion that conforms on average to the 5% damping elastic response spectrum defining the seismic action.

Nonlinear time-history analyses are very sensitive to the ground motion that is used and the following aspects should be considered:

Recorded vs Synthetic time-histories

According to Bommer and Acevedo [11] ground motion data sets can be divided into three main groups: artificial spectrum-compatible accelerograms generated using software such as SIMQKE [12], synthetic accelerograms and recorded accelerograms.

Artificial spectrum-compatible ground motions are generated by generating a power spectral density function from a smoothed response spectrum. Sinusoidal signals with random phase angles and amplitudes are derived, summed and matched to the smoothed response spectrum. The advantage of this method is that it generates ground motions that are almost exactly compatible to the smooth elastic design spectrum. Bommer and Acevedo [11] stated that the problem with these ground motions is the excessive amount of cycles of strong motion. This results in the ground motion having unreasonably high energy content.

Synthetic ground motion is generated from seismological source models and accounts for path and site effects of the earthquake event due to the geological characteristics of the location of interest. Ground motion of this type suffers from two major drawbacks according to Bommer and Acevedo [11]. A lot of parameters are required to characterise the earthquake source and therefore the engineer would have to engage the services of specialist engineers in the field of engineering seismology. The determination of the required source parameters also carries a high level of uncertainty.

Various recorded earthquake ground motion data sets are available from the website of the University of California in Berkeley [13]. Data of each event are available as acceleration time-histories (ground acceleration vs time) and response spectra for various damping ratios (spectral acceleration vs vibration period). Information regarding the geological and seismological conditions at the location of measurement is also supplied and can be used to choose appropriate ground motion data as will be discussed later.

Selection of appropriate ground motion

In this study seven ground motions were used to analyse the selected building. For this reason the selection of appropriate ground motion is discussed here.

Recorded ground motion should be chosen that are representative of the geological and seismological conditions at the location of the structure under consideration. The selection of appropriate ground motion records is important in obtaining accurate results. Dhakal, Mander and Mashiko [14] established a method to identify critical ground motions to be used in physical testing to assess different levels of seismic performances. A collection of twenty ground motion records, measured in the United States, were chosen to represent a location in New Zealand. Two important parameters that were considered were the soil type and the distance from the source to the site where the ground motion is measured.

It is also important that the response spectrum of the recorded ground motion is representative of the elastic response spectrum [15]. A good choice of recorded ground motion should therefore have a response spectrum with peak values in the same period range as that of the elastic response spectrum of the structure. This can be explained by comparing Figure 2-7 and Figure 2-8. In Figure 2-7 the period range of maximum

acceleration values of the response spectrum of the recorded ground motion differs from that of the elastic response spectrum. As the period range of large accelerations is not representative of the structure for which the elastic response spectrum was derived, this ground motion is not a good choice for a time-history analysis of the structure. In Figure 2-8 the period range of large acceleration values falls in the same range as that of the elastic response spectrum and therefore this ground motion would be a good choice for a time-history analysis of the structure provided that the soil conditions are also representative of that at the site of the structure used for analysis. Appropriate scaling factors for the ground motion histories are determined by scaling ground motion response spectra to the elastic response spectrum within a vibration period range discussed in the following section.

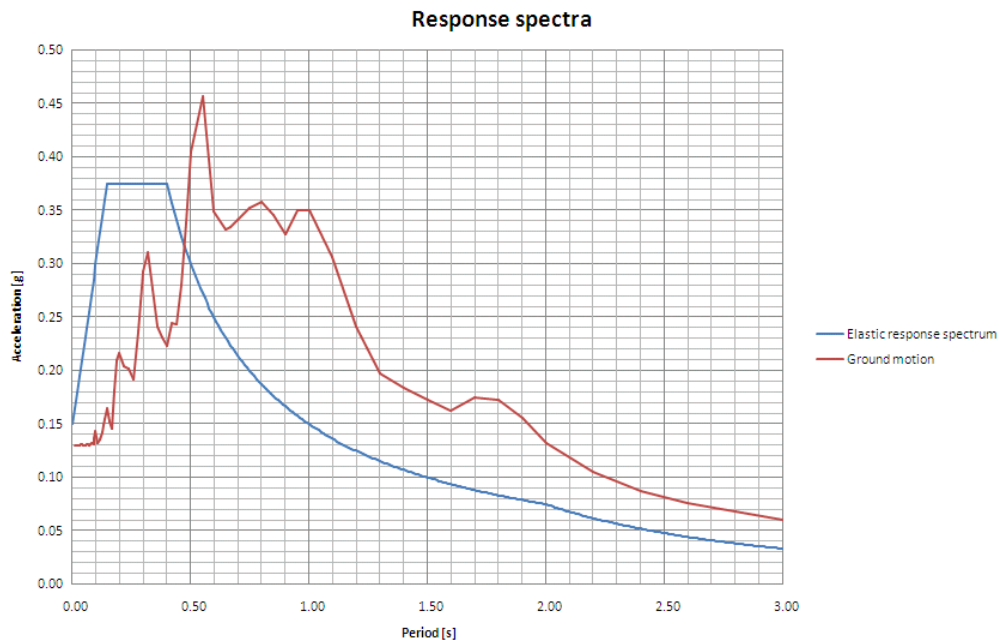


Figure 2-7: Bad comparison

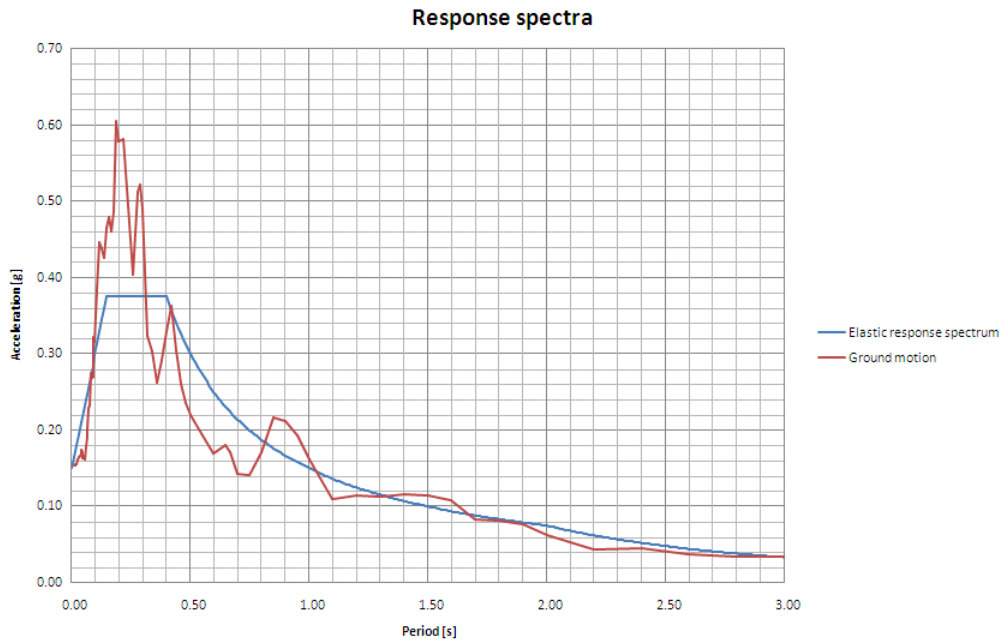


Figure 2-8: Good comparison

Scaling of ground motion data

Once appropriate ground motion data sets are chosen, the accelerograms (ground acceleration vs time) should be scaled as these data sets may have a wide variety of peak ground acceleration. Various different authors have proposed methods to scale recorded ground motion data. All of the methods have one thing in common: the ground motion data sets are scaled by a constant factor throughout to fit the elastic response spectrum. The factor required to scale the ground motion to the elastic response spectrum will not necessarily be the same as the factor required in order to scale the accelerogram of the ground motion to obtain the required peak ground acceleration and hence, the predefined peak ground acceleration applicable in a certain region will not necessarily be obtained after scaling.

In work done by Schwab and Lestuzzi [16] synthetically generated ground motion response spectra were scaled to fit the elastic response spectrum within an upper and lower limit of 25% of the elastic response spectrum. The response spectra were scaled throughout with a constant factor which was then also used to scale the accelerograms of the selected ground motion time-histories.

The NEHRP recommendations in FEMA 451 [15] describe a scaling procedure that can be followed. In this document it is prescribed that the response spectra should be scaled to fit the damped elastic response spectrum in the period range $0.2T_1$ to $1.5T_1$ where T_1

is the fundamental vibration period of the structure. The value of $0.2T_1$ is used to account for higher mode effects whilst the value of $1.5T_1$ is used to take inelastic behaviour into account which tends to increase the fundamental period.

The method used by researchers at the ETH in Zurich [2] is to scale the ground motion response spectra in the period range T_i to $T_1\sqrt{(\mu_\Delta)}$ in such a manner that the SRSS of the difference in acceleration values over this period range is as small as possible. Here T_i is the last mode that should be taken into account to obtain a cumulative effective modal mass percentage of 90% that result from an eigenvalue analysis of the structure. The factor " $\sqrt{(\mu_\Delta)}$ " takes the ductility of the structure into account and hence, accounts for inelastic behaviour which reduces the stiffness of the structure and therefore increases the fundamental period of vibration.

Number of ground motion records to be used

According to Dhakal et al [14] different ground motion records having the same peak ground acceleration will not induce equal levels of response and will not cause the same extent of damage on a structure. For this reason the results obtained by using only one ground motion time-history record may not provide accurate information regarding the response of the structure. It would be possible for another ground motion record with the same PGA to yield a more unfavourable response.

Various authors have different opinions regarding the number of ground motion records to be used when performing a nonlinear time-history analysis. According to FEMA 451 [15] two to three records are sufficient when performing linear time-history analyses whilst four to five records should be used when the structure is expected to respond into the inelastic range. According to Dazio [2] a minimum of seven ground motion records should be used. The above are the recommended minimum number of ground motion records that should be used, but various researchers have used a much larger number of records. Lestuzzi et al [17] used 164 recorded records, Dhakal et al [14] used 20 recorded records and Schwab and Lestuzzi [16] used nine recorded and 100 synthetic records.

The Designers' Guide to EN 1998-1 and EN 1998-5 [7] states that at least three ground motion records should be used. If the response of a structure is investigated by at least seven nonlinear time-history analyses, the average response quantities can be used as

the seismic demand in the relevant verifications. If fewer than seven records are used, the most unfavourable response quantity resulting from the analyses should be used.

In this study seven recorded ground motions were used as described in chapter 7.

2.2.6 Capacity spectrum method

According to Fajfar [18] the capacity spectrum method compares the capacity of a structure with the demand of earthquake ground motion on it by means of a graphical procedure. In this method the capacity of the structure can be obtained by performing a pushover analysis on the structure resulting in a lateral force-displacement response, whilst the demand of the earthquake is obtained from an Acceleration-Displacement-Response-Spectra (ADRS) diagram. This ADRS diagram gives the relationship between pseudo-acceleration (S_{pa}) and the displacement spectra (S_d). Figure 2-9 shows the concept of the capacity spectrum method.

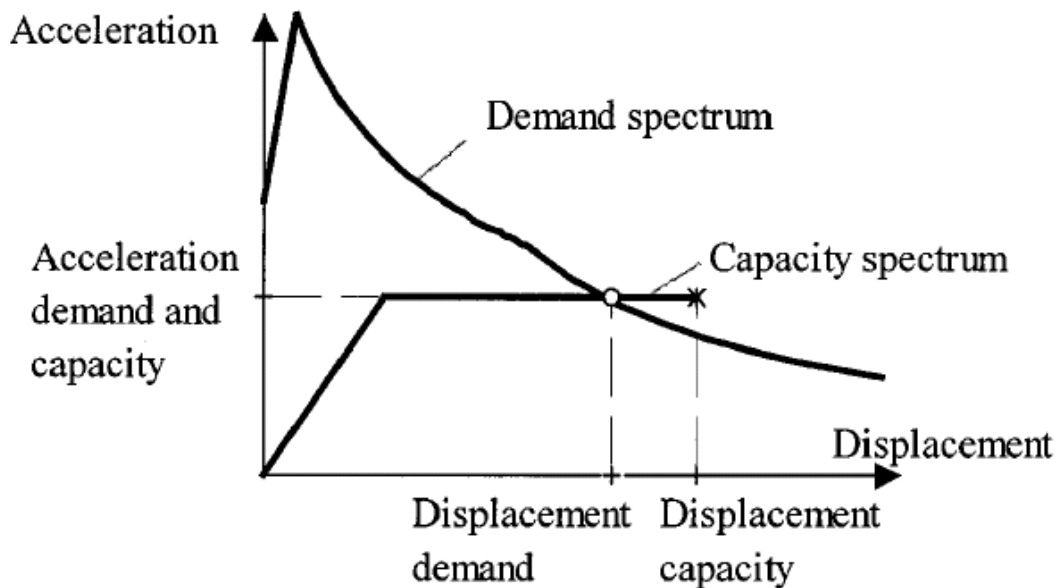


Figure 2-9: Capacity spectrum method [18]

The procedure is based on converting the base shear forces and roof displacement of the MDOF pushover curve to spectral accelerations and spectral displacements of an equivalent SDOF system respectively. These spectral values therefore define the capacity spectrum. The intersection of the capacity spectrum and the demand spectrum provides the inelastic acceleration and displacement demand of the equivalent SDOF

system. The displacement demand can be transformed back to that required for the MDOF system.

Markis and Konstantinidis [19] observed that conversion of an MDOF system to an equivalent SDOF system does not result in equivalent response when foundation rocking is taken into account. Hence, the capacity spectrum method can not be applied when foundation rocking is investigated.

The capacity spectrum method is discussed in detail by Fajfar [18].

2.3 Bilinear approximation of a capacity curve

Lateral force-displacement behaviour of structural systems and moment-curvature response of structural elements are obtained using computer software packages. As the response is expected to be nonlinear, an iterative solution procedure is implemented by these software packages. Variations in the number of iterations during each load step in the nonlinear solution usually results in a rough nonlinear response curve with yield- and ultimate values not clearly defined. It is therefore convenient to approximate the resulting curve with straight lines that clearly defines yield- and ultimate points.

The procedure of approximating a nonlinear capacity curve of a structural system with a bilinear curve with a well defined yield point is discussed in this section. Various procedures are described in different sources, all of which requires some degree of engineering judgement.

FEMA 440 [20] sets out a procedure to determine a bilinear approximation for the global force-deformation behaviour of structures with strength degradation.

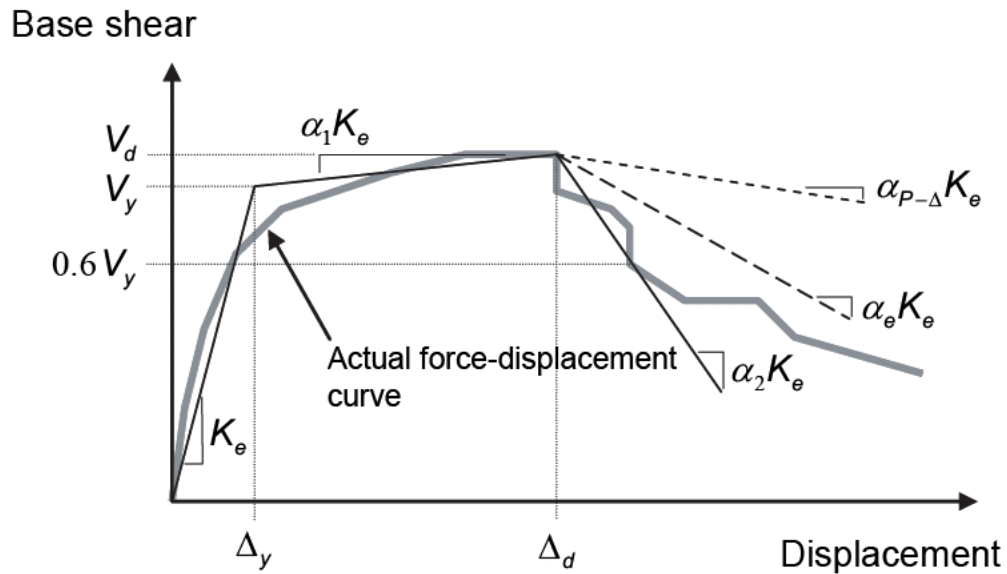


Figure 2-10: FEMA 440 force-displacement idealization [20]

As can be seen in Figure 2-10 the calculated behaviour can be replaced with an idealized relationship with an effective lateral stiffness (K_e), effective yield strength (V_y) and effective positive or negative post-yield stiffnesses ($\alpha_1 K_e$ and $\alpha_2 K_e$). The elastic part of the idealized curve starts at the origin with the post yield part ending at a point which can be either a calculated target roof displacement or the point of maximum base shear force, whichever is the least. The intersection of the two parts defines the yield point of the idealized curve. It is stated that the yield point of the idealized curve must be chosen to satisfy two conditions. The effective stiffness must be chosen such that the first segment of the idealized curve passes through the actual capacity curve at a point where the base shear is 60% of the effective yield strength. To satisfy the principle of conservation of energy, the areas between the actual and idealized curve above and below the idealization should be approximately equal. The selection of the point of 60% of the yield strength is therefore based purely on judgement.

The ATC-40 document [21] describes a slightly different procedure to that of FEMA 440. Here it is stated that the initial stiffness of the idealized curve is chosen to be equal to the initial elastic stiffness of the actual capacity curve as shown in Figure 2-11.

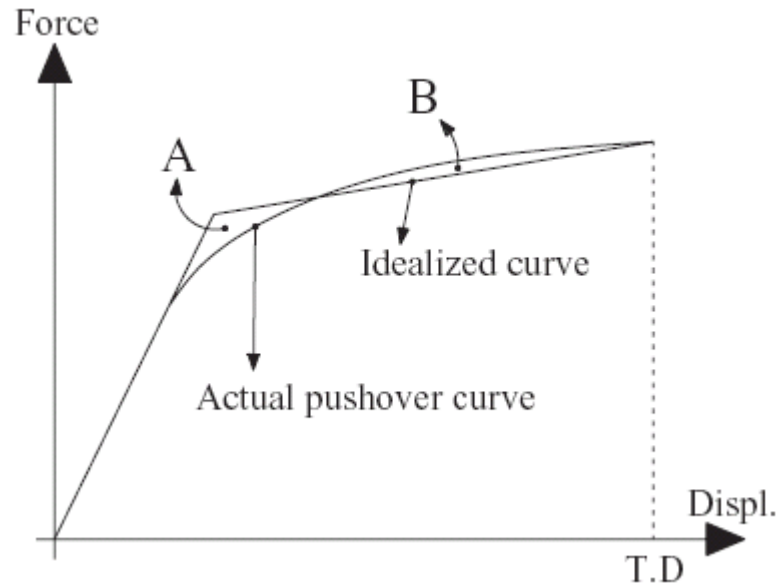


Figure 2-11: ATC-40 force-displacement idealization [22]

Again the elastic part of the idealized curve starts at the origin with the second, post yield, part ending at the point of target displacement or maximum base shear, whichever is the least with the intersection of the two parts defining the yield point. The position of the yield point should be chosen to comply with the principle of conservation of energy with areas “A” and “B” in Figure 2-11 being approximately equal and as small as possible.

In both procedures mentioned above it was the global capacity curve that was idealized with a bilinear curve. Dazio [2] describes a procedure to idealize local capacity curves which is expressed in terms of the moment-curvature relationship of a structural element. The procedure is described for a reinforced concrete section with an applied normal force and incrementally increasing bending moment. The idealized bilinear curve is shown in Figure 2-12.

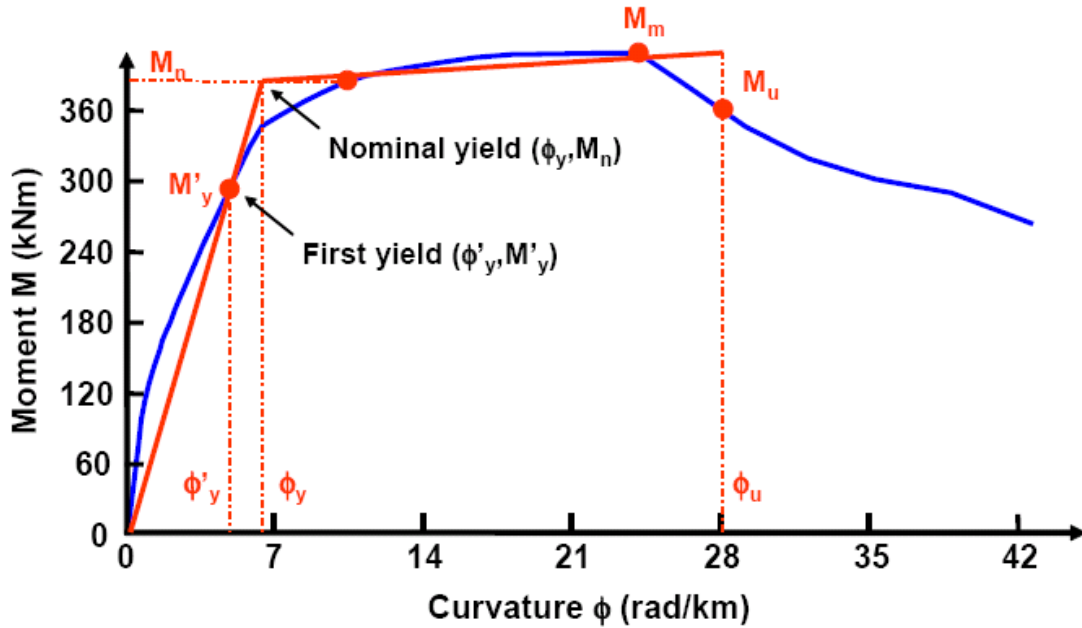


Figure 2-12: Moment-curvature idealization [2]

A four step procedure is described to determine the above bilinear idealization:

a) First yield point ($\phi'_y; M'_y$)

This is the point on the actual capacity curve where the outermost tension reinforcement bar yields for the first time.

b) Nominal yield (M_n)

This is defined as the point on the actual curve where the concrete strain exceed 0.004 or where the reinforcement strain exceed 0.015 for the first time, whichever occurs first. The bending moment at this point is termed the nominal yield bending moment.

c) Nominal yield curvature (ϕ_y)

The curvature at the nominal yield point can be determined by extrapolating between the origin and the point of first yield. The following expression is used to compute the nominal yield curvature:

$$\phi_y = \phi'_y \cdot \frac{M_n}{M'_y}$$

With these points calculated the first (elastic) part of the bilinear idealization is determined.

d) Plastic range

It is left to the engineer to interpolate the plastic region as best as possible. There is however some guidelines as to how this can be done. It is stated that the plastic region should pass through the point of maximum bending moment (M_m) and to be extended to a curvature value that corresponds to a point on the actual graph where the bending moment has dropped by 20% from the maximum value (M_u).

2.4 Effective slab width models

It can be expected that the width of slab elements modelled in framed structural systems will influence the lateral force-displacement behaviour thereof. This topic is discussed as such a framed structural system is investigated in this study.

The effective slab width to be used in the dynamic analysis of reinforced concrete flat slab frames has received much attention to date. Many different models have been proposed by different researchers. Parameters that affect the effective slab width of a flab slab frame model are the following [23]:

- The aspect ratio of the column and panels.
- The type of connection: interior-, exterior- or edge connections.
- The level of gravity load.
- Different positive and negative bending moment response.
- The amount of initial cracking.
- The presence of a drop panel.

According to clause 4.6.5.1.1.1 of the South African concrete design code SABS 0100-1 [24] a structure can be divided into frames consisting of columns and strips of slabs with an uniform width equal to half the centre distance between panels for lateral load effects. The slab width modelled at the slab-column connections is therefore prescribed as equal to that between connections.

Due to the complexity of the moment-transfer mechanism between the slab and the column under lateral loading, the assumptions made in the past regarding the effective slab width and its stiffness have been very subjective. Luo, Durrani and Conte [25]

stated that the use of the same effective slab width for both interior and exterior slab-column connections is not appropriate. They stated that different effective slab widths should be modelled at interior and exterior connections, but with the same effective slab depth at all slab-column connections. The reason for this difference in effective slab width is to account for the shear and unbalanced moment transfer at flat slab-column connections. The advantage of this method is that both the strength and stiffness calculations can be based on the same effective slab width.

The effective slab width model proposed by Luo and Durrani [26] [27] is shown in Figure 2-13.

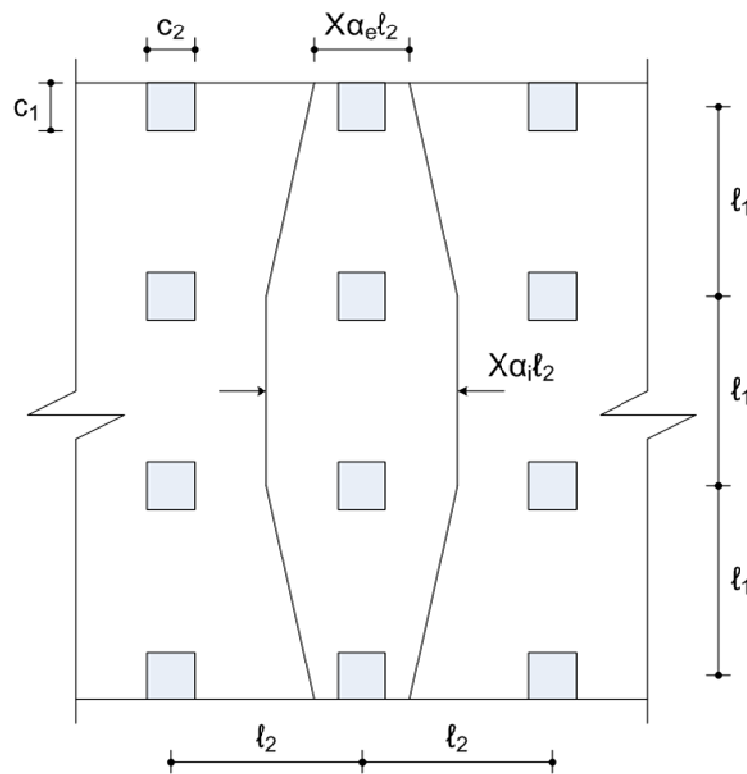


Figure 2-13: Effective slab width model proposed by Luo and Durrani [26] [27]

From Figure 2-13 the following parameters:

α_e = Exterior effective slab width factor

α_i = Interior effective slab width factor

χ = Reduction factor

Equations for the above parameters were determined empirically and are as follows:

$$\chi = 1 - \frac{0.4 \cdot V_g}{4 \cdot A_c \cdot \sqrt{f_c'}}$$

$$\alpha_e = \chi \cdot \left[\frac{K_t}{K_t + K_s} \right]$$

$$\alpha_i = \chi \cdot \left[\frac{1.02 \cdot \left(\frac{c_1}{\ell_2} \right)}{0.05 + 0.002 \cdot \left(\frac{\ell_1}{\ell_2} \right)^4 - 2 \cdot \left(\frac{c_1}{\ell_1} \right)^3 - 2.8 \cdot \left(\frac{c_1}{\ell_1} \right)^2 + 1.1 \cdot \left(\frac{c_1}{\ell_1} \right)} \right]$$

In order to determine the effective slab widths at interior and exterior slab-column connections the following parameters are therefore required:

V_g = Direct shear force due to gravity loads only.

A_c = Area of slab critical section for punching shear as specified in ACI 318-89

f_c' = Compressive strength of concrete.

c_1 = Column dimension in the bending direction of the frame.

c_2 = Column dimension normal to the bending direction of the frame.

ℓ_1 = Centre-to-centre distance between columns in the bending direction of the frame.

ℓ_2 = Centre-to-centre distance between columns in normal to the bending direction.

K_t = Torsional stiffness of torsional members in the slab as defined by the ACI Building Code.

$K_s = (4E_{cs}I)/\ell_1$ = Flexural stiffness of the slab framing into the exterior connection.

E_{cs} = Modulus of elasticity of the slab concrete.

I = Moment of inertia of the full slab width.

In the case of flat slab structures there are no torsional members such as beams at the edge of the slab. For this reason $K_t = 0$ for flat slab building structures.

Other models have also been proposed for structures where drop panels are used at slab-column connections. Dovich and Wight [23] performed experimental work on two

storey, two panel frames with drop panels. They proposed different effective slab width models to be used to determine the strength and stiffness of the frame. For both models the effective slab width at the slab-column connection were chosen as the width of the drop panel with the effective slab width being larger between slab-column connections for the model used to determine the strength of the frame. Figure 2-14 shows these effective slab width models with the top figure showing the model used for the determination of the strength of the frame. The bottom figure shows the model used to determine the stiffness of the frame.

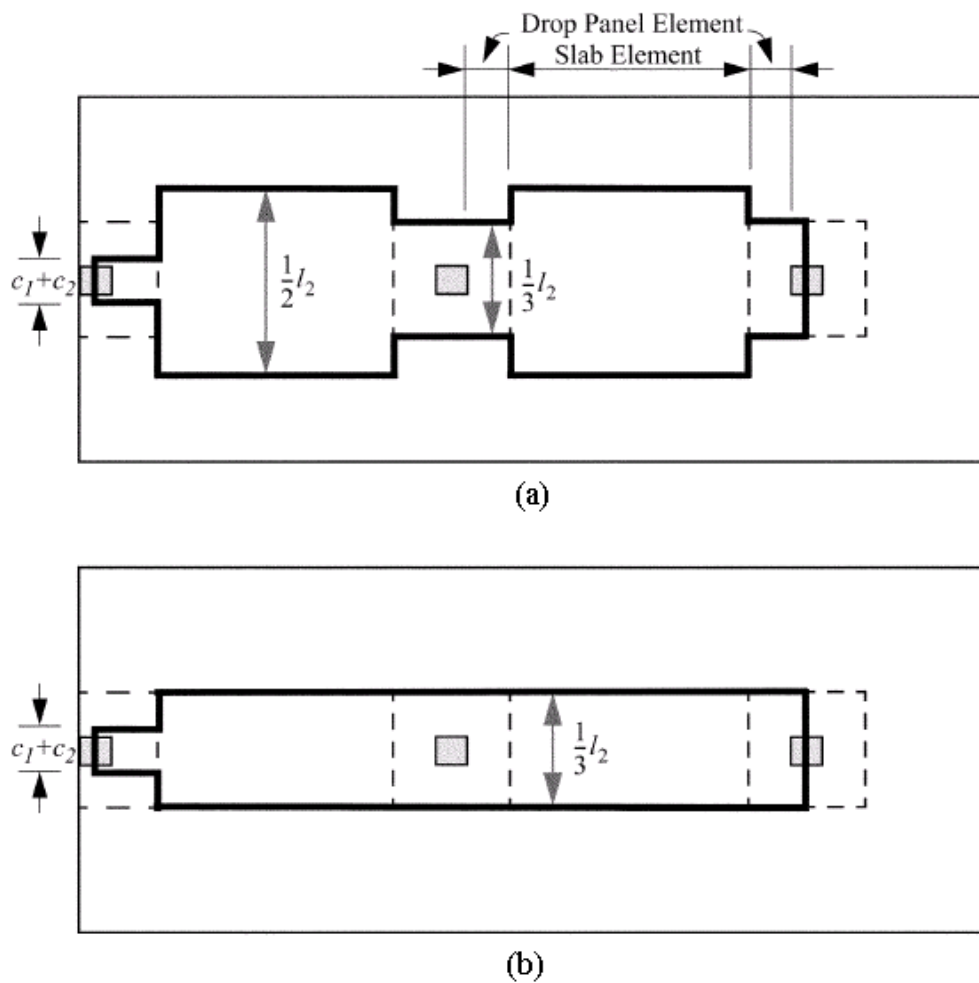


Figure 2-14: Effective slab width for strength (a) and stiffness (b) [23]

2.5 Flat slab-column connections

Failures in framed structural systems are expected to occur at slab-column connections and therefore the behaviour of these connections due to lateral loading of such frames plays an important role in this study.

Flat slabs refer to buildings consisting mostly of slabs and columns without beams. This type of construction is very often preferred to systems consisting of beams and slab, as it has the following advantages [28]:

- These buildings are aesthetically pleasing.
- Erecting and dismantling formwork is easy.
- Services are installed much easier than with other forms of construction.
- The total height of the building is reduced.

Flat slab construction however has several disadvantages such as [28]:

- The slab-column connection is much more flexible than a beam-column connection.
- The behaviour of the slab is complicated, three dimensional and non-linear.

It is important that sufficient flexural reinforcement be placed in the flat slab to resist the bending moments in the slab caused by the combined gravity and lateral loads. The slab must also be able to transfer unbalanced moments to the columns. These unbalanced moments cause additional shear forces at the flat slab-column connections that, combined with the shear force caused by gravity loads, must be resisted by the slab. The shear that must be resisted at these connections can also be expressed in terms of stresses as shown in the following:

$$v_u = \frac{V_u}{A_c} \pm \frac{\gamma_v M_u c}{J_c}$$

With: V_u = Ultimate shear force at the flat slab-column connection.

A_c = Critical area around the flat slab-column connection.

$\gamma_v M_u$ = Ultimate bending moment that is transferred to the column.

$c =$ The distance from the centroid of the critical section to the perimeter of this section.

$J_c =$ Polar moment of inertia of the critical section.

Figure 2-15 shows the position where the shear stress caused by the unbalanced bending moment ($\gamma_v M_{uc}/J_c$) needs to be added or subtracted.

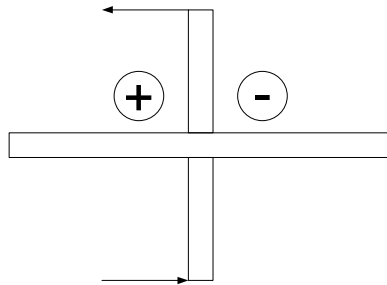


Figure 2-15: Addition or subtraction of unbalanced bending moment

Figure 2-16 shows the distribution of shear stresses at a flat slab-column connection first due to direct shear and secondly due to bending [29].

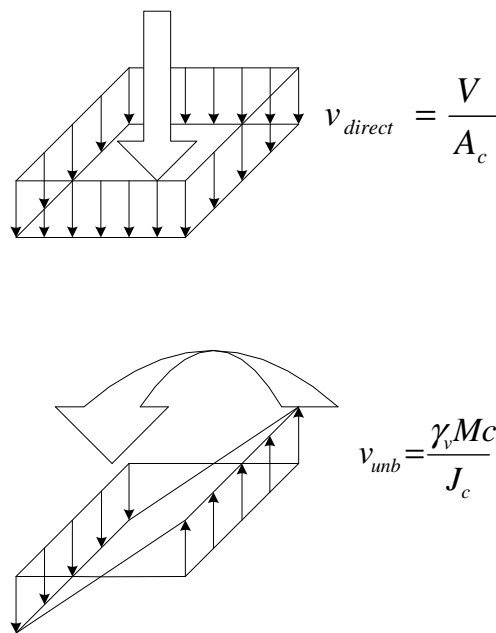


Figure 2-16: Shear stresses at a flat slab-column connection

The shear resistance of a flat slab-column connection (v_R) is obtained from the shear resistance of the slab concrete (v_c) and the shear reinforcement placed in the slab at these connections (v_s) and therefore: $v_R = v_c + v_s$ [30].

Failure due to the internal shear force exceeding the shear capacity of a connection is termed a punching shear failure. These failures are brittle and can occur rapidly. According to Theodorakopoulos and Swamy [31] variables such as concrete strength, the ratio of column size to effective slab depth, the ratio of shear strength to flexural strength, the column shape and any lateral restraints, all have an effect on the punching shear strength of flat slabs.

Though not ideal, frames consisting of flat slabs and columns can be designed as moment resisting frames to provide lateral stiffness to a building. These frames are commonly termed lateral-force-resisting-systems (LFRS). Here the frames must not only be able to withstand the lateral effect of seismic action, but also limit the lateral drift to acceptable levels. The proposed new loading code SANS 10160 [3] sets limits on the storey drift between two adjacent storeys i and j to the following:

- $d_{r\ i-j} \leq 0.025h$ for buildings with $T < 0.7s$.
- $d_{r\ i-j} \leq 0.020h$ for buildings with $T > 0.7s$.

Here “ h ” refer to the storey height and “ T ” to the fundamental period of vibration.

The flat slab-column connections in seismic regions must therefore poses adequate strength against punching shear failure and adequate ductility to undergo inelastic deformations without failure, that is, the ability to undergo the specified minimum interstorey drift ratio.

Under seismic loading it is essential that the structure is able to dissipate energy. The energy dissipated during the loading cycle that increases the shear force at a slab-column connection is represented by the area enclosed in a moment-drift hysteresis loop as shown in Figure 2-17 [32].

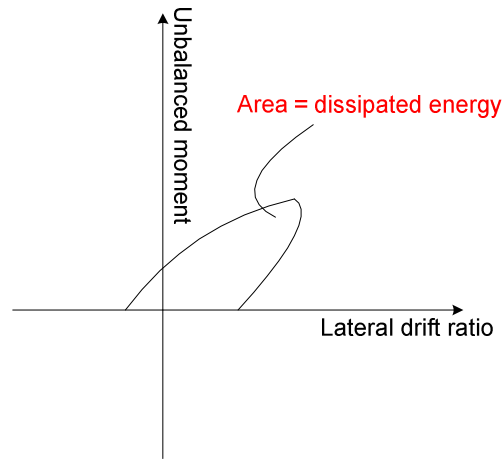


Figure 2-17: Moment-drift hysteresis loop [32]

2.6 Rigid foundation rocking

The rocking response of wall foundations is investigated in this study. Certain behaviour and modelling issues of concern to this topic is discussed in this section.

The concept of rigid foundation rocking of bridge piers has received much attention in research [33]. Rigid foundation rocking implies a foundation that rotates about one of the axes of the foundation without deformation of the foundation itself.

Assuming that the foundations of a structure and the underlying soil is firmly bonded to ensure a fixed support to the structure may lead to lateral earthquake induced forces on the structure that can produce a base shear and overturning moment that is greater than the overturning resistance due to gravity loads. This implies that a portion of the foundation would intermittently lift up for small time durations during an earthquake.

Yim and Chopra [34] stated that foundation uplift may be responsible for the good performance of seemingly unstable structures during earthquakes. Under the action of static lateral force, they found that uplift of the foundation mat is initiated when the base shear reaches a value of one-third of the critical base shear. The critical base shear is known as the base shear corresponding to the unrealizable condition of uplift of the entire foundation mat from the supporting soil except for one edge. This parameter depends only on the gravity force and slenderness-ratio parameter, which is defined as the ratio of superstructure height to half the width of the foundation.

It was found that for slender structures representative of medium to high rise structures, the base shear is reduced during an earthquake because of foundation mat uplift. The response of short structures, with short natural vibration periods, however increases. As a consequence Yim and Chopra [34] stated that increased response is of little practical consequence for medium-rise to high-rise structures.

Vibration periods that leads to an increase in response of the structure are however unrealistically short for slender structures with longer vibration periods. For this reason the increased response of very short period structures is of little practical consequence.

In the above mentioned paper it was also stated that foundation uplift generally reduces the structural deformations and forces. Foundation uplift should therefore not be prevented, and it is, on the contrary, desirable to permit it.

Analytical expressions for the moment-rotation response of a rigid foundation on a Winkler soil model (discussed later in this section) were derived by Allotey and Naggari [35]. Equations were derived for four main states. State 1 represents an elastic soil condition with no foundation uplift, state 2 represents an elastic soil condition with foundation uplift, state 3 represents yielding of the supporting soil prior to foundation uplift and finally state 4 represents a condition of yielding of the supporting soil with foundation uplift. These different states can be seen in Figure 2-18.

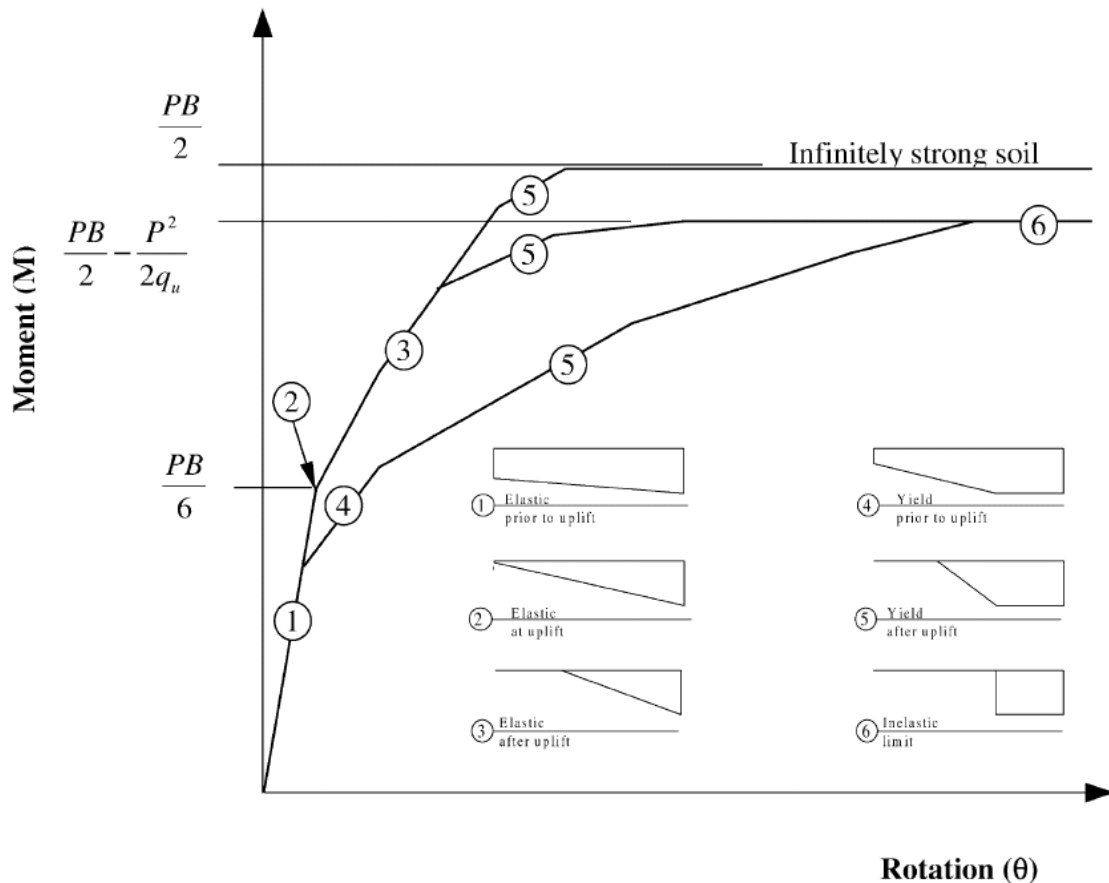


Figure 2-18: Schematic of moment-rotation response states [35]

The solution of these equations enables the full definition of the entire static moment-rotation response of the foundation. This solution can then be used to effectively study the response of a foundation where yielding of the supporting soil and foundation uplift can occur.

It has been stated by Gazettas [36] that the deformability of soil increases the natural period of a structure which in turn leads to smaller ground accelerations and stresses in the super structure and foundation. He also stated that in most cases, footing uplift helps to reduce the ductility demand of columns due to reduced deformations. Uplifting of the foundation mat also has no detriment to the vertical load carrying capacity and the consequence in terms of vertical settlement may be minor.

Overstrength factors, used in the capacity design method, may ensure that the structure does not yield due to overturning and simultaneous bearing capacity failure. The permanent rotation of the structure depends largely on the static safety factor against bearing failure as well as the frequency content of the excitation. Other structural

elements should however be designed for the associated shedding of load from the shear wall to the structural frame.

The seismic response of a 10m tall standard bridge supported on a direct foundation was investigated by Kawashima and Hosoiri [33] taking into account the inelastic rocking response of the foundation. They found that the plastic deformation of the bridge pier decreases if uplifting of the foundation occurs as a result of softening of the moment-rotation hysteresis loops of the foundation. The inelastic rocking of the foundation therefore results in an isolation effect on the response of the bridge. Jumping of the foundation did not occur at any instance during the excitation.

Markis and Konstantinidis [19] investigated the similarities and differences between the oscillatory response of a single-degree-of-freedom oscillator (regular pendulum) and the rocking response of a slender rigid block (inverted pendulum). These two systems are shown in Figure 2-19.

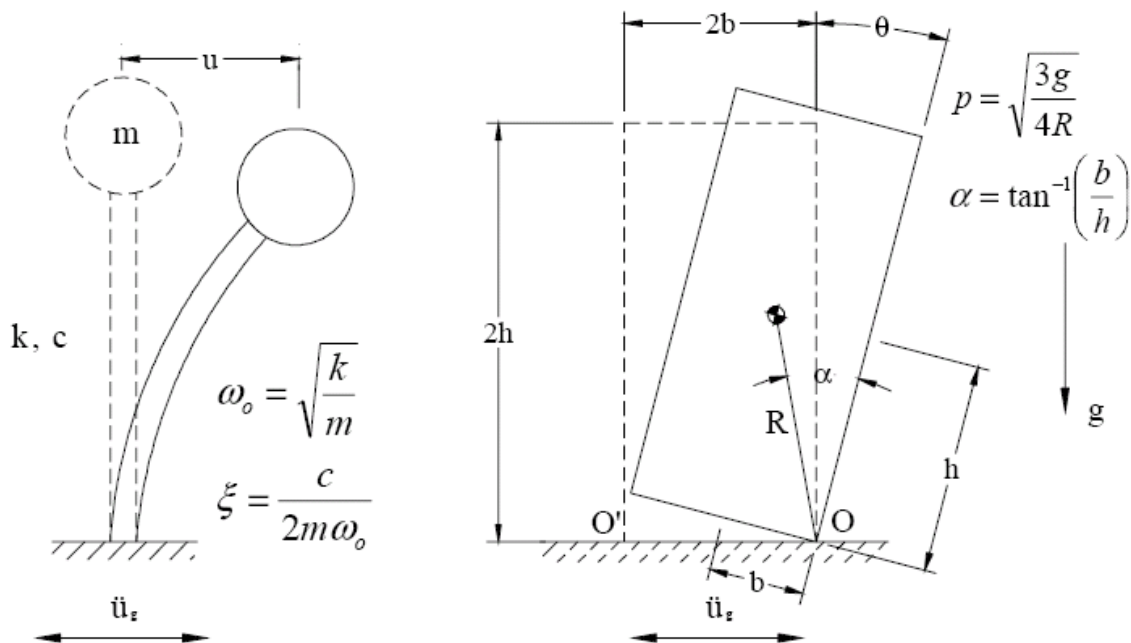


Figure 2-19: SDOF oscillator (regular pendulum) vs rocking block (inverted pendulum) [19]

The study examined the characteristics of the rocking spectrum and compared the observed trends with the response spectrum. It was found that there are fundamental differences in the mechanical structure of the two dynamic systems shown above and consequently, that the rocking structure cannot be replaced by an “equivalent” single-degree-of-freedom oscillator. The response of the one system can therefore not be used

to draw conclusions about the other. Based on these conclusions, Markis and Konstantinidis proposed that rocking spectra be used as an additional valuable measure of the intensity of ground shaking.

Anderson [37] investigated the effect of a rocking wall foundation to determine how this approach can be used to reduce wall foundation sizes, with the main response investigated being the drift ratio of the structure. Buildings having 7, 15 and 30 storeys were investigated. The shear wall and foundation, not including any other structural elements, were modelled using a number of soil springs with zero tension gap elements to allow for rocking of the wall foundation. This concept was extended to include the contribution of other structural elements for the investigation of this study.

It was confirmed that the concept of rocking foundations can reduce the size of foundations considerably to sizes smaller than that required to resist the moment capacity of the shear wall without the building falling over. The force reduction factor used for foundation design was modified in the National Building Code of Canada based on the results of his investigation.

Winkler soil model

As stated previously the moment-rotation expressions derived by Allotey and Naggari [35] for rigid foundations were based on a Winkler soil model. According to Bowles [38] a solution based on a model of a beam on elastic foundation can be used when flexural rigidity of a footing is taken into account. This solution can then be based on the classical Winkler foundation model where the foundation is considered as a bed of springs as shown in Figure 2-20.

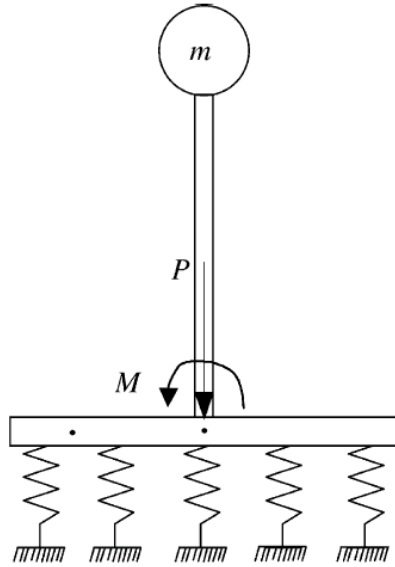


Figure 2-20: Schematic of a Winkler soil model [35]

The underlying soil of a foundation can only provide compressive resistance to a foundation and presents no tensile resistance. For this reason the spring elements that are used to model the rotation stiffness are usually modelled with “zero-gap” elements. This means that the spring elements are not connected to the foundation, but that the foundation rather only rests on the spring elements so as to prevent the spring elements from lifting up.

Bowles [38] states that the modulus of subgrade reaction (k_s , with unit kN/m^3) is used to calculate the elastic stiffness of the spring elements by multiplying this value by the contributing foundation area in plan to a certain spring element. The modulus of subgrade reaction is defined as the increment of contact pressure on the foundation ($\Delta\sigma$) and the corresponding change in deformation ($\Delta\delta$) and therefore:

$$k_s = \frac{\Delta\sigma}{\Delta\delta}$$

Since pressure is defined as the ratio of axial force and contact area, multiplying the modulus of subgrade reaction by the contributing contact area leads to a spring stiffness that describes the increment of axial force and deformation.

Many authors have used the Winkler soil model to investigate the effect of foundation rocking and some variations were used. Yim and Chopra [39] used a Winkler soil model with only two spring elements to investigate the dynamics of structures with their

foundation mat permitted to uplift from the supporting soil. This model is shown in Figure 2-21.

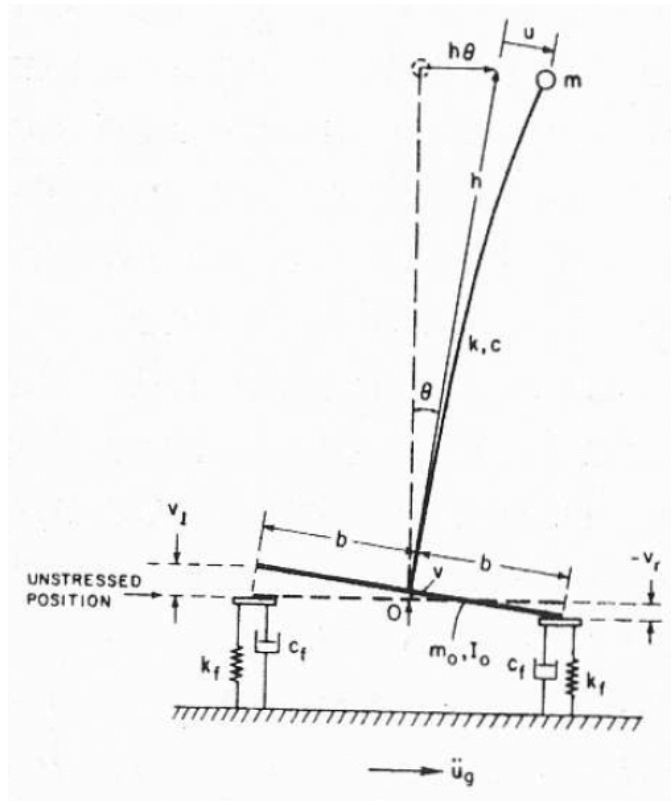


Figure 2-21: Two spring-damper Winkler soil model [39]

Winkler soil models have also been used by Yim and Chopra to investigate the dynamic response of MDOF systems with the foundation allowed to uplift in the same manner as above [40].

2.7 Confinement of concrete

Material properties were assigned to confined and unconfined concrete material in the models used to determine the lateral force-displacement behaviour of the various superstructure systems investigated in this study.

Due to Poisson's ratio effect which is enhanced by extensive micro cracking, concrete tends to expand in the direction normal to an applied compressive stress. This may lead to instability of the concrete in the core region and finally to failure.

The ultimate compressive strain of unconfined concrete is often inadequate to allow the structure to achieve the design level of ductility without extensive spalling of the cover concrete. To prevent failure of structural elements due to spalling of the cover concrete and buckling of longitudinal reinforcement, adequate transverse reinforcement should be provided to confine the compressed concrete in the core region. Attention to confinement of the core concrete should especially be given to elements in potential plastic hinge regions where inelastic material response can be expected [41].

Transverse reinforcement in conjunction with longitudinal reinforcement restrains lateral expansion of the concrete. Therefore larger compression stresses and strains can be sustained before failure occurs as can be seen from Figure 2-22 [5].

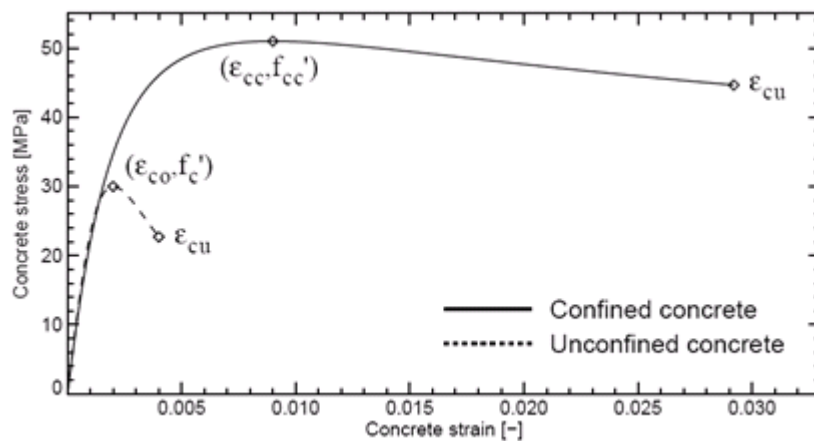


Figure 2-22: Confined and unconfined concrete stress-strain behaviour [5]

It therefore follows that adding more longitudinal and transverse reinforcement increases the confinement of the section as can be seen from Figure 2-23.

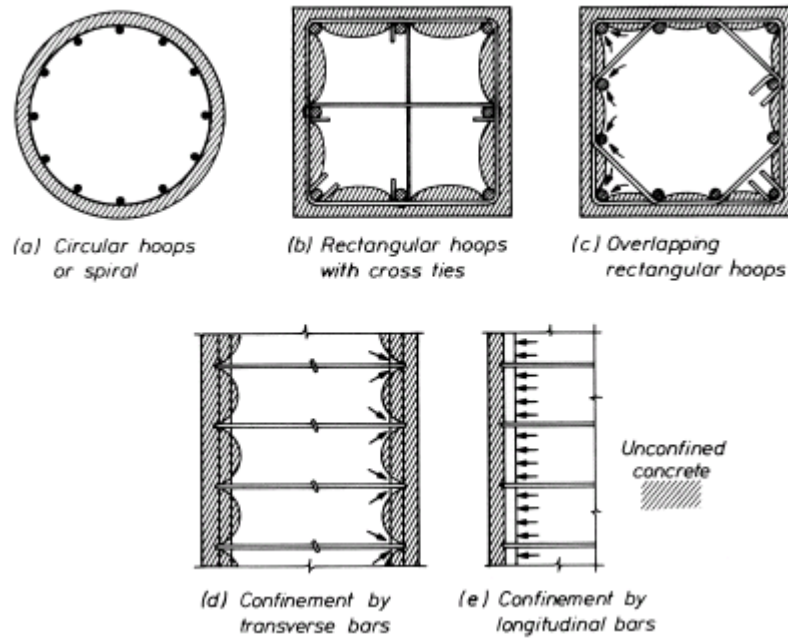


Figure 2-23: Confinement by transverse and longitudinal reinforcement [5]

Expressions to determine the stress-strain curve of confined concrete as a function of the concrete strength and amount of transverse reinforcement were derived by Mander et al. in 1988 [41]. They also stated that the compression strength of confined concrete is directly related to the effective confining stress (f_t') that can develop at yield of the transverse reinforcement.

The confined strength ratio (K) is an important parameter in seismic design and is defined by the ratio of confined concrete compressive strength (f_{cc}') to the unconfined concrete compressive strength (f_c'). This confined strength ratio can be obtained from the graph shown in Figure 2-24.

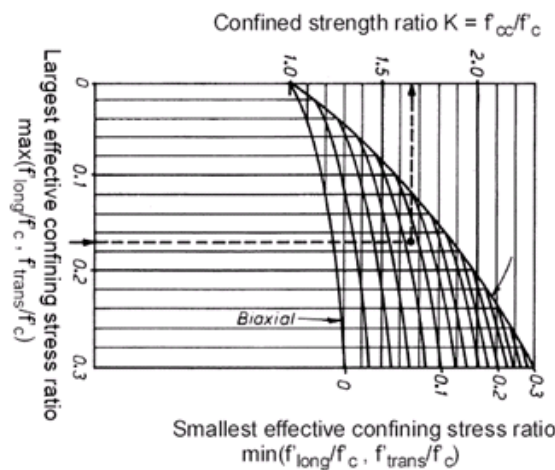


Figure 2-24: Determination of confined strength ratio [5]

With the confined strength ratio known, the confined concrete compressive strength can be calculated.

Expressions have also been proposed to compute the concrete strain at peak stress (ϵ_{cc}) and the ultimate compressive strain in the concrete section (ϵ_{cu}). These values can also be seen on the graph in Figure 2-22. These expressions are given in [5] as follows:

$$\epsilon_{cc} = 0.002 \left[1 + 5 \left(\frac{f'_{cc}}{f'_c} - 1 \right) \right]$$

$$\epsilon_{cu} = 0.004 + (1.4 \rho_s f_{yh} \epsilon_{sm} / f'_{cc})$$

A more detailed discussion of the above equations can be found in [5].

The example building structure that was used for all comparative analyses in this study is discussed in the following chapter.

Chapter 3

3 DESCRIPTION OF STRUCTURE

3.1 Objectives

This chapter presents the example building structure that was used for the purpose of comparative analyses. Figure 3-1 shows the part of the study, extruded from Figure 1-1, which is addressed in this chapter. This includes:

- Design and detailing of the building.
- Determining material properties.
- Determining failure criteria of various structural elements.

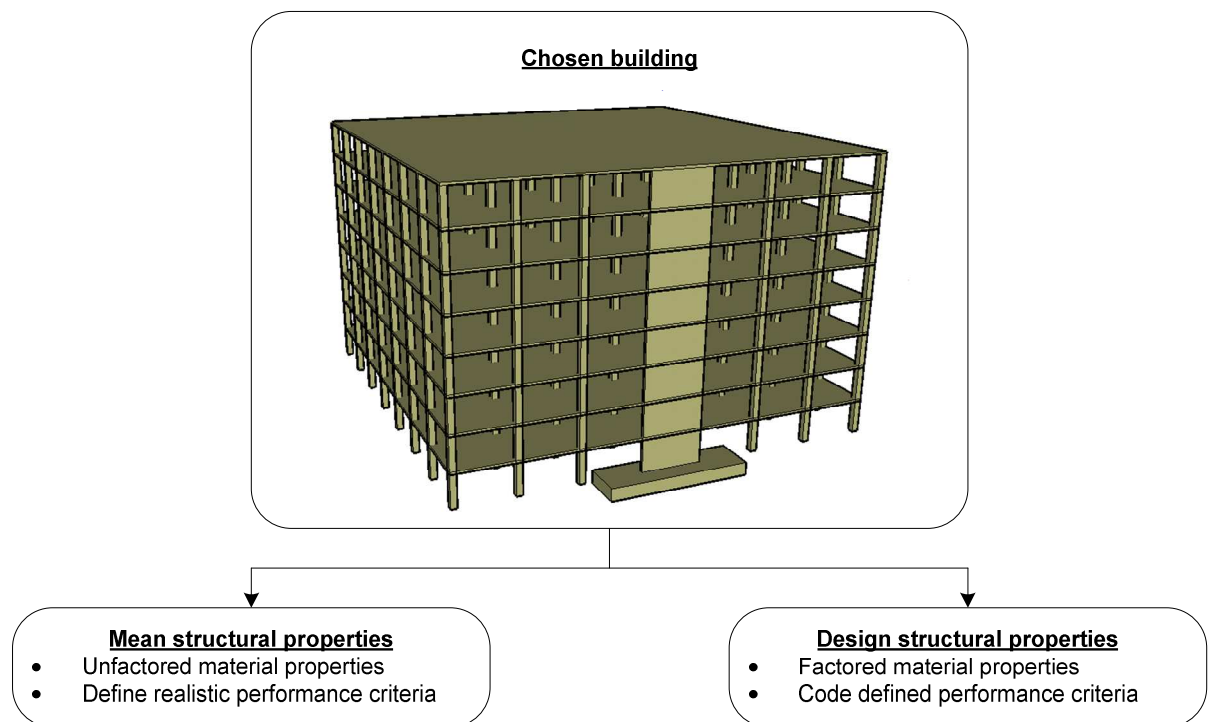


Figure 3-1: Chapter three objectives

3.2 Building design

An example building was designed in order to perform various comparative analyses. An office building for general use in the Cape Town region was chosen for the purpose of this investigation. The following properties were used:

- Provision is made for light weight partitioning = 1.5kPa in plan.
- Permanent load due to ceilings and services = 0.3kPa in plan.
- Cover to reinforcing steel = 35mm according to SABS 0100-2, Table 5 [42].
- The roof of the building is inaccessible.
- A slab thickness of 250mm is used.
- A screed thickness of 40mm is used.
- A masonry wall is provided around the perimeter of the floor slabs and has a weight of 5kPa in elevation with 20% of the wall consisting of openings.
- The building has eight floors.
- Floor to floor height is 3500mm.
- The bearing capacity of the underlying soil is 750kN/m^2 with a density of 18kg/m^3 .
- Assume that the soil has a friction angle of $\phi = 42^\circ$ as is typical in the Cape Town region.
- The building is regular in plan with a centre to centre distance of 6000mm between columns.
- Column dimensions 600mm x 600mm.
- Shear wall dimensions 6000mm x 300mm.
- The design concrete compressive strength is $f_{cu} = 30\text{MPa}$.
- The design yield strength of the reinforcing steel is $f_y = 450\text{MPa}$.

Four shear walls are placed to provide lateral stiffness to the structure in the north-south direction. In this study, ground motion will only be considered in one direction and therefore no shear walls are providing lateral stiffness in the east-west direction.

Figure 3-2 shows a plan layout of the building.

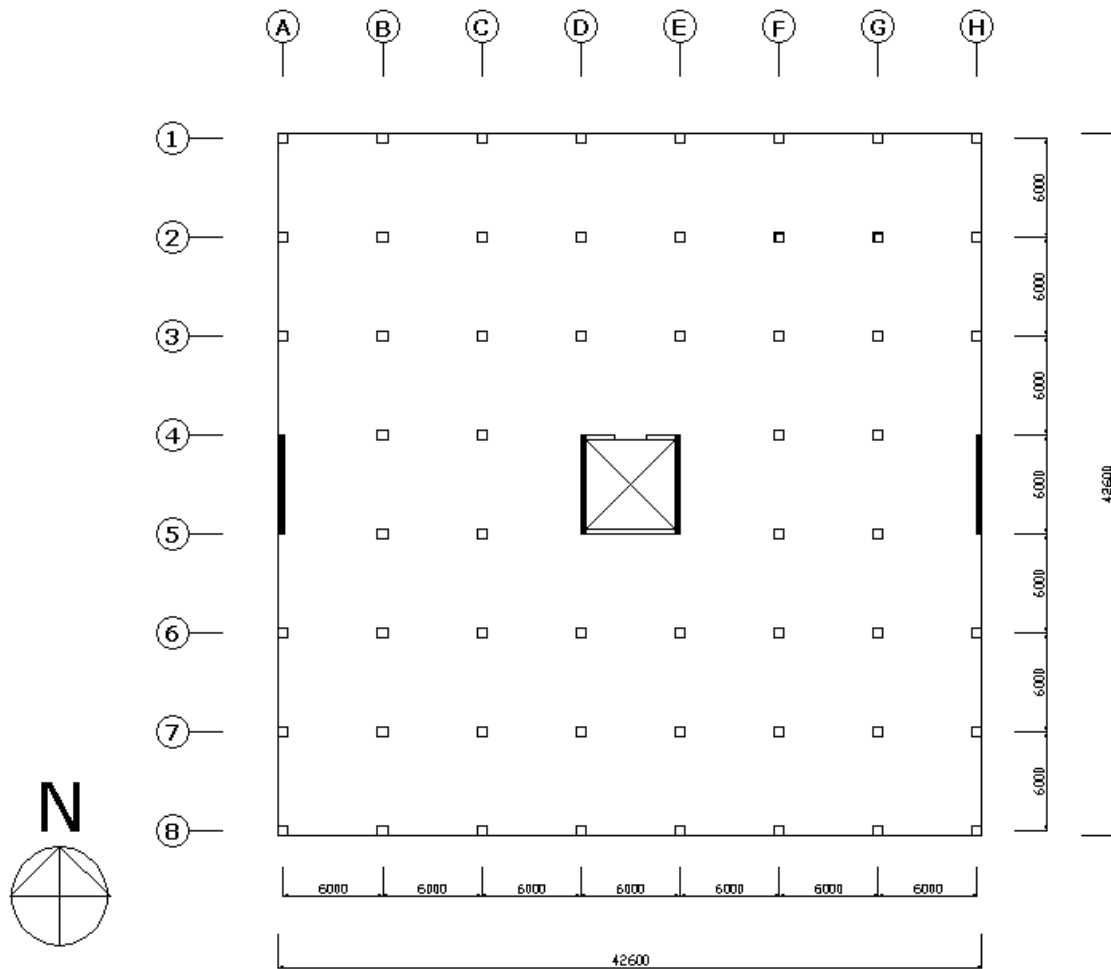


Figure 3-2: Plan layout

The structural elements in the building were designed according to the assumption that only the shear walls resist lateral forces such as wind and earthquake loads. The columns and flat slabs were therefore designed to resist gravity loads only.

The lateral response of the building is only investigated in the north-south direction and therefore the reinforcement in the flat slabs was calculated in this direction only.

Slab reinforcement

The required slab reinforcement was computed at grids A and B from the building plan layout. Table 3-1 shows the calculated reinforcement for grid A.

Table 3-1: Grid A slab reinforcement

Positive bending moment:	
Column strip:	Y12 - 250
Middle strip:	Y12 - 250
Negative bending moment:	
Centre column strip:	Y16 - 125
Remainder column strip:	Y16 - 250
Middle strip:	Y12 - 200

The reinforcement required for grid B was determined in a similar manner and is as shown in Table 3-2.

Table 3-2: Grid B slab reinforcement

Positive bending moment:	
Column strip:	Y12 - 250
Middle strip:	Y12 - 300
Negative bending moment:	
Centre column strip:	Y16 - 150
Remainder column strip:	Y16 - 300
Middle strip:	Y12 - 300

The amount of shear reinforcement that should be placed at corner -, edge -, and interior slab-column connections to prevent punching shear failures due to gravity loads were also determined. Stirrups should be placed in two rows at all slab-column connections at a centre to centre spacing of 150mm. The number of stirrups required at the slab-column connections is as follows:

- Corner slab-column connections: 20 - R8.
- Edge slab-column connections: 34 - R8.
- Interior slab-column connections: 56 - R8.

Column reinforcement

Only critical columns were considered to determine the required reinforcement in the columns. These columns are located at grids 2B, 2G, 7B and 7G. It was determined that nominal reinforcement can be placed from the second floor level to roof level. The reinforcement layout in the columns is shown in Figure 3-3.

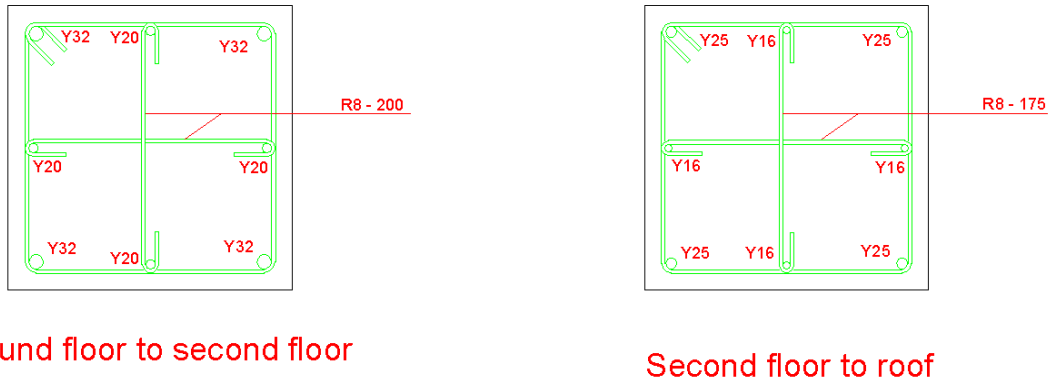


Figure 3-3: Column reinforcement detailing

Shear wall reinforcement

The shear wall on grid A is considered in the analyses and therefore the required reinforcement for this shear wall was determined using the equivalent lateral force method as set out in SANS 10160 [43]. It was determined that the plastic hinge height is six meters.

It was chosen to design the shear wall as an elastic section between fourth floor and the roof level. The reinforcement that was required in the plastic hinge height was therefore extended up to the fourth floor. Figure 3-4 shows the reinforcement layout in the plastic region of the shear wall whilst the reinforcement layout in the elastic region is shown in Figure 3-5.

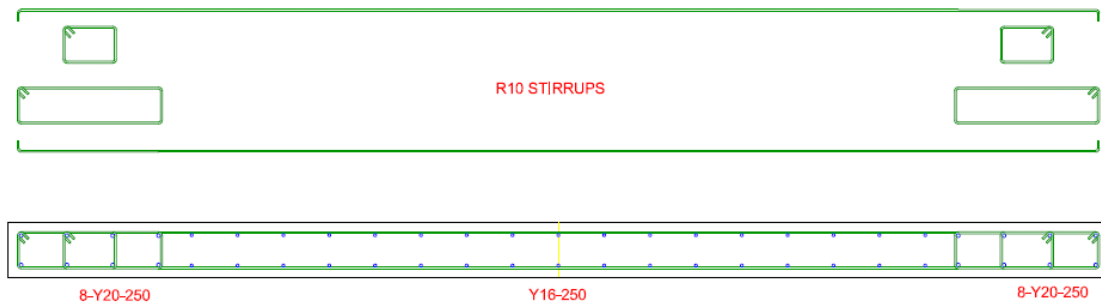


Figure 3-4: Plastic detailing of shear wall

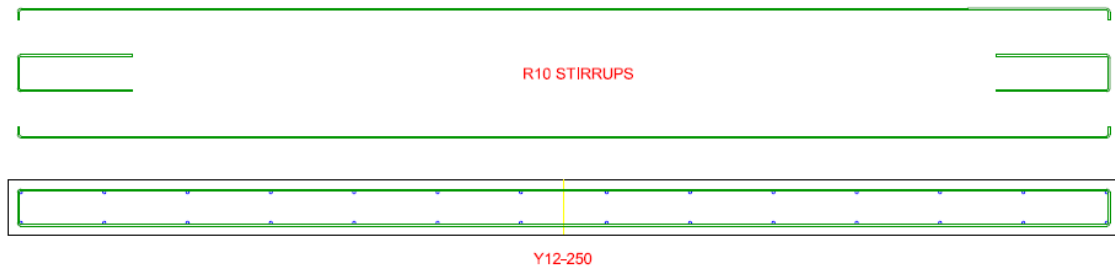


Figure 3-5: Elastic detailing of shear wall

The overstrength forces at the base of the shear wall must be used to design the wall foundation. These overstrength forces were determined to be the following:

- Overstrength bending moment: $M_{Rd}^+ = 30\ 100\text{kNm}$
- Overstrength normal force: $N_d = 4\ 165\text{kN}$
- Overstrength base shear force: $V_d^+ = 2\ 316\text{kN}$

Shear wall foundation dimensions

As stated in chapter one it was decided to investigate six different wall foundation sizes with a seventh model where no moment resistance is provided to the shear wall support. The sizes of the different foundations were determined by designing it to withstand different applied bending moments. Wall foundations are designed to withstand the overstrength bending moment at the base of the shear wall. Different foundation sizes were determined by applying different percentages of this overstrength bending moment: 0%, 20%, 40%, 60%, 80% and 100% of the overstrength bending moment. The axial force on the different foundations was kept constant.

Required foundation dimensions were determined using the *Base* module of Prokon [44]. In addition to the information provided above the following parameters were used to determine the required foundation dimensions.

- Base friction constant between concrete and soil = 0.6 (corresponding to the chosen soil friction angle of 42°).
- A load factor for overturning due to self weight (ULS) = 0.9.
- A load factor for other self weight effects (ULS) = 1.0.
- An ULS safety factor of 1.1 against both overturning and slip.

The optimum foundation size was determined for the appropriate applied bending moment. Table 3-3 shows the required foundation dimensions that were obtained.

Table 3-3: Wall foundation dimensions

Percentage of applied M_{Rd}^+	Length [m]	Width [m]	Depth [m]
100%	14.0	4.0	1.3
80%	12.0	4.0	1.3
60%	11.5	3.0	1.3
40%	9.5	3.0	1.3
20%	8.0	2.5	1.3
0%	6.5	2.0	0.8

It is important to keep in mind that the purpose of this investigation is to determine whether the size of wall foundations can be reduced by allowing rocking of the foundation. The different foundation dimensions were investigated to enable results from analyses performed later to show a trend in increasing lateral roof displacement with decreasing foundation size. Hence, the above method of determining the wall foundation sizes is considered to be satisfactory.

Foundation dimensions were determined conservatively and therefore each foundation is able to provide a bending moment resistance greater than the bending moment that was applied to determine the required dimensions. Practical dimensions were chosen and therefore it can be expected that the bending moment resistance provided by the investigated foundations will not differ by exactly the same amount as the bending moments that were applied to determine the required foundation dimensions. The bending moment resistance provided by the “40%” foundation for instance will not be exactly 60% less than the bending moment resistance of the “100%” foundation.

3.3 Material properties

To determine the lateral force-displacement behaviour of the different investigated superstructure systems using SeismoStruct, properties were required for the various material types. Material properties used in these analyses are discussed in this section.

To ensure that the correct results are obtained from analyses of different structural elements and/or structural systems it is important to define the appropriate material properties. Design codes such as SABS 0100-1 use partial material factors as safety factors to scale actual material properties for design purposes.

Material factors are therefore used in normal static design conditions leading to lower values being used for the strength of materials. This conservative approach leads to structures being designed with a greater strength than is required and generally, to stiffer structural elements. Structural overstrength is the result of this higher actual strength.

Various factors can lead to the actual strength to exceed the nominal or ideal value and are taken into account in the overstrength of a section. These factors include [5]:

- Mean material strengths that are higher than the design material strengths.
- Rounding up of member dimensions or reinforcement diameters.
- Increased structural resistance due to the effect of non-structural members.

As stated in section 2.1.4 the aim of capacity design is to design certain elements to contain plastic regions that dissipate energy with all other elements to remain elastic. To do so, the elastic elements must be strong enough, and for this reason the overstrength of the plastic regions need to be considered.

Mean material properties at overstrength does not account for any material safety factors and should therefore be used for seismic design of building structures. Design material properties should however account for these material safety factors as this is conservative in conventional design of structures.

The material properties of concrete and reinforcement steel are discussed in the following paragraphs.

3.3.1 Concrete material properties

From the above discussion it follows that the mean material properties instead of the characteristic properties are of importance in the plastic regions and therefore material properties should be used without material factors. Various different concrete material properties were considered.

Concrete Compressive Strength

The concrete compressive strength used in the design of the example building was 30MPa, cube strength. According to clause 3.3.3.2 of SABS 0100-1 [24] the partial safety factor for the strength of concrete should be taken as $\gamma_m = 1.5$.

To obtain the mean cube compressive strength of the concrete 8MPa is added to the characteristic (5th percentile value to the nominal (mean)) cube compressive strength [7]. Therefore the conversion expression is as follows:

$$f_{c,mean} = (f_{c,d} \times 1.5) + 8$$

A mean cube concrete compressive strength of **38MPa** was hence obtained using the above equation.

The cylinder concrete compressive strength can be obtained by scaling the cube compressive strength by a factor of 0.8 [46]. Therefore:

$$f_{c,mean,cyl} = f_{c,mean} \times 0.8$$

This leads to a mean cylinder compressive strength of **30.4MPa**. Table 3.1 of EN 1992-1-1:2004(E) [7] however prescribes a mean cylinder compressive strength of **33MPa** associated with the relevant concrete cube strength used in this investigation.

Concrete Tensile Strength

Concrete tensile strength should never be taken into account for the dependable strength of structural members under seismic action, because of its variable nature and due to the influence of, for instance, shrinkage on the tensile strength of the concrete.

Confined Concrete Strength Ratio (K)

The increase in compression strength of confined concrete depends on the amount of longitudinal reinforcement as well as the amount of confining reinforcement. The confinement factor (K) also depends on the yield strength of the reinforcing steel. The mean yield strength of the reinforcing steel (discussed later) and the nominal concrete compressive strength were used to calculate the confinement ratio.

Confinement ratios were calculated for the columns between ground and second floor, for columns between second floor and roof level, as well as for the confined regions of the shear wall in the plastic region. The following values were obtained:

- Columns between ground and second floor: $K = 1.049$
- Columns between second floor and roof level: $K = 1.058$
- Confined regions in plastic region of shear wall: $K = 1.100$

The calculation of these confinement factors were performed as described in [5] and can be seen in Appendix A.

The confinement ratio is therefore only used in defining the material properties of confined concrete. If a confinement ratio must be prescribed for unconfined concrete, unity should be chosen, such as for instance the case when a confinement factor is prescribed for concrete material in slab sections

Concrete Strain at Peak Stress (ϵ_{cc})

Refer to Figure 2-22 for the definition of ϵ_{cc} . The concrete strain at peak stress is a function of the confinement ratio ($K = f_{cc}'/f_c'$). This relationship is as follows [5]:

$$\epsilon_{cc} = 0.002 \left[1 + 5 \cdot \left(\frac{f_{cc}'}{f_c'} - 1 \right) \right]$$

Using the confinement ratios as described above the following values were obtained (refer to Appendix A):

- Columns between ground and second floor: $\epsilon_{cc} = 0.0025$
- Columns between second floor and roof level: $\epsilon_{cc} = 0.0026$
- Confined regions in plastic region of shear wall: $\epsilon_{cc} = 0.0030$

For unconfined concrete $K=1$ and therefore $\epsilon_{cc} = 0.002$ from the expression provided above.

Ultimate Concrete Compression Strain (ϵ_{cu})

The maximum useful strain for design purposes can be much higher than the concrete strain at peak stress. The useful strain limit occurs when the transverse confining reinforcement in a section fractures, known as the ultimate concrete compression strain.

The ultimate concrete compression strain is determined by the transverse reinforcement ratio (ρ_s), the yield strength of the transverse reinforcement (f_{yh}), the steel strain at maximum tensile stress (ϵ_{sm}) and the compressive strength of the confined concrete (f_{cc}') in the following manner [5]:

$$\epsilon_{cu} = 0.004 + (1.4 \cdot \rho_s \cdot f_{yh} \cdot \epsilon_{sm} / f_{cc}')$$

This value can be four to 16 times greater than the traditionally assumed value for unconfined concrete [5].

The following values have been calculated (refer to Appendix A):

- Columns between ground and second floor: $\epsilon_{cu} = 0.0041$
- Columns between second floor and roof level: $\epsilon_{cu} = 0.0041$
- Confined regions in plastic region of shear wall: $\epsilon_{cu} = 0.0046$

The collapse strain for unconfined concrete is prescribed in Figure 1 of SABS 0100-1 [24] as $\epsilon_{cu} = 0.0035$.

3.3.2 Reinforcement steel material properties

A yield strength value of 450MPa was used for design purposes. The mean tensile strength of the reinforcing steel is determined by conversion from the characteristic 5th percentile value of the tensile strength to the nominal tensile strength, this time by a factor of “1.1x1.15”. The following equation shows the calculation of the mean tensile yield strength of the reinforcing steel.

$$f_{y,mean} = f_{y,d} \times 1.15^{(i)} \times (1.1^{(ii)} \times 1.15^{(iii)})$$

- (i) First, the factor “1.15” is the partial material factor prescribed in clause 3.3.3.2 of SABS 0100-1 [24].
- (ii) The factor of “1.1” was prescribed by Mirza et al [47] and is used to convert the yield strength from a characteristic value to a nominal yield value together with (iii).

- (iii) SABS 920 [48] prescribes that the ultimate tensile strength of a reinforcement bar shall be at least 15% greater than the yield stress. The factor of “1.15” is therefore used to obtain the characteristic tensile strength from yield strength.

Mean tensile yield strength of **569.25MPa** was consequently obtained for the tension reinforcing steel from the expression provided above.

3.4 Performance criteria

For analysis purposes various criteria should be set that defines different failures. This is also the case when performing a pushover analysis using the structural analysis package SeismoStruct [9], where material strain limits, shear forces, element chord rotations, etc. associated with various modes of failure of certain structural elements must be prescribed.

The criteria that define various modes of failure are termed the performance criteria. Performance criteria can be defined in terms of the ultimate limit state and serviceability limit state. Ultimate limit state performance criteria include shear failures, bending moment failures and tensile and compressive material failures. Serviceability limit state performance criteria include rotation limits for structural elements and interstorey drift limits.

Mean material properties were used to determine the performance criteria to be used in numerical analyses of the various structural systems of the selected building. The following performance criteria are discussed:

- Bending moment resistance of slab elements.
- Punching shear resistance of slab-column connections.
- Steel material strain limits.
- Concrete material strain limits.
- Element rotation limits.

3.4.1 Internal force performance criteria

Flat slab bending moment resistances and punching shear resistance of flat slab-column connections were determined using mean material properties. The assumptions made in SABS 0100-1 [24] was used to determine both the sagging and hogging bending moment resistance of the column strip and middle strip of the slab on grid A and B of the example building. This assumption is based on a compression block of uniform compressive stress in the concrete with a depth of 90% of the depth of the neutral axis with no concrete tensile strength as shown in Figure 3-6.

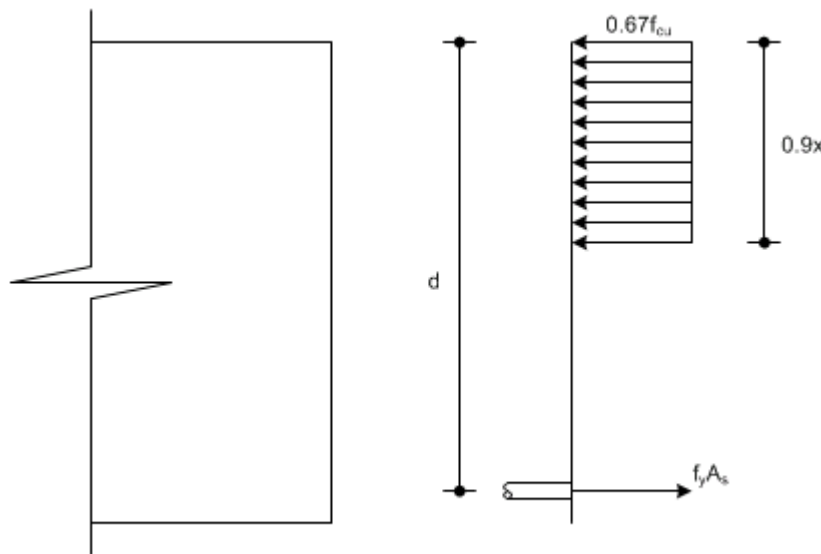


Figure 3-6: Assumption for the determination of flexural resistance

The bending moment resistance of the slab at various positions were determined to be as shown in Table 3-4.

Table 3-4: Slab bending moment resistances

Grid	Bending	Position	M_R [kNm]
A	Sagging	Column strip	92.2
A	Sagging	Middle strip	76.8
A	Hogging	Column strip	236.6
A	Hogging	Middle strip	86.1
B	Sagging	Column strip	153.6
B	Sagging	Middle strip	130.2
B	Hogging	Column strip	333.1
B	Hogging	Middle strip	130.2

Shear reinforcement in the slab at the connection of columns were calculated for three different slab-column connections:

- Interior connections with the slab continuous in both orthogonal directions.
- Edge connections with the slab only continuous in one of the orthogonal directions.
- Corner connections with the slab not continuous in any of the orthogonal directions.

The South African concrete design code SABS 0100-1 [24] was used to calculate the shear resistance of the slab at the connection of columns with the resistance given by combining the shear resistance of the punching shear reinforcement and the shear resistance provided by the slab concrete.

Table 3-5 shows the calculated punching shear resistance of the different slab-column connections.

Table 3-5: Slab-column punching shear resistance

Slab-column connection	V_R [kN]
Interior connections	1711.4
Edge connections	1076.2
Corner connections	638.6

3.4.2 Material performance criteria

Failures can also be identified by material properties such as strain limits being exceeded. Both reinforcement and concrete material strain performance criteria were specified.

As discussed previously, the mean yield strength of the reinforcement steel was calculated to be 569.25MPa. Assuming a modulus of elasticity of 200GPa results in a reinforcement steel strain yield limit of $\epsilon_y = 0.00285$. FEMA 273 [49] states that the maximum permissible strain in reinforcement steel may not exceed 0.05. The reinforcement steel ratio to identify steel fracture was therefore taken to be $\epsilon_u = 0.05$.

Concrete cover spalling occurs when the compressive resistance of cover concrete is exceeded. This will result in a decrease in the stability of longitudinal reinforcement in columns and structural walls and can result in collapse of a structure. Hence, cover

spalling was considered to be an important failure to be identified when performing nonlinear analyses. Using the expressions provided in [5] to calculate strain limits for confined concrete the strain limit of the unconfined concrete could also be determined by using a value of $K = 1.0$ for the confinement factor. This results in a compressive strain limit of **0.002** for unconfined concrete. This strain limit was chosen as the performance criteria for spalling of cover concrete.

Compressive stresses in concrete can also lead to the crushing of confined concrete. The ultimate compression strain values as discussed in section 3.3.1 were prescribed as concrete compressive strain limits associated with crushing of core concrete.

3.4.3 Element rotation performance criteria

Yielding of flexural reinforcement steel in a structural element will lead to the formation of a plastic hinge at the location of flexural failure only if the shear resistance of the section is not exceeded. Structural elements will therefore be able to undergo a greater degree of rotation in these regions. FEMA 273 [49] prescribes limits to the chord rotation of plastic hinges that can form in different structural elements, different reinforcement conditions and desired performance levels. Rotation limits were obtained from FEMA 273 for possible plastic hinges in columns, slabs as well as the shear wall in the region between ground and fourth floor.

FEMA 273 defines four main performance levels as shown in Figure 3-7 [49].

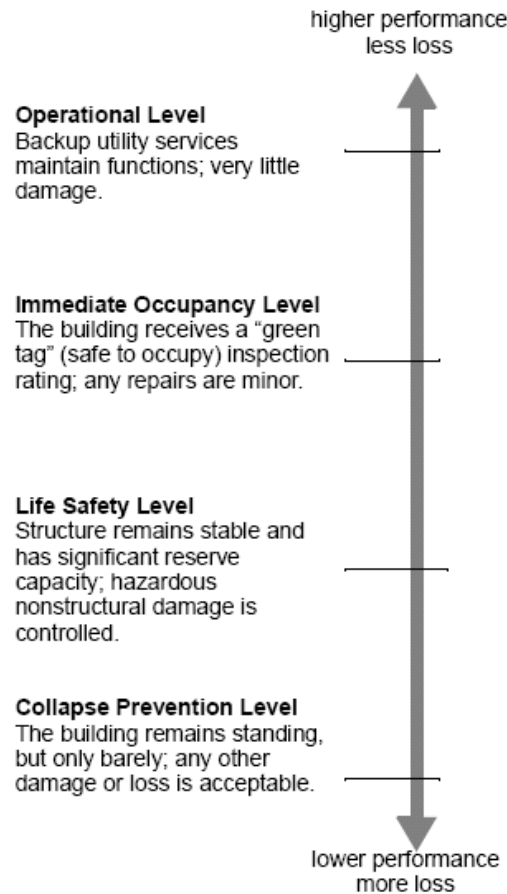


Figure 3-7: FEMA 273 building performance levels [49]

For the purpose of this investigation the plastic hinge rotation limits of *Life Safety* were chosen.

Plastic hinge rotation limit for columns

When determining the flexural resistance of the columns the axial capacity of the column was chosen equal to the applied axial force in the column. It was therefore assumed that the applied axial load in the column exceeds 70% of the axial capacity thereof. The rotation limit from FEMA 273 [49] for plastic hinges in columns where this is the case, is **0.005** radians as shown in Table 3-6.

Table 3-6: FEMA 273 column plastic hinge rotation limits [49]

Conditions	Modeling Parameters			Acceptance Criteria				
	Plastic Rotation Angle, radians		Residual Strength Ratio	Plastic Rotation Angle, radians				
				Component Type				
			Primary		Secondary			
			Performance Level					
	a	b	c	IO	LS	CP	LS	CP
iv. Columns with axial loads exceeding $0.70P_o$								
Conforming reinforcement over the entire length	0.015	0.025	0.02	0.0	0.005	0.001	0.01	0.02
All other cases	0.0	0.0	0.0	0.0	0.0	0.0	0.0	0.0

Plastic hinge rotation limit for slab-column connections

The rotation limit provided for slab-column connections for a life safety performance level is **0.015** radians as shown in Table 3-7 [49].

Table 3-7: FEMA 273 slab-column plastic hinge rotation limits [49]

Conditions	Modeling Parameters			Acceptance Criteria					
	Plastic Rotation Angle, radians		Residual Strength Ratio	Plastic Rotation Angle, radians					
				Component Type					
			Primary		Secondary				
			Performance Level						
	a	b	c	IO	LS	CP	LS	CP	
i. Slabs controlled by flexure, and slab-column connections									
$\frac{V_g}{V_o}$	Continuity Reinforcement								
≤ 0.2	Yes	0.02	0.05	0.2	0.01	0.015	0.02	0.03	0.05
≥ 0.4	Yes	0.0	0.04	0.2	0.0	0.0	0.0	0.03	0.04
≤ 0.2	No	0.02	0.02	-	0.01	0.015	0.02	0.015	0.02
≥ 0.4	No	0.0	0.0	-	0.0	0.0	0.0	0.0	0.0

Plastic hinge rotation limit for shear wall

The performance level of life safety was also chosen for the rotation limits prescribed for shear walls controlled by flexure. As can be seen from Figure 3-4 that the section of the wall where plastic deformation is expected is provided with confined boundaries. Using the mean material properties, geometry of the shear wall, as well as the

reinforcement content, the following ratios were calculated as required by FEMA 273 to determine the appropriate rotation limit for the shear wall [49]:

$$\frac{(A_s - A'_s) \cdot f_y + P}{t_w \cdot \ell_w \cdot f'_c} = 0.074 < 0.1$$

$$\frac{Shear}{t_w \cdot \ell_w \cdot \sqrt{f'_c}} = 1.31 < 3$$

Hence, as can be seen from Table 3-8, a rotation limit of **0.010** radians was used [49].

Table 3-8: FEMA 273 shear wall plastic hinge rotation limits [49]

Conditions	Plastic Hinge Rotation (radians)		Residual Strength Ratio	Acceptable Plastic Hinge Rotation (radians)						
				Component Type						
				Primary			Secondary			
				Performance Level						
	a	b	c	IO	LS	CP	LS	CP		
i. Shear walls and wall segments										
$\frac{(A_s - A'_s) f_y + P}{t_w \ell_w f'_c}$										
$\frac{Shear}{t_w \ell_w \sqrt{f'_c}}$										
Confined Boundary										
≤ 0.1	≤ 3	Yes	0.015	0.020	0.75	0.005	0.010	0.015	0.015	0.020
≤ 0.1	≥ 6	Yes	0.010	0.015	0.40	0.004	0.008	0.010	0.010	0.015
≥ 0.25	≤ 3	Yes	0.009	0.012	0.60	0.003	0.006	0.009	0.009	0.012
≥ 0.25	≥ 6	Yes	0.005	0.010	0.30	0.001	0.003	0.005	0.005	0.010
≤ 0.1	≤ 3	No	0.008	0.015	0.60	0.002	0.004	0.008	0.008	0.015
≤ 0.1	≥ 6	No	0.006	0.010	0.30	0.002	0.004	0.006	0.006	0.010
≥ 0.25	≤ 3	No	0.003	0.005	0.25	0.001	0.002	0.003	0.003	0.005
≥ 0.25	≥ 6	No	0.002	0.004	0.20	0.001	0.001	0.002	0.002	0.004

The numerical modelling procedure that was followed to determine the lateral capacity of various structural systems of the example building structure is discussed in the following chapter.

Chapter 4

4 NUMERICAL MODELLING

4.1 Objectives

This chapter discusses the numerical modelling of the various structural systems that were considered to contribute to the lateral stiffness of the building. Figure 4-1 shows the part of the study, extruded from Figure 1-1, which is addressed in this chapter. This includes:

- A description of the software package used to determine the lateral force-displacement behaviour of the various investigated superstructure systems.
- Input parameters required for these analyses.
- Determining an adequate element mesh.
- Verification of output results with regard to:
 - Calculation of internal forces.
 - Identification of bending moment failures.
 - Calculation of roof displacements.
 - Calculation of material strains.
- Lateral force-displacement capacity curves of:
 - An internal frame.
 - A shear wall.
 - An edge frame.

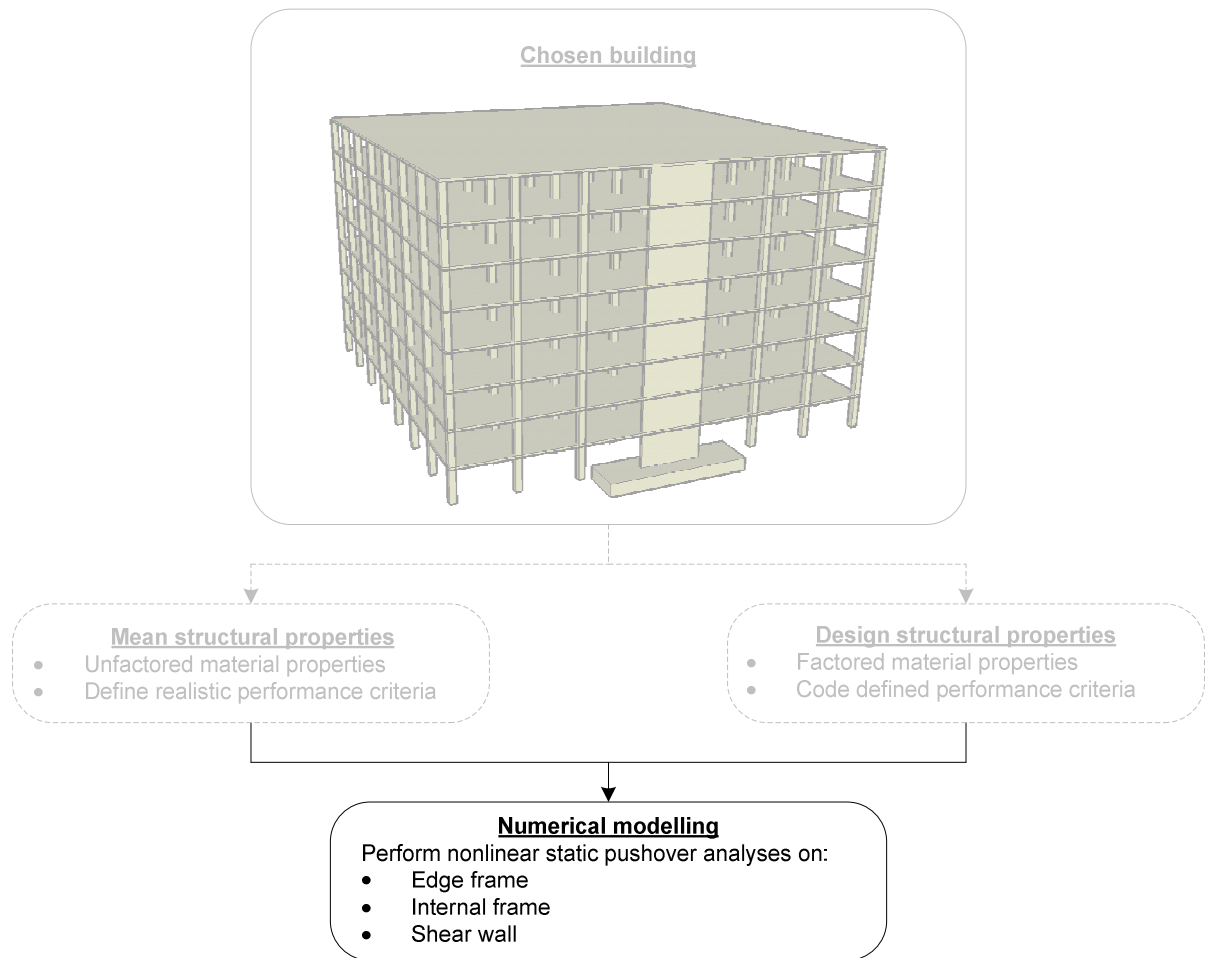


Figure 4-1: Chapter four objectives

4.2 Numerical analysis software

The structural analysis software package SeismoStruct [9] was chosen to perform the numerical modelling of the different structural systems. This is a finite element software package that can be used to investigate the large displacement behaviour of framed structures under static or dynamic loading taking various forms of nonlinearity into account. A range of different analyses can be performed using SeismoStruct such as eigenvalue analyses to determine natural vibration properties, nonlinear static pushover analyses (conventional and adaptive) to determine the capacity of structural systems, nonlinear static time-history analyses, nonlinear dynamic as well as incremental dynamic analyses.

4.2.1 Nonlinearity and modelling assumptions

Both geometric and material nonlinearity can be incorporated into a finite element model in SeismoStruct.

Geometric nonlinearity

Geometric nonlinearity of a model due to large deformations is taken into account by employing a co-rotational formulation with element displacements and the resulting internal forces defined by the movement of a local chord system. As shown in Figure 4-2 this local system consist of six basic degrees of freedom, five rotational and one translational.

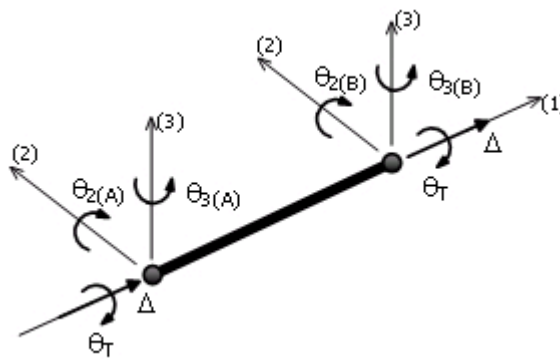


Figure 4-2: Local degrees of freedom [9]

The resulting element internal forces, Figure 4-3, and element stiffness matrix are directly transformed into the global system of coordinates, allowing large geometric nonlinearity to be accounted for.

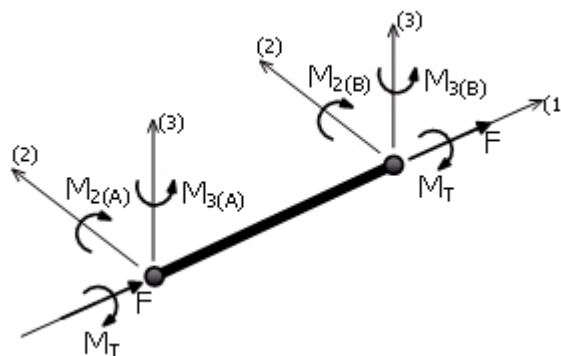


Figure 4-3: Element internal forces [9]

A constant axial strain shape function is assumed over the length of an element and therefore its application is only fully valid to model geometric nonlinearity of relatively short members. For this reason SeismoStruct propose that at least three to four elements should be used per member [9]. Another important assumption to be taken into account is that shear strains are not modelled across an element cross section and therefore a Bernoulli flexure-only beam formulation is employed, as opposed to a Timoshenko flexure-shear beam model.

Material inelasticity

Material inelasticity across an element section and length is taken into account by employing a fibre element approach. This enables the accurate representation of structural damage distribution.

The fibre modelling approach incorporated in the inelastic beam-column elements used by SeismoStruct consists of modelling the material inelasticity by dividing a section in various fibres. Each fibre in the section can be assigned a nonlinear uniaxial stress-strain response with the sectional stress-strain response of the member obtained by integrating the nonlinear behaviour of the individual fibres. This subdivision of an element into fibre elements with different material nonlinearity is shown in Figure 4-4.

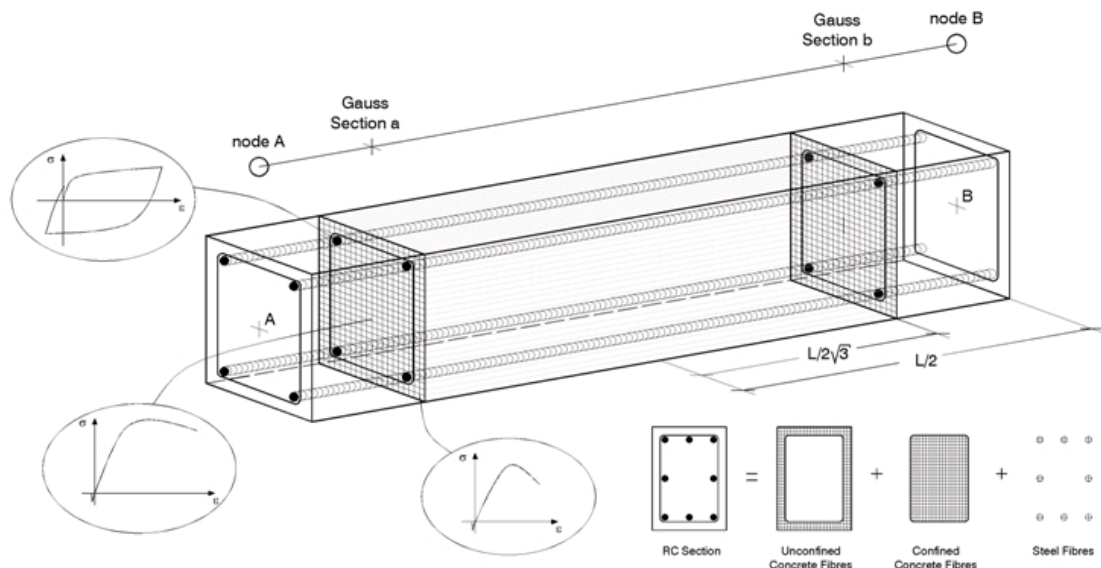


Figure 4-4: SeismoStruct element modelling [9]

If a sufficient number of fibres are employed, the distribution of material nonlinearity across a section will be accurately modelled. A two Gauss point integration scheme is

employed with the strains being computed at the Gauss sections and not the element end nodes. The spread of inelasticity along the element member length can be accurately estimated if a sufficient number of elements are used per structural member.

The help file of SeismoStruct propose that 200 to 400 fibres should be used to accurately estimate the spread of inelasticity over the cross section of a member and that five to six elements should be used per structural member to accurately estimate the spread of material inelasticity over the member length. Analyses were performed to determine the appropriate number of fibre elements for the structural systems investigated in this study and will be discussed in section 4.4.2.

4.3 Input parameters

As shown in Figure 4-1, numerical analyses were performed on three structural systems: a shear wall located on grid A of the example building (Figure 3-2), an edge frame on grid A (Figure 3-2) as well as an internal frame of the building located on grid B (Figure 3-2). The input parameters for the finite element models of the above mentioned structural systems are discussed in this section.

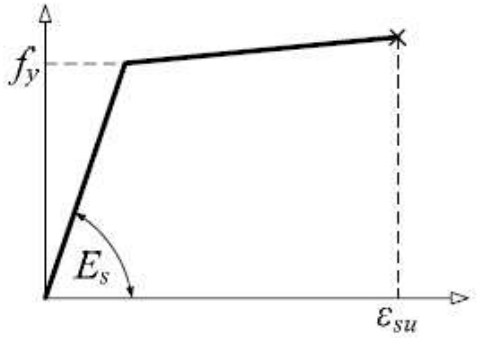
4.3.1 Material properties

Properties were prescribed for three main groups of material types: reinforcement steel, unconfined concrete, as well as confined concrete. The properties of confined concrete are highly dependent on the reinforcement detail of a section and for this reason different material properties were prescribed for the confined concrete of different sections.

Reinforcement steel

SeismoStruct provides various material types with predefined response patterns. A bilinear model including strain hardening was chosen to model reinforcement steel fibres as specified in SIA 2018 [50]. Parameters that are required to define the stress-strain characteristics of the steel model are summarised in Table 4-1.

Table 4-1: Reinforcement steel material properties

Material property	Symbol	Value	Stress-strain relationship
Modulus of elasticity [GPa]	E_s	200.0	
Yield strength [MPa]	f_y	569.25	
Strain hardening parameter [-]	μ	0.005	
Specific weight [kN/m ³]	γ_s	78.0	
Fracture strain [m/m]	ϵ_{su}	0.05	

Confined concrete

A nonlinear constant confinement material model was used to describe the stress-strain characteristic of the confined concrete material. The mean material properties discussed in chapter 3 were used. Figure 4-5 shows the stress-strain relationship defining the confined concrete.

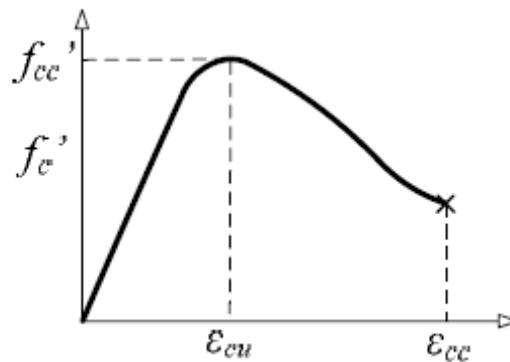


Figure 4-5: Confined concrete stress-strain relationship

Confined concrete was prescribed for the reinforcement layouts of the columns of the example building as well as for the confined zones in the plastic region of the shear wall. Calculation of the material properties of the confined concrete for the different sections is discussed in chapter 3. The prescribed parameters for the various sections are summarised in Table 4-2.

Table 4-2: Confined concrete material properties

Material property	Symbol	Ground to 2 nd floor columns	2 nd floor to roof columns	Shear wall
Compressive strength [MPa]	f_c'	33.0	33.0	33.0
Strain at peak stress [m/m]	ϵ_{cu}	0.0025	0.0026	0.0030
Confinement factor [-]	K	1.049	1.058	1.100
Specific weight [kN/m ³]	γ_c	24.0	24.0	24.0
Collapse strain [m/m]	ϵ_{cc}	0.0041	0.0041	0.0048

No tensile strength was prescribed for the confined concrete. It is also important to note that the concrete compressive strength is the cylinder strength of a 100mm × 200mm specimen.

Unconfined concrete

As unconfined concrete material response is not dependent on reinforcement detail, the same unconfined concrete material was used for all columns and shear wall elements. The nonlinear constant confinement concrete material model was used to define the response of the unconfined concrete as was used for the confined concrete but by using a confinement factor of nearly unity. For reasons related to numerical stability of the nonlinear analyses performed using SeismoStruct, a confinement factor of slightly larger than unity must be prescribed. A value of 1.001 was used for the confinement factor of the unconfined concrete. The same compressive strength and specific weight was prescribed for this material as was used to define the confined concrete. Figure 4-6 shows the stress-strain relationship assumed for the unconfined concrete.

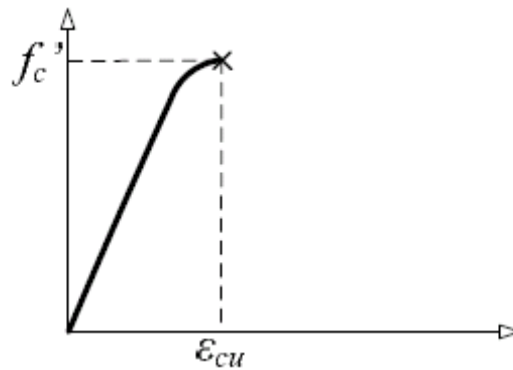


Figure 4-6: Unconfined concrete stress-strain relationship

The strain at peak stress that is applicable to unconfined concrete was calculated as 0.002 as discussed in chapter 3. The collapse strain as prescribed in SABS 0100-1 [24] was chosen.

Slab tension reinforcement has no confinement characteristics and therefore unconfined concrete was chosen for the entire slab section. It should be noted that all permanent and imposed loads in the structure other than own weight is applied on the slab of the building. To take the effect of these additional loads into account the specific weight of the slab material was increased.

For seismic design of building structures the following load combination applies [43]:

$$LC = 1.0DL + 0.3LL + 1.0EL$$

With DL = permanent loads

LL = imposed loads

EL = earthquake loads

From the assumptions made for the design of the example building the load on the slab elements can be determined (see section 3.2 for these assumptions).

Imposed loads: Office building for general use: 2.5kN/m²

Partitions: 1.5kN/m²

$$\Sigma = 4\text{kN/m}^2$$

Permanent loads:	250mm slab: 6kN/m ²
	40mm screed: 0.96kN/m ²
	Ceilings and services: 0.3kN/m ²
	$\Sigma = 7.26\text{kN/m}^2$

Combining these loads according to the appropriate load combination, results in a distributed load of **8.46kN/m²** on slab elements in plan. No distributed load can be applied to the slab in SeismoStruct and therefore the slab specific weight must be adjusted to incorporate this distributed load. The slab member depth should however be kept equal to the true depth to prevent errors in the calculation of the slab stiffness. Since a 250mm slab is used the required specific weight of the slab is as follows:

$$\gamma_{slab} = \frac{8.46\text{kN} / \text{m}^2}{0.25\text{m}} = 33.84\text{kN} / \text{m}^3$$

4.3.2 Sections

Reinforced concrete sections were defined for two column sections (ground to 2nd floor and 2nd floor to roof), two shear wall sections (ground to 4th floor and 4th floor to roof) as well as two slab sections.

Due to negative bending moments in the concrete slab at slab-column connections tension reinforcement is placed in the top layer of the slab at these locations. Between these slab-column connections, bottom tensile reinforcement is placed in the slab to resist positive bending moments resulting from gravity loads. Rules for the curtailment of reinforcement bars as set out in the South African concrete design code SABS 0100-1 [24] was used to determine the reinforcement detail in the slab and hence, alternating reinforcement bars are curtailed at different distances from slab-column connections. A simplified approximation of the reinforcement layout was used to model positions of tensile reinforcement in slab elements.

The span between two adjacent column centres was chosen as six meters. To simplify the modelling of tensile slab reinforcement it was assumed that a top and bottom layer of tension reinforcement is provided over slab-column connections and that it extends to a distance of 2100mm from the centre line of the column supports. The centre 1800mm

of slab between slab-column connections was modelled to only contain bottom tensile reinforcement. Figure 4-7 shows this assumption for the curtailment of the slab tension reinforcement.

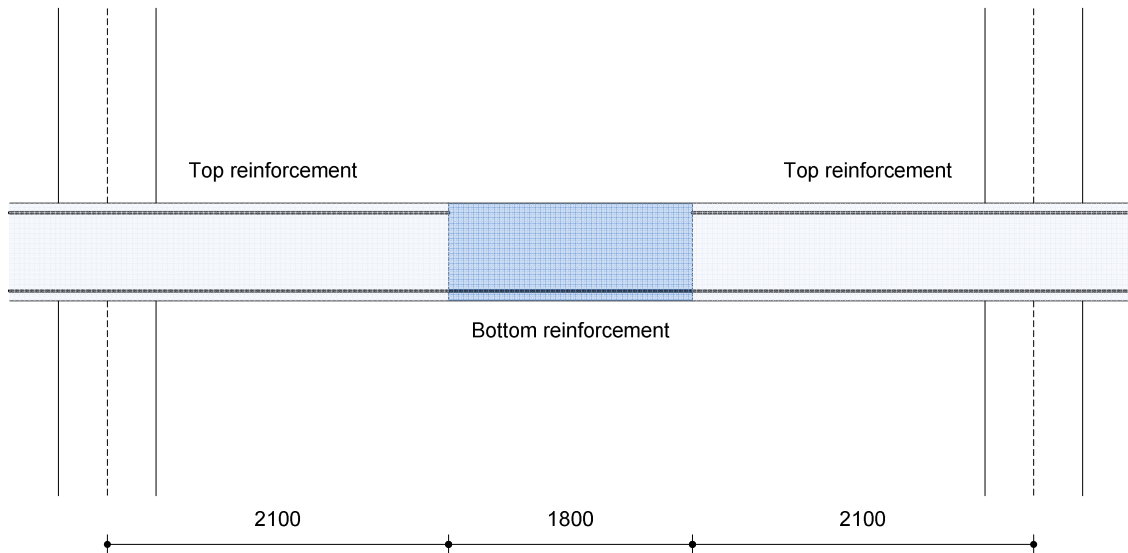
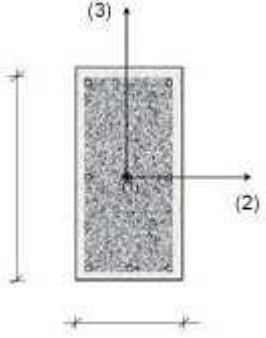
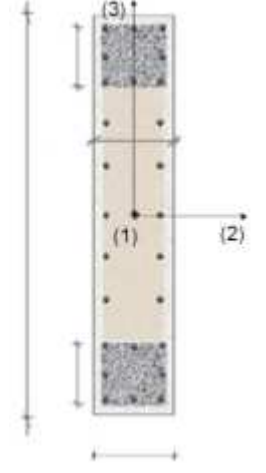


Figure 4-7: Slab reinforcement modelling

SeismoStruct provides the user with various types of sections that can be used to model different structural elements. Table 4-3 shows the section types that were chosen for the various sections.

Table 4-3: Section types [9]

Section	Section type	Default layout
Column sections	Reinforced concrete rectangular section (rcrs)	

Slab sections	Reinforced concrete asymmetric rectangular section (rcars)	
Shear wall sections	Reinforced concrete flexural wall section (rcfws)	

The coordinates and diameters of reinforcement bars are defined for each section according to the reinforcement layout of the relevant section.

4.3.3 Element classes

The element classes section in SeismoStruct is used to define the type of finite element that is to be used to model different structural members. Element types provided by SeismoStruct enable the user to model structural elements such as columns and beams, non-structural components such as masonry infill panels as well as a variety of different boundary conditions such as flexible foundations and seismic isolation of footings.

Three main groups of element types are available: beam-column elements, link elements and mass elements. As only the structural elements of the above ground structure were modelled in SeismoStruct not all of the above mentioned element types were used. All structural members in this investigation were modelled with beam-column elements.

Various different types of beam-column elements are available in SeismoStruct. These include inelastic frame elements (“infrm” and “refrm”), elastic frame elements (“elfrm”), inelastic infill panel elements (“infill”) and inelastic truss elements (“truss”).

Inelastic frame elements were used to model the columns, shear wall and slab elements in the various models as this type of element is divided into fibre elements taking into account the different material types that each of these sections consist of.

Rigid link elements

One additional element type was implemented in the model of the edge frame located on grid A of the example building. Elastic frame elements were used to create rigid link elements between the centre line of the shear wall and the node where the slab elements adjacent to the shear wall would be connected to the edge of the shear wall. The reason for the implementation of these elements can be explained by referring to Figure 4-8 and Figure 4-9.

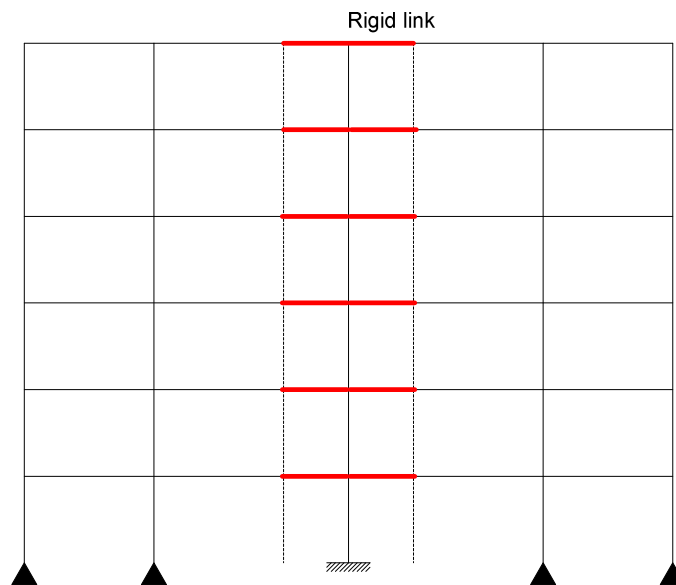


Figure 4-8: Undeformed edge frame

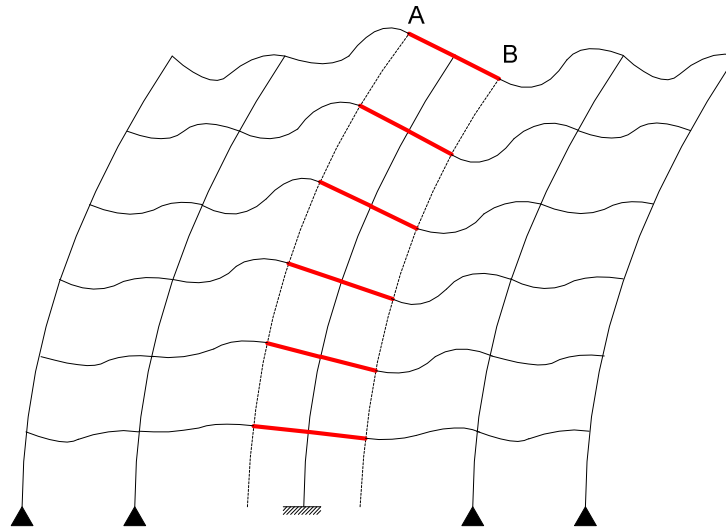


Figure 4-9: Deformed edge frame

The above figures show the centre lines of the columns, slab- and shear wall elements that would be modelled for the edge frame of an arbitrary building structure. Due to the larger dimension of the shear wall in the plane of bending, points where slab elements are connected to the shear wall will tend to lift on the one side of the deformed shear wall (point A shown in Figure 4-9) whilst the slab connections on the other side of the wall will be forced downward (point B in Figure 4-9). The deformed shape of the slab elements at the connection with the shear wall will therefore differ from that at slab-column connections where the slab-column connections tend to undergo only a slight change in elevation.

By connecting slab elements to the centre line of the shear wall in a finite element model of an edge frame, it will lead to an incorrect representation of the real lateral displacement response of the frame. It can be expected that the slab elements adjacent to the shear wall will have a small contribution to the lateral stiffness of the frame compared to the contribution of the shear wall and columns. For this reason it was decided not to model any slab elements adjacent to the shear wall as can be seen in Figure 4-10.

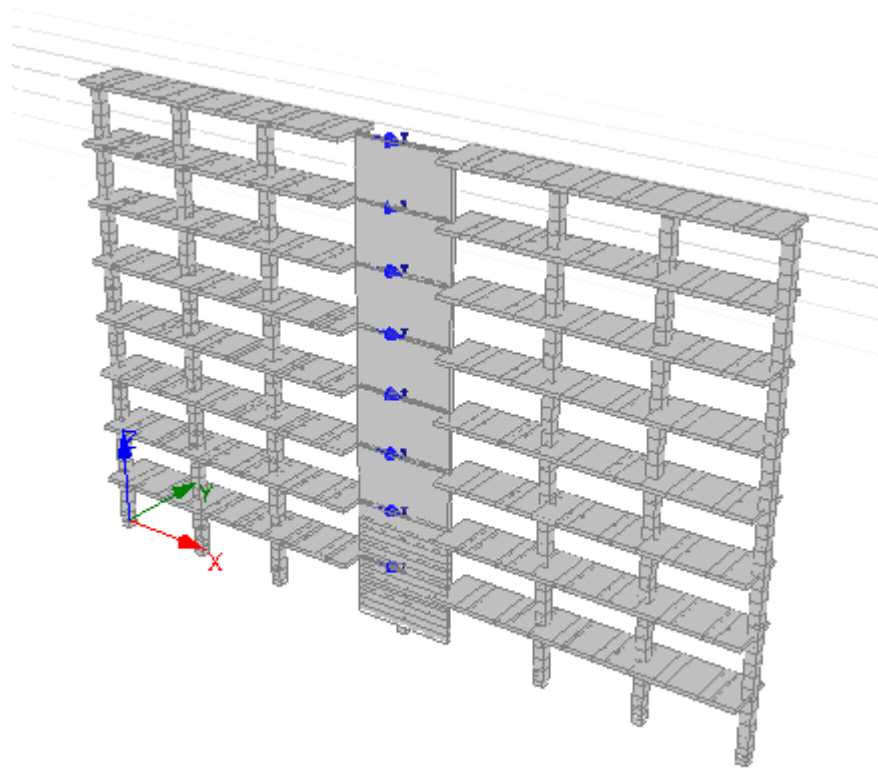


Figure 4-10: SeismoStruct edge frame model

Since the rigid links are modelled with elastic frame elements, it is required to assign elastic sectional properties to these elements. It was decided to assign sectional properties to the rigid link elements that are 100 times greater than the elastic sectional properties of the adjacent slab elements.

To calculate the required stiffness of these rigid links the following elastic material properties were chosen for the slab concrete material [24]:

- Modulus of elasticity: $E = 28\text{GPa}$
- Poisson's ratio: $\nu = 0.2$.

The first step in determining the elastic sectional properties of the rigid links would therefore be to determine elastic properties for the slab section shown in Figure 4-11.

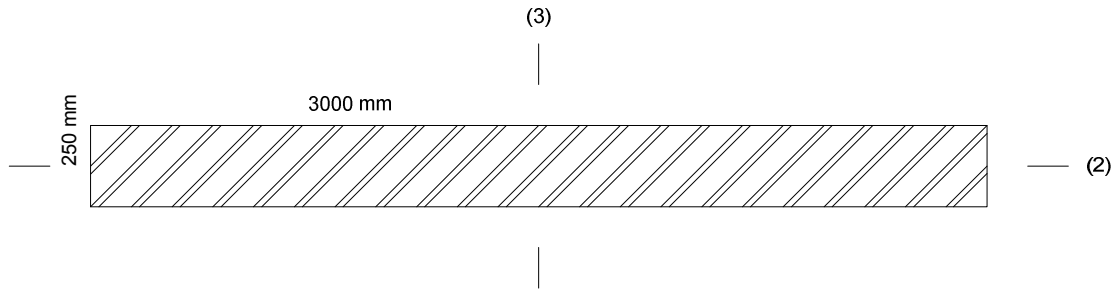


Figure 4-11: Slab element section

The elastic sectional properties of the above shown slab section is as follows:

$$A = 3 \times 0.25 = 0.75 \text{ m}^2$$

$$E = 28 \text{ GPa}$$

$$\therefore EA = 21 \times 10^6 \text{ kN}$$

$$I_2 = \frac{3 \times 0.25^3}{12} = 0.00390625 \text{ m}^4$$

$$\therefore EI_2 = 109375 \text{ kNm}^2$$

These calculated values lead to the following sectional properties being assigned to the rigid link elements:

$$EA = 2100 \times 10^6 \text{ kN}$$

$$EI_2 = 109.375 \times 10^5 \text{ kNm}^2$$

4.4 Element meshing

It is important to choose an appropriate number of elements per structural member to accurately estimate the strain distribution over the length of the member, as well as to choose the appropriate number of fibre elements per section to accurately estimate the strain distribution over the element section. The most suitable element meshing will differ for models of different element sections and therefore the only way to determine the appropriate number of elements is to perform sensitivity analyses of the required element member length and number of fibres to be used per section.

4.4.1 Elements per member length

Two sensitivity analyses were performed: one to determine the required element lengths for slab and column elements, and another to determine the required element

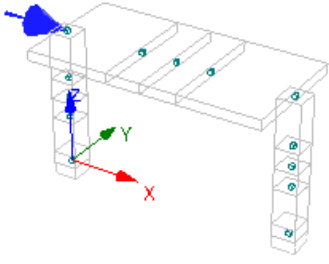
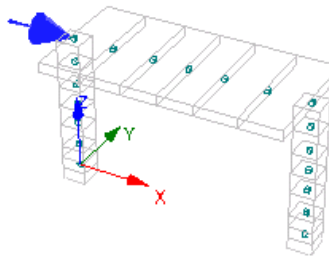
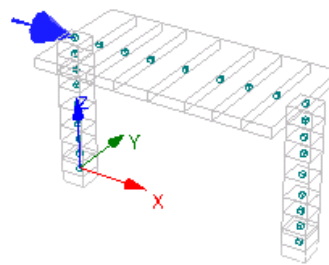
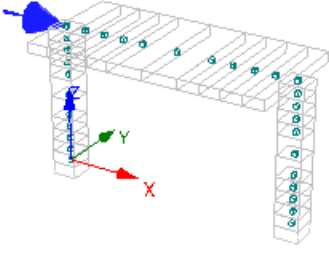
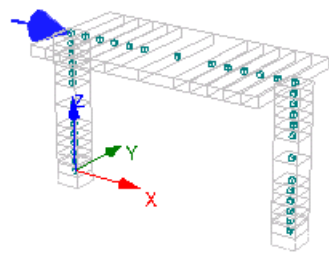
length for shear wall elements. It is stated in the SeismoStruct help file that three to four elements should be used per member.

Slab and column elements

The appropriate number of elements into which the column and slab members should be divided was determined by incrementally refining the element mesh of a simple frame consisting of two columns connected at the top by a slab member. The column dimensions and reinforcement detail were chosen to be identical to that determined for the columns of the building from ground to 2nd floor with the slab detail also identical to that used in the models of the frames. A column height of 3500mm and column spacing of 6000mm was chosen to ensure that the frame represents a panel of the internal frame situated on grid B of the example building (Figure 3-2).

A single horizontal load was applied at the top of one of the columns to perform a pushover analysis. The first mesh that was investigated was a mesh that is automatically generated by SeismoStruct (created by the “Wizard” of SeismoStruct). This meshing divides the members into four elements with the edge elements having a length of 35% of the member length and the centre elements having a length of 15% of the member length. Four other models were investigated by dividing the edge element of the Wizard mesh into two, three, four and five elements respectively. Table 4-4 shows the different models that were investigated.

Table 4-4: Sensitivity analysis models

Mesh	Elements per member	Model
Wizard	4	
Mesh01	6	
Mesh02	8	
Mesh03	10	
Mesh04	12	

The pushover curves obtained from the sensitivity analysis are shown in Figure 4-12.

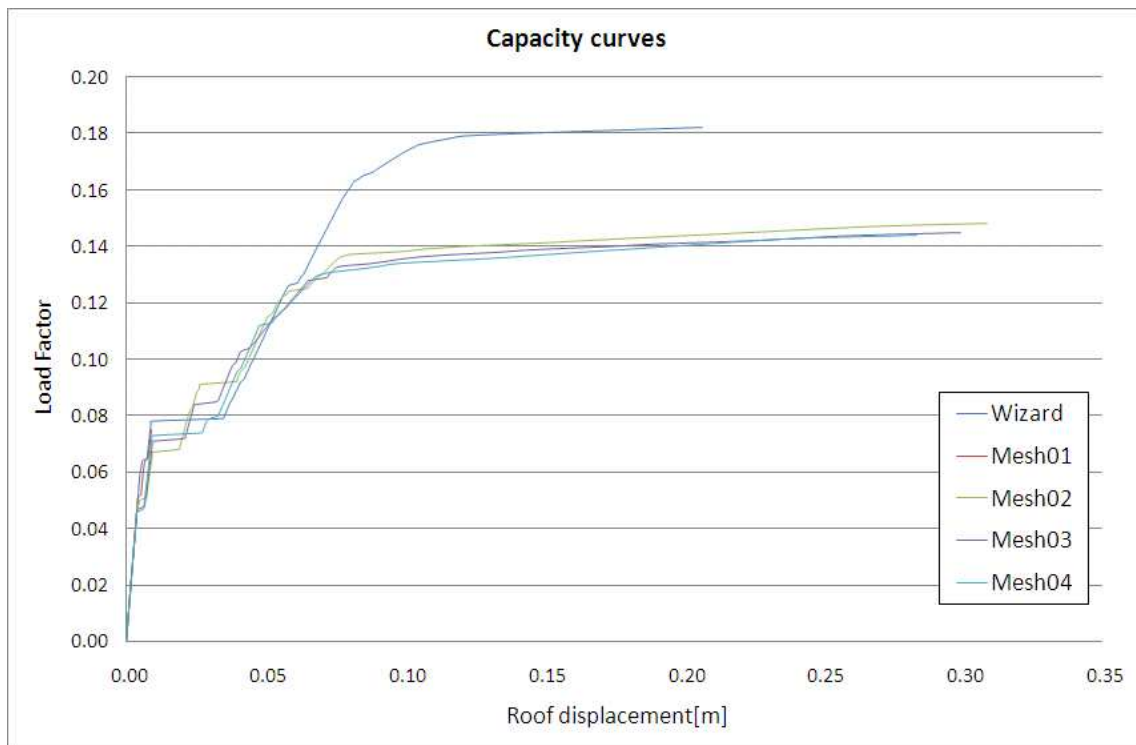


Figure 4-12: Element meshing pushover curves

Conversion was obtained between the pushover curves of Mesh03 and Mesh04 and therefore it was decided that Mesh03 would be an appropriate choice of element mesh.

In subsequent analyses that were performed on the frames using the mesh as determined above, however, led to numerical stability issues. As short element lengths lead to numerical instability, longer element lengths should be chosen.

Important bending moments in the slab elements occur at the face of columns at slab-column connections. It was therefore chosen to use an element mesh for the slab elements, at slab-column connections, that would result in one of the Gauss points of the slab element to lie at a position that would be representative of the face of the column. By using the known distance of the Gauss points from the end nodes of an element as shown in Figure 4-4, the required slab element length could be determined. Hogging moments will occur in slab elements at slab-column connections under gravity loading and therefore any element with a length shorter than the determined length will result in an overestimation of the bending moments at these connections, whilst a longer element length will result in an underestimation of the bending moments as the Gauss point will be situated further away from the column support.

To ensure numerical stability it was also decided to model each column between adjacent floor slabs with five elements as this would result in an element length close to the width of the columns. The final choice of element lengths for slab and column elements is shown in Figure 4-13.

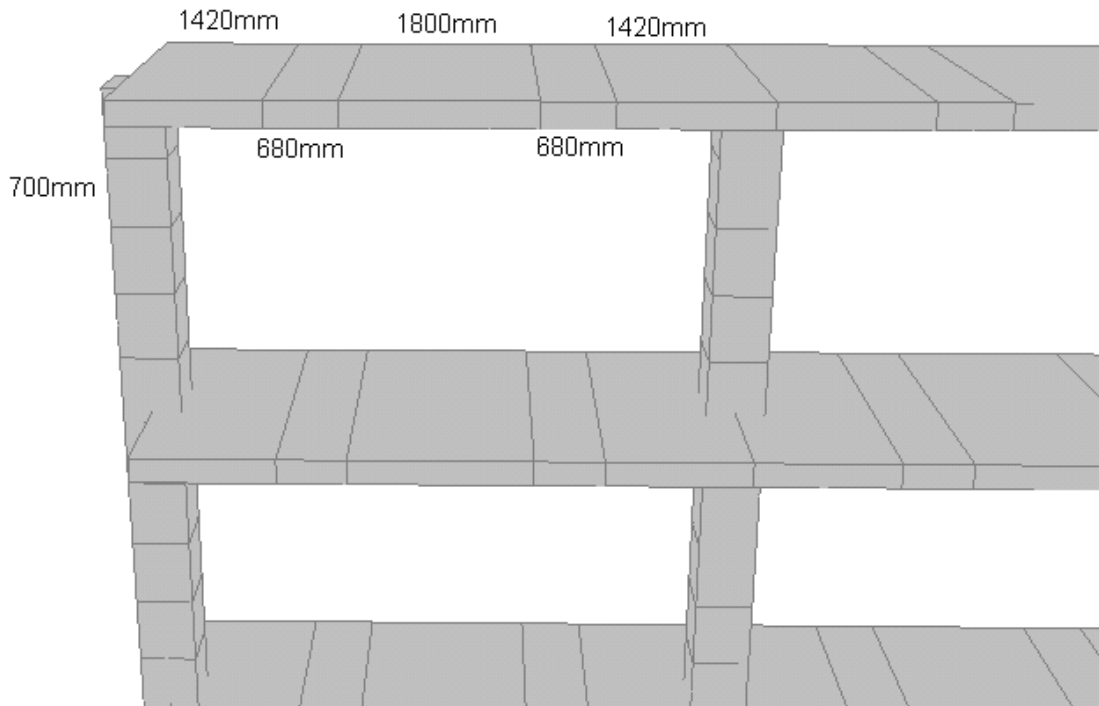


Figure 4-13: Slab and column element mesh

Shear wall elements

No plastic deformation is expected above the height of the plastic hinge region and therefore it was decided to use one shear wall element per storey outside the plastic hinge region. It can be expected that plastic deformation can occur in the bottom 6000mm of the shear wall [2]. For this reason one shear wall element per storey was chosen from the third floor upwards. Within the plastic hinge zone of the shear wall it is important to have a finer mesh as most of the deformation of the shear wall material is expected to occur in this region. Hence, and as a result of a sensitivity analysis, it was decided to use an element length of 500mm for the shear wall elements in this region, with the last element under the second floor being 1000mm long to ensure continuity of the elements.

The chosen shear wall element mesh is shown in Figure 4-14.

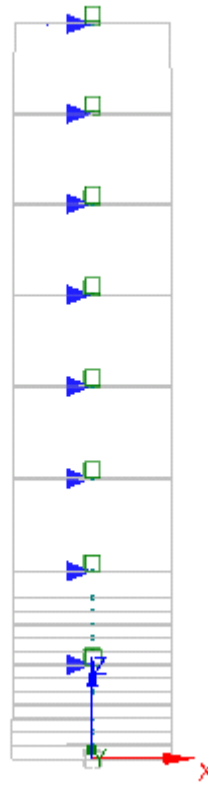


Figure 4-14: Shear wall element mesh

4.4.2 Fibre element mesh

An inelastic frame element section should be divided into a sufficient number of fibre elements to accurately estimate the spread of material inelasticity over the cross section of the element. It is stated in the help file of SeismoStruct that 100 fibre elements should be sufficient to model sections that consist of only one material type and that 200 or more fibre elements should be used to model sections that consist of more than one material. A sensitivity analysis was performed to determine the appropriate number of fibre elements to accurately estimate the spread of material inelasticity over the cross section of the elements.

Inelastic frame elements were used to model the columns, slab elements, as well as the shear wall and therefore sensitivity analyses were performed to determine the required number of fibre elements for each of these types of members.

Column element sections

The same two column frame as described in section 4.4.1 was used to determine the appropriate number of fibre elements for the column sections. Five different numbers of fibre elements per column section were investigated: 200, 300, 400, 500 and 600 fibre elements per column section.

Resulting capacity curves from the pushover analyses that were performed are shown in Figure 4-15.

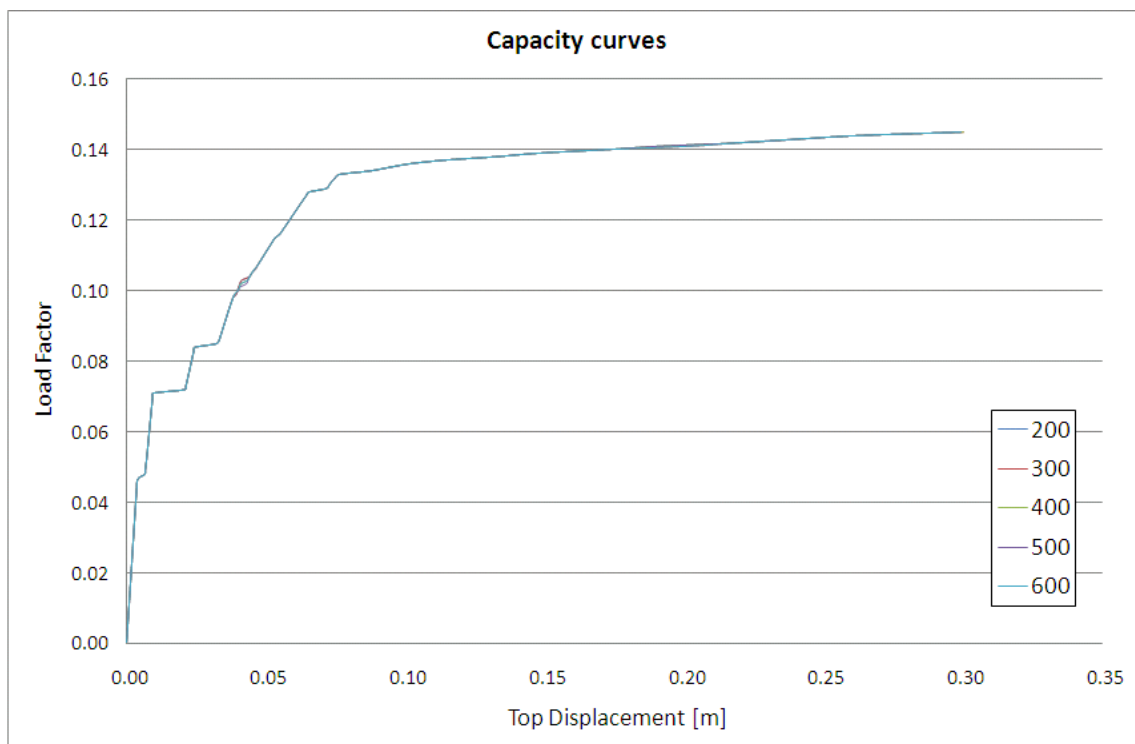


Figure 4-15: Column fibre element sensitivity analysis

All capacity curves compared quite well and therefore it was decided to use **200** fibre elements per column section.

Slab element sections

Using the same two column model, the appropriate number of fibre elements for the slab elements were determined. The same number of fibre elements was investigated as for the column elements. Again the resulting capacity curves compared quite well as can be seen from Figure 4-16 and hence, **200** fibre elements per slab element section were chosen.

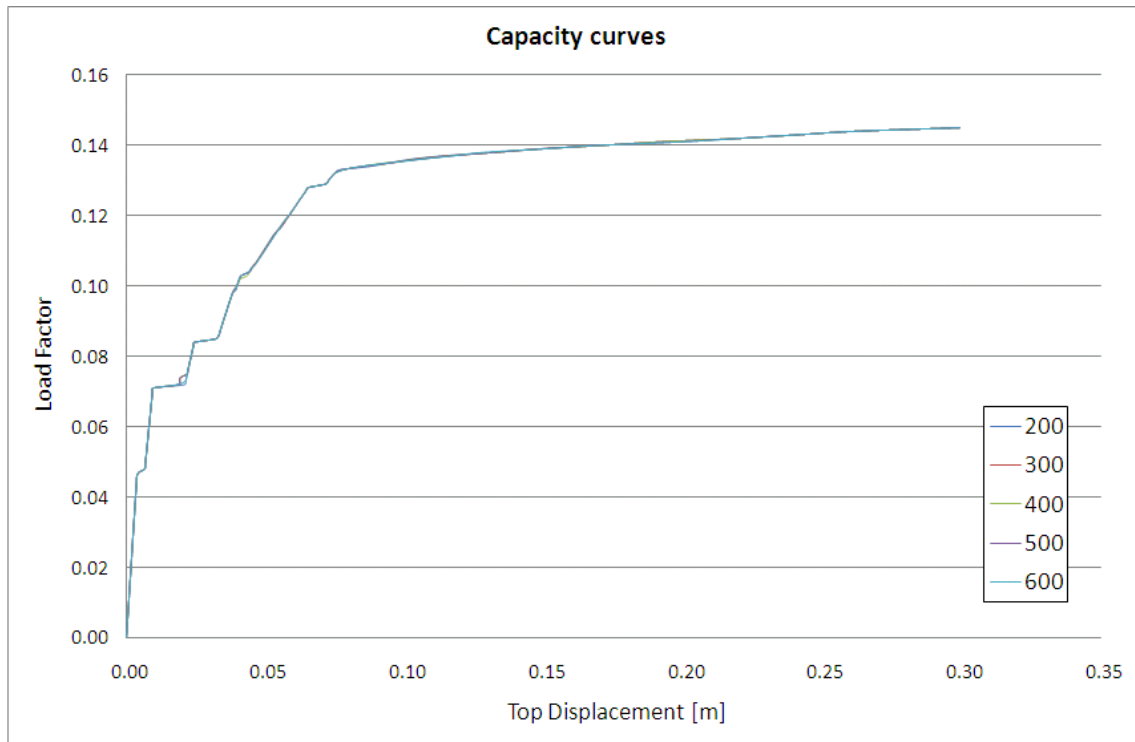


Figure 4-16: Slab fibre element sensitivity analysis

Shear wall element sections

Sensitivity analyses were performed on both shear wall reinforcement layouts used in the building. The shear wall section with the reinforcement layout as provided from ground floor to fourth floor was termed the “plastic section”, whilst the section with reinforcement layout as provided from the fourth floor to roof level was termed the “elastic section”.

The model that was used to investigate the effect of using different amounts of fibre elements per section was a ten meter high shear wall with 500mm element lengths as shown in Figure 4-17.

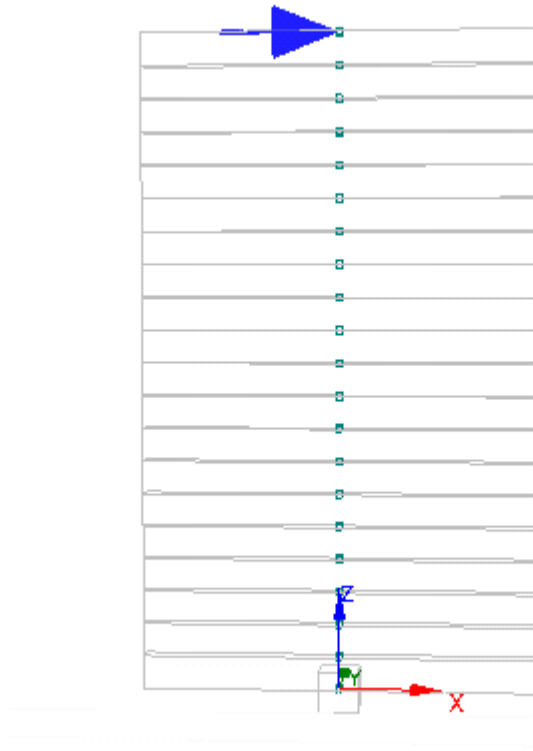


Figure 4-17: Shear wall sensitivity analysis model

Different numbers of fibre elements were investigated for the different shear wall sections used. For the plastic section 200, 500, 1000 and 1500 fibre elements were investigated, whilst 1000, 1500 and 2000 fibre elements were investigated for the elastic section. As can be seen from Figure 4-17 only one lateral load at the top of the shear wall was used to perform the pushover analyses.

Here again it was found that the resulting capacity curves compare quite well for both shear wall sections as shown in Figure 4-18 and Figure 4-19. From a previous investigation performed at the University of Stellenbosch [51] it was shown that 2000 fibre elements provided good results to determine the capacity of lateral loaded shear wall members. For this reason, and because the capacity curves obtained from the sensitivity analyses compared quite well, it was decided to employ 2000 fibre elements per shear wall section.

From Figure 4-18 and Figure 4-19 it is clear that high and low peaks were obtained on the resulting pushover curves. These peaks occur due to iterative difficulty in the nonlinear solution performed by the solver of SeismoStruct. The solver performs a number of iterations per displacement increment until convergence is obtained. If the

displacement increment is chosen too large, or the maximum number of iterations allowed per displacement increment is chosen too small, the number of iterations could be insufficient to achieve convergence. This may result in unrealistically high or low lateral force values being calculated by the solver. By reducing the displacement increment and/or increasing the number of iterations allowed per displacement increment, smoother pushover curves can be obtained.

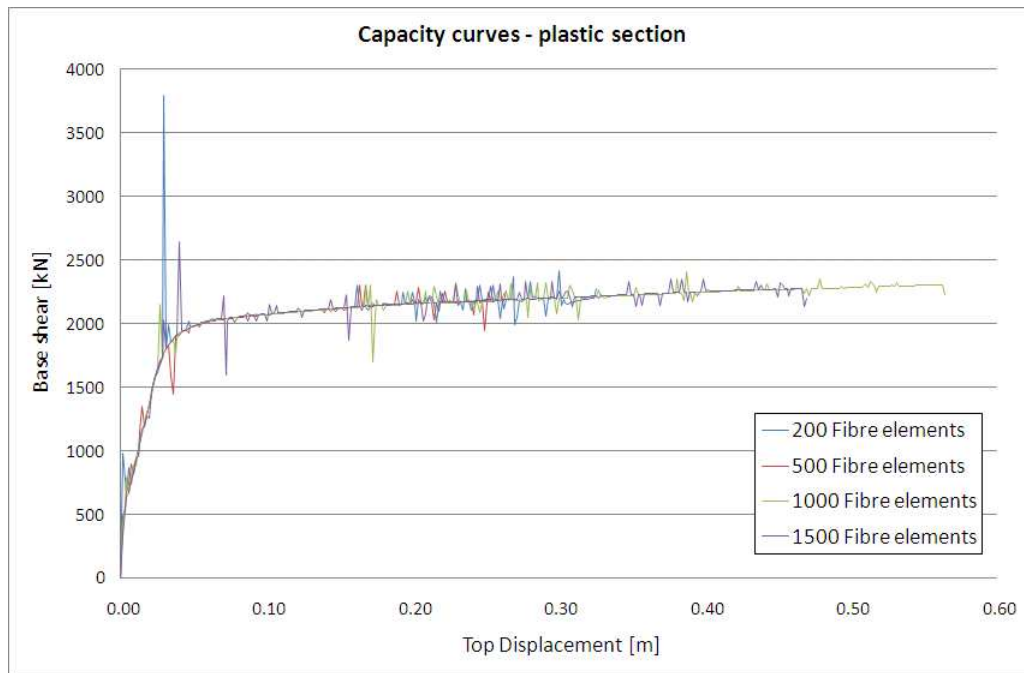


Figure 4-18: Shear wall fibre element sensitivity analysis – plastic section

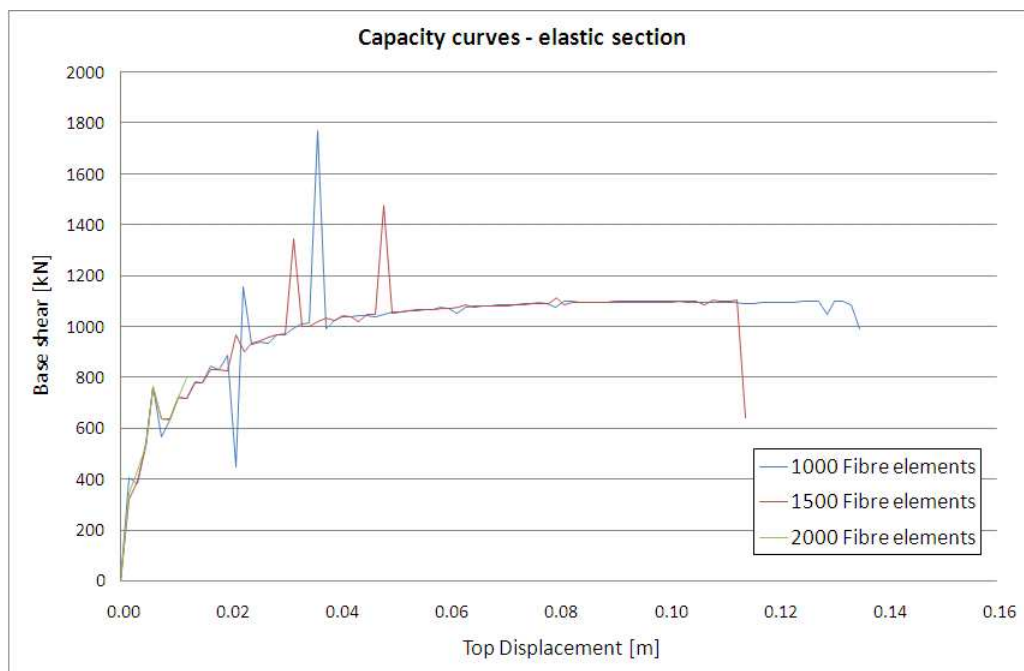


Figure 4-19: Shear wall fibre element sensitivity analysis – elastic section

4.5 Verification of software

To ensure that the pushover analyses performed using SeismoStruct provide accurate estimations of the capacities of different structural systems against lateral loading, different verification analyses were performed. These investigations include the following:

- The calculation of internal forces.
- The identification of bending moment failures.
- The calculation of roof displacements.
- The calculation of material strains.

4.5.1 Slab element internal forces

It is essential that the internal forces in a structural system are correctly calculated by the software to ensure that failures within the system can be correctly determined. These internal forces change incrementally from that due to gravity loading as the lateral applied loading increases.

To determine whether internal forces are calculated correctly with only gravity loads applied, the bending moments and shear forces in the first floor slab of the internal frame situated on grid B of the example building (Figure 3-2) was investigated. Results obtained from SeismoStruct were compared to that resulting from a model of the slab in Prokon [44].

SeismoStruct

The bending moments and shear forces in the first floor slab of the internal frame were investigated taking only the own weight of the slab into account.

Prokon

A model of the first floor slab was analysed using the *Continuous Beam* module provided by Prokon [44] as shown in Figure 4-20.

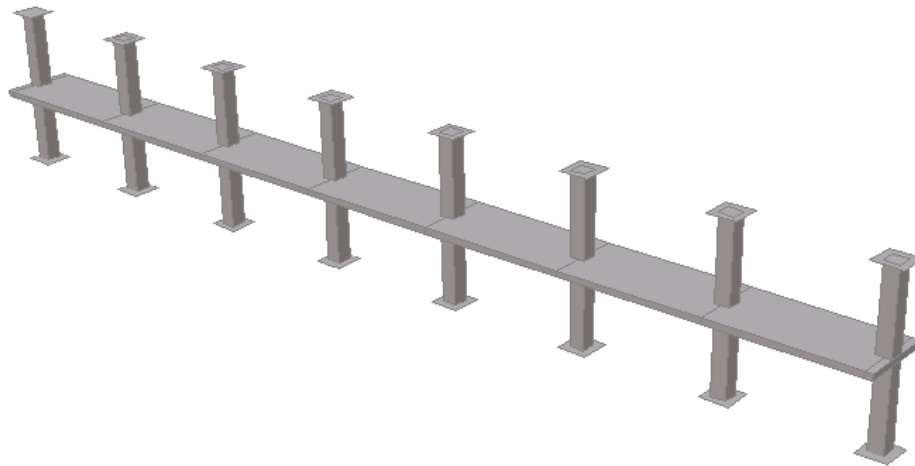


Figure 4-20: Continuous Beam model

Only linear material properties can be analysed in this module. Since the slab is only loaded with its own weight it is assumed that the slab element material will remain elastic. The elements provided by Prokon allow quadratic interpolation of bending moments and therefore linear interpolation of shear forces.

From the output of the analysis a maximum sagging moment of 28.26kNm was obtained in the first span with a maximum hogging moment of 56.22kNm at the first interior support. The maximum shear force in the slab was obtained at the first interior support with a value of 55.16kN.

Comparison of results

Bending moment and shear force results as obtained from SeismoStruct and Prokon compared quite well as shown in Figure 4-21 and Figure 4-22.

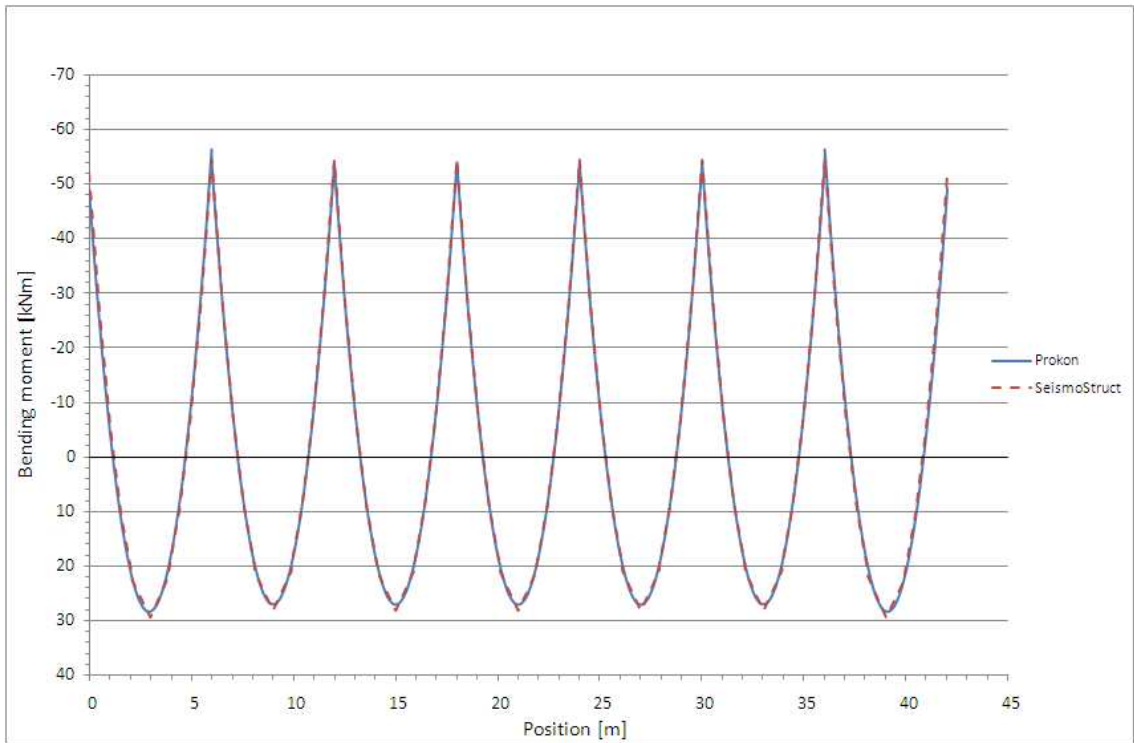


Figure 4-21: Bending moment results

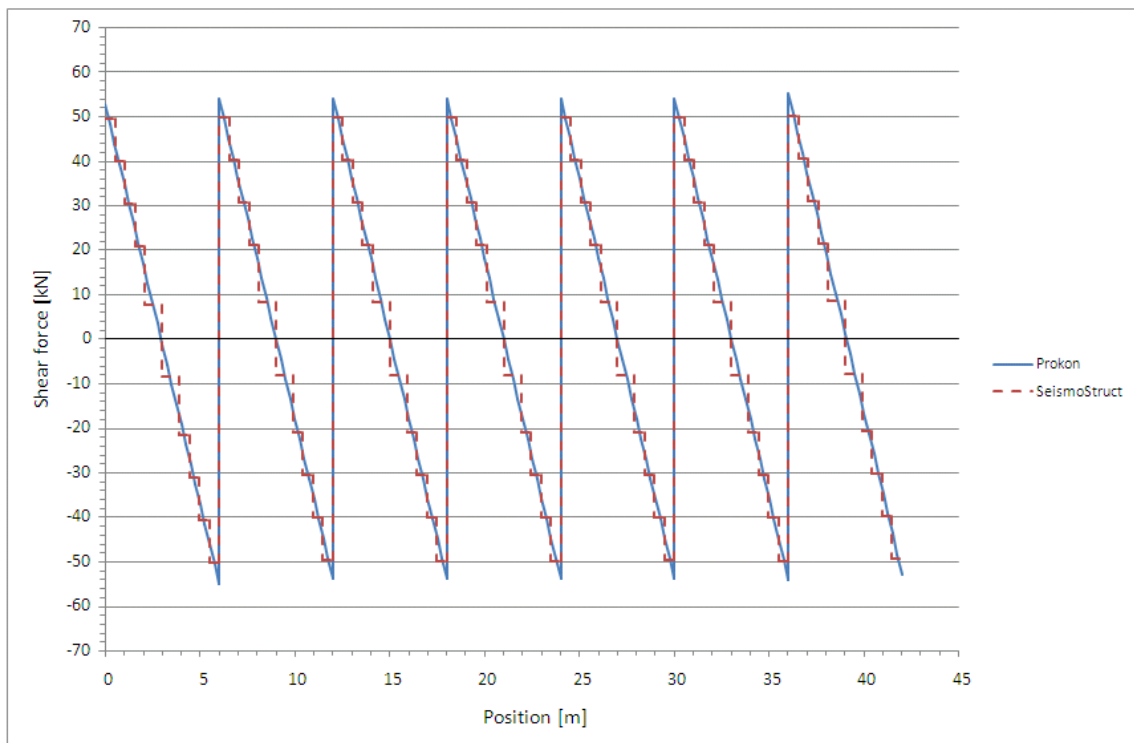


Figure 4-22: Shear force results

A summary of the values of the maximum internal forces are shown in Table 4-5.

Table 4-5: Critical internal forces – first floor slab

Source	Sagging moment [kNm]	Hogging moment [kNm]	Shear force [kN]
SeismoStruct	29.32	54.49	50.22
Prokon	28.26	56.22	55.16

Since the results as obtained from SeismoStruct and Prokon compare quite well it can be stated with confidence that the initial internal forces in the slab elements are computed accurately by SeismoStruct when no lateral loads are applied to the structure.

4.5.2 Bending moment failure

Bending moments in slab elements exceeding the flexural capacity of these elements are expected to be a critical mode of failure. The correct identification of a bending moment failure by the software was therefore investigated.

Material strain limits were set in SeismoStruct as performance criteria for the tensile reinforcement in slab elements with the aim of identifying the formation of a plastic hinge. Tensile strains develop in the slab tensile reinforcement due to bending moments with the bending moment resistance of the slab determined by the amount of tensile reinforcement placed in the slab. It is therefore expected that the material strain limit in the tensile reinforcement should be reached when the bending moment capacity of the slab is exceeded.

To investigate whether internal slab bending moments exceeds its flexural capacity when a steel yielding material strain limit is reached, a simple frame was modelled in SeismoStruct. The frame consists of two columns and of three floor slab members connecting the columns. Reinforcement details and member dimensions were chosen to be identical to that of the example building and the same performance criteria were set as determined earlier. A pushover analysis was performed on the frame using a triangular distribution of incremental lateral forces. The frame is shown in Figure 4-23.

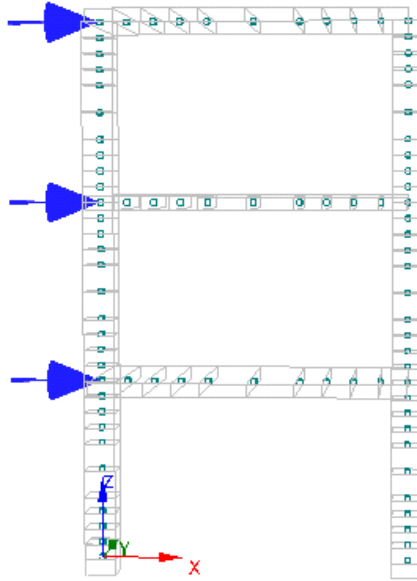


Figure 4-23: Three storey frame model

From the output of the pushover analysis it was found that the steel material yield strain limit was first reached in the slab element at the slab-column connection of the first floor and the column to which the lateral loading was applied. The strain limit was reached when a base shear value of 148.251kN was reached and the corresponding bending moment in the relevant element was calculated as $M_U = 168.78\text{kNm}$ and resulted in tension in the bottom reinforcement layer.

The critical slab element was provided with 17 Y16 reinforcement bars in the top layer and seven Y16 reinforcement bars in the bottom layer. The seven Y16 reinforcement bars were used to calculate the bending moment resistance as these bars are in tension. Using the mean material factors as discussed in section 3.3, the sagging moment resistance of the slab at this position was hand calculated as $M_R = 160.96\text{kNm}$. It is therefore clear that the bending moment resistance of the slab was indeed exceeded and that a plastic hinge could therefore be expected to have developed in the slab.

It was therefore assumed that the calculated steel material strain limit was correct and that this enabled SeismoStruct to correctly identify the formation of a plastic hinge.

4.5.3 Roof displacement

The control node when performing a pushover analysis is typically situated at roof level. This results in a capacity curve showing the nonlinear relationship between the

base shear force and lateral roof displacement. For this reason it is essential that the calculation of the lateral roof displacement is accurate. To investigate the roof displacement calculated by SeismoStruct, the same two-column, three floor slab frame described in section 4.5.2 was employed. It was decided to compare the roof displacement calculated by SeismoStruct to that predicted for the same frame using the *Frame* module of Prokon [44].

Only elements with linear elastic material properties can be analysed in this module of Prokon and therefore the material properties of the frame in SeismoStruct was adjusted to have only linear elastic material properties as to ensure comparable results from the two analyses. A target loading on the frame as well as the number of increments that should be used to apply the incremental load is defined in SeismoStruct by the user. For the purpose of this investigation a target base shear value of 2000kN with a target roof displacement of 1.5m was chosen. A response control pushover analysis was performed with 1000 lateral roof displacement increments chosen. It was chosen to investigate the roof displacement at the tenth increment leading to lateral loads on the first, second and third floor as follows:

$$\begin{Bmatrix} F_1 \\ F_2 \\ F_3 \end{Bmatrix} = \begin{Bmatrix} 13.024kN \\ 26.047kN \\ 39.071kN \end{Bmatrix}$$

These loads were consequently also applied to the frame in Prokon and the roof displacements obtained from the two analyses compared. A lateral roof displacement of **13.50mm** was obtained from the SeismoStruct output, whilst the result from Prokon was **14.28mm**. It was decided that the 5.5% difference in the results are acceptable for the purpose of this investigation and hence, that SeismoStruct provides acceptably accurate estimations of lateral roof displacements during an elastic analysis.

4.5.4 Strain calculation

Correct identification of failures in structural systems associated with material strain limits depend on the accuracy by which strain limits are determined as well as the calculation of material strains by the software. The accuracy of the material strains calculated by the software was therefore investigated.

The estimation of strains in fibre elements is highly dependent on the length of the element. It is therefore essential that the calculated strains should be investigated for the chosen element mesh. Steel material strain calculation in the internal frame located on grid B of the example building was investigated.

As stated previously a steel material yield strain limit of $\epsilon_{sy} = 0.00285$ was calculated and used as one of the performance criteria. The steel yielding criteria was exceeded in a slab element on the seventh floor. This value for steel material strain was investigated by calculating a steel strain value from the chord rotation of the elements where the failure was identified, as the chord rotation is not dependant on the element length.

At the location (and lateral force value) where the strain limit was identified an internal bending moment of $M_u = 204.458\text{kNm}$ and a chord rotation of $\theta = 0.0121$ radians were calculated by SeismoStruct. The length of the relevant element was 1420mm and taking this element length into consideration the curvature was calculated as follows:

$$\phi = \frac{\theta}{\ell} = \frac{0.0121}{1.42} = 0.00852\text{m}^{-1}$$

Bernoulli beam theory is employed in the frame elements used by SeismoStruct and therefore the assumption is made that sections that are initially plane and orthogonal to the neutral axis of the element will remain plane and orthogonal to the deformed neutral axis. The steel material strain was therefore calculated using the curvature determined above. By using the assumptions for beam bending as provided in the South African concrete design code SABS 0100-1 [24] the bending moment resistance could be calculated. The strain distribution of the code assumption is shown in Figure 4-24.

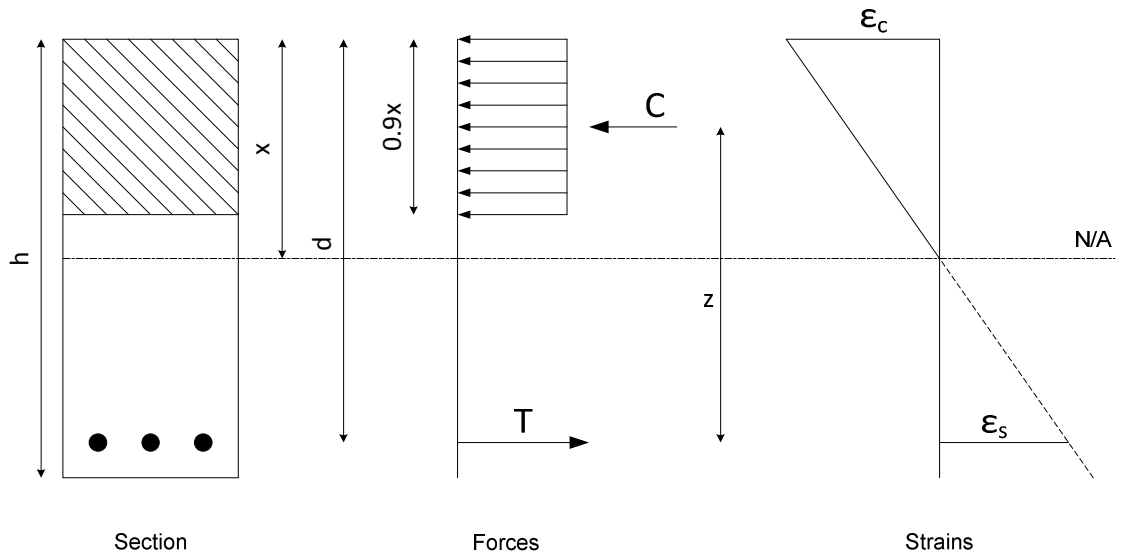


Figure 4-24: SABS 0100-1 bending assumption

From the above, strains can be related to curvature by calculating the slope of the strain distribution over the section:

$$\phi = \frac{\varepsilon_s}{d - x}$$

$$\therefore \varepsilon_s = \phi \cdot (d - x)$$

The depth of the neutral axis (x) should therefore be calculated by setting the resistance bending moment equal to the internal bending moment.

$$M_u = T \cdot z$$

$$\therefore M_u = f_{ym} \cdot A_s \cdot (d - 0.45x)$$

$$\therefore x = \frac{d}{0.45} - \frac{M_u}{0.45 \cdot f_{ym} \cdot A_s}$$

The steel material properties as determined in section 3.3 were used for this calculation. It leads to a steel material strain of $\varepsilon_s = 0.0027$. The strains are therefore as summarized in Table 4-6.

Table 4-6: Internal frame strain investigation

Case	Strain
Performance limit	0.00285
Identified	0.00286
Hand calculation	0.00270

The strain values compare well, showing a 5.3% difference between the performance limit and the value obtained from simple hand calculations.

As the calculation of the element chord rotation is not sensitive to the length of an element and the strains determined above compare reasonably well, it can be stated that the steel material strains determined by SeismoStruct compare well with the value corresponding to the relevant internal bending moment. Calculation of the internal forces were verified in section 4.5.1 and since it was found that the internal force calculation is accurate, it follows that the results obtained from SeismoStruct for the chosen element mesh can be considered suitable.

4.6 Capacity curves

Using SeismoStruct to perform pushover analyses on structural systems of the example building, capacity curves were determined for the internal frame, shear wall and edge frame. Two patterns of lateral loading were used as discussed earlier.

4.6.1 Internal frame

The internal frame that was investigated is shown in Figure 4-25.

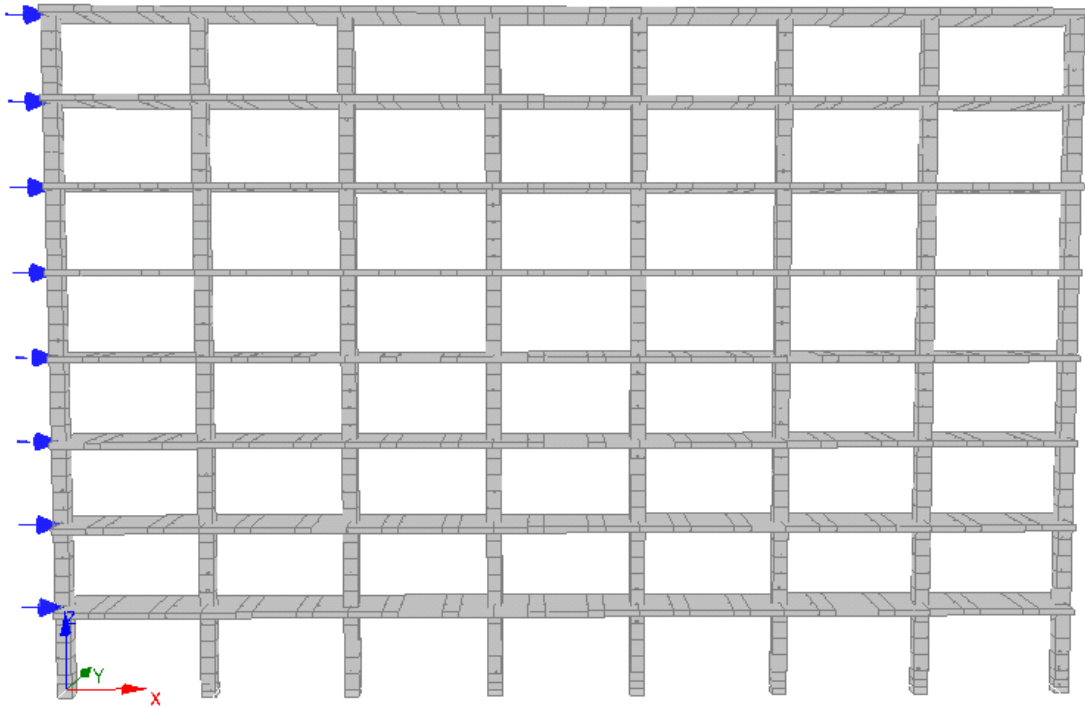


Figure 4-25: Internal frame

Displacement controlled pushover analyses were performed whereby a constant lateral roof displacement increment is defined. The lateral loads required to obtain the lateral roof displacement is calculated during each displacement increment. A lateral roof displacement increment of 1.5mm was chosen.

Nonlinear response is obtained from the result of a pushover analysis as the material strains enter the inelastic range. The resulting nonlinear pushover curve up to the value of maximum base shear therefore defines the lateral force-displacement capacity of the structure. Using the procedure described in FEMA 440 [20], a bilinear approximation could be made of the nonlinear capacity curve obtained from the pushover analysis.

Two pushover analyses were performed on the frame: one using a uniformly distributed lateral loading pattern and another using a triangular distributed lateral loading pattern. Points where different performance criteria were first exceeded were also plotted on the capacity curves. The capacity curves that were obtained from the pushover analyses as well as the bilinear approximation of these curves are shown in Figure 4-26 and Figure 4-27.

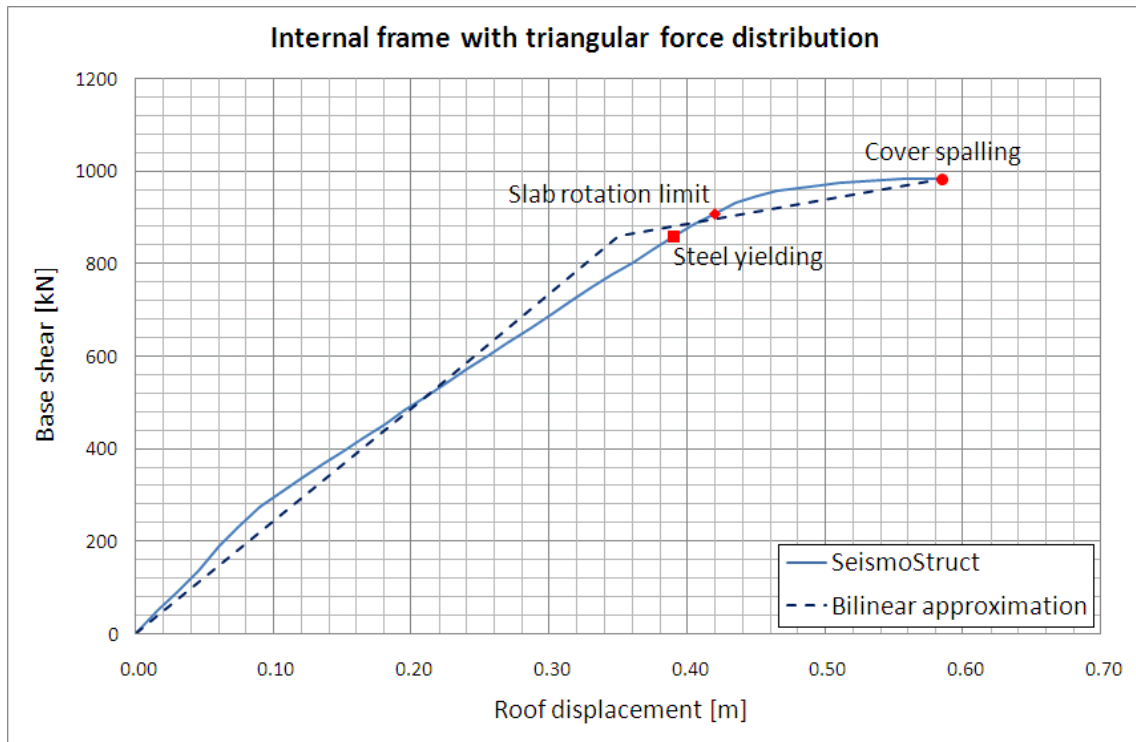


Figure 4-26: Internal frame, triangular force distribution

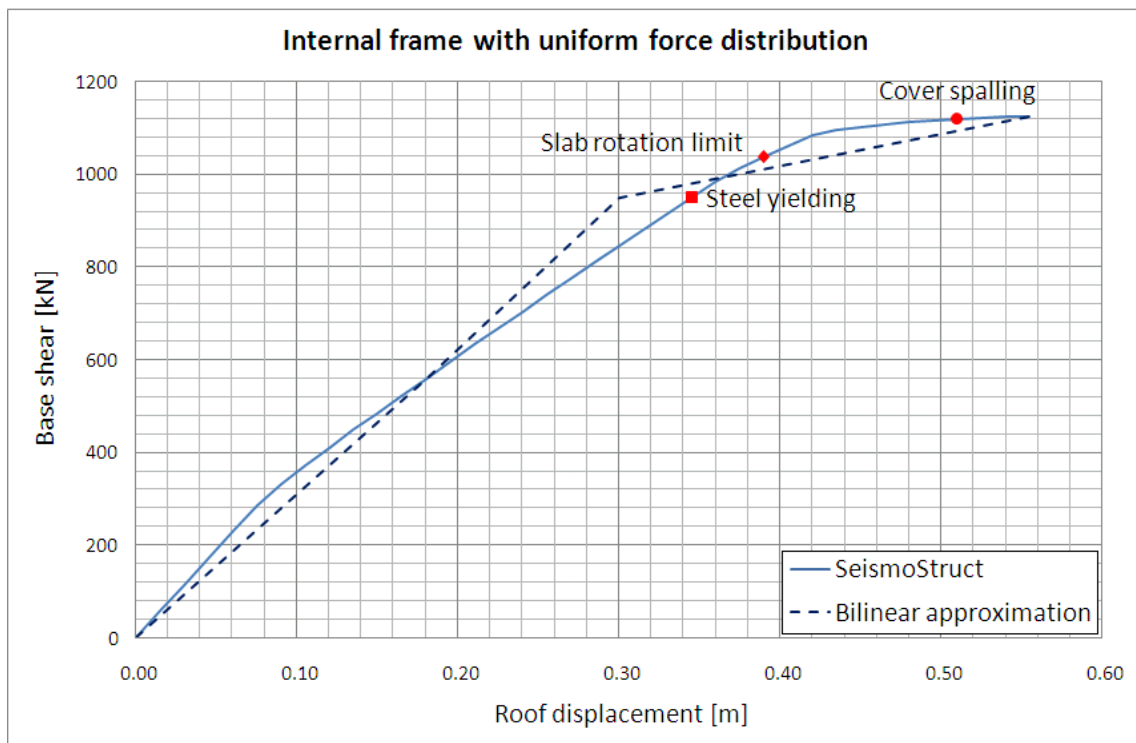


Figure 4-27: Internal frame, uniform force distribution

From the above it is clear that the steel material yield limit is reached before the slab plastic hinge rotation limit is reached. This can be expected as a plastic hinge should first form before the maximum permitted plastic hinge rotation is reached. The

compressive strain limit of cover concrete is reached near the end of both of the capacity curves.

As stated in the designers' guide to EN 1998-1 and EN 1998-5 [7] only the most unfavourable capacity curve of the two lateral load approximations should be used for further investigation. The most unfavourable result will be the curve that results in the largest lateral roof displacement for a given base shear force. For this reason the most unfavourable result will be the lower of the two curves when drawn on the same axis.

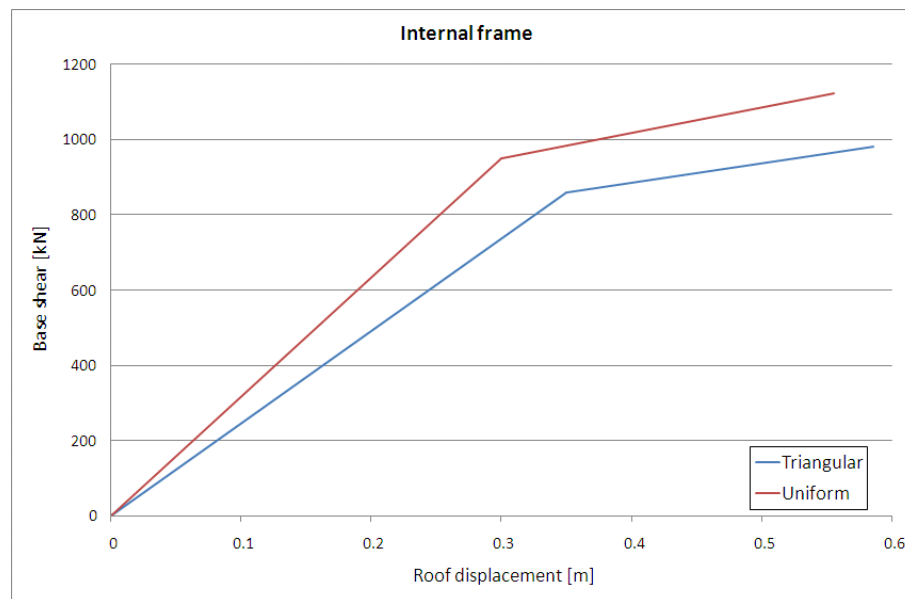


Figure 4-28: Internal frame comparison

From Figure 4-28 it is clear that the capacity curve from the pushover analysis using a triangular lateral force distribution is the most unfavourable result.

Values that define the bilinear approximation of the capacity curve obtained by applying a triangular lateral force distribution are shown in Table 4-7.

Table 4-7: Internal frame capacity curve

Position	Roof displacement [mm]	Base shear [kN]
Start	0.0	0.000
60% Yield	210.0	511.109
Yield	350.0	857.950
Ultimate	585.0	981.737

4.6.2 Shear wall

The lateral force-displacement behaviour of the shear wall is discussed in this section.

No slab elements were modelled with the shear wall and therefore the gravity load effect of the contributing slab area had to be taken into account by adding lumped mass at the various floor levels. The contributing slab area for gravity loading on the shear wall was taken to be half the slab span between the wall and adjacent columns. The contributing slab area is as shown in Figure 4-29 with a length of 12 meters and a width of 3 meters. With the slab density as calculated in section 4.3.1 the lumped mass at each floor level was calculated as:

$$Mass = Density \times Volume$$

$$\therefore M = \frac{33.84kN/m^3}{9.81m/s^2} \times (12m \times 3m \times 0.25m) = 31050kg$$

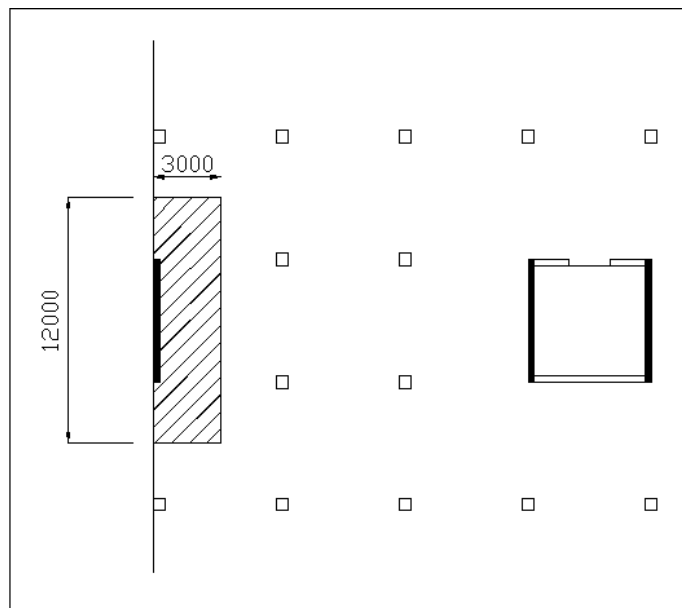


Figure 4-29: Contributing slab area to shear wall

These permanent lumped masses as well as the incrementally increasing lateral forces were applied at the same nodes located at the different floor levels as shown in Figure 4-14.

It was found that a displacement increment of 0.67mm resulted in a smooth capacity curve from the output of the response control pushover analyses. Positions of

performance criteria being reached for the first time are shown on the capacity curves. Figure 4-30 and Figure 4-31 show the resulting capacity curves.

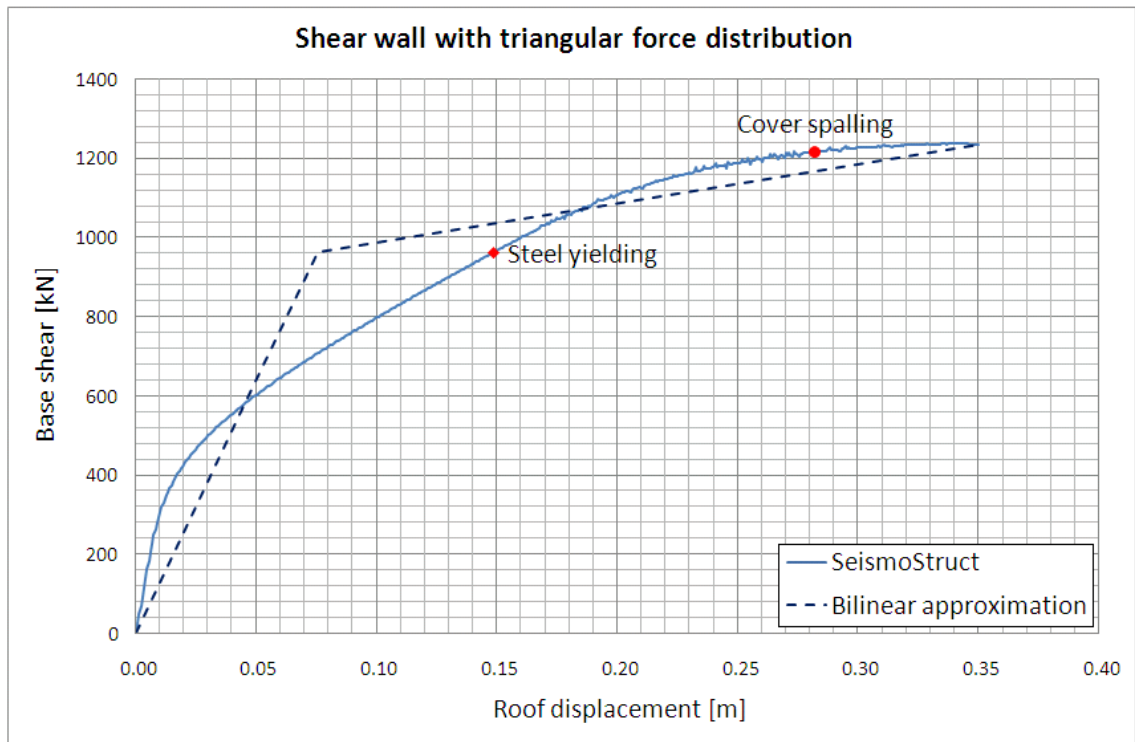


Figure 4-30: Shear wall, triangular force distribution

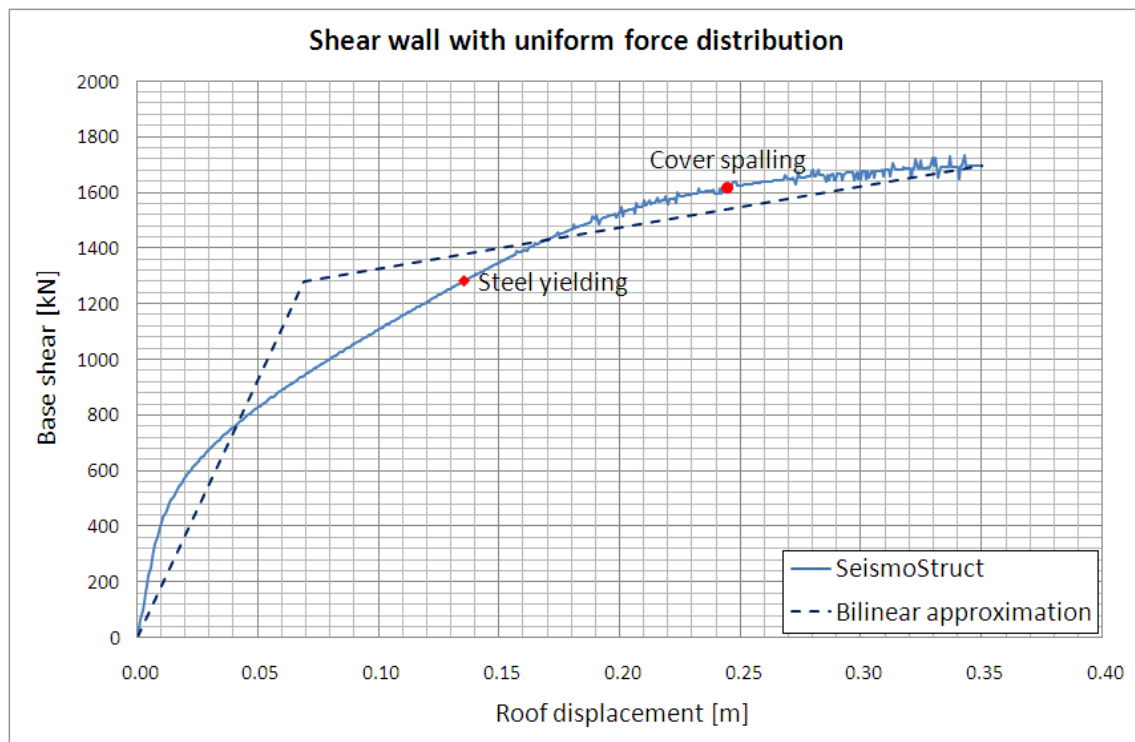


Figure 4-31: Shear wall, uniform force distribution

Locations where identified performance criteria are first reached compare well between the two resulting capacity curves. In both cases the steel material yield strain and compressive cover concrete strain limits are reached.

The procedure described in FEMA 440 was used to determine a bilinear approximation for the capacity curves. Comparing the bilinear approximations of the capacity curves it is clear that the triangular distribution of lateral forces was the most unfavourable loading pattern as shown in Figure 4-32.

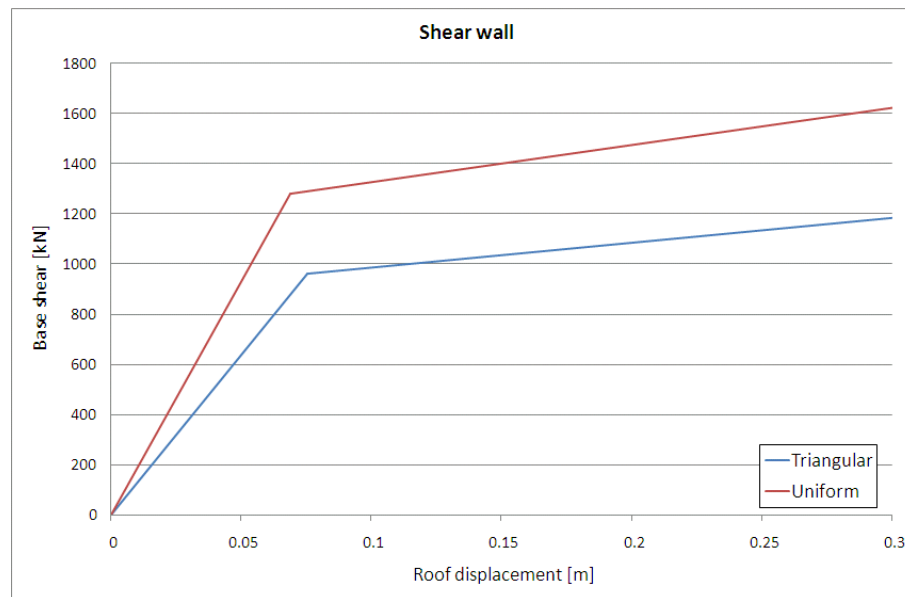


Figure 4-32: Shear wall comparison

Values that define the bilinear approximation of the capacity curve obtained by applying a triangular lateral force distribution are as shown in Table 4-8.

Table 4-8: Shear wall capacity curve

Position	Roof displacement [mm]	Base shear [kN]
Start	0.0	0.000
60% Yield	45.3	579.910
Yield	75.6	961.915
Ultimate	350.0	1234.067

4.6.3 Edge frame

The lateral force-displacement behaviour of the edge frame located on grid A of the example building (Figure 3-2) is discussed in this section.

For the edge frame it was observed that a displacement increment of 2mm resulted in a smooth capacity curve. Performance criteria limits that were exceeded in the pushover analysis of the edge frame, using a triangular- and uniform lateral load distribution, were:

- Steel material yield strain limit.
- Cover concrete compressive strain limit.
- Core concrete compressive strain limit.
- Steel material fracture strain limit.

Bilinear approximations of the capacity curves were determined by following the procedure described in FEMA 440 with resulting capacity curves as shown in Figure 4-33 and Figure 4-34.

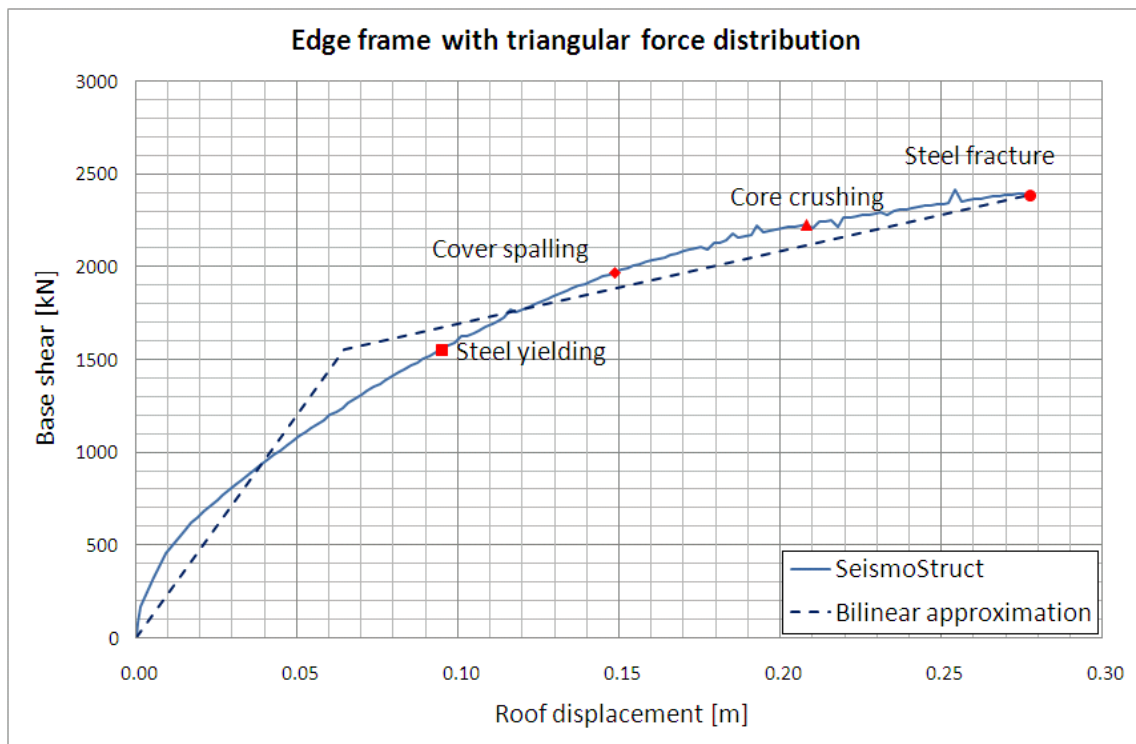


Figure 4-33: Edge frame, triangular force distribution

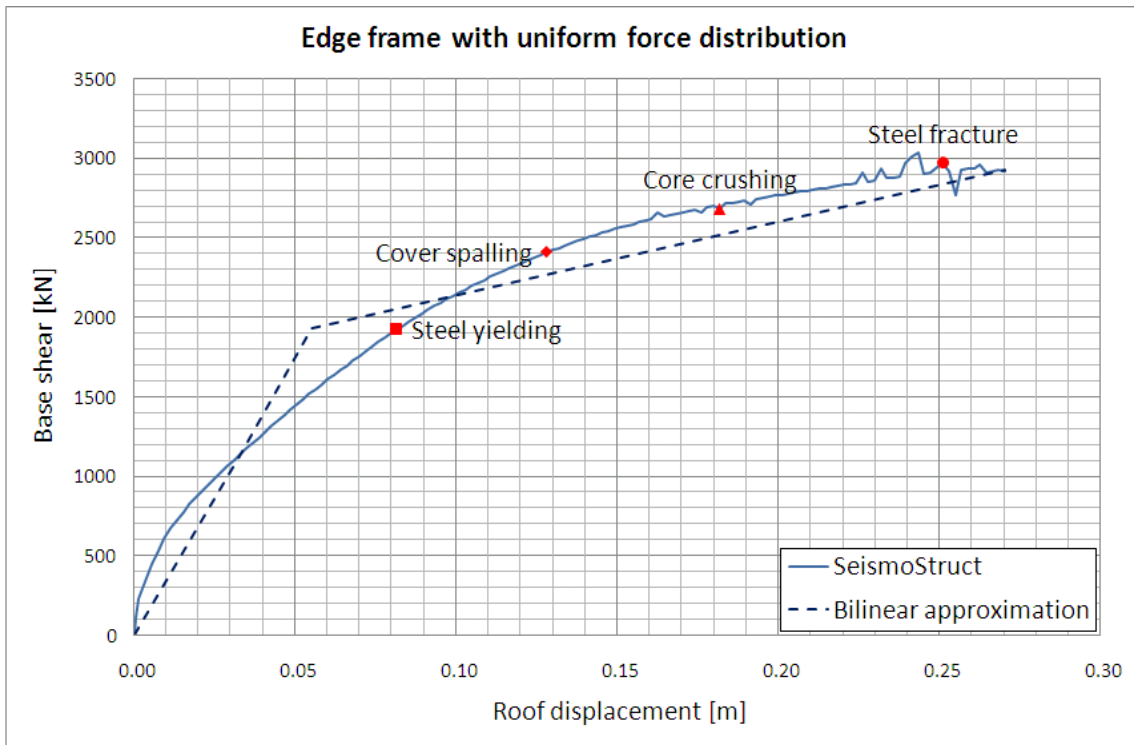


Figure 4-34: Edge frame, uniform force distribution

Comparing the bilinear approximations of the two capacity curves in Figure 4-35 it is clear that the triangular lateral force distribution is the most unfavourable loading pattern.

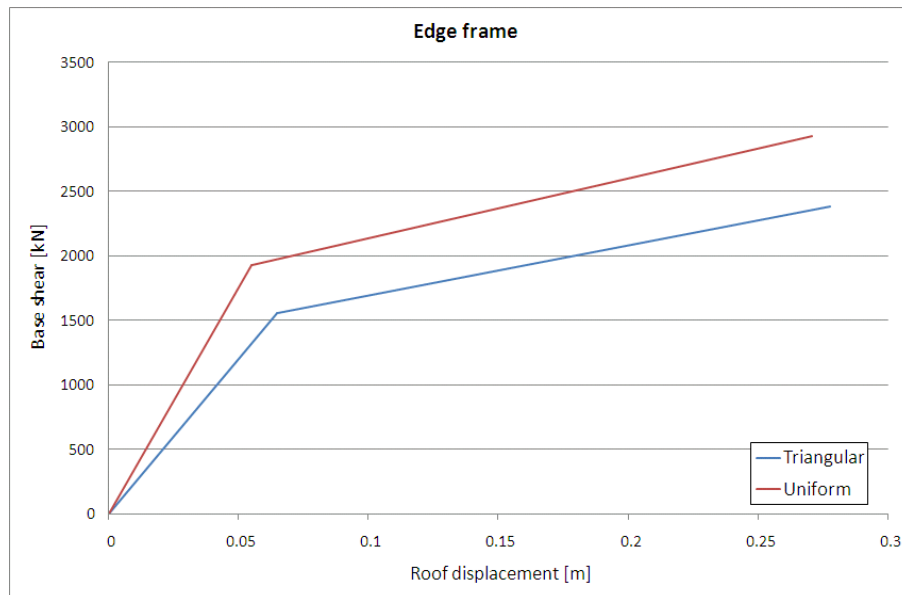


Figure 4-35: Edge frame comparison

Values that define the bilinear approximation of the capacity curve obtained by applying a triangular lateral force distribution are as shown in Table 4-9.

Table 4-9: Edge frame capacity curve

Position	Roof displacement [mm]	Base shear [kN]
Start	0.0	0.000
60% Yield	38.7	930.260
Yield	64.6	1551.417
Ultimate	277.5	2384.493

It is shown in chapter seven that it is not required to include the contribution of the edge frame to the structural system of the building. The lateral force-displacement behaviour of the shear wall, the internal frame, and the moment-rotation behaviour of the wall foundation, was therefore used in subsequent analyses.

The nonlinear moment-rotation capacity curves that were determined for the various foundation sizes are discussed in the next chapter.

Chapter 5

5 FOUNDATION BEHAVIOUR

5.1 Objectives

The nonlinear response of the various wall foundation sizes is discussed in this chapter. Allotey and Naggar [35] derived analytical equations for the moment-rotation response of a rigid foundation. These equations were applied to determine the nonlinear moment-rotation behaviour of the chosen foundation sizes. Figure 5-1 shows the part of the study, extruded from Figure 1-1, which is addressed in this chapter. The following are presented:

- First, soil parameters that influence the foundation behaviour.
- A discussion of the different conditions of foundation response follows.
- Thereafter a comparison of the nonlinear behaviour of the various foundation sizes that were investigated is discussed.
- Verification of the nonlinear foundation behaviour follows.
- Finally, conversion of the units of the foundation capacity curve is discussed.

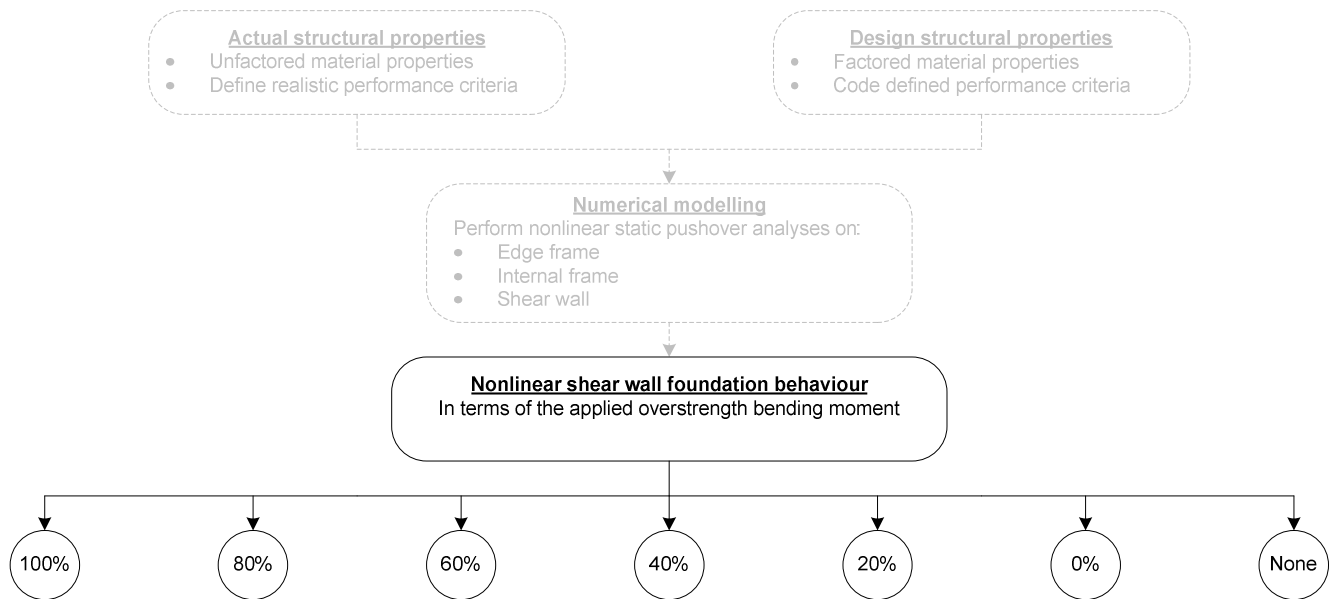


Figure 5-1: Chapter five objectives

5.2 Foundation parameters

Various soil and foundation properties are required to determine the nonlinear response of rigid foundations. Parameters have been chosen that are appropriate to this investigation and are discussed in this section.

Poisson's ratio (μ)

It is suggested by Bowles [38] that the typical range of values for the Poisson's ratio for sand and gravelly sand is 0.3 to 0.4. As this type of soil was chosen for the example building, a value of $\mu = 0.4$ was chosen.

Static stress-strain modulus (E_s)

The static stress-strain modulus of soil is commonly used to compute estimates of foundation settlement. For any given soil type a wide range of values are possible for this parameter and it is therefore suggested by Bowles [38] that field values from in situ testing should be used where possible. For loose sand and gravel a range of values between 50MPa and 150MPa is suggested. A value of $E_s = 50\text{MPa}$ was chosen for the purpose of this investigation.

Plane strain modulus (E'_s)

Bowles [38] provides an expression for the calculation of the plane strain modulus:

$$E'_s = \frac{E_s}{1 - \mu^2}$$

A value of $E'_s = 59.5\text{MPa}$ was calculated for the example in this investigation. This parameter is used in the calculation of the modulus of subgrade reaction, as will be discussed later.

Influence factors (I_F, I_1, I_2, I_S)

Influence factors (I_F, I_1, I_2, I_S) are used to calculate the modulus of subgrade reaction, as will be discussed later. Bowles [38] provides a chart that is used to determine the factor I_F . This influence factor depends on the dimensions of the foundation and values are provided graphically for a range of foundation depth to length ratios between 0.5 and 10. Wall foundations typically have foundation depth to length ratios of less than 0.5 and therefore a value of $I_F = 1$ was assumed for the purpose of this investigation.

Expressions are provided by Bowles [38] to calculate values for the influence factors I_1 and I_2 .

$$I_1 = \frac{1}{\pi} \left[M \ln \frac{(1 + \sqrt{M^2 + 1}) \sqrt{M^2 + N^2}}{M(1 + \sqrt{M^2 + N^2 + 1})} + \ln \frac{(M + \sqrt{M^2 + 1}) \sqrt{1 + N^2}}{M + \sqrt{M^2 + N^2 + 1}} \right]$$

$$I_2 = \frac{N}{2\pi} \tan^{-1} \left(\frac{M}{N \sqrt{M^2 + N^2 + 1}} \right)$$

Parameters “M” and “N” depends on the foundation dimensions.

Using the influence factors I_1 and I_2 together with Poisson’s ratio, the Steinbrenner influence factor (I_S) can be determined from the equation:

$$I_S = I_1 + \frac{1 - 2\mu}{1 - \mu} I_2$$

Influence factors I_F and I_S are subsequently used directly to calculate the modulus of subgrade reaction.

Modulus of subgrade reaction (k_s)

The modulus of subgrade reaction is described by Bowles [38] as a conceptual relationship between soil pressure and deflection that is used in the analysis of foundations. If the symbol “ q ” is used to describe soil pressure under a foundation and “ δ ” is used to describe the settlement of the foundation, the modulus of subgrade reaction can be expressed as:

$$k_s = \frac{q}{\delta}$$

As the soil pressure and resulting foundation deflection is dependent on the soil properties, foundation dimensions, and loading on the foundation, other expressions were also derived using the parameters discussed earlier. For the purpose of this investigation it was chosen to use an expression provided in [38] as derived by A.S. Vesic:

$$k_s = \frac{1}{B \cdot E'_s \cdot I_s \cdot I_F}$$

In the above equation “ B ” denotes the width of the foundation. Using this expression, results in an estimation of the modulus of subgrade reaction. Bowles [38] provides a table with a range of typical values to be used to assess the calculated value. A value of between 4800kN/m³ and 128000kN/m³ can apply to the modulus of subgrade reaction for loose to dense sands. The value calculated for each investigated foundation size was compared to this typical range of values to ensure realistic results.

Chi (X) – dimensionless parameter

Another important parameter that defines the nonlinear rocking response of rigid foundations is the inverse of the foundation bearing capacity safety factor under vertical load, X . This parameter is calculated as the ratio of applied normal load on the foundation per meter of foundation width to the bearing capacity of the underlying soil:

$$X = \frac{P}{q_u B}$$

In the above expression “P” denotes the normal force per meter foundation width [kN/m], “ q_u ” the soil bearing capacity [kN/m²] and “B” the width of the foundation [m]. It was stated by Allotey and Nagggar [35] that X-values of less than 0.5 implies that the foundation mat will lift up from the underlying soil before yielding of the soil occurs. Values of greater than 0.5 indicate that the underlying soil will yield before foundation uplift. Figure 5-2 shows the resulting soil pressure under a foundation when X is less than 0.5, whilst Figure 5-3 shows the soil pressure when X is greater than 0.5.

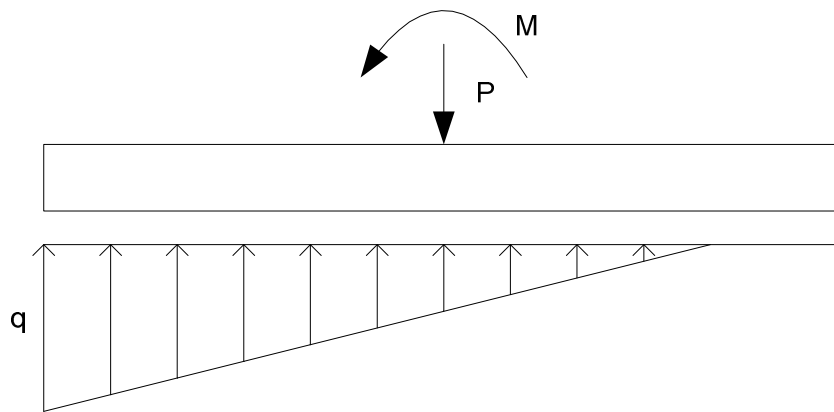


Figure 5-2: Foundation uplift prior to yielding of soil

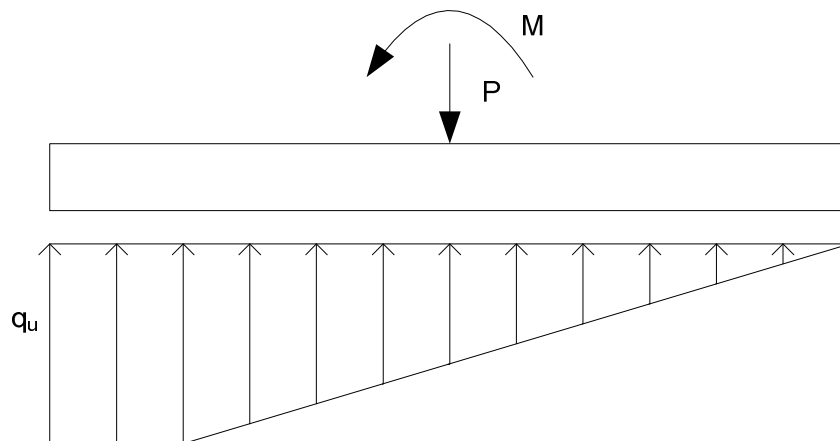


Figure 5-3: Soil yielding prior to foundation uplift

It was determined that all the foundations investigated in this study had X-values of less than 0.5 and hence, all the investigated foundations were expected to lift up prior to yielding of the underlying soil.

5.3 Conditions of foundation behaviour

As the X -value defines a sequence of the behaviour of rigid foundations under rocking response, it can be expected that the nonlinear moment-rotation response of foundations will differ for X -values of above and below 0.5. Allotey and Naggar [35] provided expressions to determine this nonlinear response for the two situations. In this calculation the ratio of soil stiffness to its strength (denoted with “ Ψ ”) also plays an important role and is expressed as follows:

$$\Psi = \frac{k_v \cdot L}{q_u}$$

In this expression “ L ” denotes the foundation length and “ k_v ” the stiffness of the spring elements of the Winkler soil model which is related to the modulus of subgrade reaction.

Expressions are provided by Allotey and Naggar [35] for a normalized nondimensional moment:

For $X \leq 0.5$:

$$M_{qL} = \begin{cases} \frac{\psi\theta}{12}, & 0 \leq \theta \leq \frac{2\chi}{\psi} \\ \frac{\chi}{6} \left(3 - 2 \sqrt{\frac{2\chi}{\psi\theta}} \right), & \frac{2\chi}{\psi} \leq \theta \leq \frac{1}{2\psi\chi} \\ \frac{1}{2} (\chi - \chi^2) - \frac{1}{24\psi^2\theta^2}, & \theta \geq \frac{1}{2\psi\chi} \end{cases}$$

For $X \geq 0.5$:

$$M_{qL} = \begin{cases} \frac{\psi\theta}{12}, & 0 \leq \theta \leq \frac{2(1-\chi)}{\psi} \\ \frac{(1-\chi)}{6} \left(3 - 2 \sqrt{\frac{2(1-\chi)}{\psi\theta}} \right), & \frac{2(1-\chi)}{\psi} \leq \theta \leq \frac{1}{2\psi(1-\chi)} \\ \frac{1}{2} (\chi - \chi^2) - \frac{1}{24\psi^2\theta^2}, & \theta \geq \frac{1}{2\psi(1-\chi)} \end{cases}$$

Using the ultimate soil bearing capacity (q_u), foundation length (L), and foundation width (B), this normalized moment is transformed to the bending moment capacity for a given rigid rotation as follows [35]:

$$M = M_{qL} \cdot q_u \cdot L^2 \cdot B$$

Expressions are also provided by Allotey [35] for the different conditions of rigid foundation rocking response:

- A condition of elastic response.
- A condition of initial uplift of the foundation prior to yielding of the soil.
- A condition of initial yielding of the underlying soil prior to foundation uplift.
- A condition of combined soil yielding and uplift of the foundation.

As the bending moment applied to the foundation increase the foundation can either uplift or the underlying soil could yield. The condition of combined foundation uplift and soil yielding could occur if the applied bending moment increases further. This sequence is shown in Figure 5-4.

The above mentioned conditions therefore follow upon each other and bending moments and rotations at foundation performance points can be determined from the various conditions:

- From the elastic condition, the condition of soil yielding or foundation uplift can be determined, depending on which condition is achieved first.
 - The condition of initial uplift of the foundation occurs first if $X < 0.5$.
 - The condition of initial soil yielding is reached first if $X > 0.5$.
- The point of soil yielding can be determined from the condition of initial uplift of the foundation if $X < 0.5$.
- The point of foundation uplift can be determined from the condition of initial soil yielding if $X > 0.5$.
- The ultimate bending moment resistance (when $\theta \rightarrow \infty$) can be determined from the condition of combined soil yielding and foundation uplift.

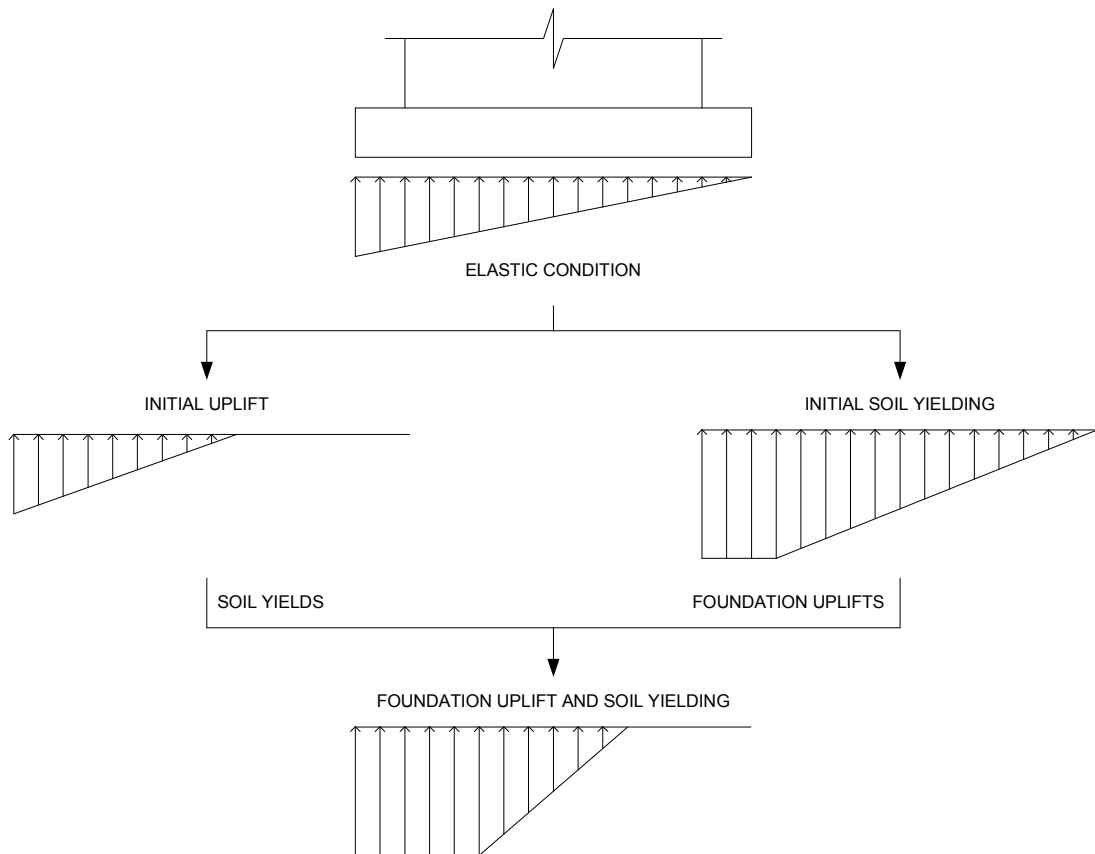


Figure 5-4: Rigid foundation rocking response

5.4 Comparison of nonlinear behaviour

As discussed earlier it was decided to investigate foundations designed with 0%, 20%, 40%, 60%, 80% and 100% of the overstrength bending moment of the shear wall applied to the foundation. This led to foundations determined in section 3.2. These sizes are shown in Table 5-1.

Table 5-1: Investigated wall foundation dimensions

Percentage M_{Rd}^+ applied	Length (L)	Width (B)	Depth (D)
100%	14.0 m	4.0 m	1.3 m
80%	12.0 m	4.0 m	1.3 m
60%	11.5 m	3.0 m	1.3 m
40%	9.5 m	3.0 m	1.3 m
20%	8.0 m	2.5 m	1.3 m
0%	6.5 m	2.0 m	0.8 m

Using the expressions provided by Allotey and Naggar [35] the nonlinear rigid rocking response of the wall foundations were determined together with positions where uplift

of the foundations and yielding of the underlying soil occur for the first time. Figure 5-5 shows the resulting moment-rotation capacity curves for the investigated foundations.

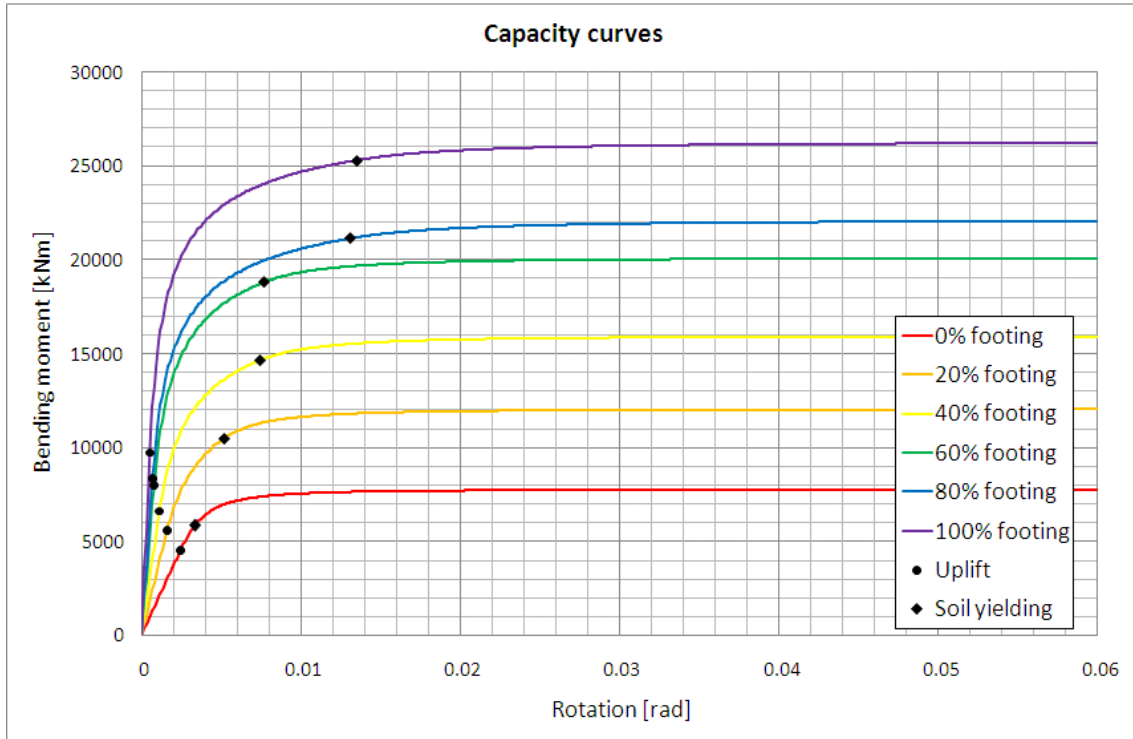


Figure 5-5: Foundation capacity curves

The ultimate moment capacities of the foundations were determined to be as shown in Table 5-2.

Table 5-2: Ultimate moment capacities

Foundation	$M_{R,ultimate}$ [kNm]
100%	26264
80%	22099
60%	20094
40%	15929
20%	12034
0%	7754

From Table 5-2 it is clear that there is not a linear relationship between foundation size and the applied bending moment. This is because these percentages merely refer to the percentage of shear wall overstrength bending moment *applied* to determine the required foundation dimensions. Even a 0% foundation has definite dimensions and

hence, will provide a nominal amount of bending moment resistance. Expressed as a percentage of the 100% foundation properties, the concrete volume and ultimate bending moment resistance of the other foundations are as shown in Table 5-3.

Table 5-3: Foundation comparison

Foundation size	Concrete volume	$M_{R,ultimate}$
100%	100.0%	100.0%
80%	85.7%	84.1%
60%	61.6%	76.5%
40%	50.9%	60.6%
20%	36.0%	45.8%
0%	14.3%	29.5%

5.5 Verification of procedure to analyse foundation behaviour

A spreadsheet was set up to determine the nonlinear rocking response of the foundations that were investigated. To validate the results obtained from this spreadsheet the parameters used in a previous study [52] was implemented in the spreadsheet and the results compared.

In the investigation that was used for the validation, nonlinear rigid foundation response to seismic action was determined for bridge pier foundations. The expressions as presented by Allotey and Naggar [35] were used in this investigation and therefore the results obtained from Kuhn [52] were expected to be identical to that obtained from the spreadsheet. The parameters of interest to the investigated foundation are as follows:

- Soil bearing capacity: $q_u = 1688\text{kN/m}^2$
- Soil density: $\rho = 18\text{kg/m}^3$
- Poisson's ratio: $\mu = 0.4$
- Static stress-strain modulus: $E_s = 50\text{MPa}$
- Width of foundation: $B = 3.8\text{m}$
- Length of foundation: $L = 7.4\text{m}$
- Depth of foundation: $D = 0.9\text{m}$
- Applied bending moment: $M' = 21951.43\text{kNm}$
- Applied normal force: $N' = 7100\text{kN}$

It was calculated that $\alpha < 0.5$ and therefore foundation uplift is expected to occur before the underlying soil yields. The ultimate bending moment resistance was calculated as $M_{R,ultimate} = 22340\text{kNm}$ and the bending moments and rotations at positions of foundation uplift and yielding of the underlying soil was calculated to be the following:

Table 5-4: Foundation performance point

Position	M [kNm]	Θ [rad]
Foundation uplift	8757	0.0034
Soil yielding	21031	0.0381

Identical moment rotation curves were obtained as shown in Figure 5-6. Data was only presented by Kuhn [52] for foundation rotation values up to 0.015 radians and therefore this was the only available range in which to compare the results.

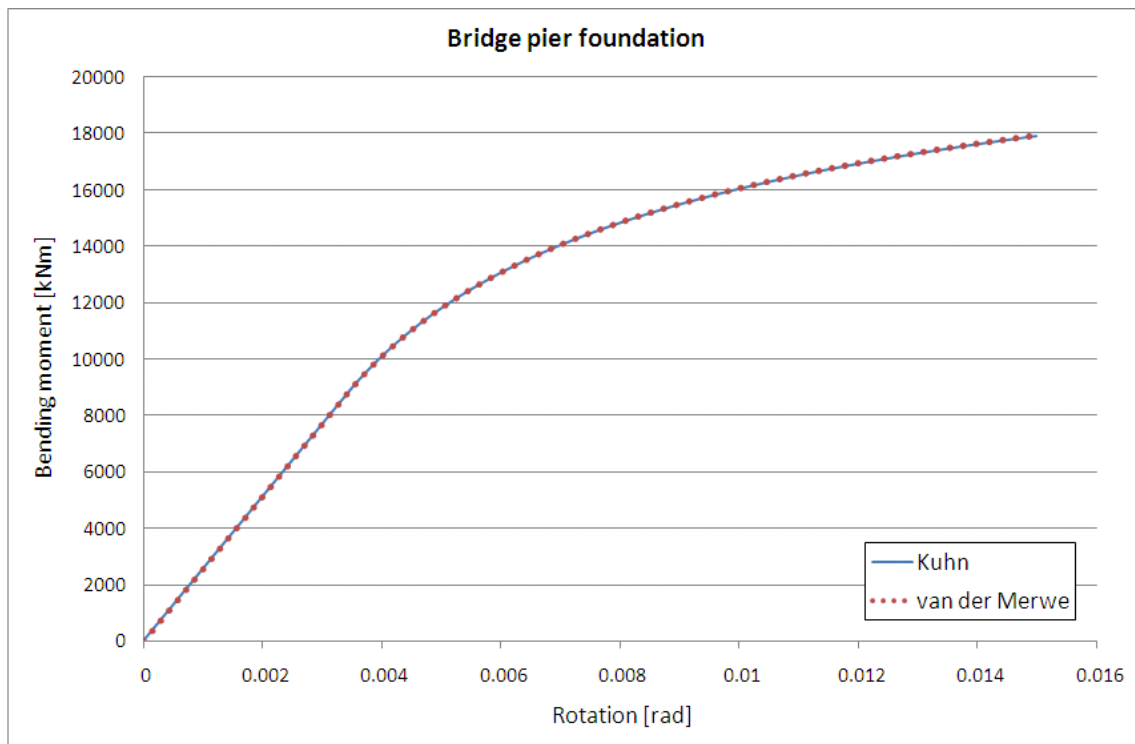


Figure 5-6: Moment-rotation validation curves

It is therefore assumed that the results in this study obtained with the spreadsheet used for the investigated foundation sizes are accurate.

5.6 Conversion of capacity curve

The structural systems considered in this study consist of:

- An internal reinforced concrete frame consisting of columns and slab elements.
- Either a shear wall or an edge frame consisting of a shear wall, columns and slab elements in the plane of the shear wall.
- A wall foundation.

In this section, it is shown how the capacity curve of the wall foundation is converted so that the capacity curves of all investigated systems are expressed in the same units.

The capacity curves that were obtained for the investigated foundations as discussed in section 5.4 results in nonlinear moment-rotation curves. These can be seen as the nonlinear rotational stiffness of the various foundation sizes. When modelling the foundation with a rotational spring element, this curve would therefore describe the nonlinear stiffness of the rotational spring element. Rotational stiffness is defined as the slope of the moment-rotation curve and hence, the unit of the stiffness is the ratio of bending moment and rotation (kNm/rad).

Capacity curves that show the relationship between base shear and lateral roof displacement were determined in chapter 4. These curves therefore define the nonlinear lateral stiffness of the various systems that were investigated with the slope of the curve being the lateral stiffness. The unit of this lateral stiffness is therefore defined by the ratio of base shear and lateral roof displacement (kN/m).

If the nonlinear stiffness of the rocking foundation and the various above ground structural systems are to be combined, the units of the nonlinear stiffness should be the same. It will therefore be required to convert capacity curves to ensure that the axes of the curves define the same parameters. For this reason the capacity curves of the rocking foundations were also converted to curves showing the relationship between the base shear force that corresponds to the relevant base bending moment, and the lateral roof displacement caused by a rotating foundation.

Equivalent lateral force methods assume a distribution of the base shear force in a predefined pattern, $\{\phi\}$, over the height of a structure. These forces can be used to

determine the bending moment that results at the base of a shear wall. Assuming a rigid shear wall, the conversion can be explained by considering Figure 5-7.

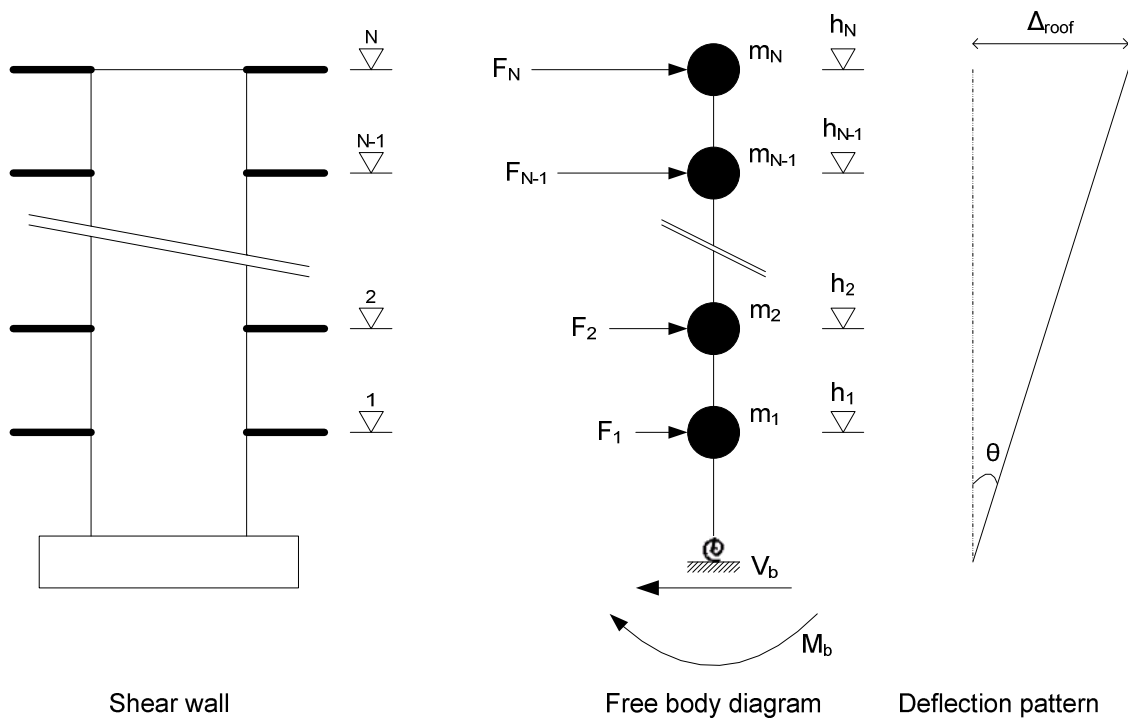


Figure 5-7: Moment-rotation and base shear-roof displacement relationship

The lateral distribution of the base shear force over the height of the shear wall as well as the height of every floor can be expressed in vector notation:

$$\{F\} = \begin{Bmatrix} F_1 \\ F_2 \\ \dots \\ F_{N-1} \\ F_N \end{Bmatrix} = \{\phi\} \cdot V_b$$

$$\{h\} = \begin{Bmatrix} h_1 \\ h_2 \\ \dots \\ h_{N-1} \\ h_N \end{Bmatrix}$$

For horizontal force and moment equilibrium of the structure:

$$V_b = \sum_{i=1}^N F_i$$

$$M_b = \sum_{i=1}^N F_i \cdot h_i = \{F\}^T \{h\} = V_b \cdot \{\phi\}^T \{h\}$$

The pattern of lateral force distribution is decided upon by the engineer and the height vector is determined by the geometry of the structure and therefore the above moment equilibrium expression can be used to equate a bending moment value to the relevant base shear value:

$$V_b = \frac{M_b}{\{\phi\}^T \{h\}}$$

If the shear wall is assumed to remain rigid as shown in Figure 5-7, a relationship between the rotation of the footing and the lateral roof displacement of the shear wall can be determined:

$$\sin \theta = \frac{\Delta_{roof}}{h_N}$$

For small rotations it is known that $\sin \theta \approx \theta$ and therefore: $\theta \approx \frac{\Delta_{roof}}{h_N}$.

This allows the conversion of rigid footing rotation to the lateral roof displacement of the rigid shear wall using the following expression:

$$\Delta_{roof} = \theta \cdot h_N$$

The example building that was investigated consists of eight storeys with a vertical spacing of 3.5m between floor slabs. A triangular distribution of lateral forces was found to be critical for all above ground structures and hence, this force distribution pattern was also used in the conversion of the foundation capacity curves. Therefore the height vector, $\{h\}$ with meter units, and lateral loading pattern vector, $\{\phi\}$, are as follows:

$$\{h\} = 3.5 \begin{Bmatrix} 1 \\ 2 \\ 3 \\ 4 \\ 5 \\ 6 \\ 7 \\ 8 \end{Bmatrix}; \quad \{\phi\} = \frac{1}{36} \begin{Bmatrix} 1 \\ 2 \\ 3 \\ 4 \\ 5 \\ 6 \\ 7 \\ 8 \end{Bmatrix}$$

Note that the factor of “1/36” is used to normalize the shape vector to ensure horizontal equilibrium of the structure. Expressions to convert the moment-rotation response of the foundations to the corresponding base shear-roof displacement response are therefore the following:

$$V_b = \frac{6M_b}{119}$$

$$\Delta_{roof} = 28 \cdot \theta$$

Earthquake ground motion histories were selected and scaled in order to perform nonlinear time-history analyses. The procedure followed to choose appropriate ground motions and scaling these ground motion data are discussed in the following chapter.

Chapter 6

6 TIME-HISTORY DATA

6.1 Objectives

In order to perform nonlinear time-history analyses with real ground motion accelerograms it was necessary to obtain appropriate time-history data and to scale the selected data. The procedure followed to accomplish the aforementioned is discussed in this chapter. Figure 6-1 shows the part of the study, extruded from Figure 1-1, which is addressed in this chapter. This includes first selecting a sufficient number of ground motion time-histories and then scaling these ground motion data sets to be representative of the expected site conditions and seismic hazard.

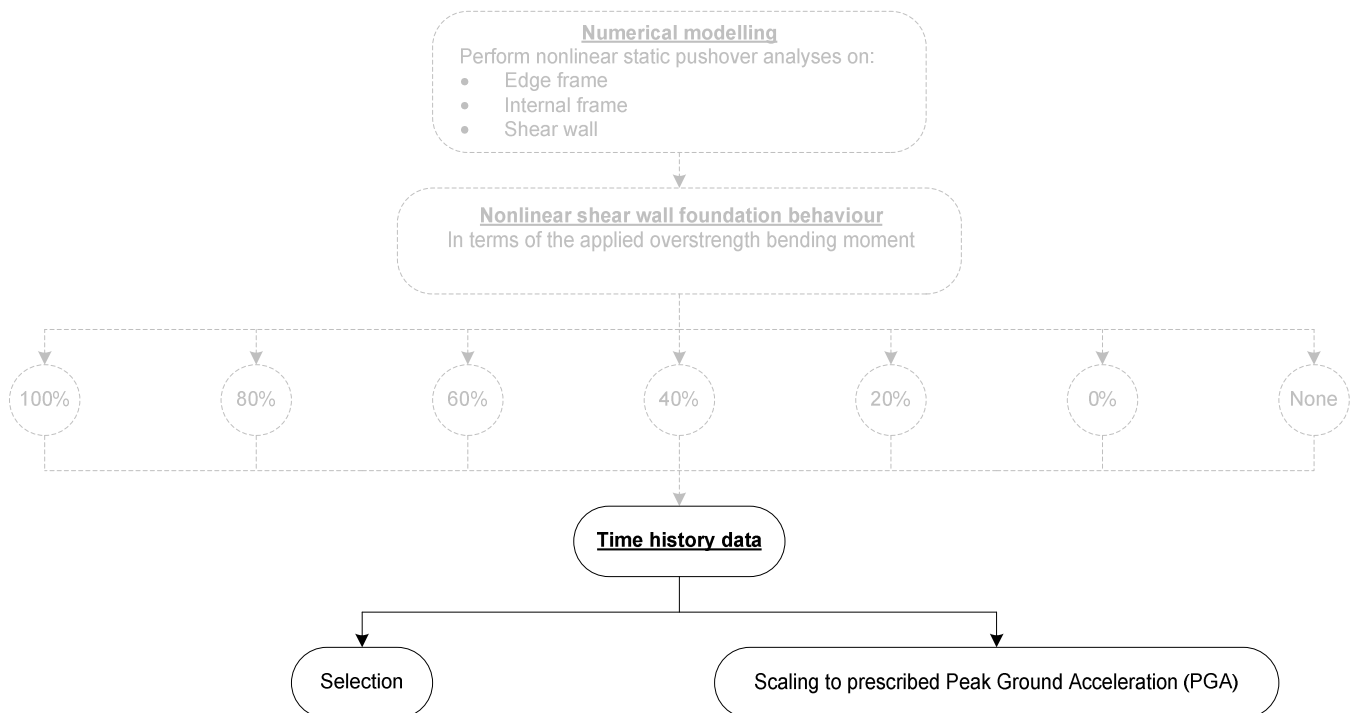


Figure 6-1: Chapter six objectives

6.2 Selection of real ground motion

Various ground motion data sets are freely available on the internet and it is left to the engineer to choose the most appropriate ground motions as well as the most appropriate number of ground motions to be used in time-history analyses. As stated in section 2.2.5 the selection of appropriate ground motion data is dependent on the geological and seismological conditions at the location of the structure being considered.

For the purpose of this investigation the 20 ground motion data sets used by Dhakal et al [14] were used as an initial set of ground motions from which to select appropriate ground motions to perform nonlinear time-history analyses. Here ground motion data sets were chosen that are appropriate for firm soils with a moderate distance from the location where the ground motion was measured to the source of the earthquake. All ground motion data sets were recorded in the United States of America.

Two properties that are essential for the choice of 20 ground motion data sets are the expected site conditions and the distance of the site from a fault zone [14]. The “Campbell’s GEOCODE” and the “Closest Distance to Fault Rupture”, denoted by R^* , are used to define these properties respectively [13]. The chosen ground motion data sets had R^* -values ranging from 15.1km to 31.7km. Campbell’s GEOCODE describes different soil types with alphabetical letters A to F:

- A: Firm soil
- B: Very firm soil
- C: Soft rock
- D: Firm rock
- E: Shallow rock
- F: Extremely soft or loose soils such as beach sand

Campbell’s GEOCODE classifications A, B and C were used to choose the set of 20 ground motions. Ground motions can be freely downloaded from the PEER Strong Motion Database [13] and the set of 20 ground motion records are shown in Table 6-1.

Table 6-1: Initial set of 20 ground motion data [13]

No	Event	Year	Station	Component (ϕ)	R* [km]	PGA [g]	Campbell's GEOCODE
1	Loma Prieta	1989	Agnews State Hospital	90	28.2	0.159	A
2	Imperial Valley	1979	Plaster City	135	31.7	0.057	A
3	Loma Prieta	1989	Hollister Diff. Array	255	25.8	0.279	A
4	Loma Prieta	1989	Anderson Dam	270	21.4	0.244	B
5	Loma Prieta	1989	Coyote Lake Dam	285	22.3	0.179	B
6	Imperial Valley	1979	Cucapah	85	23.6	0.309	A
7	Loma Prieta	1989	Sunnyvale Colton Ave	270	28.8	0.207	A
8	Imperial Valley	1979	El Centro Array #13	140	21.9	0.117	A
9	Imperial Valley	1979	Westmoreland Fire Sta.	90	15.1	0.074	A
10	Loma Prieta	1989	Hollister South & Pine	0	28.8	0.371	A
11	Loma Prieta	1989	Sunnyvale Colton Ave	360	28.8	0.209	A
12	Superstition Hills	1987	Wildlife Liquefaction Array	90	24.4	0.180	A
13	Imperial Valley	1979	Chihuahua	282	28.7	0.254	A
14	Imperial Valley	1979	El Centro Array #13	230	21.9	0.139	A
15	Imperial Valley	1979	Westmoreland Fire Sta.	180	15.1	0.110	A
16	Loma Prieta	1989	WAHO	0	16.9	0.370	C
17	Superstition Hills	1987	Wildlife Liquefaction Array	360	24.4	0.200	A
18	Imperial Valley	1979	Plaster City	45	31.7	0.042	A
19	Loma Prieta	1989	Hollister Diff. Array	165	25.8	0.269	A
20	Loma Prieta	1989	WAHO	90	16.9	0.638	C

As stated in section 2.2.5 it was decided to use seven ground motion histories from the above set of 20 for nonlinear time-history analyses. The elastic response spectrum of the structure is required to select the most appropriate data sets. Calculation of this response spectrum is discussed in the following section.

6.2.1 Elastic response spectrum

The procedure as described in the Swiss code [53] was used. Ground type A from this code corresponds to ground type 1 of SANS 10160 [43] and the following parameters are provided to determine the elastic response spectrum.

- $S = 1.0$
- $T_B = 0.15 \text{ s}$
- $T_C = 0.4 \text{ s}$
- $T_D = 2.0 \text{ s}$

Other parameters that were required as discussed below:

Damping ratio (ξ)

A damping ratio of 5% was chosen for the example building and therefore $\xi = \mathbf{0.05}$.

Peak ground acceleration ($a_{g,d}$)

As shown in Figure 2-4 a PGA of 0.15g was prescribed by the Council of Geoscience for the Cape Town region. Therefore $\mathbf{a_{gd} = 0.15g}$ was chosen.

Correction factor (η)

This dimensionless parameter depends on the damping ratio and can be calculated from the following equation:

$$\eta = \sqrt{\frac{1}{0.5 + 10\xi}} \geq 0.55$$

For the chosen 5% damping ratio: $\mathbf{\eta = 1.0}$.

Expressions are given in SIA 261 to determine the elastic response spectrum in the various period intervals. These expressions are as follows [53]:

$$0 \leq T \leq T_B : S_e(T) = a_{gd} \cdot S \cdot \left[1 + \frac{(2.5\eta - 1) \cdot T}{T_B} \right]$$

$$T_B \leq T \leq T_C : S_e(T) = 2.5 \cdot a_{gd} \cdot S \cdot \eta$$

$$T_C \leq T \leq T_D : S_e(T) = 2.5 \cdot a_{gd} \cdot S \cdot \eta \cdot \frac{T_C}{T}$$

$$T_D \leq T : S_e(T) = 2.5 \cdot a_{gd} \cdot S \cdot \eta \cdot \frac{T_C \cdot T_D}{T^2}$$

The resulting elastic response spectrum is as shown in Figure 6-2.

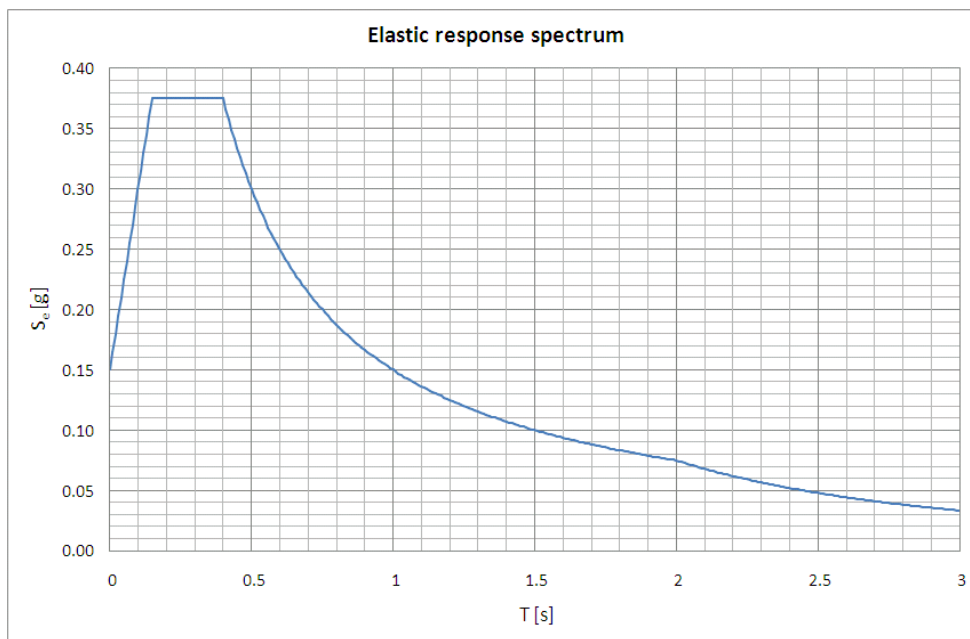


Figure 6-2: Elastic response spectrum

6.2.2 Final choice of ground motion data

The procedure to select the most appropriate ground motion data is discussed in section 2.2.5. This procedure entails scaling the 5% damped response spectra of the various ground motion data sets to the elastic response spectrum and seeing how well the elastic response spectrum represents the ground motion response spectrum. The seven ground motion response spectra that best fit the shape of the elastic response spectrum were chosen for the nonlinear time-history analyses. These seven ground motions were numbers 1, 2, 4, 5, 8, 14 and 15 from Table 6-1.

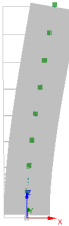
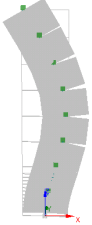

Appendix B shows the response spectra of the seven selected ground motions fitted to the elastic response spectrum of the structure.

6.3 Scaling of selected ground motion

As mentioned in section 2.2.5 recorded ground motion must be scaled to fit the elastic response spectrum of the structure. Clearly it will not be possible to fit the whole earthquake response spectrum to fit the elastic response spectrum and for this reason the response spectra are scaled only within a range of period values in which the structure can be expected to vibrate.

For the purpose of scaling the chosen recorded ground motions it was assumed that the shear wall will have a dominant effect on the vibrating response of the building. Natural vibration periods of the shear wall were therefore used to determine the period range in which to scale the earthquake response spectra. An eigenvalue analysis was performed on the shear wall using SeismoStruct. Enough modes of vibration must be considered that will result in a cumulative effective modal mass of 90% of the total mass as discussed in section 2.2.2, and it was determined that the first three modes of vibration should be considered. The results from the eigenvalue analysis for the first three modes of vibration are shown in Table 6-2.

Table 6-2: Shear wall natural vibration periods

Mode	Period	Cumulative mass	Deformed shape
1	$T_1 = 1,264 \text{ s}$	64.95%	
2	$T_2 = 0.201 \text{ s}$	84.96%	
3	$T_3 = 0.071 \text{ s}$	91.85%	

Eigenvalue analyses are performed assuming linear material vibration response. To account for the increase in natural vibration periods due to nonlinear material behaviour the upper limit of the scaling period range was chosen to be $1.5T_1$ as used by Naeim et al [54].

The range of period values in which the recorded earthquake ground motion was scaled to fit the elastic response spectrum was therefore between $T_3 = 0.071\text{s}$ and $1.5T_1 = 1.896\text{s}$. Spectral acceleration values over the entire period range were scaled by a constant factor to obtain a best fit with the elastic response spectrum within the determined period range. It was attempted to obtain a scaling factor that ensures an equal area between the two curves above and below the elastic response spectrum as well as attempting to obtain a good fit between the curves at the fundamental period of vibration. Figure 6-3 shows this graphical procedure for the second ground motion data set (“ATH02”) from the initial set of twenty.

Appendix B shows the scaled response spectra of the chosen ground motions.

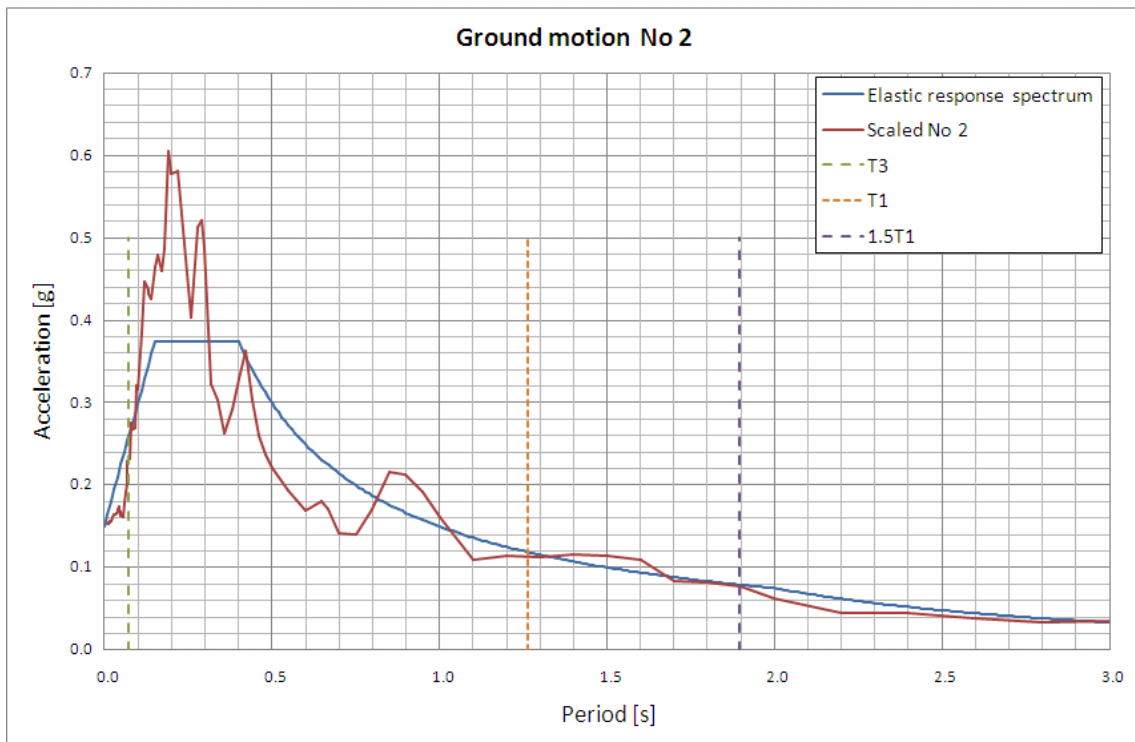


Figure 6-3: Scaling of ground motion data set number two

Table 6-3 shows the scaling factors that were determined for the seven chosen ground motion data sets.

Table 6-3: Ground motion scaling factors

Ground motion	ATH01	ATH02	ATH04	ATH05	ATH08	ATH14	ATH15
Scaling factor	0.90	2.70	0.60	0.65	1.20	1.30	1.60

The scaling factors determined above were then used to scale the accelerograms of these ground motion data sets. Resulting peak ground accelerations after scaling are as shown in Table 6-4.

Table 6-4: Ground motion PGA

Ground motion	ATH01	ATH02	ATH04	ATH05	ATH08	ATH14	ATH15
PGA [g]	0.14	0.15	0.15	0.12	0.14	0.18	0.18

Appendix B shows the scaled ground acceleration time-histories.

Nonlinear time-history analyses were performed on a simplified model that incorporates different structural systems. Simplified modelling of the different structural systems, the determination of inelastic material response for the various components, as well combining these systems into one lateral load resisting system, are discussed in chapter 7.

Chapter 7

7 NONLINEAR MODELLING OF COMBINED MODEL

7.1 Objectives

Figure 7-1 shows the part of the study, extruded from Figure 1-1, which is addressed in this chapter.

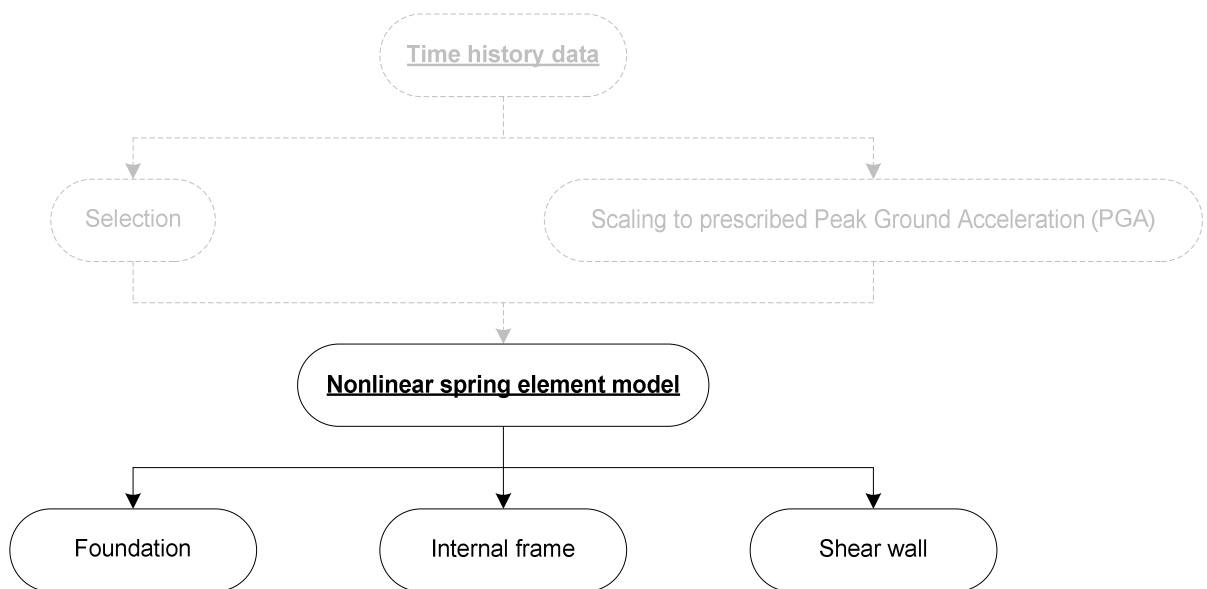


Figure 7-1: Chapter seven objectives

For the final analyses of the selected building, a simplified model was developed. Such a model would reduce computational effort. This chapter presents steps to compute this model.

First, the combined stiffness of the wall foundation and edge frame was investigated. From this investigation it was found that the edge frame was not needed, and that the following elements should be included in the simplified model:

- The shear wall
- The wall foundation
- The internal frame

The next step was to determine the geometry of the three elements of the simplified model. This included the choice of element type and lumped mass.

Finally, nonlinear material properties were assigned to the elements used to model the shear wall and internal frame to ensure the accurate representation of the lateral force-displacement behaviour of these systems, as presented in chapter four. Damping coefficients were determined for both systems to ensure that 5% viscous damping is obtained.

7.2 Choice of structural systems

It is shown in this section that the edge frame is not needed in the simplified model of the edge element. The edge element would consist of the shear wall and its foundation. For this purpose, the elastic stiffness of the wall foundation and edge frame, located on grid A of the example building (Figure 3-2), is investigated.

Three components were identified to contribute to the lateral stiffness of the structure. These are:

- An internal frame.
- A wall foundation
- Either an edge frame or a shear wall

In chapter 4 the capacity curves of these elements were discussed. Chapter 5 discussed the nonlinear rocking capacity of the various investigated foundation sizes. In this chapter these capacity curves are used to investigate the seismic response when these systems are combined into one lateral load resisting system.

Rocking foundation response is expected to act as a mechanism of energy dissipation and it is possible for this mechanism to be more dominant than the mechanism due to plastic rotation of the shear wall. For this reason it was decided to investigate whether the edge frame should be included in the combined model at all. This was done by

investigating the combined effect of the initial elastic lateral stiffness of the wall foundation and that of the edge frame.

It is assumed that the same lateral roof displacement will apply to all frames when the investigated building is loaded laterally. From this assumption it follows that the lateral roof displacement of the investigated internal frame (grid B, Figure 3-2) will be equal to the roof displacement resulting from the combined stiffness of the edge frame (grid B, Figure 3-2) and the wall foundation.

This concept can be explained by representing the lateral stiffness of the different systems with spring elements. From the above discussion it follows that the spring elements of the wall foundation and the edge frame should be connected in series to ensure that the total lateral displacement is equal to the sum of the displacements of these two systems. As the total displacement resulting from these two systems should be equal to the displacement of the internal frames it follows that the internal frame spring element should be connected in parallel with the other two elements. The resulting combination of stiffness would therefore be as shown in Figure 7-2.

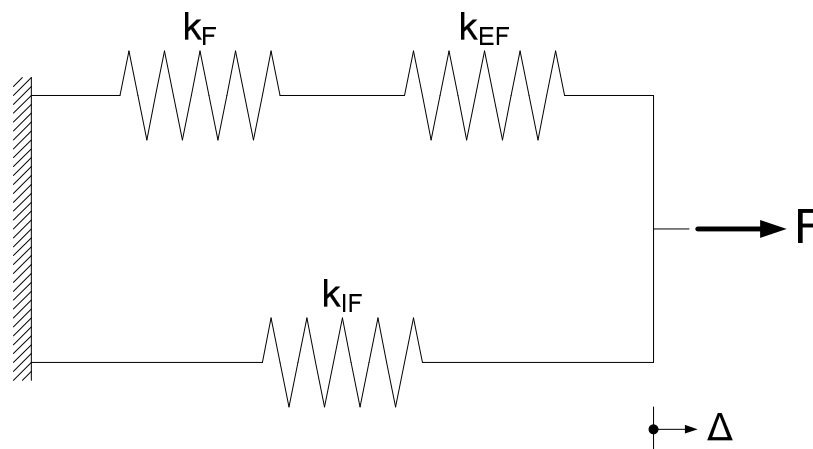


Figure 7-2: Lateral stiffness combination of systems

In Figure 7-2, “ k_F ” refers to the nonlinear stiffness of the wall foundation, “ k_{EF} ” that of the edge frame and “ k_{IF} ” that of the internal frame. The stiffness of the foundation and that of the investigated edge frame can be added to produce the stiffness of the whole edge element located on grid A of the example building (Figure 3-2).

7.2.1 Stiffness contribution

If the subscript “e” denotes the combined effect of the wall foundation and the edge frame it is clear that for spring elements connected in series, the total displacement is equal to the sum of the displacement of the different components:

$$\Delta_F + \Delta_{EF} = \Delta_e$$

All components connected in series will experience the same internal force and will be equal to the internal force of the combined spring element, and hence:

$$F_F = F_{EF} = F_e$$

As stiffness is defined as the ratio of force and the displacement in the direction of the applied force, the addition of displacement can be expressed as follows:

$$\frac{F_F}{k_F} + \frac{F_{EF}}{k_{EF}} = \frac{F_e}{k_e} = \frac{F_e}{k_F} + \frac{F_e}{k_{EF}}$$

Dividing by F_e throughout, the effective stiffness can be expressed in terms of the stiffness of the various components:

$$\frac{1}{k_F} + \frac{1}{k_{EF}} = \frac{1}{k_e} \Rightarrow k_e = \frac{k_F \cdot k_{EF}}{k_F + k_{EF}}$$

The above expression can be used to determine the combined stiffness of the edge frame and the wall foundation.

7.2.2 Elastic comparison

To determine the contribution of the foundation and edge frame to the combined stiffness of the whole edge element located on grid A of the example building (Figure 3-2), it was decided to compare the elastic stiffness of each of these systems to their combined elastic stiffness. The initial slope of the nonlinear capacity curves of these systems were used as the elastic stiffness. Note that the capacity curves used for the foundation are that of the converted curve showing the relationship of base shear to lateral roof displacement.

Combination of the foundation and edge frame was only investigated for the 40%, 60%, 80% and 100% foundation sizes to determine whether a trend can be observed. The elastic stiffness of relevance is shown in Table 7-1.

Table 7-1: Elastic stiffness

System	Stiffness
Edge frame	70 080.4 kN/m
100% footing	32 963.1 kN/m
80% footing	21 386.5 kN/m
60% footing	17 994.6 kN/m
40% footing	10 494.7 kN/m

Combining the elastic edge frame stiffness with that of the various foundation sizes resulted in a combined stiffness that is lower than either of the two components for all investigated foundation sizes. The combined stiffness differs only slightly from that of the foundation stiffness. This difference between the elastic foundation stiffness and the combined elastic stiffness decreases with decreasing foundation size, that is, for smaller elastic foundation stiffness. This can be seen from Figure 7-3 that shows the combined stiffness using the 100% foundation size and Figure 7-4 showing the result using the 40% foundation.

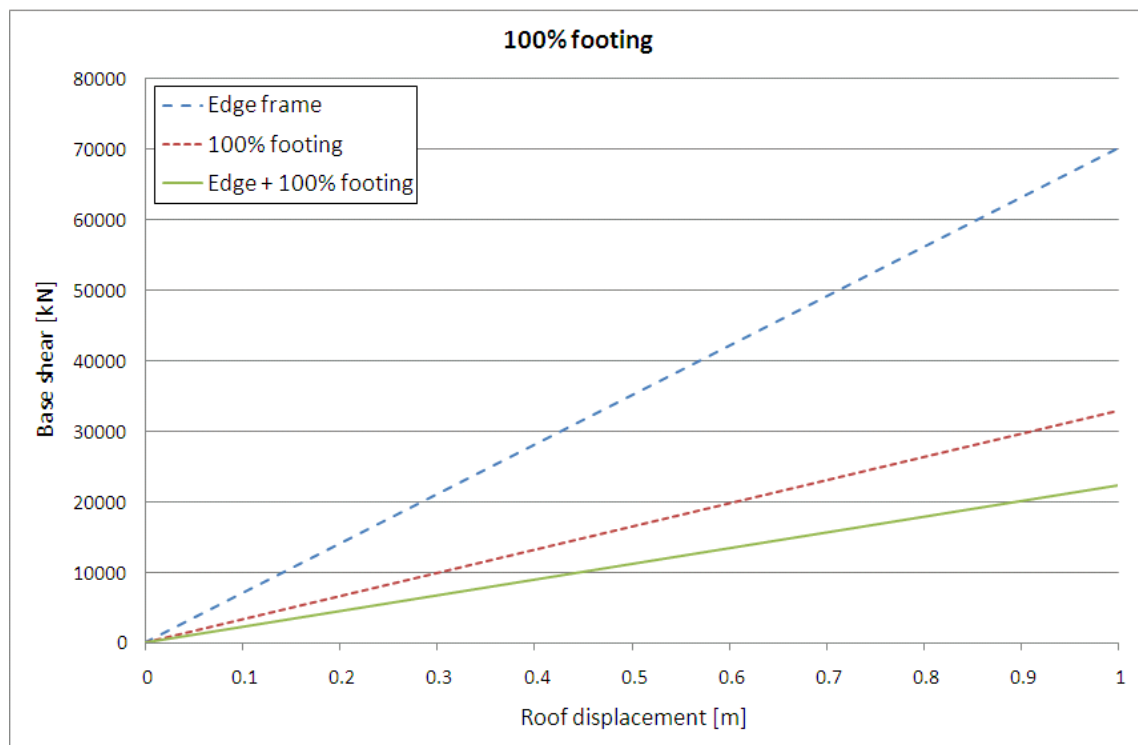


Figure 7-3: Edge frame + 100% footing elastic comparison

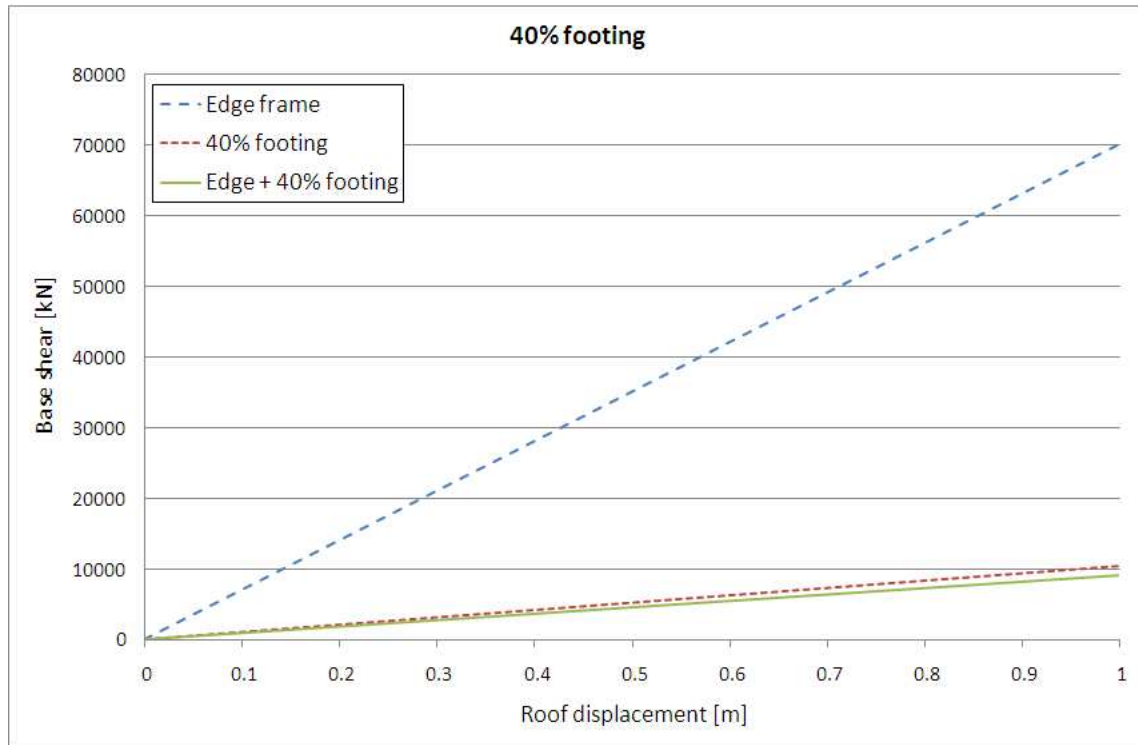


Figure 7-4: Edge frame + 40% footing elastic comparison

A summary of the combined elastic stiffness are shown in Table 7-2.

Table 7-2: Combined elastic stiffness

System	Elastic stiffness
Edge frame + 100% footing	22 418.3 kN/m
Edge frame + 80% footing	16 386.0 kN/m
Edge frame + 60% footing	14 318.1 kN/m
Edge frame + 40% footing	9 127.8 kN/m

Due to the combined elastic stiffness being close to that of the wall foundation it was concluded that the effect of the edge frame can be neglected for the sake of simplicity with only the effect of the foundation being taken into account.

Some superstructure member should however be attached to the foundation to ensure that the rotation of the footing results in lateral roof displacement. For the purpose of achieving lateral roof displacement the shear wall is included in the model. This combined foundation and shear wall model could therefore have geometry similar to that shown by the free body diagram of Figure 5-7.

7.3 Component geometry

Simplified geometries were chosen to represent the various structural systems to reduce the number of elements and nodes in the combined model that will lead to a reduction in computational effort when performing nonlinear time-history analyses. The finite element analysis system Strand7 [55] was chosen to perform the nonlinear time-history analyses. This software package allows the modelling of nonlinear spring elements, various types of link elements, beam elements and lumped mass elements, all of which were used for the combined model as will be discussed later.

In section 7.2 it was shown that the edge frame is not needed in the simplified model. The simplified model would therefore consist of the following elements:

- The wall foundation
- The shear wall
- The internal frame

The properties of these components are discussed in the following paragraphs.

7.3.1 Wall foundation

Nonlinear rocking response of the various foundation sizes were determined resulting in a moment-rotation relationship for the foundations. A spring element with nonlinear rotation stiffness was chosen to represent the foundation. This enables the direct use of the nonlinear moment-rotation response to describe the stiffness of the spring element.

7.3.2 Shear wall

Rotation of the footing will result in lateral roof displacement and therefore it was decided to include the shear wall in the combined model. Displacement of the centre line of the shear wall relative to the foundation is equivalent to that of a cantilever beam and hence, the shear wall was modelled with a beam element that includes lumped mass representing the contributing mass of floor slab at the various floor levels as shown in Figure 7-5.

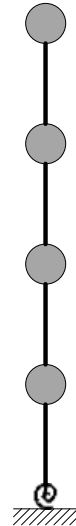


Figure 7-5: Shear wall model concept (schematic)

Equal mass were modelled at each floor level as the example building structure is regular in plan and elevation. As discussed in section 4.3.1 the equivalent density of the slab concrete material is $\gamma = 33.84 \text{ kN/m}^3$ to include imposed loads. The mass at each floor level of the shear wall represents the three meter wide edge frame strip of slab. The following lumped mass was obtained at each floor level:

$$m = \text{Density} \times \text{Area} \times \text{Depth} = 33.84 \times 42.6 \times 3 \times 0.25 \times 1000 / 9.81 = 110213 \text{ kg}$$

7.3.3 Internal frame

It is important that the simplified model that accounts for the nonlinear response of the internal frame is able to accurately represent the displaced shape of the frame. From the pushover analysis performed in SeismoStruct the displaced shape was found to be as shown in Figure 7-6.

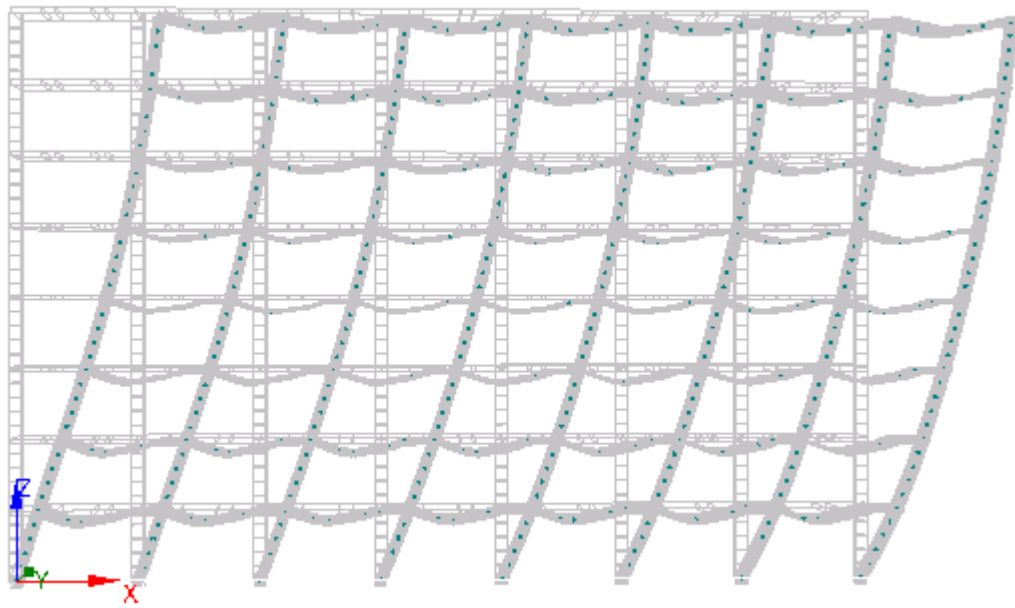


Figure 7-6: Displaced internal frame

To enable the simplified model to displace in the same manner as the internal frame it was decided to use a model consisting of two columns with nonlinear material behaviour and lumped mass at the various floor levels. Slab elements were not included in the simplified model. Column material properties would therefore be determined to accurately represent the lateral force-displacement behaviour of the internal frame.

Rigid link elements were connected between the two columns at every floor level to ensure equal lateral displacement and rotation of the columns at every floor level.

The column foundations are designed to provide no bending moment resistance and therefore pinned supports were provided to the columns. This will also result in the displaced shape to better represent the displaced shape of the frame. Figure 7-7 shows the concept of the simplified model to represent the internal frame.

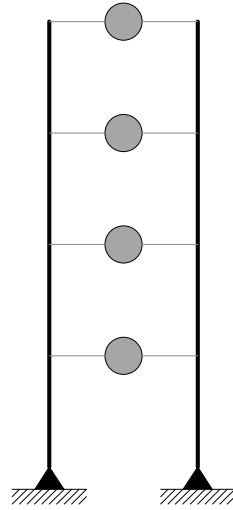


Figure 7-7: Internal frame model concept (schematic)

Contributing permanent and imposed loads on the slabs were included in the masses modelled at the floor levels in much the same way as done for the shear wall model. Here the contributing slab width used to determine the mass at every floor level was chosen to be midway between the adjacent grids of columns, resulting in a six meter width of contributing slab. The mass at every floor level was calculated as:

$$m = \text{Density} \times \text{Area} \times \text{Depth} = 33.84 \times 42.6 \times 6 \times 0.25 \times 1000 / 9.81 = 220426 \text{ kg}$$

7.3.4 Combined model

It was already stated that the shear wall model was connected to the rotational spring element representing the foundation rocking response at the base of the wall. As the total lateral displacement resulting from the combination of shear wall and foundation is equal to lateral displacement of the internal frame, these systems were connected by link elements ensuring equal lateral displacement of the systems at every floor level. Figure 7-8 shows the concept of the combined model.

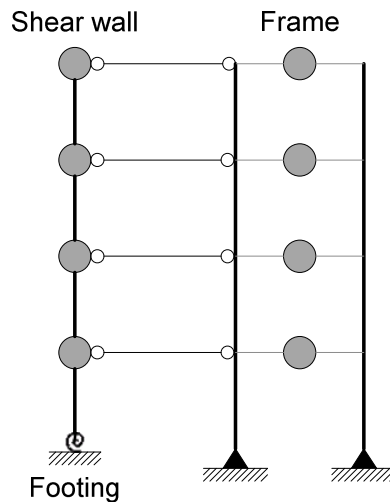


Figure 7-8: Combined model concept (schematic)

Nonlinear material properties were assigned to both the elements of the shear wall and two-column frame models to ensure an accurate representation of the displaced shape due to lateral loading. This is discussed in the following section.

7.4 Nonlinear material response

It has been shown in section 7.2 that the shear wall, wall foundation, and internal frame should be included in the simplified model. The procedure to determine nonlinear material properties for the simplified model is presented in the following paragraphs.

Nonlinear material response is required to describe the nonlinear behaviour of the two superstructure systems as discussed in chapter 4. These superstructure systems, as shown in Figure 7-8, consist of an internal frame and a shear wall. Nonlinear material response, the hysteretic response assigned to the simplified model, as well as required damping coefficients are discussed in this section.

In this section the bilinear approximations of the lateral force-displacement behaviour curves of these superstructure systems were used to determine nonlinear moment-curvature material response for the beam elements used to model the shear wall and internal frame.

7.4.1 Shear wall

As simplification, the lateral force-displacement behaviour determined for the shear wall in section 4.6.2 was represented as a bilinear curve. The bilinear curve was used as reference to determine a nonlinear moment-curvature material response for the simplified model. The following parameters had to be defined for a bilinear approximation of the moment-curvature material response:

- Elastic stiffness
- Yield curvature
- Ultimate curvature

The procedure followed to determine this material response is discussed in the following paragraphs.

Standard parameters

Standard properties of the beam elements representing the shear wall and the mass used at all floor levels were the following:

- Lumped mass of **m = 110212.8kg** at every floor level.
- Shear wall material density of **$\rho = 2400\text{kg/m}^3$** to represent the density of reinforced concrete.
- A viscous damping ratio of **$\xi = 5\%$** was chosen.
- Poisson's ratio of **v = 0.2** as was prescribed to the concrete material of the SeismoStruct model.
- Beam element dimensions of **6000mm x 300mm** were used to represent the section of the shear wall with the strong axis of the section providing stiffness in the plane of the two-dimensional model.

Bilinear capacity curve and lateral loads

The bilinear approximation of the shear wall capacity curve (Figure 4-30) defines a yield point and ultimate point as described in Table 7-3.

Table 7-3: Bilinear approximation of shear wall capacity

	Base shear force (F) [kN]	Roof displacement (Δ) [m]
Yield point (y)	961.915	0.0756
Ultimate point (u)	1234.067	0.3500

Distributing the above base shear forces in a triangular pattern over the height of the shear wall will result in applied forces as shown in Table 7-4.

Table 7-4: Lateral force distribution – shear wall

Floor level	F_y [kN]	F_u [kN]
1	26.7	34.3
2	53.4	68.6
3	80.2	102.8
4	106.9	137.1
5	133.6	171.4
6	160.3	205.7
7	187.0	240.0
8	213.8	274.2

Elastic stiffness

An iterative procedure was followed to determine the required elastic stiffness of the shear wall model. Linear static analyses were performed applying the lateral force distribution of the yield base shear force and the resulting lateral roof displacement was obtained. It was found that using an elastic modulus of $E = 10.45\text{GPa}$ results in a lateral roof displacement of 0.0756m which is equal to the required lateral roof displacement of the wall when the yield base shear is applied.

Yield point of the moment-curvature response

Performing a linear static analysis with the lateral force distribution of the yield base shear force, resulted in a bending moment of $M_y = 19\,078.0\text{kNm}$ at the base of the wall model. The lateral forces applied here will result in elastic material response with larger lateral forces resulting in inelastic material response. For this reason this bending moment corresponds to the point where inelastic material response is initiated. The bending moment at the base of the shear wall model was considered because this is the point of maximum bending moment in the wall model due to lateral loading, and therefore the position where inelastic material response will start.

The curvature of the section that corresponds with the observed bending moment was determined using the elastic modulus determined above. Strong axis bending applies and therefore the moment of inertia is as follows:

$$I = \frac{b \cdot h^3}{12} = \frac{0.3 \times 6^3}{12} = 5.4 m^4$$

Assuming a linear distribution of bending stress over the section will result in the following yield stress:

$$\sigma_y = \frac{M_y \cdot y}{I} = \frac{(19077.975 \times 10^{-3}) \cdot (3)}{5.4} = 10.599 MPa$$

The yield strain associated with this stress was calculated using the elastic modulus:

$$\varepsilon_y = \frac{\sigma_y}{E} = 10.599 / 10450 = 0.001014$$

Curvature is defined as the slope of the strain distribution, which will be linear with the assumption of linear stress distribution over the section. As the section is assumed to remain elastic at this bending moment value it was also assumed that the neutral axis will remain at the centre of the section. The yield curvature was calculated as the following:

$$\phi_y = \frac{2 \cdot \varepsilon_y}{h} = \frac{2 \times 0.001014}{6} = 3.38 \times 10^{-4} m^{-1}$$

This results in the yield point of the nonlinear moment-curvature response of the material being: $(\phi_y; M_y) = (3.38 \times 10^{-4}; 19\ 078.0) [m^{-1}; kNm]$.

Ultimate point of the moment-curvature response

Applying forces greater than that resulting from the yield base shear force should result in nonlinear material response of the model and therefore linear static analysis is inappropriate for a base shear force larger than yield. Applying the lateral force distribution corresponding to the ultimate base shear force resulted in a maximum bending moment obtained at the base of the shear wall equal to $M_u = 24\ 475.6 kNm$.

Nonlinear moment-curvature material response was defined with the *yield point* as described above and the *ultimate bending moment* equal to that mentioned in the previous paragraph. An iterative procedure was followed to determine the required ultimate curvature value that will result in the ultimate roof displacement as determined in section 4.6.2. This procedure is shown in Figure 7-9.

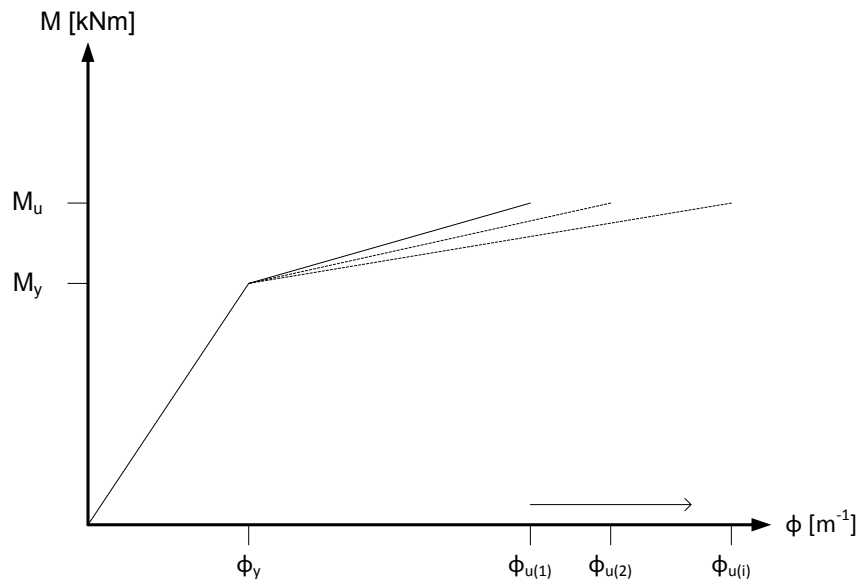


Figure 7-9: Determining ultimate curvature

A larger ultimate curvature value results in a decreased slope of the post-yield moment-curvature response as the ultimate moment value is kept constant. This leads to reduced post-yield stiffness of the material and increased lateral roof displacement.

The nonlinear material response was prescribed to the shear wall material. Nonlinear static analyses were then performed with the lateral roof displacement investigated. It was observed that a lateral roof displacement of 0.3503m is obtained when an ultimate curvature of $\phi_u = 0.0048\text{m}^{-1}$ is prescribed. This roof displacement differs from the required ultimate roof displacement (section 4.6.2) by only 0.09% and it was therefore assumed that this curvature value results in a sufficiently accurate lateral roof displacement.

The ultimate point of the moment-curvature material response is therefore: $(\phi_u; M_u) = (0.0048; 24\,475.6) [\text{m}^{-1}; \text{kNm}]$.

Figure 7-10 shows the resulting shear wall moment-curvature response.

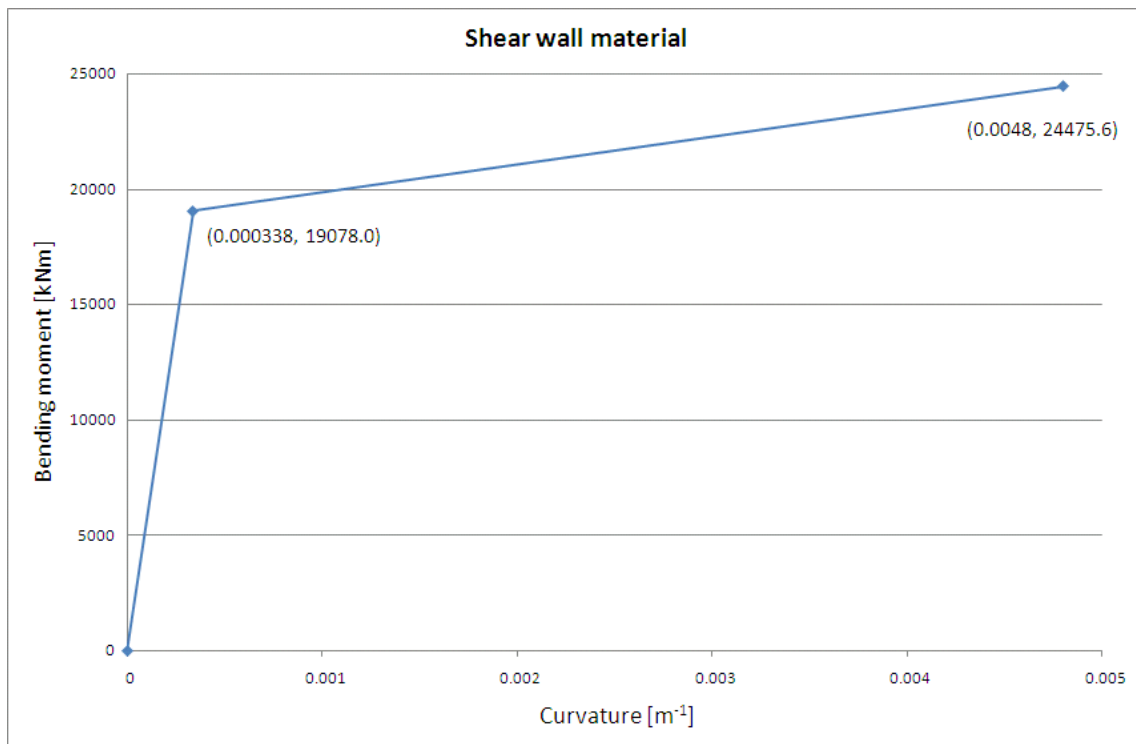


Figure 7-10: Shear wall moment-curvature material response

7.4.2 Internal frame

The same procedure as for the shear wall was followed to determine the nonlinear moment-curvature response of the internal frame material. The following parameters had to be defined for a bilinear approximation of the moment-curvature material response:

- Column size
- Elastic stiffness
- Yield curvature
- Ultimate curvature

This procedure is described in the following paragraphs.

Standard parameters

Modelling the internal frame with a single element will result in cantilever bending behaviour and not frame behaviour. A two-column frame was therefore chosen to represent the nonlinear response of the internal frame. The number of columns modelled is therefore reduced from eight to two. Sectional dimensions of the columns are of little importance as the material properties are determined to result in sufficient stiffness of the model to represent the frame response. As the eight columns of the

internal frame is reduced to only two columns in the simplified model, it was decided to choose sectional dimensions that will result in an inertia moment of roughly four times that of one of the internal frame columns.

The moment of inertia for one column of the internal frame is as follows:

$$I = \frac{b^4}{12} = \frac{0.6^4}{12} = 0.0108m^4$$

If the simplified model column dimension is denoted by “ x ”, it will follow that:

$$\frac{x^4}{12} = 0.0108 \times 4 \Rightarrow x = 0.849m$$

Column dimensions of the simplified model were subsequently chosen as **850mm×850mm**. Other parameters include the following:

- A lumped mass of **$m = 220425.6\text{kg}$** at each floor level.
- Material density of **$\rho = 2400\text{kg/m}^3$** to represent concrete material.
- A viscous damping ratio of **$\xi = 5\%$** was chosen.
- Poisson’s ratio of **$\nu = 0.2$** as prescribed to the concrete material of the SeismoStruct model.

Bilinear capacity curve and lateral loads

The bilinear approximation of the internal frame capacity curve (Figure 4-26) needs to define a yield point and ultimate point as described in Table 7-5.

Table 7-5: Bilinear approximation of internal frame capacity

	Base shear force (F) [kN]	Roof displacement (Δ) [m]
Yield point (y)	857.9	0.3500
Ultimate point (u)	981.7	0.5850

Distributing the above base shear forces in a triangular pattern over the height of the frame will result in applied forces as shown in Table 7-6.

Table 7-6: Lateral force distribution – internal frame

Floor level	F_y [kN]	F_u [kN]
1	23.8	27.3
2	47.7	54.5
3	71.5	81.8
4	95.3	109.1
5	119.2	136.3
6	143.0	163.6
7	166.8	190.9
8	190.7	218.2

Elastic stiffness

The lateral load distribution corresponding to the yield base shear force was applied to the model and linear static analyses performed iterating through values for the elastic modulus of the column material. A lateral roof displacement of 0.3502m was observed when an elastic modulus of **E = 2.845GPa** was prescribed. The 0.06% difference between this lateral roof displacement and the target roof displacement (Table 7-5) was assumed to be negligible.

Yield point of the moment-curvature response

The yield point of the moment-curvature response for the column elements had to be found. With the lateral load distribution as used above and performing a linear static analysis, it was observed that the maximum bending moment in the columns were obtained just below the connection between the column and the rigid link element at first floor level as shown in Figure 7-11.

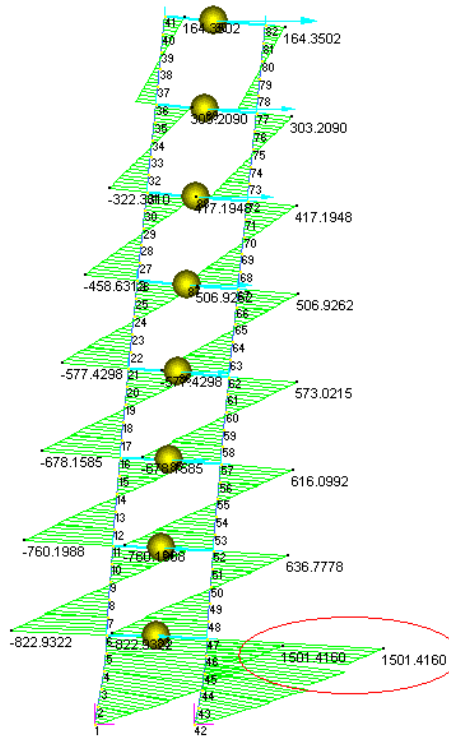


Figure 7-11: Bending moment diagram: internal frame model

It was observed that the bending moment at this position was $M_y = 1\,501.4\text{kNm}$.

Making the same assumptions as was made for the shear wall model it follows that:

$$I = \frac{d^4}{12} = \frac{0.85^4}{12} = 0.0435\text{m}^4$$

The maximum stress in the section due to the yield bending moment is therefore:

$$\sigma_y = \frac{M_y \cdot y}{I} = \frac{(1501.416 \times 10^3) \cdot (0.425)}{0.0435} = 14.669\text{MPa}$$

$$\varepsilon_y = \frac{\sigma_y}{E} = \frac{14.669}{2845} = 0.00516$$

The resulting curvature can therefore be determined using the strain calculated above.

$$\phi_y = \frac{2 \cdot \varepsilon_y}{d} = \frac{2 \times 0.00516}{0.85} = 0.01213\text{m}^{-1}$$

The yield point of the moment-curvature was therefore determined to be: $(\phi_y; M_y) = (0.01213; 1\,501.4) [\text{m}^{-1}; \text{kNm}]$.

Ultimate point of the moment-curvature response

The next step was to determine the ultimate curvature for the frame columns. Applying the lateral force distribution corresponding to the ultimate base shear force resulted in a maximum bending moment in the column of $M_u = 1\,718.0\text{kNm}$ at the same location as with the yield base shear applied. Following the same procedure as for the shear wall model, it was determined that defining an ultimate curvature of $\phi_u = 0.244\text{m}^{-1}$ resulted in a lateral roof displacement of 0.5851m by performing a nonlinear static analysis. The 0.02% difference between this obtained displacement and the ultimate lateral roof displacement of the bilinear force-displacement behaviour (section 4.6.1) was considered to be negligible.

The ultimate point of the nonlinear moment-curvature response of the simplified internal frame model is therefore defined as: $(\phi_u; M_u) = (0.244; 1\,718.0) [\text{m}^{-1}; \text{kNm}]$.

Figure 7-12 shows the resulting nonlinear moment-curvature material response assigned to the column elements of the simplified internal frame model.

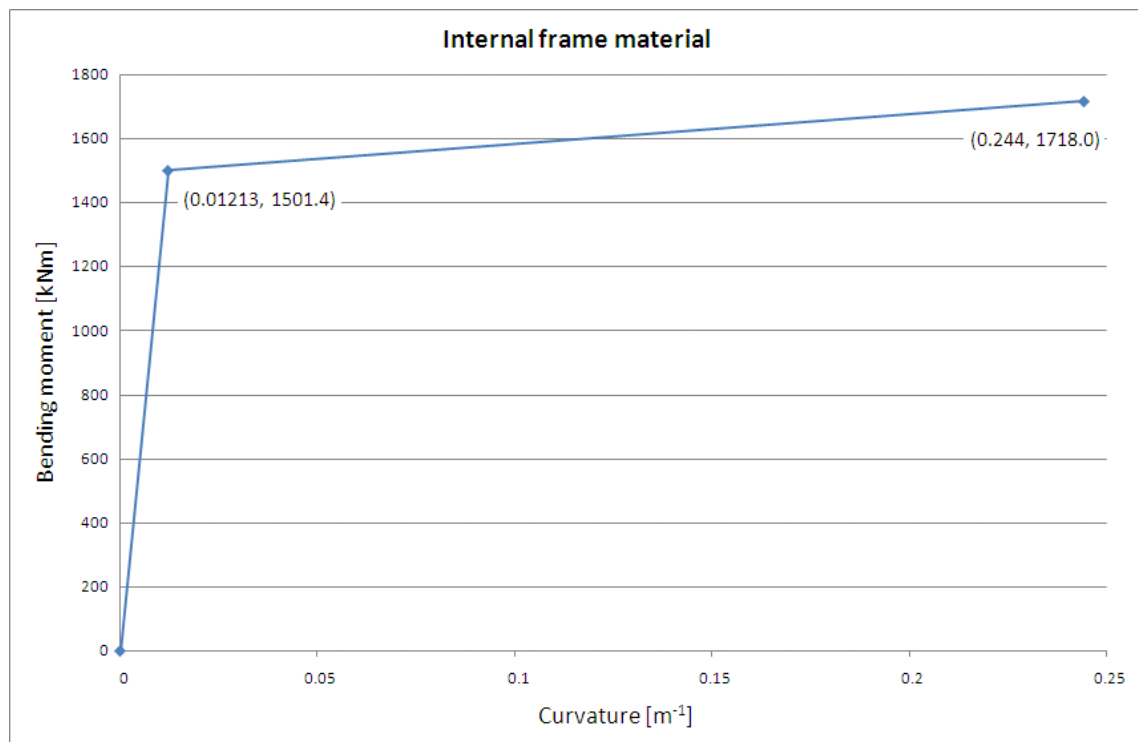


Figure 7-12: Internal frame moment-curvature material response

7.4.3 Hysteretic response properties

The nonlinear material behaviour had to be defined for the Strand7 model and is discussed in this section.

Nonlinear material behaviour can be implemented by Strand7 in different ways. The way in which the nonlinearity is applied will depend on the chosen *type of nonlinearity*, as well as the specified *hardening rule*.

Type of nonlinearity

The user is given a choice between *Elastic* and *Elastic-Plastic* nonlinear material behaviour. Elastic material behaviour is used when a nonlinear stress-strain relationship exists but no plastic deformation is allowed. Therefore this choice of nonlinearity will result in all applied strains to be recovered during unloading. Repetitive loading and unloading will follow the same deformation path.

Elastic-Plastic material behaviour refers to material that can exhibit plastic deformation. If the stress in the material exceeds the specified yield value, strains will result that comprise of elastic and plastic strain: $\epsilon_{\text{total}} = \epsilon_{\text{elastic}} + \epsilon_{\text{plastic}}$. Elastic strain will be recovered during unloading but plastic strain will not be recovered, resulting in hysteretic behaviour.

Hardening rule

Various hardening rules are available to the user to define the type of hysteretic behaviour of repetitive loading and unloading. *Isotropic hardening* describes hysteretic behaviour of which the compressive and tensile yield strengths are equal. *Kinematic hardening* is used when the elastic range in compression and tension is equal. The compressive and tensile yield deformations are, however, not equal. Increasing tensile yield deformation will therefore result in a reduced compressive yield deformation and vice versa [55].

Inelastic material response is of importance in this investigation and therefore *Elastic-Plastic* nonlinear behaviour was defined to ensure plastic deformation. Capacity curves of the various structural systems were obtained by performing static analyses loading these systems in only one direction. For the purpose of this investigation it was assumed that the capacity of the structural systems would be the same for lateral loading

in both directions. An *Isotropic hardening* rule was therefore chosen to describe the hysteretic behaviour.

7.5 Damping properties

Time-history analyses were performed in Strand7 using the *Nonlinear Transient Dynamic* procedure. As the name implies, this dynamic procedure is able to account for inelastic material response. Damping effects for beam elements are taken into account by prescribing a damping coefficient per cubic meter of beam element material with unit kNs/m/m³. It was therefore necessary to determine damping coefficients for the shear wall and frame models that will result in a 5% viscous damping ratio.

The procedure followed to determine appropriate damping coefficients is discussed in the following paragraphs, first for the shear wall material and then for the column material of the internal frame model.

7.5.1 Theoretical response

Theoretical expressions for the vibration response of a structure forced at its resonance frequency are provided by A.K. Chopra [8]. These expressions include the effect of damping. The displacement response of a system forced at resonance frequency is described by the following equation [8]:

$$u(t) = (u_{st})_0 \cdot \frac{1}{2\xi} \cdot \left[e^{-\xi\omega_n t} \left(\cos(\omega_D t) + \frac{\xi \cdot \sin(\omega_D t)}{\sqrt{1-\xi^2}} \right) - \cos(\omega_n t) \right]$$

In the above equation:

- $\omega_D = \omega_n \cdot \sqrt{1-\xi^2}$ = damped natural frequency.
- $(u_{st})_0$ = maximum displacement due to the statically applied force.
- ξ = Percentage of critical damping (expressed as a ratio).

Plotting the relationship of $\frac{u(t)}{(u_{st})_0}$ and $\frac{t}{T_n}$ results in a theoretical response for a 5% damped system as shown in Figure 7-13. As can be seen from Figure 7-13 the response is contained in an envelope in both directions of displacement.

Chopra [8] also provides expressions for these envelopes.

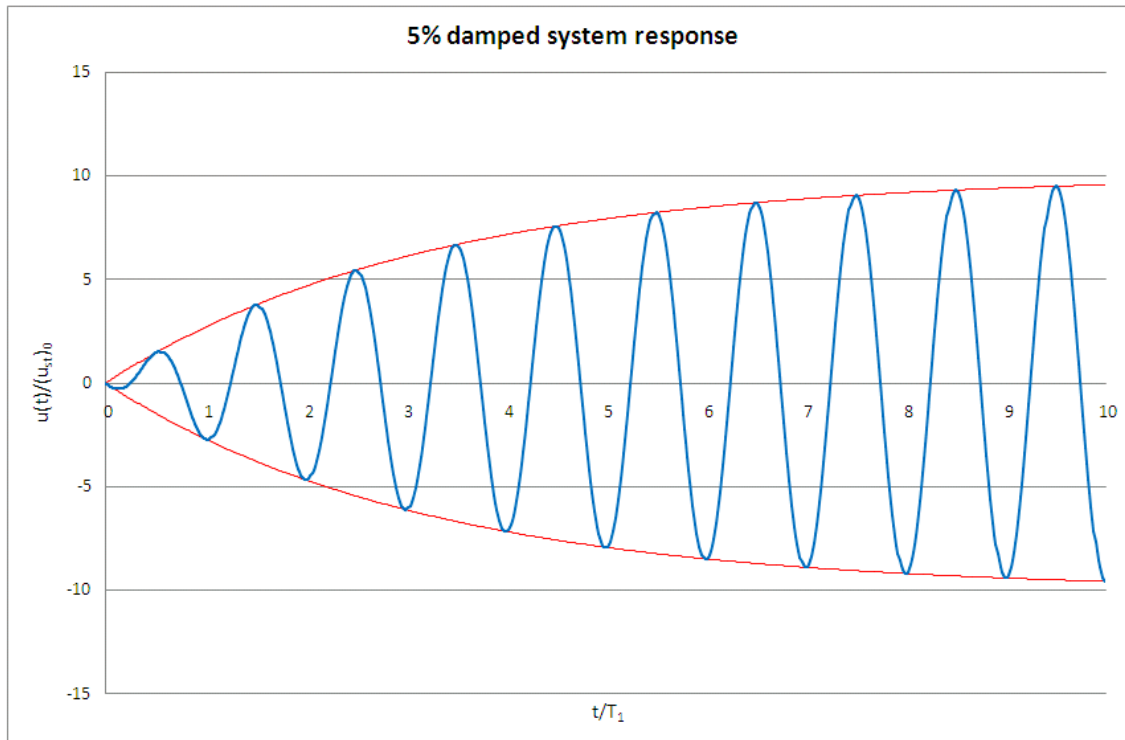


Figure 7-13: Response of a 5% damped system to a sinusoidal force at resonance frequency

7.5.2 Shear wall material damping coefficient

An iterative procedure was followed to determine the damping coefficient for the shear wall elements required to obtain the response shown in Figure 7-13.

Maximum value of static deformation

A linear static analysis was performed on the shear wall model applying 100kN lateral forces at every floor level. The roof displacement due to these applied loads was $(\mathbf{u}_{st})_0 = 45.6\text{mm}$.

Fundamental mode of vibration

It was decided to apply the lateral forces harmonically at the fundamental frequency and therefore this mode of vibration was to be found. *Natural Frequency Analysis* was

performed to obtain the fundamental mode of vibration. The fundamental frequency was found to be $f_1 = 0.807\text{Hz}$. Therefore:

$$T_1 = \frac{1}{f_1} = \frac{1}{0.807} = 1.240s$$

$$\omega_1 = \frac{2\pi}{T_1} = \frac{2\pi}{1.240} = 5.068\text{rad} / s$$

Harmonic analysis

The 100kN lateral forces at each floor level were then applied harmonically according to the following forcing function:

$$F(t) = F_0 \cdot \sin(\omega_1 t) = 100 \cdot \sin(5.068 \cdot t)$$

This harmonic analysis was performed prescribing a damping coefficient to the shear wall model material. The damping coefficient value was changed iteratively and the ratio of dynamic displacement to static displacement compared with the theoretical curve shown in Figure 7-13.

It was found that the ratio compared well with the theoretical curve when prescribing a damping coefficient of $c = 12.6\text{kNs/m/m}^3$ to the shear wall material as shown in Figure 7-14.

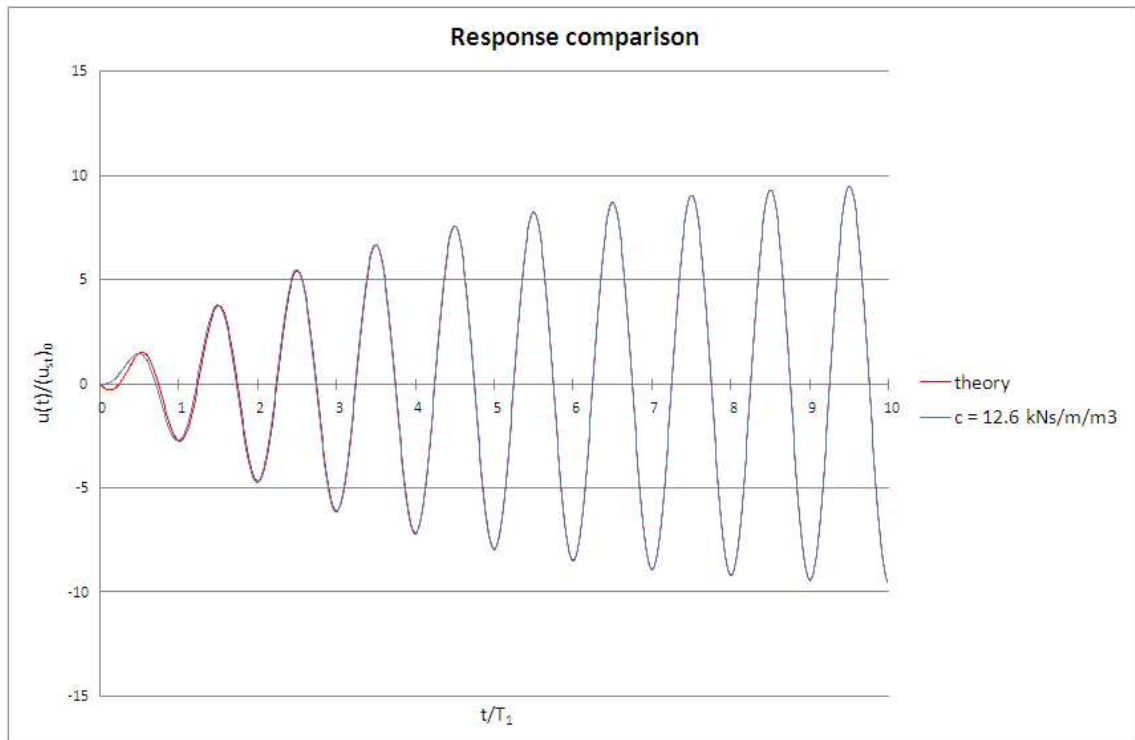


Figure 7-14: Shear wall harmonic response

7.5.3 Internal frame material damping coefficient

The same procedure was followed to determine the required damping coefficient for the column material of the simplified model of the internal frame. The following results were obtained:

Maximum value of static deformation

Performing a linear static analysis with 100kN lateral forces applied at every floor level resulted in a static lateral roof displacement of $(\mathbf{u}_{st})_0 = 253.4\text{mm}$.

Fundamental mode of vibration

From a *Natural Frequency Analysis* it was found that the fundamental mode of vibration was $\mathbf{f}_1 = 0.245\text{Hz}$ and therefore:

$$T_1 = \frac{1}{f_1} = \frac{1}{0.245} = 4.085\text{s}$$

$$\omega_1 = \frac{2\pi}{T_1} = \frac{2\pi}{4.085} = 1.538\text{rad/s}$$

Harmonic analysis

The 100kN forces were then applied harmonically at a forcing frequency equal to the fundamental frequency of the model:

$$F(t) = F_0 \cdot \sin(\omega_1 t) = 100 \cdot \sin(1.538 \cdot t)$$

It was observed that a damping coefficient of $\mathbf{c} = 8.7\text{kNs/m/m}^3$ for the column elements resulted in a lateral displacement response that compares well with the theoretical curve as shown in Figure 7-15.

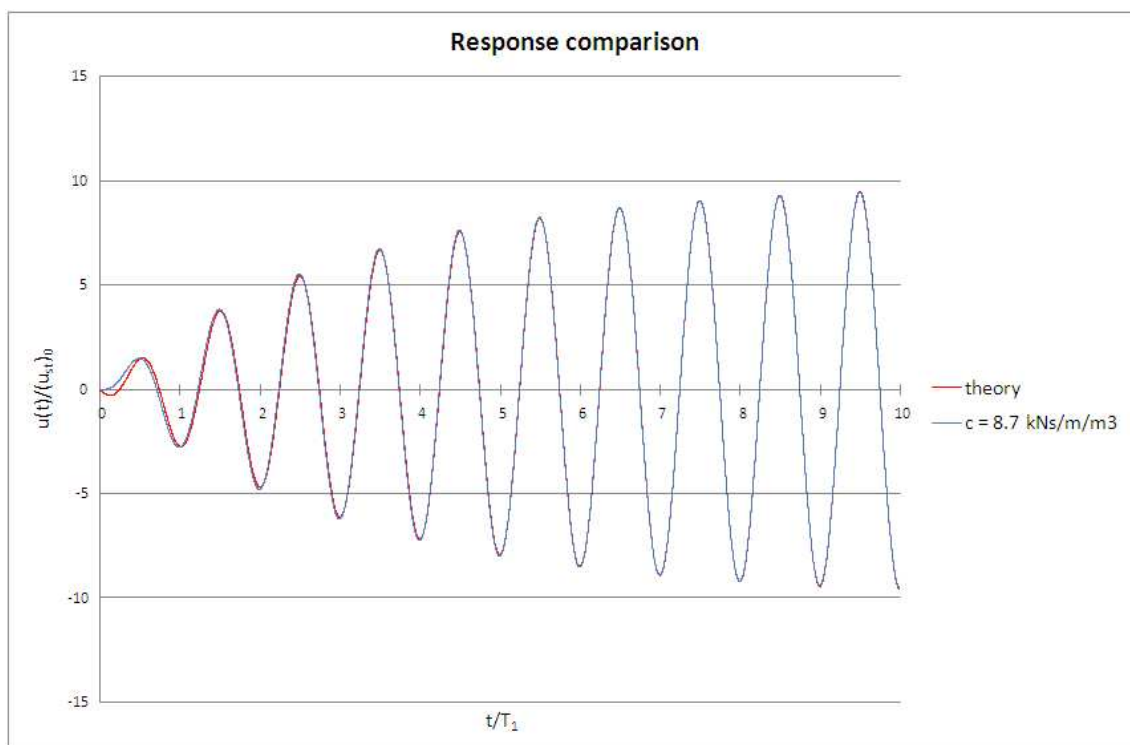


Figure 7-15: Internal frame harmonic response

Chapter eight discusses the results from the nonlinear time-history analyses as well as the assessment of the results on a local and global level.

Chapter 8

8 ANALYSES, RESULTS AND ASSESSMENT

8.1 Objectives

Figure 8-1 shows the part of the study, taken from Figure 1-1, which is addressed in this chapter. This includes:

- Determining an appropriate time step to be used in nonlinear time-history analyses of the investigated models.
- A discussion of the procedure and relevant parameters used in the software package *Strand7* to perform the time-history analyses.
- The response quantities that were used for assessment of the various structural systems.
- Assessment of the building on a local and global level.

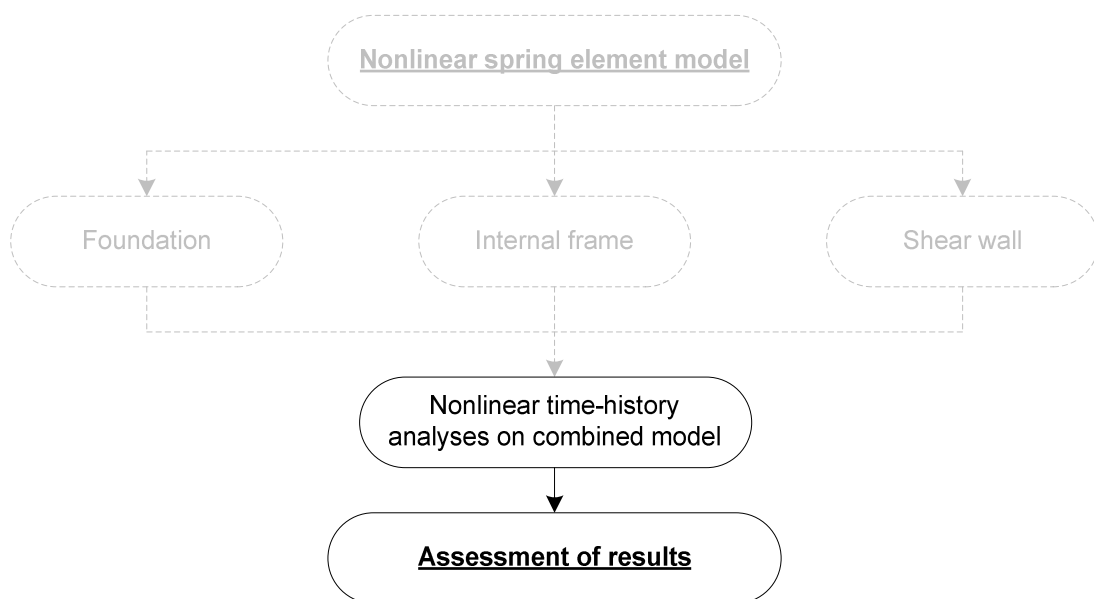


Figure 8-1: Chapter eight objectives

8.2 Nonlinear time-history analyses

Nonlinear time-history analyses were performed using the *Nonlinear Transient Dynamic* procedure of Strand7. The simplified models described in chapter seven were investigated with the six different foundation sizes as well as a model where no rotational stiffness is provided to the shear wall support, resulting in seven different models being investigated. The seven chosen ground motion accelerograms discussed in chapter 6 were used to perform nonlinear time-history analyses on each of the models. A total of 49 analyses were therefore carried out.

A discussion of the appropriate time step for nonlinear time-history analyses, a description of the software procedure used, and the output results used for assessment purposes are discussed in the following paragraphs.

8.2.1 Determining the appropriate time-step

Recorded ground motion histories obtained from the PEER Strong Motion Database [13] provides accelerograms with a time step of 0.005 seconds. It was decided to investigate whether a larger time-step could be used for the nonlinear time-history analyses in order to reduce computational effort. Various time-step increments were investigated for two accelerograms applied to the internal frame model, comparing the lateral roof displacement response.

Total accelerogram of ATH01 ground motion data set

The first ground motion that was investigated was the Loma Prieta event recorded at Agnews State Hospital, referred to as “ATH01” in this study. Refer to event number one in Table 6-1. This scaled accelerogram was applied to the frame for the total duration of the recorded ground motion. Four time-step increments were investigated. As the time increment of the recorded data is 0.005 seconds, it is assumed that using a time-step of $\Delta t = 0.005\text{s}$ will result in a suitably accurate result and was the first time-step investigated. The other time-step values investigated were 0.01s, 0.02s and 0.1s. Resulting maximum lateral roof displacement for the different time-step values are shown in Table 8-1.

Table 8-1: Time-step investigation results – ATH01

Δt [s]	Roof displacement [mm]	Difference from 0.005s value
0.005	76.2	0.00%
0.010	74.8	1.84%
0.020	74.5	2.23%
0.100	87.8	13.21%

Using a time-step of $\Delta t = 0.01$ s will half the computational effort and the resulting maximum lateral roof displacement does not differ much from the minimum time-step value. A time-history comparison of the lateral roof displacement response of the frame model for the time-step values of 0.005s and 0.01s are shown in Figure 8-2.

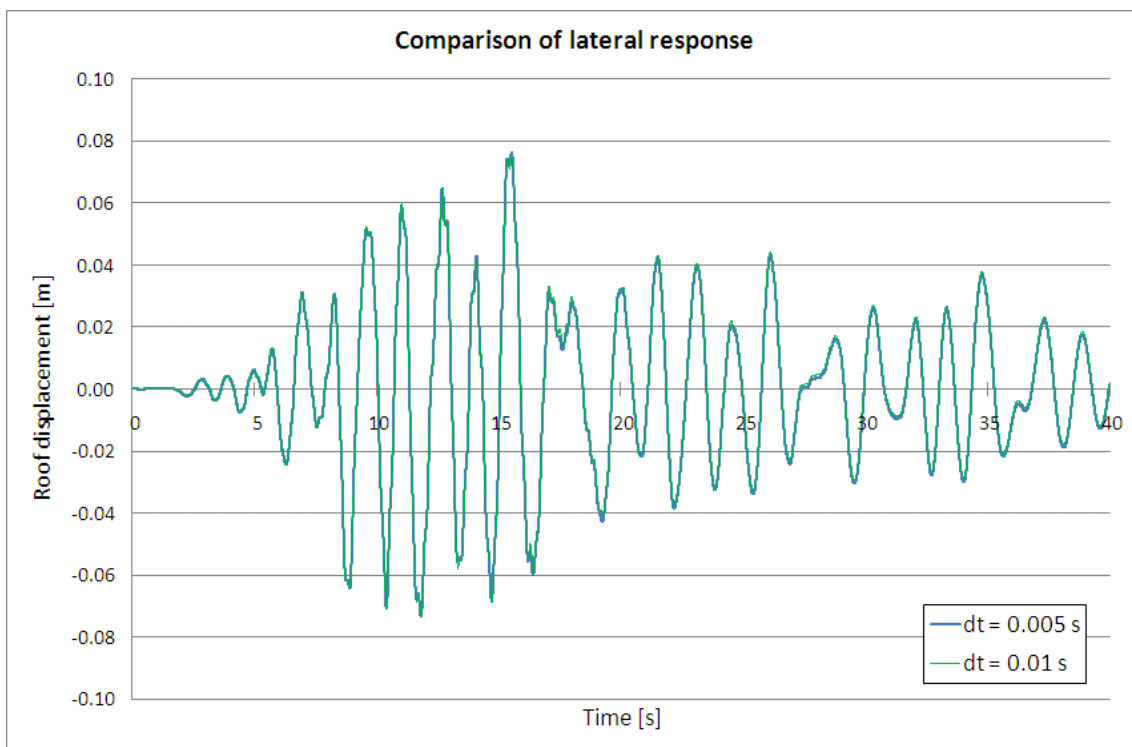


Figure 8-2: Comparison of lateral roof displacement – ATH01

From Figure 8-2 it is clear that the lateral displacement response of the frame is calculated sufficiently accurate using a time-step of $\Delta t = 0.01$ s.

Region of maximum acceleration of ATH04 ground motion data set

The influence of a larger time-step was also investigated applying the Loma Prieta event recorded at Anderson Dam, referred to as “ATH04” in this study. Refer to event number four in Table 6-1. Here it was decided to only investigate the time period where

maximum ground acceleration had been recorded. The range of ground acceleration values from 5 seconds to 15 seconds of the scaled accelerogram was therefore chosen as shown in Figure 8-3.

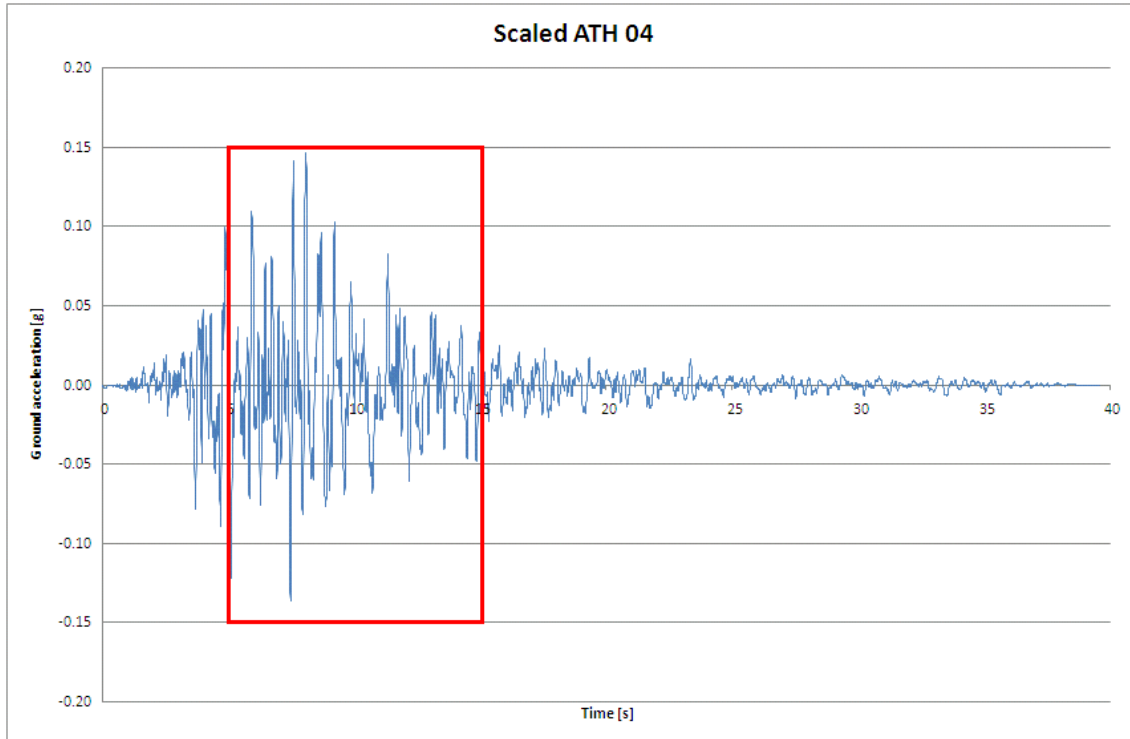


Figure 8-3: ATH04 region of maximum ground acceleration

Time-step values investigated were 0.005s, 0.01s, 0.02s, 0.05s, 0.08s and 0.1s. The maximum lateral displacement response for the different investigated time-step values are shown in Table 8-2.

Table 8-2: Time-step investigation results – ATH04

Δt [s]	Roof displacement [mm]	Difference from 0.005s value
0.005	137.3	0.00%
0.010	137.6	0.22%
0.020	139.3	1.44%
0.050	146.6	6.34%
0.080	158.2	13.21%
0.100	202.1	32.06%

From Table 8-2 it is clear that a time-step value of $\Delta t = 0.01s$ results in a maximum lateral displacement response sufficiently close to that obtained implementing the

smallest time-step. A good comparison of the total lateral displacement response of the frame is obtained between these two time-step values as shown in Figure 8-4.

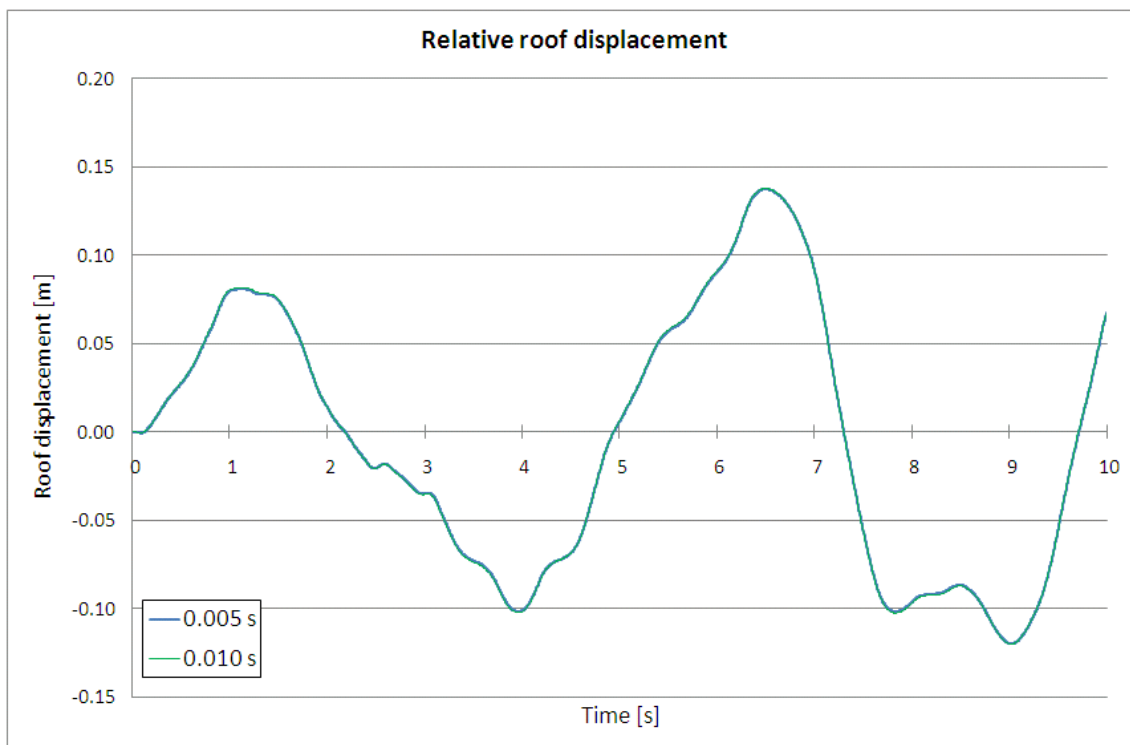


Figure 8-4: Comparison of lateral roof displacement – ATH04

All subsequent nonlinear time-history analyses were therefore performed using a time-step of $\Delta t = 0.01\text{s}$.

8.2.2 Nonlinear Transient Dynamic procedure

The *Nonlinear Transient Dynamic* procedure provided by Strand7 [55] is able to apply time dependant acceleration of restrained nodes taking nonlinearity into account. This was therefore the preferred procedure for the nonlinear time-history analyses. The following conditions must be defined by the user:

Initial Conditions

Initial velocities and accelerations of all free nodes are prescribed in each of the global axis directions. The structure is assumed to be static prior to a seismic event and therefore zero values were prescribed here.

Base Acceleration

Time dependant acceleration of all restrained nodes is prescribed by a direction vector and a table reference prescribing the time dependant acceleration in that direction. The values in the direction vector are used to scale the acceleration table prescribed in that direction. Required output results are also chosen here to be either total or relative displacement, velocity or acceleration. Total results were chosen because the relative quantities can be obtained by comparing the absolute results at different nodes from the output. The Newmark- β method was implemented to solve the time-history analyses with $\beta = \frac{1}{2}$ and $\alpha = \frac{1}{4}$ [55].

Node History

Nodes where output is required must be chosen by the user. All possible displacement, velocity and acceleration output were chosen at the base and roof nodes of the model.

8.2.3 Response quantities for result assessment

Different response quantities were used to assess the various structural systems:

- Lateral roof displacement was used to assess the response of the internal frame.
- Rotation of the foundation spring element was used to investigate failures associated with the foundations.
- As the capacity curve of the shear wall was determined by assuming a fixed support to the shear wall, it follows that the lateral roof displacement, taking footing rotation into account, was used to assess the shear wall response.

The results that were obtained from the output of the analyses will be discussed in the following sections.

8.3 Local assessment of results

The performance of each individual component of the investigated lateral load resisting system was evaluated as well as the performance level of the combined system on a global level.

- First, the lateral roof displacement response is used to investigate failures in the internal frame.
- Footing rotation response is used to assess foundation performance.
- Lateral roof displacement of the shear wall model relative to the footing rotation is then used to investigate failures in the shear wall model.
- Finally, the lateral roof displacement response is used to assess the performance level of the entire building structure.

8.3.1 Internal frame

Lateral roof displacement response obtained from the time-history analyses was used to investigate whether failures can be expected to occur in the internal frame. The same response quantities were therefore used for the local assessment of the internal frame and the global assessment of the entire structure.

From the lateral force-displacement curve of the internal frame applying a triangular distribution of the base shear force (section 4.6.1), it was observed that failures were first identified at the following lateral roof displacements:

- Steel yielding: 390mm
- Slab rotation limit: 420mm
- Cover spalling: 585mm

Seven recorded ground motion accelerograms, scaled to fit the elastic response spectrum, were used to perform time-history analyses on each of the seven models with different foundation responses. Roof displacement response relative to that of the base nodes was investigated from the output of the analyses and the maximum lateral displacement was obtained from this response. As discussed in section 2.2.5 the average response can be investigated when at least seven ground motions are investigated and therefore the average maximum lateral displacement was also calculated for each case.

The maximum lateral roof displacement response resulting from the various analyses (measured in millimetre) are shown in Table 8-3.

Table 8-3: Lateral roof displacement response [mm]

Event	Model foundation size						
	100%	80%	60%	40%	20%	0%	None
ATH01	181.6	199.4	195.5	208.9	197.4	188.9	154.1
ATH02	76.4	83.0	87.5	90.3	102.9	120.5	178.3
ATH04	66.1	70.7	67.9	74.2	92.3	75.9	112.5
ATH05	121.7	125.7	125.1	118.7	102.4	86.8	141.8
ATH08	147.3	145.5	174.3	144.3	138.4	138.3	155.3
ATH14	112.3	131.6	142.3	150.9	143.5	139.4	255.6
ATH15	227.2	240.6	248.2	268.2	289.2	308.3	360.8
AVERAGE	133.2	142.4	148.7	150.8	152.3	151.2	194.1
STD DEV	53.0	56.0	58.1	63.0	65.0	72.9	79.6

A graphical representation of the above results is shown in Figure 8-5.

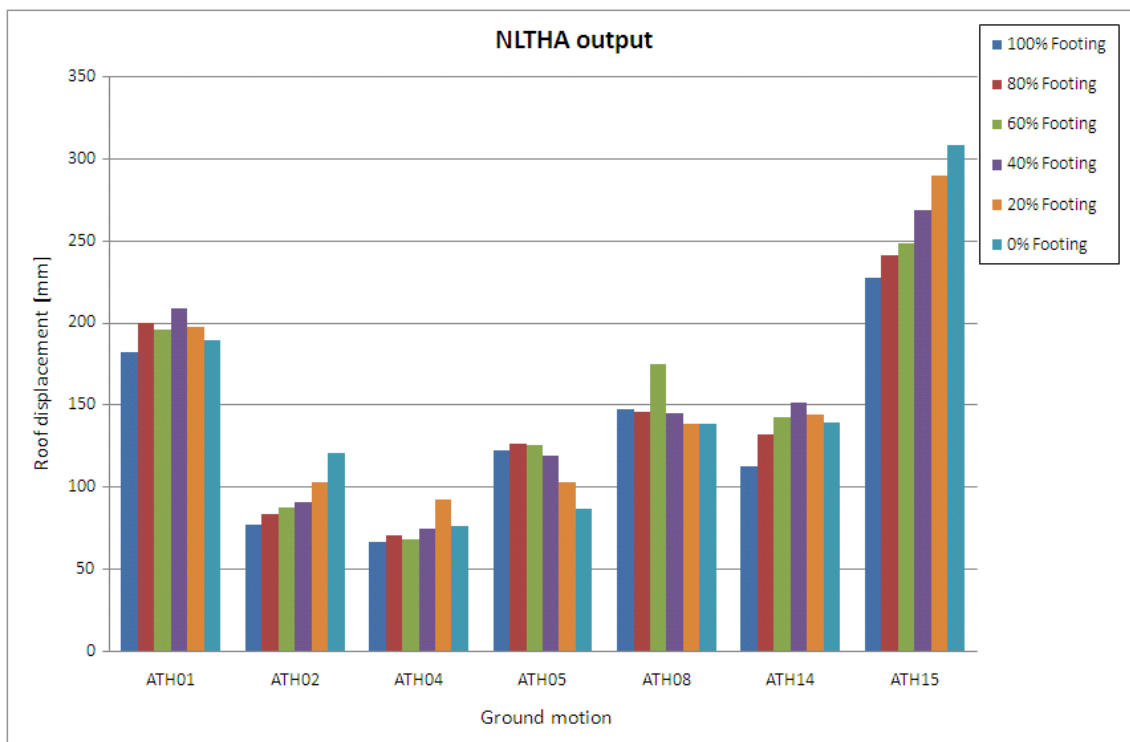


Figure 8-5: Graphical representation of maximum displacement response

Eurocode 8 specifies that at least three artificial, recorded or simulated ground motion records should be used as input for nonlinear time-history analyses. If the response of a structural system is obtained from at least seven nonlinear time-history analyses, it is

specified that the average of the response quantities from all these analyses may be used as the action effect in subsequent evaluations. If less than seven ground motion records are used, the most unfavourable response quantity from the analyses should be used [7].

As seven recorded ground motions were used in this investigation the average response of each model may be evaluated. The standard deviations between the lateral roof displacement responses obtained from the various ground motions are quite large as shown in Table 8-3. It therefore follows that ground motion leading to more severe lateral displacement response is a significant possibility. For this reason it was chosen to not only assess the mean response, but also the maximum response obtained from each investigated model. Ground motion number 15 from Table 6-1, "ATH15", resulted in the most unfavourable response for each of the investigated models.

Figure 8-6 shows the average and maximum lateral displacement response.

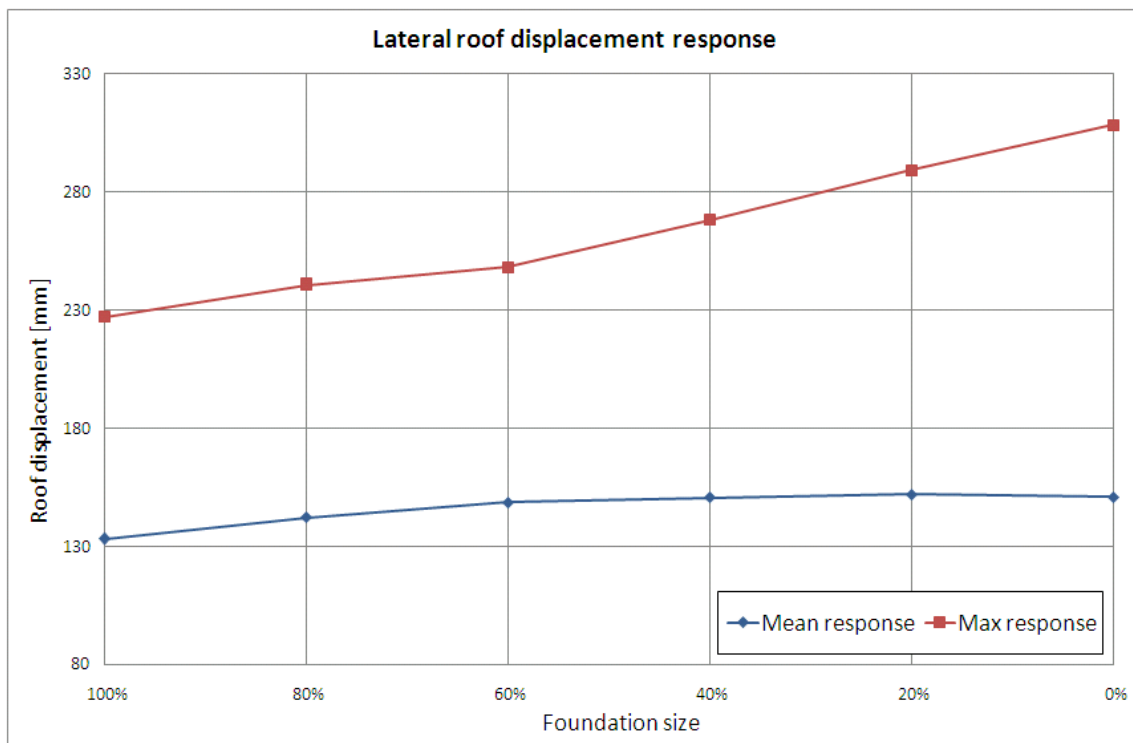


Figure 8-6: Lateral displacement response

A general increasing trend in lateral displacement is observed for both the average and maximum response with the exception that the mean lateral displacement response of the foundation size determined to resist zero percent of the shear wall overstrength bending moment is slightly smaller than that of the foundation size determined to resist 20% of the same bending moment.

The increase in lateral displacement response between successive foundation sizes is not constant. This can be contributed to the fact that the increase in ultimate bending moment resistance between successive foundations is not constant as can be seen from Table 5-2.

An increasing trend in lateral displacement response with decreasing foundation size can be expected as the bending moment resistance of the foundation decreases with decreasing size. The response of the structure to ground motion can result in nonlinear material response and therefore the natural vibration periods of the structure will tend to increase. For this reason the natural vibration periods of the structure will be unknown and will differ as the response of the structure becomes increasingly nonlinear. The 5% damped response spectra of the various recorded ground motions differ in shape and none of these response spectra are smooth. The resulting peak ground acceleration from different ground motion response spectra can therefore be expected to differ at the same natural vibration period.

For this reason it is clear that the lateral displacement response from random excitation can not be predicted precisely and this could be the reason for the smaller average lateral displacement response obtained with the “0%” foundation size than with the “20%” foundation size.

From the output it is can also be observed that none of the performance criteria limits are reached for any of the response quantities. It can therefore be stated that no flexural failures are expected in the internal frame.

8.3.2 Foundations

Rotation response of the spring element used to model the rotational stiffness of the foundations was used to assess failures associated with the various foundation sizes. Rocking of the foundations is expected and therefore the only performance criteria investigated in the local assessment of the foundations were yielding of the underlying soil. Footing rotation limits associated with yielding of the underlying soil were determined from the capacity curves of the foundations as discussed in chapter 5. These limits are shown in Table 8-4.

Table 8-4: Footing rotation associated with soil yielding

Foundation size	Footing rotation [rad]
100%	0.0135
80%	0.0131
60%	0.0077
40%	0.0075
20%	0.0052
0%	0.0033

Maximum footing rotations, measured in radians, from each nonlinear time-history analysis of the model with the various foundation sizes were as shown in Table 8-5.

Table 8-5: Footing rotation response [radians]

Event	Model foundation size					
	100%	80%	60%	40%	20%	0%
ATH01	0.0028	0.0038	0.0043	0.0056	0.0057	0.0054
ATH02	0.0013	0.0015	0.0017	0.0023	0.0034	0.0047
ATH04	0.0010	0.0014	0.0012	0.0024	0.0027	0.0026
ATH05	0.0021	0.0036	0.0035	0.0033	0.0037	0.0038
ATH08	0.0026	0.0029	0.0033	0.0037	0.0040	0.0049
ATH14	0.0015	0.0021	0.0025	0.0036	0.0038	0.0044
ATH15	0.0034	0.0061	0.0064	0.0071	0.0081	0.0096
AVERAGE	0.0021	0.0031	0.0033	0.0040	0.0045	0.0050
STD DEV	0.0008	0.0015	0.0016	0.0016	0.0017	0.0020

For the same reason as discussed in the local assessment of the internal frame, both the average response and maximum response were investigated. The ground motion “ATH15” generally resulted in the most unfavourable response.

A graphical representation of the footing rotation response and the rotation limit associated with soil yielding is presented in Figure 8-7 for the average and maximum rotation response.

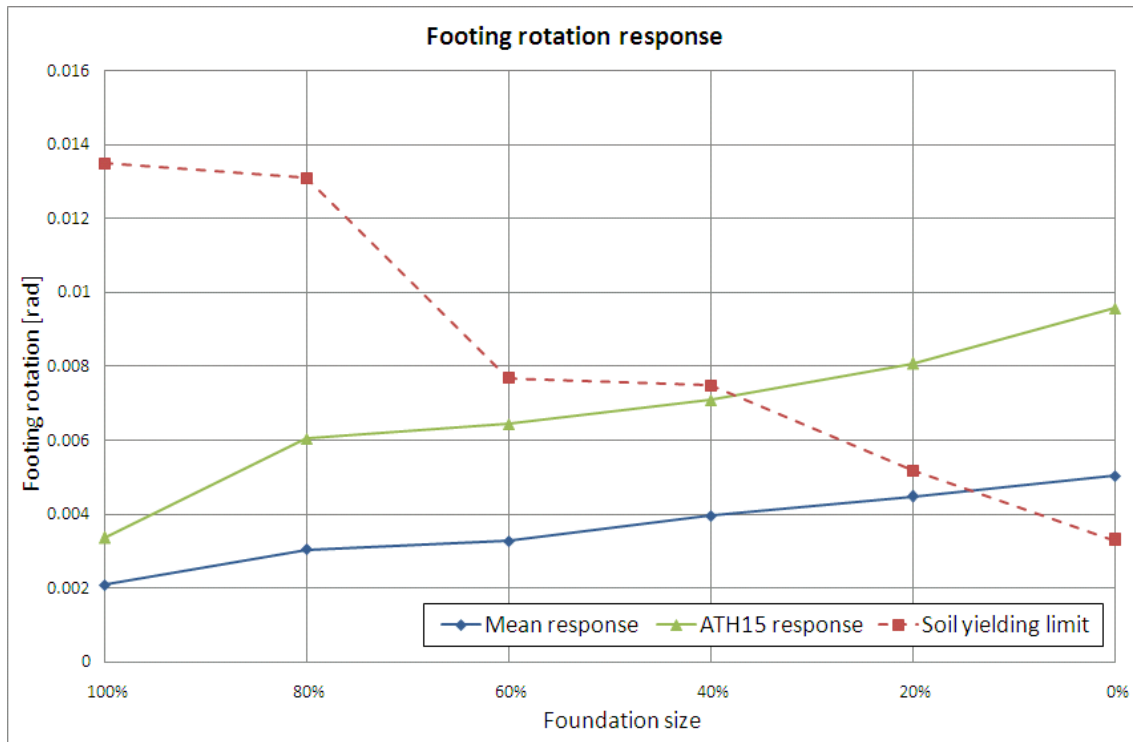


Figure 8-7: Footing rotation response

The following is observed:

- The average rotation response of the “0%” footing exceeds the soil yielding performance criteria by **34%**.
- The maximum rotation response of the “20%” footing exceeds this limit by **35.8%**.
- The maximum rotation response of the “0%” footing exceeds the soil yielding limit by **65.6%**.

It follows that yielding of the underlying soil can be expected only for very small wall foundation sizes.

8.3.3 Shear wall

Lateral roof displacement response obtained from the time-history analyses was used to investigate whether failures can be expected to occur in the shear wall. From the lateral force-displacement curve of the shear wall determined by distributing the base shear force in a triangular pattern over the height of the wall (section 4.6.2), failures were first identified at the following lateral roof displacements:

- Steel yielding: 148.7mm
- Cover spalling: 282mm

Lateral roof displacement cannot be used directly to assess the shear wall response as the footing rotation will tend to influence strains in the shear wall, depending on the direction of lateral roof displacement relative to the rotation of the shear wall footing. The capacity curve of the shear wall was determined by assuming a fixed moment support to the bottom of the shear wall and therefore the lateral displacement that should be used for assessment of the shear wall response is the relative lateral displacement as shown by Δ_{rel} in Figure 8-8.

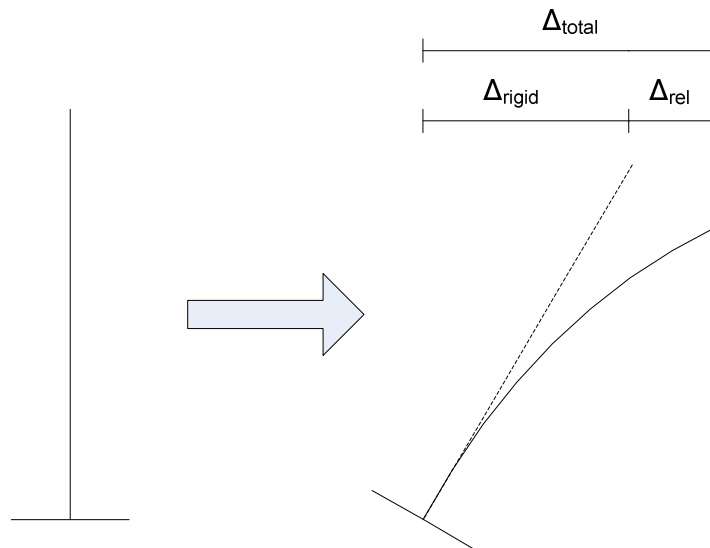


Figure 8-8: Relative shear wall displacement

Footing rotations used to investigate the foundation response were transformed to lateral roof displacement of a rigid wall. If this calculated displacement act in the same direction as the lateral roof displacement, shear wall material strains will be reduced. With this calculated displacement acting in the opposite direction as the roof displacement, shear wall material strains will however increase. Relative lateral displacement response of the shear wall, measured in millimetre, was determined to be as shown in Table 8-6.

Table 8-6: Relative shear wall roof displacement [mm]

Event	Model foundation size					
	100%	80%	60%	40%	20%	0%
ATH01	120.5	102.6	87.0	80.1	67.8	60.1
ATH02	64.0	59.5	60.9	62.1	75.5	85.0
ATH04	56.2	56.3	54.5	65.3	63.8	64.3
ATH05	84.6	84.3	78.6	75.0	82.1	74.9
ATH08	103.5	92.4	92.8	91.0	83.8	71.3
ATH14	70.3	73.9	77.1	73.6	86.8	94.9
ATH15	155.5	133.0	92.7	81.0	78.1	74.4
AVERAGE	93.5	86.0	77.7	75.4	76.8	75.0
STD DEV	32.8	24.7	13.9	9.1	7.8	11.0

From Table 8-6 it is observed that the maximum displacement responses occur at different ground motions for models with different foundation sizes:

- “ATH15” results in the maximum response for the foundation sizes determined to resist 100% and 80% of the shear wall overstrength bending moment.
- “ATH08” results in the maximum response for the foundation sizes determined to resist 60% and 40% of the shear wall overstrength bending moment.
- “ATH14” results in the maximum response for the foundation sizes determined to resist 20% and 0% of the shear wall overstrength bending moment.

A graphical representation of the output results with the relevant performance criteria limits is shown in Figure 8-9 for the average and maximum lateral displacement response respectively.

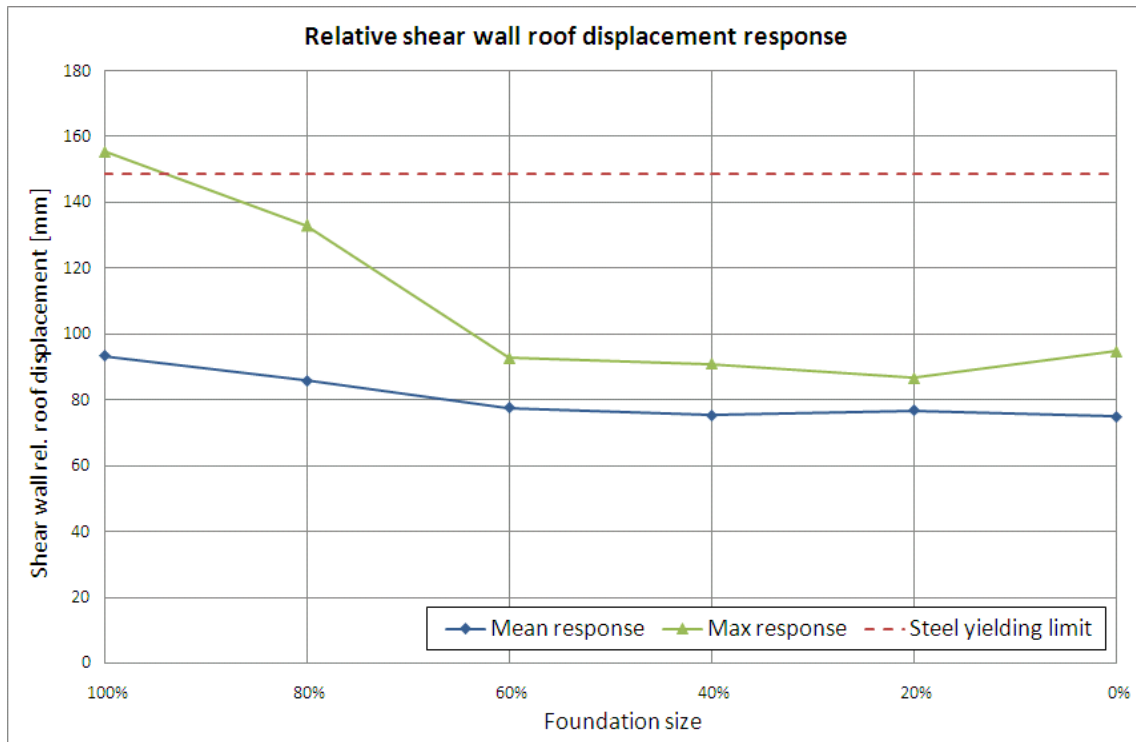


Figure 8-9: Relative shear wall lateral roof displacement response

A general decrease in relative lateral roof displacement is observed with diminishing footing size. The rocking effect of the foundation therefore generally has the effect of reducing strains in the shear wall and hence, decreases the relative lateral roof displacement response of the shear wall. This phenomenon is well known. Booth and Key [6] mentioned that collapse of structures resulting from the failure of the moment capacity of foundations is comparatively rare. Paulay and Priestley [5] stated that the satisfactory seismic response of some structures can only be attributed to foundation rocking.

The observed generally reducing trend of lateral displacement is therefore expected. No failures are observed from the average response. The roof displacement associated with the steel yielding performance criteria is however exceeded by **4.4%** for the maximum response of the model with the “100%” footing subjected to ground motion ATH15.

It is therefore clear that the response of the shear wall is improved by the rocking action of the wall foundation, as observed by previous researchers. For the model with a wall foundation size determined to resist the full shear wall overstrength bending moment, it can be expected that a plastic hinge mechanism should form in the shear wall near the foundation to dissipate energy. Steel material strain in the shear wall is therefore

expected to approach the yielding strain limit as the foundation size increases and that the steel yielding strain limit should be exceeded for the foundation size that resist the full shear wall overstrength bending moment. This is indeed observed from the most unfavourable output results.

From the above evaluation of response results it is clear that the mechanism of energy dissipation changes from a plastic hinge mechanism in the shear wall, when large wall foundations are present, to a foundation rocking mechanism when smaller wall foundations are used.

8.4 Global assessment of results

Assessment of the lateral roof displacement of the combined models that were investigated was performed using performance levels as described in the Vision 2000 report on *Performance Based Seismic Engineering of Buildings* [56].

8.4.1 Vision 2000 performance levels

According to the Vision 2000 report [56] *a performance level is an expression of the maximum desired extent of damage to a building, given that a specific earthquake design level affects it. The condition of structural elements, nonstructural elements and contents are all considered in the performance levels, as are availability of site utilities necessary to building function.*

Four performance levels are defined in the Vision 2000 report for structures displaced beyond the elastic response and are the following [56]:

Fully Operational

Essentially no damage has occurred in this performance level and the consequences to the building users are negligible. The building can be occupied and all equipment and services associated with basic occupancy and function are available for use. Repair of the building is generally not required.

Operational

Building structures in this performance level experience moderate nonstructural damage and light structural damage. This damage to the structure is limited and does not affect

the safety thereof for occupancy. The structure would be safe for occupancy for its normal intended function, immediately after the earthquake. Damage to some contents, utilities and nonstructural elements may result in the disruption of some normal functions of the building.

Life Safe

Building structures with moderate structural and nonstructural damage is classified in the *Life Safe* performance level. The lateral stiffness of the structure and the ability thereof to resist additional lateral loads has been reduced but some resistance against collapse remain. Some electrical and mechanical equipment may not function. It would be possible to repair the building but it may not be economically feasible.

Near Collapse

This is an extreme damage state in which the vertical and lateral load resistance of the building structure have been substantially compromised. Partial or total collapse may result from aftershocks. All vertical load resisting elements continue to function although debris hazards may have occurred. This structure will most likely be unsafe for occupancy and repair may not be technically or economically feasible.

Displacement limits determined by the capacity curve of the total lateral load resisting system of the building have been prescribed by the Vision 2000 report for the various performance levels. The yield displacement (Δ_y), ultimate displacement (Δ_u) and plastic displacement ($\Delta_p = \Delta_u - \Delta_y$) are used to define these performance levels. The building structure is assumed to have deformed elastically if the lateral displacement does not exceed the yield displacement of the capacity curve of the lateral load resisting system of the building and it is assumed that the building collapses if the lateral displacement exceeds the ultimate lateral displacement of the capacity curve.

Lateral displacement limits of the various performance levels are the following:

- Elastic: $0 \leq \Delta \leq \Delta_y$
- Fully Operational: $\Delta_y \leq \Delta \leq \Delta_y + 0.3\Delta_p$
- Operational: $\Delta_y + 0.3\Delta_p \leq \Delta \leq \Delta_y + 0.6\Delta_p$
- Life Safe: $\Delta_y + 0.6\Delta_p \leq \Delta \leq \Delta_y + 0.8\Delta_p$
- Near Collapse: $\Delta_y + 0.8\Delta_p \leq \Delta \leq \Delta_y + \Delta_p$
- Collapsed: $\Delta_y + \Delta_p \leq \Delta$

It was therefore required that a capacity curve be determined for the investigated combined lateral load resisting system to enable global assessment of the lateral roof displacements. The global capacity curve is discussed in the following section.

8.4.2 Global capacity curve

A capacity curve of the investigated combined lateral load resisting system requires the combination of capacity curves of each structural system included in the combined model: the internal frame, shear wall and wall foundation. The spring analogy describing how the various structural systems contribute to the total stiffness of the investigated model was discussed in section 7.2. Global stiffness of the combined system can be determined by replacing the different elements in the spring analogy with only one spring element representing the global stiffness as shown in Figure 8-10.

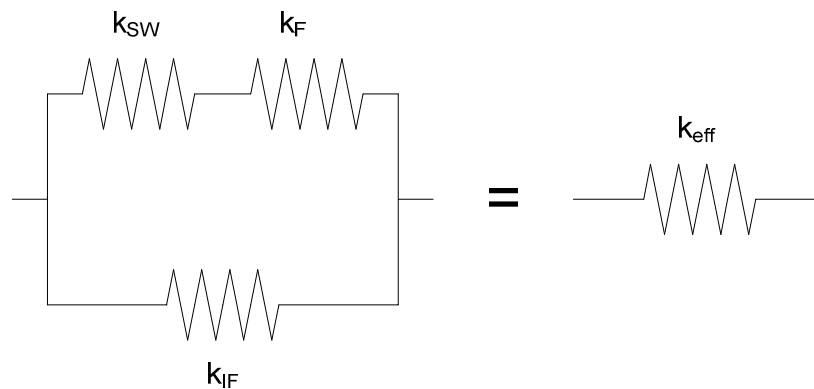


Figure 8-10: Spring analogy for global stiffness

Here the spring elements represent the following:

- k_{SW} = Capacity of the shear wall.
- k_F = Capacity of the wall foundation.
- k_{IF} = Capacity of the internal frame.
- k_{eff} = Effective stiffness of the global system.

In the same manner as was done in section 7.2 the effective stiffness of the global system can be determined by the following expression:

$$k_{eff} = k_{IF} + \frac{k_{SW} \cdot k_F}{k_{SW} + k_F}$$

The stiffness of a structural system is defined as the slope of the capacity curve which describes the nonlinear relationship between base shear force (V_i) and lateral roof displacement (Δ_i) and therefore:

$$k_i = V_i / \Delta_i$$

To determine a global capacity curve representing the relationship between base shear force and lateral roof displacement of the combined system, base shear values at any given displacement value can therefore be determined in the same manner as for the stiffness:

$$V_{eff} = V_{IF} + \frac{V_{SW} \cdot V_F}{V_{SW} + V_F}$$

Where, at a given lateral roof displacement:

- V_{SW} = Shear wall base shear value.
- V_F = Wall foundation base shear value.
- V_{IF} = Internal frame base shear value.
- V_{eff} = Base shear force of the global system.

Global capacity curves were determined for each model with varying foundation sizes. For each model it was observed that the yield displacement and ultimate displacement of the resulting global capacity curve compared well with that of the shear wall capacity curve. A bilinear approximation of the global capacity curve was determined using the yield- and ultimate displacement values of the shear wall capacity curve. This procedure was also followed by Schwarz et al. [57] for a model combining the capacity of a shear wall and reinforced concrete frame.

Figure 8-11 shows the global capacity curve determined for the model consisting of the internal frame, shear wall, and wall foundation of which the foundation size was determined by applying the full shear wall overstrength bending moment.

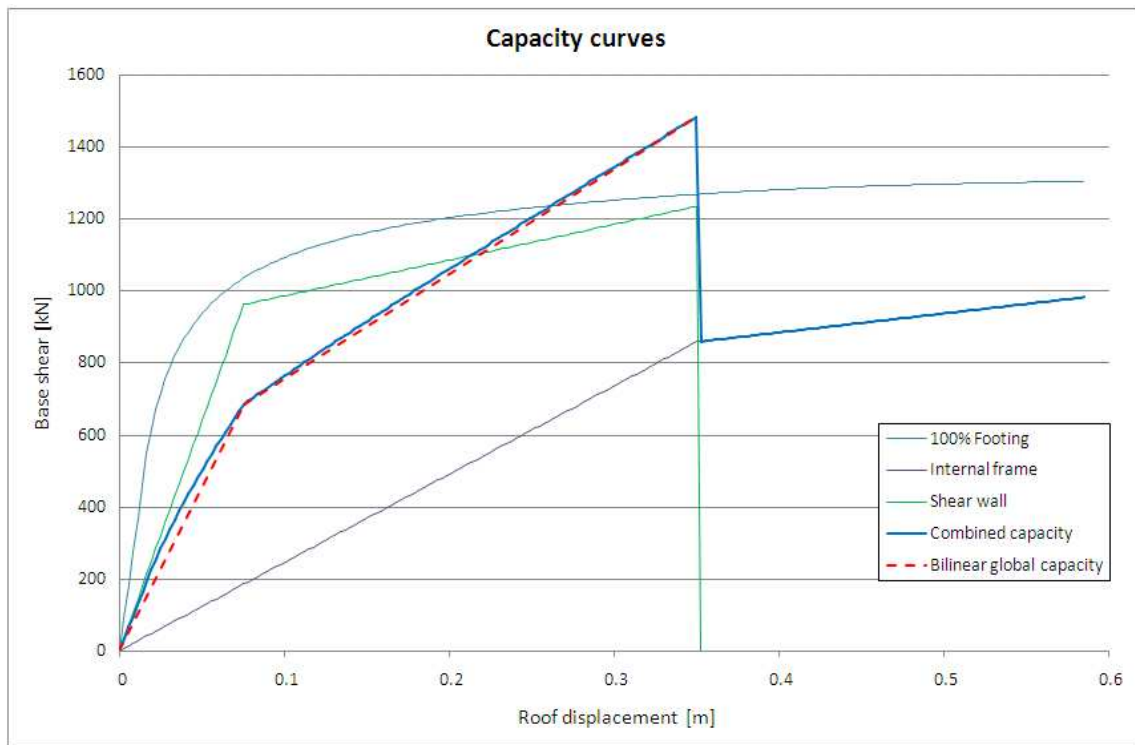


Figure 8-11: Global capacity curve of model with foundation of full overstrength moment

It is therefore clear that the lateral load capacity of the shear wall dominates the global effect. The stiffness of the shear wall is much greater than that of the internal frame and for smaller wall foundations the shear wall is the structural element with the greatest stiffness. It can therefore be expected that the shear wall will have a greater influence on the global lateral load capacity than the other structural systems.

A comparison of the global capacity curves of the various models are shown in Figure 8-12. As could be expected, a decreasing capacity was observed with decreasing foundation size.

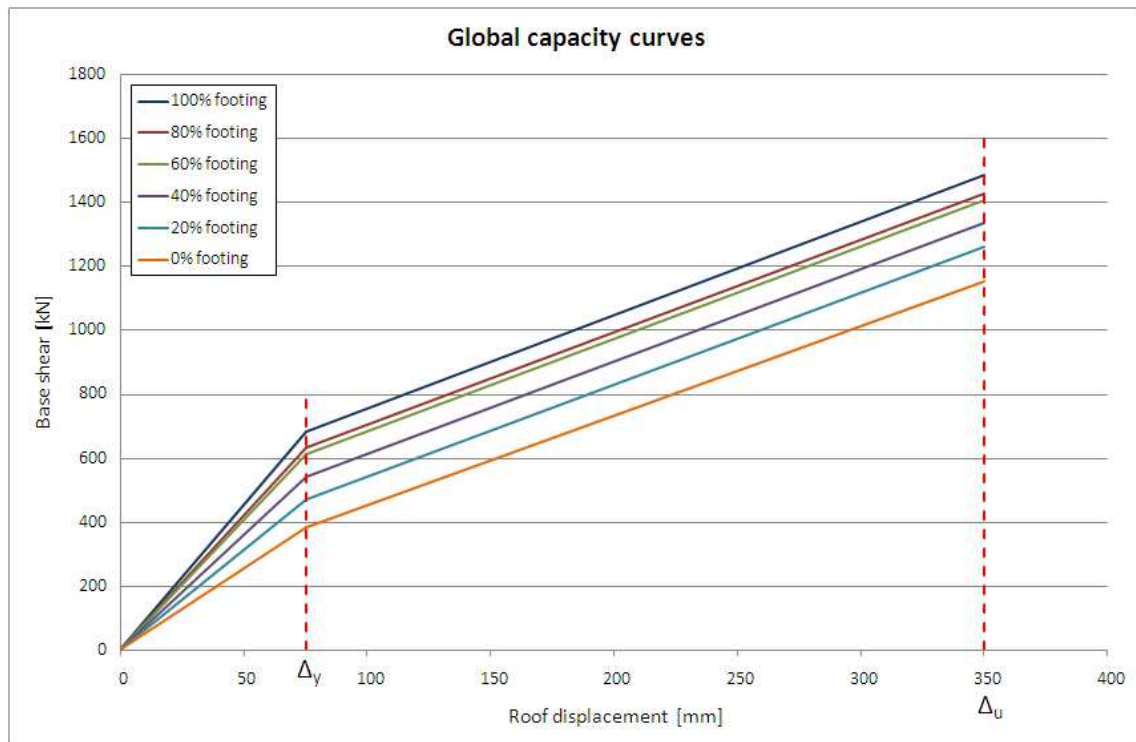


Figure 8-12: Comparison of bilinear global capacity curves

From the above discussion it follows that the same yield- and ultimate lateral roof displacement values are applicable for all investigated models and equal to that obtained from the lateral force-displacement behaviour of the shear wall (section 4.6.2). The relevant lateral displacement values are:

- Yield displacement: $\Delta_y = 76\text{mm}$ (Figure 8-12)
- Ultimate displacement: $\Delta_u = 350\text{mm}$ (Figure 8-12)
- Plastic displacement range: $\Delta_p = \Delta_u - \Delta_y = 274\text{mm}$

These displacement values were used to assess the lateral roof displacements that resulted from the nonlinear time-history analyses.

8.4.3 Global assessment

With the yield- and ultimate lateral roof displacement values as defined in section 8.4.2 the performance levels discussed in section 8.4.1 are defined as follows:

- Elastic: $0 \leq \Delta \leq 76$ [mm]
- Fully operational: $76 \leq \Delta \leq 158.2$ [mm]
- Operational: $158.2 \leq \Delta \leq 240.4$ [mm]

- Life Safe: $240.4 \leq \Delta \leq 295.2$ [mm]
- Near Collapse: $295.2 \leq \Delta \leq 350$ [mm]
- Collapsed: $350 \leq \Delta$ [mm]

The lateral roof displacement of the lateral load resisting system as shown in Table 8-3 are therefore assessed using these displacement limits. A graphical representation of the lateral roof displacement response quantities and the above performance level displacement limits are shown in Figure 8-13 for the average and maximum response respectively.

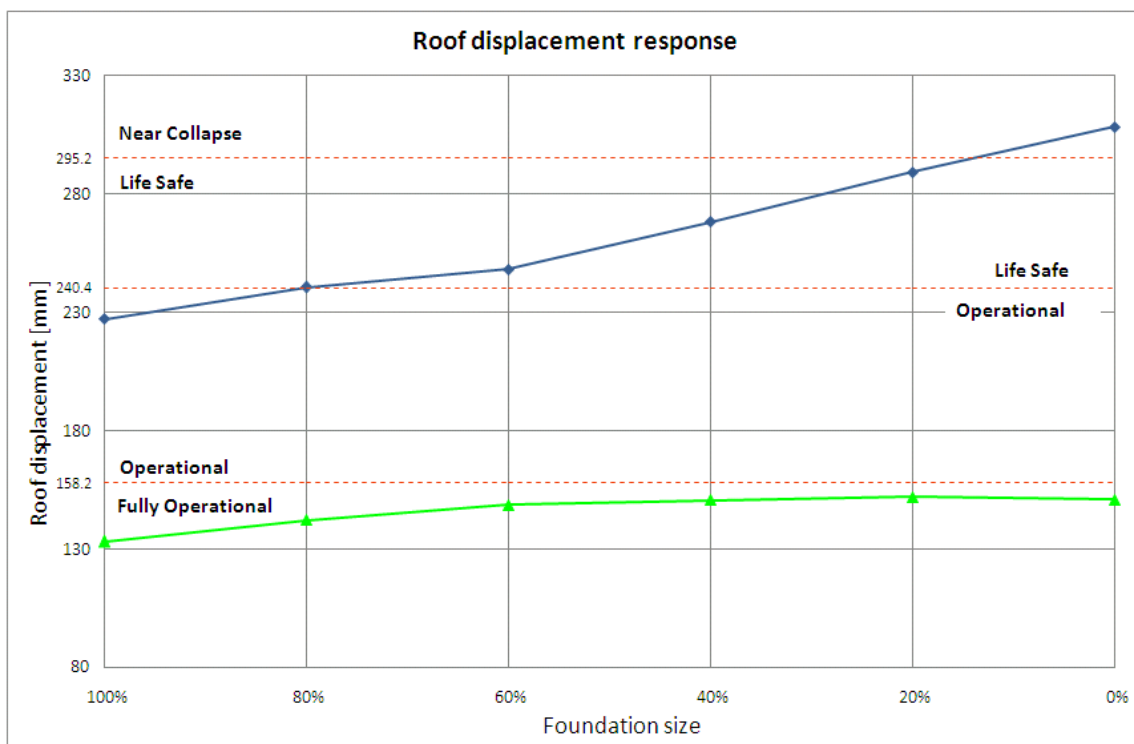


Figure 8-13: Lateral roof displacement response

It is observed that all average lateral roof displacement response quantities are within the displacement limits defining the *Fully Operational* performance level. Maximum lateral roof displacement response however result in various performance levels being achieved for the different foundation sizes as shown in Table 8-7.

Table 8-7: Global assessment of foundation sizes (maximum response)

Foundation size	Performance level
100%	<i>Operational</i>
80%	<i>Life Safe</i>
60%	<i>Life Safe</i>
40%	<i>Life Safe</i>
20%	<i>Life Safe</i>
0%	<i>Near Collapse</i>
None	<i>Collapsed</i>

From this assessment it is clear that the size of the wall foundation can be significantly reduced whilst limiting the damage to a moderate level and ensuring that life safety is protected.

The Vision 2000 report prescribes performance objectives associated with building structures for different occupancies and uses [56]. Buildings containing large quantities of hazardous materials, the release of which would result in extensive hazard to the public are defined as *Safety Critical Facilities*. The minimum performance level associated to this type of building is *Fully Operational*.

Building structures that are critical to post-earthquake operations are classified as *Essential Facilities* and includes hospitals, police stations, fire stations, emergency control centres and shelters for emergency response vehicles. The minimum performance level associated to this building type is *Operational*.

Building structures not classified in the above categories are classified as *Basic Facilities* and would include the building structure investigated in this study. The minimum performance level associated with this type of building is *Life Safe*. Wall foundation sizes able to resist 20% or more of the shear wall overstrength bending moment are therefore sufficient to comply with the minimum performance level objective of the Vision 2000 report.

Chapter nine discuss the conclusions and recommendations that can be made from this study.

Chapter 9

9 SUMMARY, CONCLUSIONS AND RECOMMENDATIONS

9.1 Summary

This study aims to investigate the feasibility of reducing the size of wall foundations in areas of moderate seismicity for buildings with no basement level. The investigation is aimed at allowing shear wall foundation rocking and taking into account the contribution of structural frames to the lateral stiffness of the structure.

An example building with no basement level was chosen. Shear wall rocking was investigated by reducing the foundation size from that required to resist the full shear wall overstrength bending moment to one designed to resist no bending moment.

Lateral force-displacement behaviour was determined for the shear wall, the wall foundation and a reinforced concrete frame. A simplified model was used to represent the combined lateral stiffness of these systems. Time-history analyses were performed on this model.

Response quantities were assessed on a local and global level and results showed that a significant reduction in wall foundation size is possible when allowing the foundation to rock and taking into account the contribution of structural frames to the lateral stiffness of the structure.

9.2 Conclusions

From the output of the nonlinear time-history analyses conclusions can be made regarding the performance of the investigated structure. Assessment of the response

quantities were performed on a global and local level and conclusions can be made from these assessments.

9.2.1 Global performance

From the maximum lateral roof displacement response it is clear that the wall foundation size could be reduced significantly whilst still limiting damage to structural and nonstructural elements to a moderate level, as defined by the *Life Safe* performance level [56]. With a foundation designed to withstand the entire shear wall overstrength bending moment only light structural damage occurs.

Lateral roof displacement tends to increase as the wall foundation size, and resulting foundation bending moment resistance, decrease. It is observed that some measure of moment resistance should still be provided to the shear wall in order to prevent extreme structural damage.

9.2.2 Internal frame performance

From the assessment of the lateral roof displacement response of the internal frame no flexural failures were observed. Large lateral displacement of the frame however increase shear forces at flat slab-column connections and could lead to punching shear failures occurring prior to the bending capacity of the slab being exceeded. Punching shear failures were not investigated in this study.

9.2.3 Foundation performance

It is observed from the wall foundation response that foundation rocking tends to increase with decreasing foundation size. This is expected, as the bending moment capacity of the foundations decrease with decreasing size.

Footing rotations associated with yielding of the underlying soil are only approached for foundation sizes designed to resist 40% or less of the shear wall overstrength bending moment. Rocking of the wall foundation increases as the foundation size decreases and yielding limits, as well as resulting lateral roof displacements, tend to increase with decreasing foundation size. It can therefore be stated that the contribution of the rocking shear wall foundation to energy dissipation increase with decreasing wall foundation size.

9.2.4 Shear wall performance

A decreasing trend is observed in the lateral roof displacement of the shear wall relative to the rotation of the wall foundation. When rocking of the wall foundation is limited, a plastic hinge mechanism in the lower part of the shear wall is used to dissipate energy. It is therefore expected that the steel yielding strain limit of the shear wall reinforcement would be exceeded when the wall foundation is large enough to resist the full shear wall overstrength bending moment. From the maximum response of the model when the aforementioned foundation size was used, it was observed that a plastic hinge would indeed form in the shear wall.

As the foundation size decreases, and as a result contribute to energy dissipation to a greater extent, the required contribution of the shear wall plastic hinge mechanism to energy dissipation will decrease. From the relative roof displacement response of the shear wall it is observed that the relative shear wall roof displacement decreases with decreasing foundation size. Hence, the shear wall response approaches that of a rigid wall element as the foundation size decrease, resulting in a smaller contribution to energy dissipation by the shear wall.

9.2.5 Overall performance

From the assessment of the response quantities it follows that it would be possible to reduce the wall foundation size of the investigated building structure by roughly 40% of volume. It should be noticed that this reduction is valid for the investigated building structure of this study and that different site conditions, as well as building geometry and use, could lead to different results.

The aim of this thesis was to investigate the feasibility of reducing the size of shear wall foundations in areas of moderate seismicity for buildings with no basement level. From the discussion of the assessment of the response quantities it follows that allowing the shear wall foundation to rock, could result in significantly smaller shear wall foundations being required.

9.3 Recommendations

This study was limited to the investigation of an example building structure with certain site conditions and building geometry in order to determine if the reduction of wall foundation sizes is feasible. It was concluded that the size of wall foundations can be reduced significantly by taking into account the contribution of shear wall rocking to dissipate energy. Future investigations are however required to investigate the following:

Number of storeys

The effect of the number of storeys should be investigated. A building with eight storeys was investigated in this study. Buildings with more and less storeys should be investigated.

Number of bays

Building geometry that includes different numbers of bays in the plane of stiffness of the lateral load resisting system should be investigated. This parameter is expected to be less critical than the number of storeys due to the restricted amount of damaged observed in the assessment of the internal frame.

Punching shear failures

Punching shear should be considered as a failure mechanism. This was excluded from the current study.

To do so, the capacity curve of the internal frame should be determined using elements that are able to calculate shear strain effects more accurately. These elements should be able to account for the increase in punching shear forces due to unbalanced bending moment transfer.

Influence of soil type

It is expected that the soil type will play an important role in the dynamic response of the wall foundation and as a result influence the response of the superstructure. The influence of different soil types should be investigated as other soil types could lead to yielding of the underlying soil to the foundation to occur prior to foundation uplift.

For this reason it is recommended that future study be performed investigating the sensitivity of the dynamic building response to the characteristics of the supporting soil. Further study should specifically be focussed on the effect of different static stress-strain modulus values (E_s) for the supporting soil.

Effective slab width

Different researchers have proposed various effective slab width models to be used for reinforced concrete frames loaded laterally. The simplified model proposed by the South African concrete design code, SABS 0100-1 [24], has been used in this study. It is recommended that future investigation be focussed on the sensitivity of the lateral force-displacement behaviour of reinforced concrete frames using the various proposed effective slab width models.

Foundation sliding failure

Uplifting of the shear wall foundation and yielding of the underlying soil were the only performance criteria prescribed to the investigated footings. Sliding failure of the foundations was therefore not investigated. The simplified model that was used in this study could be improved to include the possibility of this mode of foundation failure by adding nonlinear lateral spring elements to the shear wall support to model the lateral stiffness of the foundation.

Soil yielding could be expected to occur earlier than a sliding failure and for this reason it is the opinion of the author that soil yielding remains a more critical mode of failure than sliding.

REFERENCES

REFERENCES

1. Tarbuck E.J., Lutgens F.K., *Earth, An Introduction to Physical Geology: Seventh Edition*. 2002: Prentice Hall.
2. Dazio A., *Postgraduate Short Course, Seismic Design of Building Structures*. 2009: University of Stellenbosch, Stellenbosch, South Africa.
3. *SABS 0160-1989: The general procedures and loadings to be adopted in the design of buildings*. 1993: South African Bureau of Standards, Pretoria.
4. Kijko A., Graham G., Bejaichund M., Roblin D., Brandt M.B.C., *Probabilistic Peak Ground Acceleration and Spectral Seismic Hazard Maps of South Africa*, Report No 2003-0053, Council for Geoscience, 2003.
5. Paulay T., Priestley M.J.N., *Seismic Design of Reinforced Concrete and Masonry Buildings*. 1992: Wiley Interscience Publications.
6. Booth E., Key D., *Earthquake design practice for buildings: Second Edition*. 2006: Thomas Telford.
7. Fardis M.N., Carvalho E., Elnashai A., Faccioli E., Pinto P., Plumier A., *Designers' Guide to EN 1998-1 and EN 1998-5, Eurocode 8: Design of structures for earthquake resistance. General rules, seismic actions, design rules for buildings, foundations and retaining structures*. 2005: Thomas Telford.
8. Chopra A.K., *Dynamics of Structures: Theory and Application to Earthquake Engineering: Third Edition*. 2007: Prentice Hall.
9. SEISMOSOFT, *SeismoStruct - A computer program for static and dynamic nonlinear analysis of framed structures*, [online]. Available from URL: <http://www.seismosoft.com> (2007)
10. Krawinkler H., Seneviratna G.D.P.K., *Pros and cons of a pushover analysis of seismic performance evaluation*. *Engineering Structures*, 1998. **20**: p. 452-464.

11. Bommer J.J., Acevedo A.B., *The use of Real Earthquake Accelerograms as input to Dynamic Analysis*. Journal of Earthquake Engineering, 2004. **8**: p. 43-91.
12. SIMQKE - *Conditional Earthquake Ground Motion Simulator*, Version 2.1. May 1999.
13. PEER Strong Motion Database. University of California, Berkeley. Available from URL: <http://peer.berkeley.edu/smcat/search.html>
14. Dhakal R.P., Mander J.B., Mashiko N., *Earthquake Records for Multi-Level Seismic Performance Assessment of Structures*. Department of Civil Engineering, University of Canterbury, Christchurch, New Zealand, 2006.
15. *FEMA 451: NEHRP Recommended Provisions: Design Examples*. 2006: Prepared by the Building Seismic Safety Council for the Federal Emergency Management Agency (FEMA) of the Department of Homeland Security, Washington, D.C.
16. Schwab P., Lestuzzi P., *Assessment of the seismic non-linear behaviour of ductile wall structures due to synthetic earthquakes*. Bulletin of Earthquake Engineering, 2007. **5**: p. 549-569.
17. Lestuzzi P., Belmouden Y., Trueb M., *Non-linear seismic behaviour of structures with limited hysteretic energy dissipation capacity*. Bulletin of Earthquake Engineering, 2007. **5**: p. 549-569.
18. Fajfar P., *Capacity Spectrum Method based on inelastic demand spectra*. Earthquake Engineering and Structural Dynamics, 1999. **28**: p. 979-993.
19. Markis N., Konstantinidis D., *The Rocking Spectrum and the Shortcomings of Design Guidelines*. PEER Report 2001/07, Pacific Earthquake Engineering Research Center, College of Engineering, Aug. 2001.
20. *FEMA 440: Improvement of Nonlinear Static Seismic Analysis Procedures*. 2005: Prepared by the Applied Technology Council (ATC-55 Project); Prepared

- for the Department of Homeland Security, Federal Emergency Management Agency (FEMA), Washington, D.C.
21. ATC, 1996, *Seismic evaluation and retrofit of concrete buildings*, Vol. 1, ATC-40, Applied Technology Council, Redwood City, California.
 22. Azimi H., Galal K., Pekau O.A., *Incremental Modified Pushover Analysis*. The Structural Design of Tall and Special Buildings, 2008.
 23. Dovich L.M., Wight J.K., *Effective Slab Width Model for Seismic Analysis of Flat Slab Frames*. ACI Structural Journal, Nov-Dec 2005. **102**(6): p. 868-875.
 24. *SABS 0100-1: The structural use of concrete, Part 1: Design*. 2000: South African Bureau of Standards, Pretoria.
 25. Luo Y.H., Durrani A., Conte J., *Seismic Reliability Assessment of Existing R/C Flat-Slab Buildings*. Journal of Structural Engineering, Oct 1995. 121(10): p. 1522-1530.
 26. Luo Y.H., Durrani A.J., *Equivalent Beam Model for Flat-Slab Buildings - Part I: Interior Connections*. ACI Structural Journal, Jan-Feb 1995. **92**(1): p. 115-124.
 27. Luo Y.H., Durrani A.J., *Equivalent Beam Model for Flat-Slab Buildings - Part II: Exterior Connections*. ACI Structural Journal, Mar-Apr 1995. **92**(2): p. 250-257.
 28. Dunaiski P.E., *The Response of Flat Slab-Column Connections of Reinforced Concrete to High-Cycle Lateral Motion of Low Amplitude*. University of Stellenbosch, 1990.
 29. Wallace J.W., Kang T.H.K., Rha C., *Seismic Performance of Flat Plate Systems*. Department of Civil and Environmental Engineering, University of California, Los Angeles.
 30. Robertson I.N., Kawai T., Lee J., Enomoto B., *Cyclic Testing of Slab-Column Connections with Shear Reinforcement*. ACI Structural Journal, Sep-Oct 2002. **99**(5): p. 605-613.

31. Theodorakopoulos D.D., Swamy R.N., *Ultimate punching shear strength analysis of slab-column connections*. Cement & Concrete Composites, 2002. **24**: p. 509-521.
32. Megally S., Ghali A., *Seismic behaviour of slab-column connections*. Canadian Journal of Civil Engineering, 2000. **27**: p. 84-100.
33. Kawashima K., Hosoiri K., *Rocking Isolation of Bridge Columns on Direct Foundations*. Proceedings FIB-Symposium, Concrete Structures in Seismic Regions, Paper no 118, Athens.
34. Yim C., Chopra A., *Earthquake Response of Structures with Partial Uplift on Winkler Foundation*. Earthquake Engineering and Structural Dynamics, 1984. **12**: p. 263-281.
35. Allotey N., Nagggar M.H.E., *Analytical moment-rotation curves for rigid foundations based on a Winkler model*. Soil Dynamics and Earthquake Engineering, 2003. **23**: p. 367-381.
36. Gazzetas G., *Seismic Design of Foundations and Soil Structure Interaction*. Paper K7, First European Conference on Earthquake Engineering and Seismology. Geneva, Switzerland, 2006.
37. Anderson D.D., *Effect of foundation rocking on the seismic response of shear walls*. Canadian Journal of Civil Engineering, 2003. **30**: p. 360-365.
38. Bowles J.E., *Foundation Analysis and Design, Fifth Edition*. 1996: McGraw-Hill.
39. Yim S.C.S., Chopra A.K., *Dynamics of Structures on Two-Spring Foundation Allowed to Uplift*. Journal of Engineering Mechanics, July 1984. **110**(7): p. 1124-1146.
40. Yim S.C.S., Chopra A.K., *Simplified Earthquake Analysis of Multistorey Structures with Foundation Uplift*. Journal of Structural Engineering, Dec 1985. **111**(12): p. 2708-2731.

41. Mander J.B., Priestley M.J.N., Park R., *Theoretical Stress-Strain Model for Confined Concrete*. Journal of Structural Engineering, Aug 1988. **114**(8): p. 1804-1826.
42. *SABS 0100-2: The structural use of concrete, Part 2: Materials and execution of work*. 2000: South African Bureau of Standards, Pretoria.
43. *SANS 10160: Basics of Structural Design and Actions for Buildings and Industrial Structures, Part 4: Seismic actions and general requirements for buildings*. 2008 Draft. South African National Standard. South African National Bureau of Standards, Pretoria.
44. PROKON version 2.4, 2008; Prokon Software Consultants;
<http://www.prokon.com>
45. *BS EN 1992-1-1: 2004: Eurocode 2: Design of concrete structures - Part 1-1: General rules and rules for buildings*. British Standard, 2000.
46. Illston J.M., Domone P.L.J., *Construction Materials, their nature and behaviour*, Third Edition. 2001: Spon Press.
47. Mirza S.A., MacGregor, *Variability of Mechanical Properties of Reinforcing Bars*. Journal of the Structural Division, May 1979. **105**: p. 921-937.
48. SANS 920: Steel bars for concrete reinforcement, 2005: South African National Standard. South African National Bureau of Standards, Pretoria.
49. *FEMA 273, NEHRP Guidelines for the Seismic Rehabilitation of Buildings*. 1997: Prepared by the Applied Technology Council (ATC-33 Project) for the Building Seismic Safety Council, Washington, D.C.
50. *SIA 2018: Überprüfung bestehender Gebäude bezüglich Erdbeben Anhang A* ed. 2004, Zürich: Schweizerischer Ingenieur und Architektenverein.
51. Spathelf C.A., *Assessment of the Behaviour Factor for the Seismic Design of Reinforced Concrete Structural Walls according to SANS 10160: Part 4*. University of Stellenbosch, 2008.

-
52. Kuhn M., *Seismische Analyse bestehender Schweizer Brücken mittels numerischer Methoden*, Eidgenössische Technische Hochschule Zürich, 2007.
 53. *SIA 261: Actions on Structures*. 2003: Swiss Society of Engineers and Architects (SIA), Zurich, Swiss Standards Organisation SN 505 261.
 54. Naeim F., Alimoradi A., Pezeshk S., *Selection and Scaling of Ground Motion Time Histories for Structural Design Using Genetic Algorithms*. *Earthquake Spectra*, May 2004. **20**(2): p. 413-426.
 55. Strand7 - Finite Element Analysis System. Release 2.3.8, 2005.
<http://www.strand7.com>
 56. Structural Engineers Association of California (SEAOC), *Vision 2000: Performance Based Seismic Engineering of Buildings*. Sacramento, California, 1995.
 57. Schwarz S., Leibovich E., Yankelevsky D.Z., *Assessment of the Seismic Resistance and Seismic Safety of Existing Multistory Residential Buildings*, *Structural Engineering International*, 2009, **2**, p. 165-173.

APPENDICES

Appendix A

A CONFINEMENT CALCULATIONS

This appendix presents the calculation of the following parameters [5] [41]:

- Confinement factor (K)
- Concrete strain at peak stress (ϵ_{cc})
- Ultimate concrete compressive strain (ϵ_{cu})

These parameters were calculated for the following structural elements:

- Ground to second floor columns.
- Second floor to roof level columns.
- Shear wall sections.

A.1 Ground to second floor columns

Column width: 600mm

Concrete cover: 35mm

Stirrup diameter: 8mm

Stirrup spacing: 200mm

Clear distance between adjacent longitudinal bars: $w_i' = 215\text{mm}$

$$b_c = 522\text{mm}$$

$$d_c = 522\text{mm}$$

$$s' = 192\text{mm}$$

$$A_s = 4474\text{mm}^2$$

$$A_{\text{core}} = 272484\text{mm}^2$$

$$\rho_{cc} = 0.0164$$

$$k_e = \frac{\left(1 - \sum_{i=1}^n \frac{(w_i')^2}{6b_c d_c}\right) \cdot \left(1 - \frac{s'}{2b_c}\right) \cdot \left(1 - \frac{s'}{2d_c}\right)}{(1 - \rho_{cc})} = 0.524$$

$$A_{sx} = A_{sy} = 150.8\text{mm}^2 \quad (\text{Three R8 stirrups})$$

$$\rho_{sx} = \frac{A_{sx}}{s \cdot d_c} = 0.0014$$

$$\rho_{sy} = \frac{A_{sy}}{s \cdot b_c} = 0.0014$$

Lateral confining stresses in the x and y directions:

Characteristic yield strength of stirrups: 250MPa

$$f_{yh} = 316.25\text{MPa}$$

$$f'_{lx} = k_e \cdot \rho_x \cdot f_{yh} \quad \text{and} \quad f'_{ly} = k_e \cdot \rho_y \cdot f_{yh}$$

$$f'_{lx} = f'_{ly} = 0.239\text{MPa}$$

Characteristic concrete compressive strength: 30MPa

$$f'_c = 33\text{MPa}$$

$$f'_\ell / f'_c = 0.0073$$

Confinement coefficient:

$$K = \frac{f'_{cc}}{f'_c} = -1.254 + 2.254 \sqrt{1 + \frac{7.94 \cdot f'_\ell}{f'_c}} - \frac{2f'_\ell}{f'_c}$$

Therefore: **K = 1.049**

$$f'_{cc} = K \cdot f'_c = 34.63 \text{ MPa}$$

Concrete strain at peak stress:

$$\epsilon_{cc} = 0.002 \left[1 + 5 \left(\frac{f'_{cc}}{f'_c} \right) - 1 \right] = 0.0025$$

Ultimate concrete compressive strain (collapse strain):

$$\epsilon_{sm} = 0.0018$$

$$\epsilon_{cu} = 0.004 + \frac{1.4 \cdot \rho_s \cdot f_{yh} \cdot \epsilon_{sm}}{f'_{cc}} = 0.0041$$

A.2 Second floor to roof columns

Column width: 600mm

Concrete cover: 35mm

Stirrup diameter: 8mm

Stirrup spacing: 175mm

Clear distance between adjacent longitudinal bars: $w_i' = 224\text{mm}$

$$b_c = 522\text{mm}$$

$$d_c = 522\text{mm}$$

$$s' = 167\text{mm}$$

$$A_s = 2767\text{mm}^2$$

$$A_{\text{core}} = 272484\text{mm}^2$$

$$\rho_{cc} = 0.0102$$

$$k_e = \frac{\left(1 - \sum_{i=1}^n \frac{(w_i')^2}{6b_c d_c}\right) \cdot \left(1 - \frac{s'}{2b_c}\right) \cdot \left(1 - \frac{s'}{2d_c}\right)}{(1 - \rho_{cc})} = 0.538$$

$$A_{sx} = A_{sy} = 150.8\text{mm}^2 \quad (\text{Three R8 stirrups})$$

$$\rho_{sx} = \frac{A_{sx}}{s \cdot d_c} = 0.0017$$

$$\rho_{sy} = \frac{A_{sy}}{s \cdot b_c} = 0.0017$$

Lateral confining stresses in the x and y directions:

Characteristic yield strength of stirrups: 250MPa

$$f_{yh} = 316.25\text{MPa}$$

$$f'_{\ell x} = k_e \cdot \rho_x \cdot f_{yh} \quad \text{and} \quad f'_{\ell y} = k_e \cdot \rho_y \cdot f_{yh}$$

$$f'_{\ell x} = f'_{\ell y} = 0.281\text{MPa}$$

Characteristic concrete compressive strength: 30MPa

$$f'_c = 33\text{MPa}$$

$$f'_\ell / f'_c = 0.0085$$

Confinement coefficient:

$$K = \frac{f'_{cc}}{f'_c} = -1.254 + 2.254 \sqrt{1 + \frac{7.94 \cdot f'_\ell}{f'_c}} - \frac{2f'_\ell}{f'_c}$$

Therefore: **K = 1.058**

$$f'_{cc} = K \cdot f'_c = 34.91 \text{MPa}$$

Concrete strain at peak stress:

$$\epsilon_{cc} = 0.002 \left[1 + 5 \left(\frac{f'_{cc}}{f'_c} \right) - 1 \right] = 0.0026$$

Ultimate concrete compressive strain (collapse strain):

$$\epsilon_{sm} = 0.0018$$

$$\epsilon_{cu} = 0.004 + \frac{1.4 \cdot \rho_s \cdot f_{yh} \cdot \epsilon_{sm}}{f'_{cc}} = 0.0041$$

A.3 Shear wall

Note that only the edge regions are confined.

Wall length: 6000mm

Wall thickness: 300mm

Concrete cover: 50mm

Stirrup diameter: 10mm

Stirrup spacing: 100mm

Clear distance between adjacent longitudinal bars: $w_1' = 230\text{mm}$

$w_2' = 140\text{mm}$

$b_c = 780\text{mm}$

$d_c = 190\text{mm}$

$s' = 90\text{mm}$

$A_s = 2513\text{mm}^2$

$A_{\text{core}} = 148200\text{mm}^2$

$\rho_{cc} = 0.0170$

$$k_e = \frac{\left(1 - \sum_{i=1}^n \frac{(w_i')^2}{6b_c d_c}\right) \cdot \left(1 - \frac{s'}{2b_c}\right) \cdot \left(1 - \frac{s'}{2d_c}\right)}{(1 - \rho_{cc})} = 0.438$$

$A_{sx} = 471.24\text{mm}^2$ (Six R10 stirrups)

$$\rho_{sx} = \frac{A_{sx}}{s \cdot d_c} = 0.0248$$

$A_{sy} = 314.16\text{mm}^2$ (Four R10 stirrups)

$$\rho_{sy} = \frac{A_{sy}}{s \cdot b_c} = 0.0040$$

Lateral confining stresses in the x and y directions:

Characteristic yield strength of stirrups: 250MPa

$f_{yh} = 316.25\text{MPa}$

$$f'_{lx} = k_e \cdot \rho_x \cdot f_{yh} \quad \text{and} \quad f'_{ly} = k_e \cdot \rho_y \cdot f_{yh}$$

$$f'_{\ell x} = 3.437 \text{ MPa}$$

$$f'_{\ell y} = 0.558 \text{ MPa}$$

Characteristic concrete compressive strength: 30MPa

$$f'_c = 33 \text{ MPa}$$

Smallest confining stress ratio: $f'_{\ell 1} / f'_c = 0.0169$

Largest confining stress ratio: $f'_{\ell 2} / f'_c = 0.1041$

Confinement coefficient:

From Figure 2-24: **K = 1.100**

$$f'_{cc} = K \cdot f'_c = 36.30 \text{ MPa}$$

Concrete strain at peak stress:

$$\epsilon_{cc} = 0.002 \left[1 + 5 \left(\frac{f'_{cc}}{f'_c} \right) - 1 \right] = 0.0030$$

Ultimate concrete compressive strain (collapse strain):

$$\epsilon_{sm} = 0.0018$$

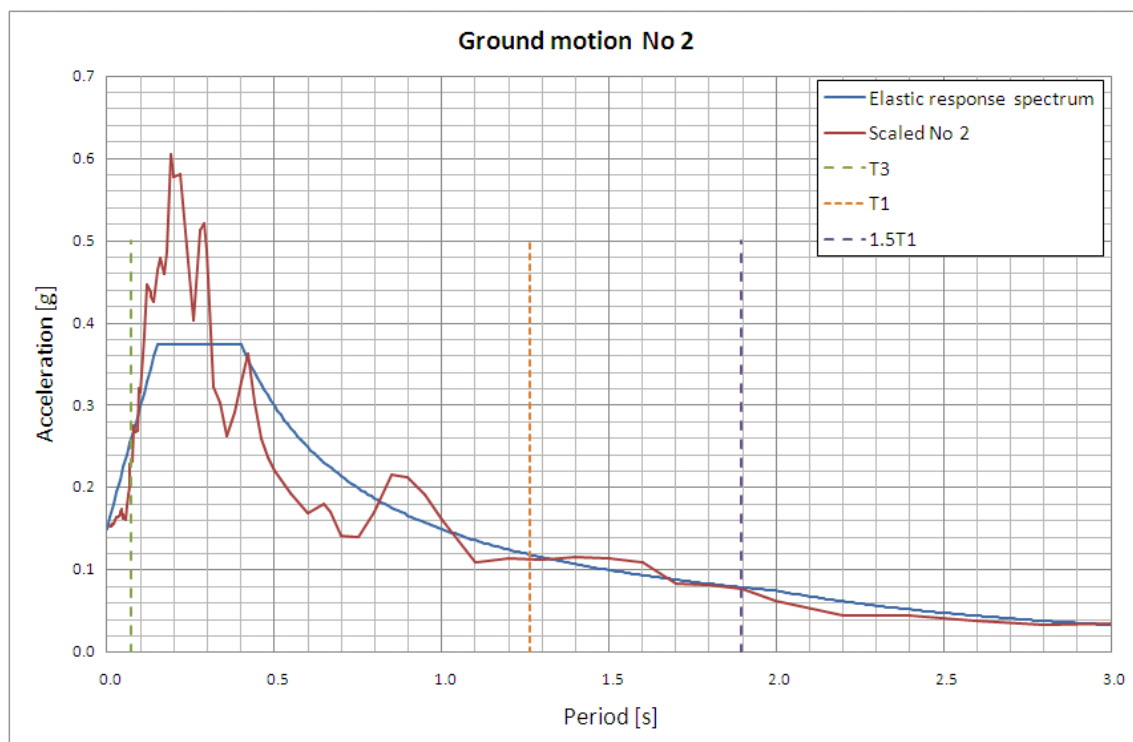
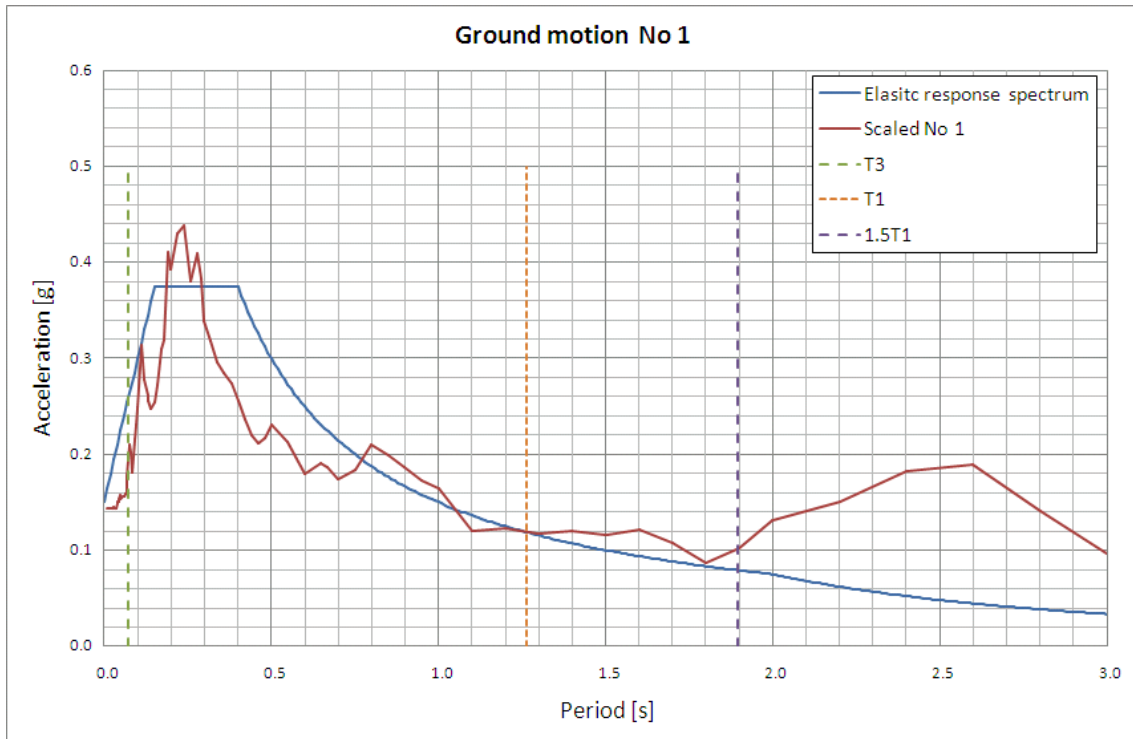
$$\epsilon_{cu} = 0.004 + \frac{1.4 \cdot \rho_s \cdot f_{yh} \cdot \epsilon_{sm}}{f'_{cc}} = 0.0046$$

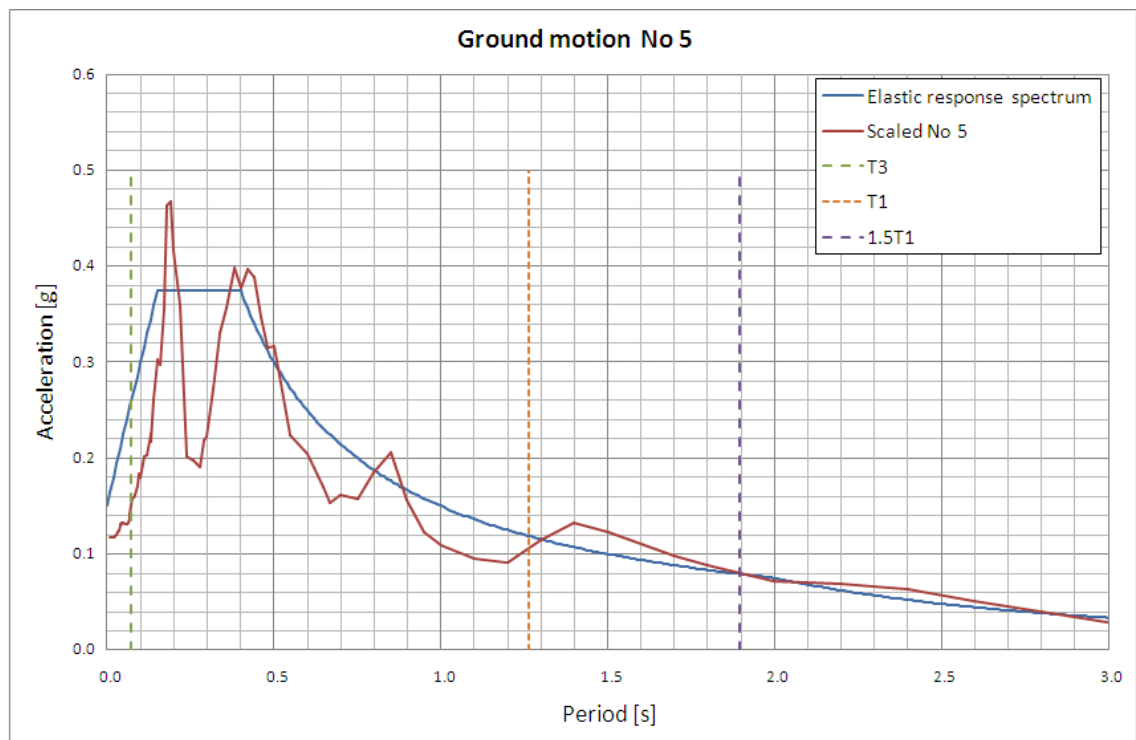
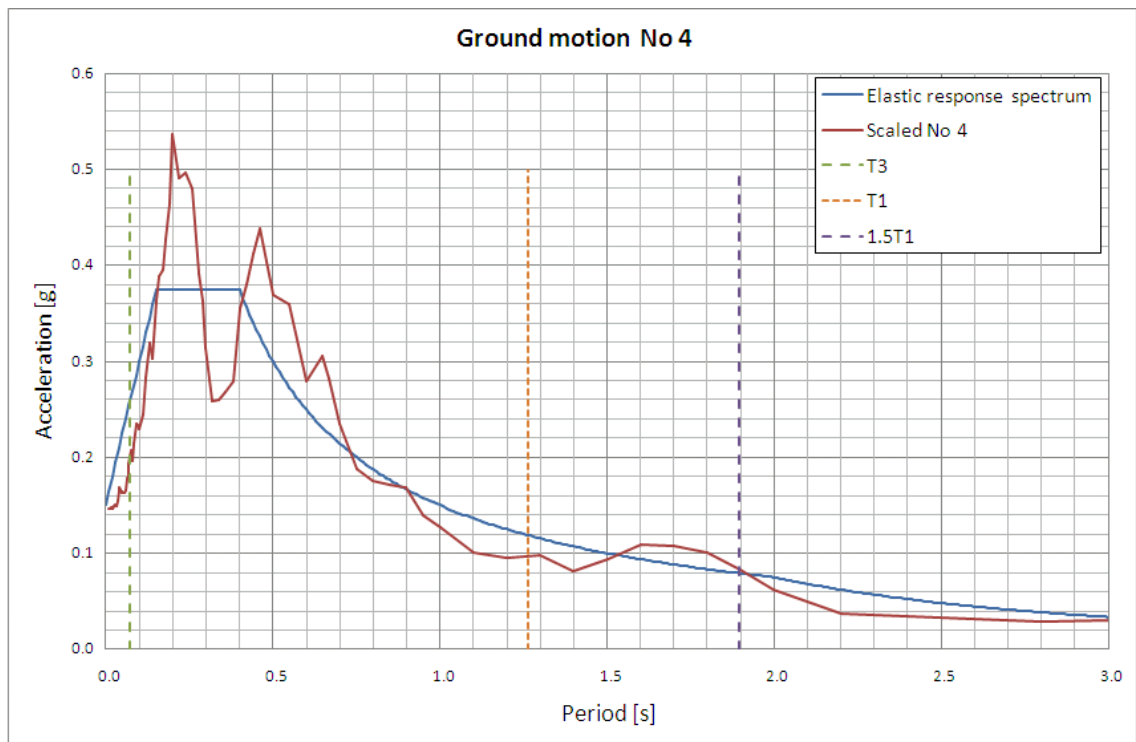
Appendix B

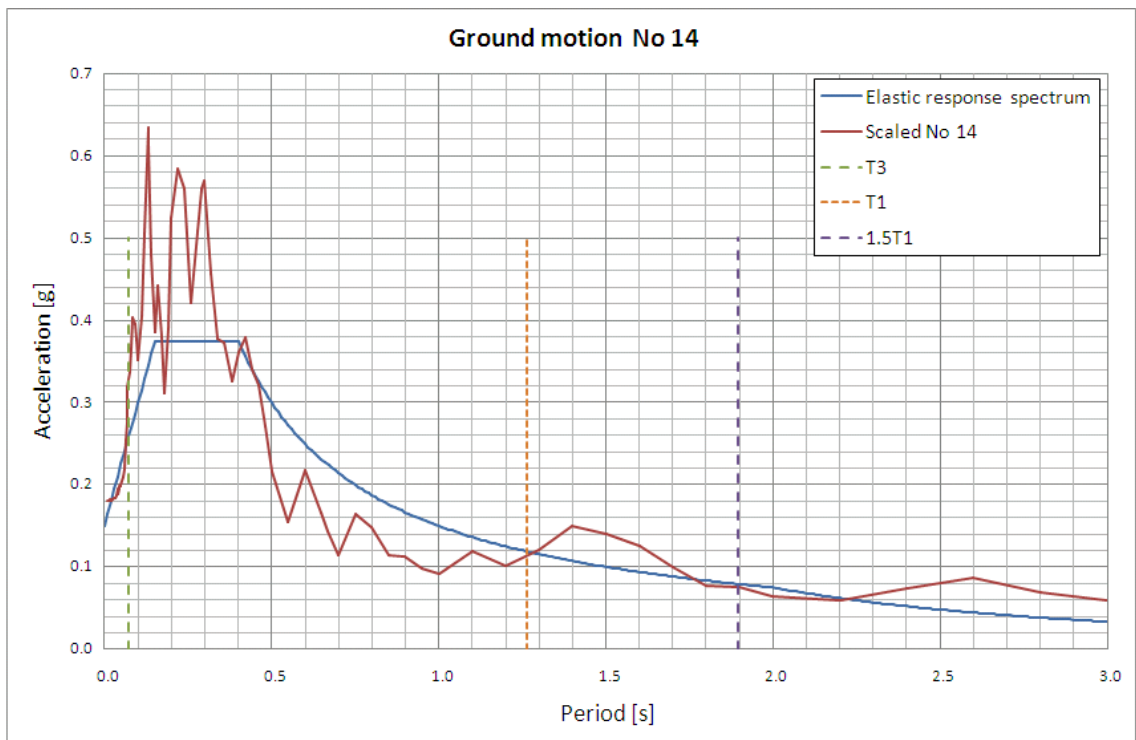
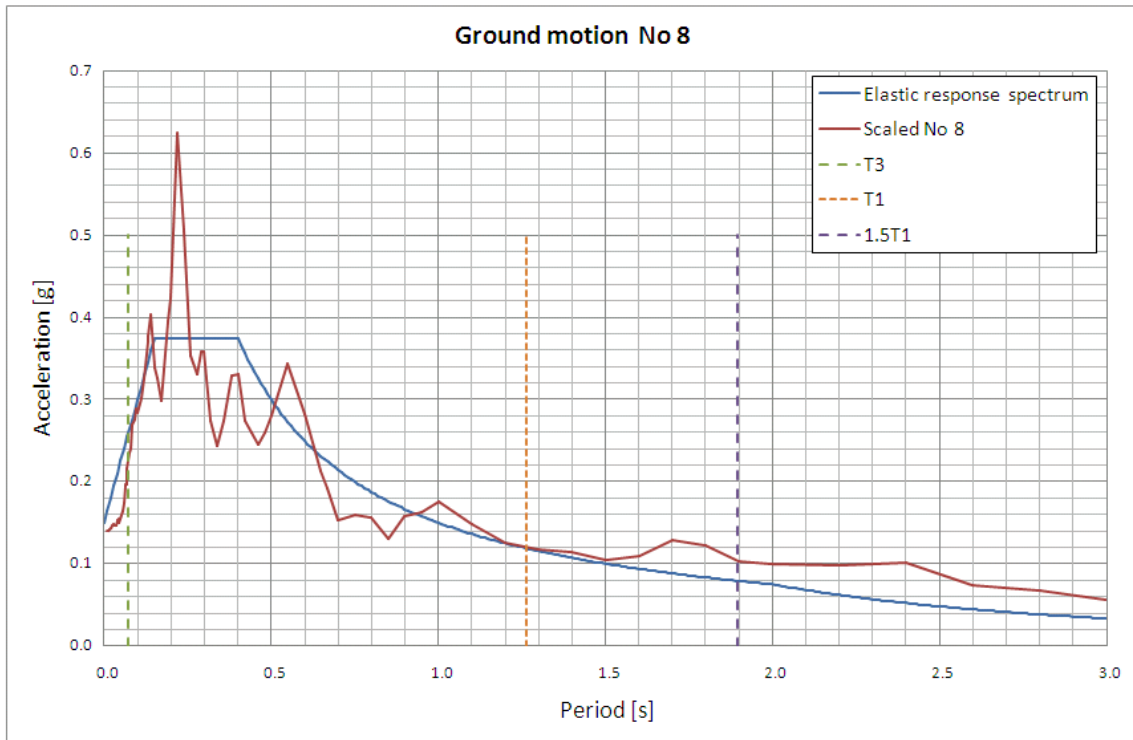
B GROUND MOTION

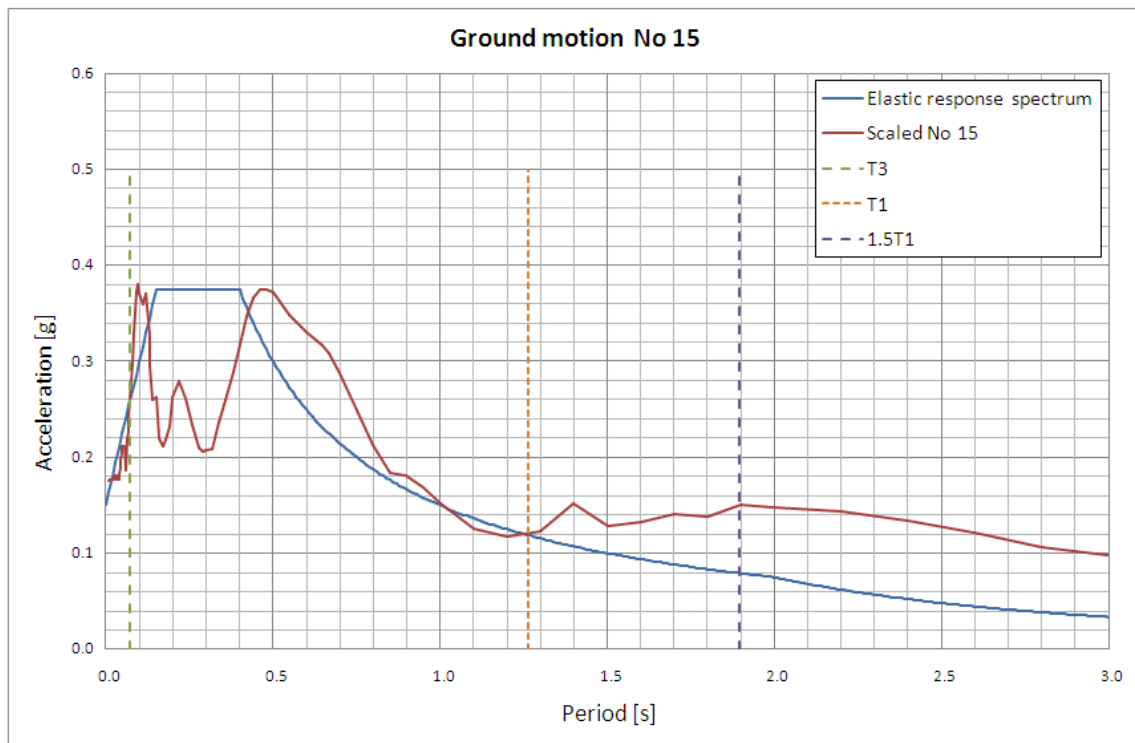
This appendix presents the scaled ground motion response spectra used in this study. The scaled ground motion time-histories are also presented.

B.1 Scaled response spectra









B.2 Scaled accelerograms

